

**CARDIFF SCHOOL OF ENGINEERING  
CARDIFF UNIVERSITY**

# **Modelling of Repair Techniques for Masonry Arch Bridges**

**Mahmoud Miri**

**BSc, MSc**

**THESIS SUBMITTED TO CARDIFF UNIVERISTY IN CANDIDATURE FOR THE  
DEGREE OF DOCTOR OF PHILOSOPHY**

**OCTOBER 2005**

UMI Number: U584743

All rights reserved

INFORMATION TO ALL USERS

The quality of this reproduction is dependent upon the quality of the copy submitted.

In the unlikely event that the author did not send a complete manuscript and there are missing pages, these will be noted. Also, if material had to be removed, a note will indicate the deletion.



UMI U584743

Published by ProQuest LLC 2013. Copyright in the Dissertation held by the Author.  
Microform Edition © ProQuest LLC.

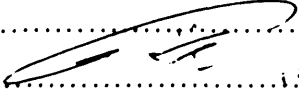
All rights reserved. This work is protected against  
unauthorized copying under Title 17, United States Code.



ProQuest LLC  
789 East Eisenhower Parkway  
P.O. Box 1346  
Ann Arbor, MI 48106-1346

**DECLARATION**

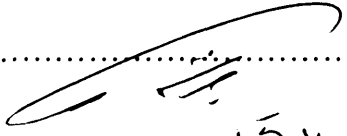
This work has not previously been accepted in substances for any degree and is not concurrently submitted in candidature for any degree.

Signed..........(Candidate)

Date.....15, 11, 2005.....

**STATEMENT 1**

This thesis is the result of my own investigation, except where otherwise stated. Other sources are acknowledged by explicit references.

Signed..........(Candidate)

Date.....15, 11, 2005.....

**STATEMENT 2**

I hereby give consent for my thesis, if accepted, to be available for photocopying and for interlibrary loan, and for the title and summary to be made available to outside organisations.

Signed..........(Candidate)

Date.....15, 11, 2005.....

## DEDICATION

*To my family,*

*Maryam, Mehrnaz and Mehrad*



## **AKNOWLEDGEMENTS**

First, I would like to thank my supervisor Prof. Tim Hughes for his great assistance, support and encouragement during the research work.

The facilities provided by Civil Engineering within the Cardiff School of Engineering, are hereby gratefully acknowledged. Thanks to the technical staff particularly Mr Harry Lane for flying the Centrifuge and frequent assistance with testing. Thanks also to Len, for helping with soils testing. Thanks also to Richard and Abba the other research students who provided a great research environment in the masonry research group.

This programme of research would have been impossible without financial support of the Iranian Ministry of Science Research and Technology who funded me during my stay at Cardiff University. Thanks also to the Iranian government for their funding.

Most importantly, I would like to thank my family, particularly my wife and kids for their continued support and encouragement throughout the course of this research.

## ABSTRACT

Small scale centrifuge models were used to study the behaviour of arches repaired using different techniques. The models under test were 1/12<sup>th</sup> scale replicas of a 6 metre single span three ring arch. Two types of arch geometry, with span/rise of 4 and 2, were studied as a shallow and deep arch geometry. The models were tested in a centrifuge under a steady equivalent gravity of 12g.

Two types of 2-D and 3-D arch models were studied which had the same geometry but different in the addition of spandrel walls. The 3-D models were built with spandrel walls but without any wing walls or parapet. Both 2-D and 3-D arch models were tested under rolling and failure loads. The models were usually tested with fourteen passes of a rolling load and then up to the observation of first signs of failure to enable them to be suitable for applying a repair method. The repaired models were tested using the same procedure but up to the full failure load. To understand the behaviour of the arch models under unsymmetrical loads different roller weights were applied at different positions. The arch deflection and the soil/masonry interaction in arch extrados were measured in all the tests and compared with each other.

Plastic mesh reinforcement, stitching, and concrete slab on top of the soil backfill were applied as repair methods to the 2-D arch models. A review of the results has shown an increase in arch stiffness, decrease in deflections and a significant improvement in the ultimate load carrying capacity. A significant effect on the pressure distribution on the arch barrel was observed due to the application of the concrete slab on top of the backfill. Stitching of arch barrel and the barrel to the spandrels, applying partial saddle concrete and strengthening of spandrel wall using reinforced concrete were tested in the 3-D arch models. The results showed improvements in the stiffness and ultimate arch load carrying capacity due to these repair techniques.

The results provide a valuable data base for validation of numerical models and an initial attempt to use them with a commercial finite element program is included.

## TABLE OF CONTENT

List of Tables.....	ix
List of Figures.....	x
List of Plates.....	xiii
<b>1 Introduction .....</b>	<b>1-1</b>
1.1 Background .....	1-1
1.2 Objective of research .....	1-3
1.3 Layout of thesis .....	1-3
<b>2 Literature review .....</b>	<b>2-1</b>
2.1 History .....	2-1
2.2 General assumption of masonry arch.....	2-2
2.3 Analysis and assessment of arch bridge.....	2-3
2.3.1 Elastic method.....	2-4
2.3.2 Plastic method .....	2-8
2.3.3 Finite element method .....	2-10
2.4 Experimental work on arch bridges .....	2-12
2.4.1 Load test on full scale bridges.....	2-13
2.4.2 Load test on model scale bridges .....	2-15
2.5 Centrifuge Modelling.....	2-17
2.5.1 Principles of centrifuge modelling .....	2-17
2.5.2 Masonry arch centrifuge modelling.....	2-19
2.6 Defects and repair of masonry arch bridges.....	2-20
2.6.1 Common defects affecting masonry arch bridges .....	2-21
2.6.2 Tests on arch bridges with defect.....	2-22
2.6.3 Test on repaired arch bridge.....	2-23
2.7 Repair and strengthening techniques .....	2-24
2.7.1 Saddling.....	2-24
2.7.2 Sprayed concrete .....	2-25
2.7.3 Repointing.....	2-25
2.7.4 Retro-reinforcement of masonry .....	2-26
2.7.5 Archtec (Cintec Anchor).....	2-27
2.7.6 MARS (Masonry Arch Repair and Strengthening System).....	2-28
<b>3 Material Properties.....</b>	<b>3-1</b>
3.1 Introduction .....	3-1
3.2 Mortar tests.....	3-1
3.2.1 Compressive tests.....	3-2
3.2.2 Specimens and procedures.....	3-2
3.2.3 Tests results and discussion .....	3-3
3.2.4 Flexural tests .....	3-4

3.2.5 Stress strain .....	3-5
3.2.6 Mortar tests results, discussion and conclusions .....	3-6
3.3 Brick tests.....	3-6
3.3.1 Bulk density and compression tests .....	3-7
3.3.2 Stress strain and Poisson's ratio tests .....	3-8
3.3.3 Bricks test results and discussions.....	3-9
3.4 Backfill tests .....	3-9
3.4.1 Particle size distribution and compaction tests.....	3-9
3.4.2 Shear test.....	3-10
3.4.3 Backfill tests results and discussion .....	3-11
3.5 Micro concrete tests .....	3-11
3.5.1 Micro concrete compression tests .....	3-12
3.5.2 Test results and discussion.....	3-12
3.5.3 Flexural tests .....	3-13
3.6 Masonry tests.....	3-13
3.6.1 Uniaxial compression tests .....	3-13
3.6.2 Bond tensile strength .....	3-15
3.7 Materials tests conclusions.....	3-15
<b>4 Experimental tests and procedure.....</b>	<b>4-1</b>
4.1 Introduction .....	4-1
4.2 Test arrangement .....	4-2
4.3 Tests programme .....	4-3
4.4 Arch model geometry and properties.....	4-5
4.4.1 Bricks.....	4-5
4.4.2 Mortar .....	4-6
4.4.3 Backfill .....	4-7
4.5 Instrumentation.....	4-8
4.5.1 Displacement measurement .....	4-8
4.5.2 Soil/masonry interaction measurement.....	4-9
4.5.3 Test observation instruments .....	4-10
4.6 Loading system.....	4-10
4.6.1 Rolling load system .....	4-10
4.6.2 Increasing load system.....	4-11
4.7 Model construction procedure .....	4-11
4.7.1 Arch barrel construction .....	4-11
4.7.2 Spandrel wall construction.....	4-12
4.7.3 Backfilling procedure .....	4-14
4.8 Instrument installation .....	4-15
4.9 Centrifuge preparation .....	4-16
4.10 Centrifuge tests procedure.....	4-16
4.10.1 Benchmark tests procedure .....	4-16
4.10.2 Repaired tests procedure .....	4-18
4.11 Repair techniques.....	4-18
4.11.1 The 2-D repair techniques and applying procedure.....	4-19
4.11.2 The 3-D repair techniques and applying procedure.....	4-20

<b>5</b>	<b>Benchmark tests and results</b> .....	<b>5-1</b>
5.1	Introduction .....	5-1
5.2	The 2-D benchmarks tests .....	5-2
5.3	The 2-D benchmark results .....	5-3
5.3.1	Rolling load results.....	5-3
5.3.2	Increasing load results .....	5-11
5.3.3	Post test observations .....	5-15
5.4	The 3-D benchmark tests .....	5-16
5.5	The 3-D benchmark tests results.....	5-16
5.5.1	Rolling load results.....	5-18
5.5.2	Increasing load results .....	5-24
5.6	The 2-D and the 3-D test results comparison .....	5-26
5.7	Conclusions .....	5-27
<b>6</b>	<b>Repaired tests and results</b> .....	<b>6-1</b>
6.1	Introduction .....	6-1
6.2	Repaired tests and results .....	6-2
6.3	Plastic mesh.....	6-3
6.3.1	Repair details .....	6-3
6.3.2	Rolling load results.....	6-3
6.3.3	Ultimate load results.....	6-4
6.3.4	Post test observations .....	6-5
6.4	Relieving slab .....	6-5
6.4.1	Rolling load results.....	6-5
6.4.2	Ultimate load results.....	6-9
6.4.3	Post test investigation .....	6-12
6.5	Stitching .....	6-13
6.5.1	Stitching repair details .....	6-13
6.5.2	Rolling load results.....	6-13
6.5.3	Ultimate load results.....	6-14
6.5.4	Post test investigation .....	6-16
6.6	Partially saddled concrete.....	6-16
6.6.1	Repair details .....	6-16
6.6.2	Rolling load results.....	6-17
6.6.3	Ultimate load results.....	6-19
6.6.4	Post test investigation .....	6-20
6.7	Spandrel walls strengthening.....	6-21
6.7.1	Rolling load results.....	6-22
6.7.2	Ultimate load results.....	6-23
6.7.3	Post test results.....	6-25
6.8	Conclusions .....	6-26
<b>7</b>	<b>Finite Element model</b> .....	<b>7-1</b>
7.1	Introduction .....	7-1
7.2	Linear elastic FE model .....	7-2

7.3 Stress analysis under self weight .....	7-3
7.3.1 Pressures on the arch extrados .....	7-3
7.3.2 Stress in the arch barrel.....	7-5
7.3.3 Parametric studies .....	7-6
7.4 Non-linear FE model .....	7-7
7.4.1 Analysis procedure .....	7-7
7.4.2 Load application.....	7-8
7.5 Modelling of failure of arch barrel .....	7-9
7.5.1 Arch barrel model results.....	7-10
7.5.2 Parametric study.....	7-11
7.6 Modelling arches with backfill .....	7-12
7.7 Results of arch model with backfill .....	7-13
7.7.1 Failure load results .....	7-14
7.7.2 Rolling load results.....	7-16
7.8 Backfill depth effect.....	7-17
7.9 Arch model with repair .....	7-19
7.10 Repair model results .....	7-19
7.11 Conclusions .....	7-20
<b>8 Conclusions and recommendations .....</b>	<b>8-1</b>
8.1 Introduction.....	8-1
8.2 Conclusions .....	8-1
8.3 Recommendations for future research .....	8-5

## LIST OF TABLES

Table 2-1: Model test results (Royles and Hendry 1991).....	2-29
Table 2-2: Centrifuge scaling law (Cheney and Fragaszy 1984).....	2-30
Table 2-3: Fault, repair and strengthening on arch bridges (Page 1993).....	2-31
Table 3-1: Mortar tests, specimens and related standards.....	3-16
Table 3-2: Engineering properties of mortar (compression strength).....	3-16
Table 3-3: Engineering properties of mortar (modulus of rupture).....	3-16
Table 3-4: Mortar tests results.....	3-17
Table 3-5: Modulus of elasticity and Poisson’s ratio (bricks).....	3-17
Table 3-6: Bricks test results.....	3-17
Table 3-7: Backfill tests.....	3-17
Table 3-8: Backfill materials properties.....	3-18
Table 3-9: Micro concrete tests.....	3-18
Table 3-10: Engineering properties of micro concrete (compression strength).....	3-18
Table 3-11: Engineering properties of micro concrete (modulus of rupture).....	3-19
Table 3-12: Masonry compression strength and modulus of elasticity.....	3-19
Table 3-13: Arch bridges material properties.....	3-20
Table 4-1: 2-D arch models and their repair methods.....	4-26
Table 4-2: 3-D arch models and their repair methods.....	4-26
Table 4-3: Major dimensions of arch models under test.....	4-26
Table 4-4: Material properties of models.....	4-26
Table 4-5: 3-D tests applied rolling loads.....	4-27
Table 5-1: 2-D benchmark model details.....	5-29
Table 5-2: Load cycle and arch condition after each test.....	5-29
Table 5-3: 3-D benchmark model details.....	5-30
Table 5-4: Roller weight (kg) for load cases for 3-D tests.....	5-30
Table 6-1: 2-D tests details and repair methods.....	6-28
Table 6-2: 3-D tests details and repair methods.....	6-28
Table 6-3: Load cycle and arch condition after each test.....	6-29
Table 6-4: Roller weight for load cases for 3-D repair tests.....	6-29
Table 6-5: Arch model stiffness and ultimate load.....	6-30
Table 6-6: Arch deflections (mm) under the different load cases.....	6-31
Table 7-1: Material properties, linear elastic FE model.....	7-22
Table 7-2: Failure load with different modulus of elasticity.....	7-22
Table 7-3: Failure load with different tensile strength.....	7-22
Table 7-4: Material properties, non-linear FE model.....	7-22
Table 7-5: Numerical arch failure load with different tensile strength of barrel material.....	7-23

## LIST OF FIGURES

Figure 2-1: Typical masonry arch bridge .....	2-32
Figure 2-2: Response of arch bridge to applied load .....	2-32
Figure 2-3: Pippard's real and analytical arch model .....	2-33
Figure 2-4: Mechanism with equilibrating forces (Page 1993).....	2-33
Figure 2-5: Heyman's arch model .....	2-34
Figure 2-6: Centrifuge scale model.....	2-34
Figure 3-1: Mortar flexural test specimen .....	3-22
Figure 3-2: Backfill size distribution curve .....	3-22
Figure 3-3: Maximum bulk density of limestone backfill .....	3-22
Figure 3-4: Shear box test on backfill materials .....	3-23
Figure 3-5: Masonry test specimens (triplet).....	3-23
Figure 3-6: Masonry test specimens (walette).....	3-23
Figure 3-7 : Masonry bond wrench test setting .....	3-24
Figure 4-1: General view of 2-D models.....	4-28
Figure 4-2: General view of 3-D models.....	4-28
Figure 4-3: Arch barrel and model instruments locations .....	4-29
Figure 5-1: Typical arch deflection under rolling load (S2D-1B) .....	5-31
Figure 5-2: Arch deflection under rolling load (S2D-1B).....	5-32
Figure 5-3: Arch deflection under the rolling load (D2D-1B).....	5-32
Figure 5-4: Radial deflection of arch under the rolling load (2-D tests) .....	5-33
Figure 5-5: Pass number effect on arch deflection (S2D-1B, 50% span).....	5-34
Figure 5-6: Average arch deflection under rolling load (forward direction).....	5-34
Figure 5-7: Average arch deflection under rolling load (backward direction) .....	5-34
Figure 5-8: Arch response to the roller load in forward and backward movement.....	5-35
Figure 5-9: Pressure on extrados of arch barrel under self weight.....	5-35
Figure 5-10: Typical recorded pressures on arch extrados under rolling load (S2D-1B, 75% span) .....	5-36
Figure 5-11: Comparison of the theoretical and measured values (shallow arches).....	5-36
Figure 5-12: Change in pressure under rolling load (2-D tests) .....	5-37
Figure 5-13: Pass number effect on soil/ masonry interaction (S2D-1B) .....	5-38
Figure 5-14: Effect of roller movement direction on soil/masonry interaction (S2D-2B) .....	5-38
Figure 5-15: Load/deflection at different span positions (S2D-2B) .....	5-38
Figure 5-16: Load/deflection at different sections.....	5-39
Figure 5-17: Load/deflection at front and middle of arch (D2D-1B, 25% span).....	5-40
Figure 5-18: Load/deflection at front and middle of arch (S2D-1B, 75% span) .....	5-40
Figure 5-19: Arch deflection under the increasing load.....	5-40
Figure 5-20: Pressures on back and front sensors under increasing load.....	5-42
Figure 5-21: Pressures on arch extrados under increasing load.....	5-42
Figure 5-22: Arch condition after benchmark tests (2-D models) .....	5-43
Figure 5-23: General view of 3-D arches with instrument locations .....	5-45
Figure 5-24: Arch deflection at different sections under the rolling load (S3D-1B) .....	5-47
Figure 5-25: Average 3-D shallow arch deflections under the rolling load (pass F7) .....	5-48
Figure 5-26: Arch deflections under different load cases (3-D shallow) .....	5-49
Figure 5-27: 3-D deep arch deflection under the rolling load (pass F7) .....	5-50
Figure 5-28: Pressure under rolling load at different sections (3-D, pass F7).....	5-51
Figure 5-29: Change in pressure under rolling load (deep arch pass F6).....	5-52
Figure 5-30: Maximum pressures under the rolling load .....	5-53
Figure 5-31: Front edge average pressures under the different rolling load cases.....	5-54



Figure 5-32: Back edge average pressures under the different rolling load cases .....	5-55
Figure 5-33: Different load cases and the UK practice load distribution .....	5-56
Figure 5-34: Arch deflections under increasing load (3-D tests).....	5-57
Figure 5-35: Pressures on the arch extrados under increasing load (3-D tests).....	5-58
Figure 5-36: 2-D and 3-D average arch displacements under rolling load.....	5-59
Figure 6-1: Arch deflection for different roller positions at 50% of the span .....	6-32
Figure 6-2: Pressures on arch extrados at 75% of the span .....	6-32
Figure 6-3: Load deflection curve under load position .....	6-32
Figure 6-4: Pressures on different locations of the arch barrel (S2D-2B & S2D-2R).....	6-33
Figure 6-5: Arch condition and hinge locations after test (S2D-2R) .....	6-33
Figure 6-6: Shallow arch deflections under the rolling load .....	6-34
Figure 6-7: Deep arch deflections under the rolling load.....	6-35
Figure 6-8: At-rest pressures at different locations of the arch barrel.....	6-36
Figure 6-9: Influence of concrete slab repair on pressure (shallow arch) .....	6-36
Figure 6-10: Influence of pass number and direction (sensor at 75% span, S2D-3R) .....	6-37
Figure 6-11: Influence of concrete slab repair on pressure (deep arch) .....	6-38
Figure 6-12: Arch load deflections at different sections (shallow arch) .....	6-39
Figure 6-13: Arch load deflections at different sections (deep arch).....	6-40
Figure 6-14: Pressures at different locations of arch barrel (S2D-3B & S2D-3R) .....	6-41
Figure 6-15: Pressures at different locations of arch barrel (D2D-1B & D2D-1R).....	6-41
Figure 6-16: Arch condition after test (S2D-3R).....	6-42
Figure 6-17: Arch condition after test (D2D-1R) .....	6-42
Figure 6-18: Deflections under the rolling load at 50% of span (S3D-1B & S3D-1R) .....	6-43
Figure 6-19: Arch load deflection comparison (S3D-1B& S3D-1R).....	6-43
Figure 6-20: Soil/arch interface pressure comparison (S3D-1B & S3D-1R) .....	6-43
Figure 6-21: Arch condition after test (S3D-1B & S3D-1R).....	6-44
Figure 6-22: Arch deflections under rolling load.....	6-45
Figure 6-23: Pressures under different rolling loads at 20% of the span (S3D-2R) .....	6-46
Figure 6-24: Pressures at different locations of the arch barrel under the rolling Load Case 1 ...	6-47
Figure 6-25: Arches deflections under increasing load.....	6-48
Figure 6-26: Soil/arch interface pressure comparison (S3D-2B & S3D-2R) .....	6-48
Figure 6-27: Pressures recorded by pairs of sensors at 75% of the span (S3D-2R).....	6-48
Figure 6-28: Arch condition after tests (S3D-2B & S3D-2R).....	6-49
Figure 6-29: Arch deflection under rolling load (S3D-3R & S3D-3B).....	6-50
Figure 6-30: Load/deflection comparison (S3D-3B & S3D-3R).....	6-50
Figure 6-31: Soil/arch interface pressure comparison (S3D-3B & S3D-3R) .....	6-51
Figure 6-32: Pressure/displacement at different position of the shallow arch.....	6-51
Figure 6-33: Load/deflection comparison (D3D-1B, D3D-1R).....	6-51
Figure 6-34: Soil/arch interface pressure comparison (D3D-1B & D3D-1R).....	6-52
Figure 6-35: Shallow arch test condition before and after test (S3D-3B & S3D-3R).....	6-53
Figure 6-36: Deep arch test condition before and after test (D3D-1B & D3D-1R).....	6-54
Figure 6-37: 2-D arch ultimate load capacity .....	6-55
Figure 6-38: 3-D arch ultimate load capacity .....	6-56
Figure 7-1: General view of 2-D shallow arch FE model .....	7-24
Figure 7-2: General view of 2-D deep arch FE model .....	7-24
Figure 7-3: Direction of stresses .....	7-24
Figure 7-4: Normal stress on shallow arch barrel extrados .....	7-25
Figure 7-5: Normal stress on deep arch barrel extrados.....	7-25
Figure 7-6: Shear stress on the shallow and deep arch extrados.....	7-25
Figure 7-7: Normal stress inside of the shallow arch barrel .....	7-26
Figure 7-8: Shear stress inside of the shallow arch barrel .....	7-26

Figure 7-9: Barrel extrados pressures with different material properties.....	7-26
Figure 7-10: Shallow arch barrel non-linear model .....	7-27
Figure 7-11: Shallow arch barrel at failure.....	7-27
Figure 7-12: The effect of residual force norm on failure load .....	7-27
Figure 7-13: The effect of displacement norm on failure.....	7-27
Figure 7-14: Non-linear FE model (shallow arch).....	7-28
Figure 7-15: Non-linear FE model (deep arch) .....	7-28
Figure 7-16: Shallow arch deformation at failure load .....	7-28
Figure 7-17: Deep arch deformation at failure load.....	7-29
Figure 7-18: Numerical and experimental results comparison (shallow arch).....	7-29
Figure 7-19: Numerical and experimental deflections comparison (deep arch).....	7-29
Figure 7-20: Numerical and experimental pressures comparison (shallow arch).....	7-30
Figure 7-21: Numerical and experimental pressures comparison (deep arch).....	7-31
Figure 7-22: Shallow arch deflections at different sections under roller load.....	7-31
Figure 7-23: Pressures at different arch barrel positions (shallow arch).....	7-32
Figure 7-24: Arch deflection against roller location at 50% of span (deep arch).....	7-32
Figure 7-25: Backfill depth effect on arch deflection (75% deep arch).....	7-33
Figure 7-26: Backfill depth effect on predicted extrados pressure (68% deep arch).....	7-33
Figure 7-27: Shallow repaired arch predicted hinge position.....	7-33
Figure 7-28: Deep repaired arch predicted hinge position .....	7-34
Figure 7-29: Load/arch deflection (repaired shallow arch).....	7-34
Figure 7-30: Load/arch deflection (repaired deep arch).....	7-34
Figure 7-31: Change in pressures against increasing load (repaired shallow arch).....	7-35
Figure 7-32: Change in pressures against increasing load (repaired deep arch).....	7-35

## LIST OF PLATES

Plate 1-1: Pol-Khajoo, in Isfahan, Iran.....	1-5
Plate 3-1: Mortar tests .....	3-25
Plate 3-2: Compression bricks test.....	3-25
Plate 3-3: Stress strain relationship brick test.....	3-26
Plate 3-4: Masonry test (triplet).....	3-26
Plate 3-5: Masonry test (walette).....	3-27
Plate 4-1: 2-D shallow arch model construction procedure.....	4-30
Plate 4-2: 2-D deep arch model construction procedure .....	4-31
Plate 4-3: Load system .....	4-32
Plate 4-4: 3-D arch model construction procedure .....	4-33
Plate 4-5: Plastic mesh repair method .....	4-34
Plate 4-6: Concrete slab repair method .....	4-35
Plate 4-7: Partial concrete slab repair method .....	4-36
Plate 4-8: Spandrel wall strengthening method .....	4-37
Plate 6-1: General view of plastic mesh reinforcement (S2D-2R) .....	6-57
Plate 6-2: Arch condition after test (S2D-2R) .....	6-57
Plate 6-3: Arch condition after test (S2D-3R) .....	6-58
Plate 6-4: Arch condition after test (D2D-1R).....	6-59
Plate 6-5: Arch condition after benchmark test (S2D-1B) .....	6-60
Plate 6-6: Arch condition after repair test (S3D-1R) .....	6-61
Plate 6-7: Arch condition after benchmark (S3D-2B).....	6-62
Plate 6-8: Arch condition after test (S3D-2R) .....	6-63
Plate 6-9: Arch condition after benchmark test (S3D-3B) .....	6-64
Plate 6-10: Arch condition after test (S3D-3R) .....	6-64

# 1 Introduction

## 1.1 Background

Masonry arch bridges are a major part of the transport system around the world. In the UK there are about 40,000 masonry arch bridges in use, the majority of them were built between the 17<sup>th</sup> and the 19<sup>th</sup> centuries. A small but significant population of the masonry arch bridges from the 19<sup>th</sup> century is present on the local roads of the United States (Roberts and Boothby 1999).

Si-O-Se-Pol (33 arches) is a famous arch bridge built at the beginning of the 17<sup>th</sup> century at Zayandeh Rud located in Isfahan, in central Iran. The bridge is made of bricks and stone of 295.0m length and 13.8m width. The bridge is a multi span arch with 33 spans. Pol-Khajoo is one of the other famous bridges in Iran, Isfahan, which was made of stone and bricks and built between 1642 and 1667. The bridge is 110.0m long and a little over 20.0m wide for most of its course. Both of these bridges are in good condition and in use now. Plate 1-1 shows a general view of Pol-Khajoo bridge. In many countries the arch bridges are still in use as a major part of their transport system. The world's longest single span masonry arch bridge, Jiuxigou Bridge, was built in Sichhuna, China, in 1972 with a span, rise, and width of 116.0m, 14.5m, and 7.5m respectively. The ring thickness varies from 1.6m to 2.2m. The arch was built in random stonework and took only a year to complete.

Masonry arch bridges are now carrying loads much more than they were designed to carry by their builders. The maximum allowable axial load was increased from 9.0 tonnes to 10.0 tonne in 1984 under new European Commission Directives and has

increased to 11.5 tonnes since January 1999. Bridges are now being assessed to the new EC loading requirements. It has become evident that many bridges are not strong enough, either because they have deteriorated over time or their design was inadequate for current loads (Page 1996). The current assessment methods are based on past experimental research work which was carried out on real arches and full scale or small scale models. Significant experiments on single arches have been carried out and reported by Hendry (Hendry 1986; Hendry et al. 1985), Page (Page 1987; Page 1988; Page 1989), Melbourne et al (Melbourne et al. 1995; Melbourne and Walker 1988; Melbourne and Walker 1990), Hughes et al (Hughes et al. 1998) and others. Most of the early tests on the arch bridges and their results were reported by Page (Page 1993). These experiments were initially directed at load assessment and have provided significant understanding on the response of these types of structures to loads.

Most of the existing structures in use are more than hundred years old and therefore there is significant interest in repair and strengthening techniques. In recent years experimental work has moved more from assessing existing capacity towards investigations of methods to increase capacity. The effect of various strengthening methods on full scale arches was reported by Sumon (Sumon 1998) and Melbourne et al (Melbourne et al. 1995). Baralos (Baralos 2002) applied different types of strengthening method to 1/12<sup>th</sup> scale 2-D single span arch models. In most of the above referenced works 2-D arch models were studied. However it is known that a significant number of arch bridge defects are due to transverse effects. Lateral earth pressure on spandrel and wing wall tends to cause the overturning of the walls and often causes longitudinal cracks between the spandrel and the arch ring. Longitudinal cracks can also be caused by the lane directionality in the loading but these tend to be on the centreline rather than at the spandrel ring interface. Additionally the backfill downward pressure due to self weight and traffic loads on the barrel, which is restrained in each side between two relatively stiff spandrel walls, may cause transverse bending in the arch barrel. This suggests that 3-D and spandrel wall effects on these structures should also be considered. The 3-D numerical and experimental works by Fanning and Boothby (Fanning and Boothby 2001a; Fanning and Boothby 2001b) and Boothby and Roberts (Boothby and Roberts 2001) have shown bending effect and transverse behaviour of arches under service load tests.

In a survey of 98 arch bridges by Page et al (Page et al. 1991) it was shown that 23 bridges had longitudinal cracks and 69 bridges had spandrel wall defects. Despite the magnitude of this problem little research has been carried out on understanding the behaviour of 3-D models and to the author's knowledge very little specifically on the effect of strengthening on 3-D arch behaviour under service and ultimate loads.

## 1.2 Objective of research

The research work described in this thesis continues the series of research work at Cardiff University using centrifuge models to study masonry arch behaviour. This research is particularly focused on the effect of applying different repair methods to 2-D and the 3-D masonry arch models. The particular objectives of this thesis were:

- To review existing research information related to the masonry arch behaviour and repair methods.
- To provide details of the behaviour of the repaired arches by undertaking tests on repaired models under rolling and increasing loads.
- To modify the existing repair methods and provide information on comparison between applying the various repair techniques for masonry arch bridges.
- To obtain further understanding on the behaviour of masonry arch bridges from numerical analysis.

## 1.3 Layout of thesis

This thesis is divided into 8 chapters:

Chapter 1: This contains the background, aim of the research and finally outlines of the thesis.

Chapter 2: A brief review of both theoretical and experimental works is presented in Chapter 2. The analysis and assessment methods are presented and then experimental work on masonry arch bridges are considered, this was followed by a comprehensive review of the technique of geotechnical centrifuge modelling and in particular its

application of the modelling of masonry arch bridges. The final section covers the various repair and strengthening techniques of masonry arch bridges.

Chapter 3 describes the tests on materials employed in the centrifuge models. This includes tests on bricks, mortar, micro concrete and the backfill which was used for the arch model building. It details the main properties of materials used during the research. The chapter presents also the results of the tests on masonry assemblies.

The experimental programme and test procedures are presented in Chapter 4. The first section of this chapter includes the test programmes, arch model details and instrumentation. Details of the devices used to monitor the tests are given and covers the transducers and pressure sensors. Test preparation procedures are detailed followed by the repair technique methods applied to the arch models.

Chapter 5 covers the results of the first stage of the model tests prior to the application of any repairs. This includes a description of the results under the rolling and increasing load up to the observation of the first sign of failure. The 3-D behaviour of the arch models is investigated, especially under unsymmetrical rolling loads.

Chapter 6 details the effect of applying various repairs to the arches and compares the results of each. Arch deflections, pressures on the arch extrados and the ultimate load capacity are described. The repaired arch behaviour is compared to the benchmark arches and the effect of each repair identified.

In Chapter 7, the results of a 2-D Finite Element analysis of the arch model are detailed. The FE model was constructed using an available commercial FE package and the behaviour of the numerical and experimental models is compared to each other. This includes the arch deflections and the pressures on the extrados of the arches under rolling and increasing loads. At the end of this chapter the effect of adding the concrete slab repair to the numerical model are detailed and compared with the experimental results.

Chapter 8; the final chapter presents the main conclusions of the work and the recommendations for further research.



**Plate 1-1: Pol-Khajoo, in Isfahan, Iran**



## 2 Literature review

### 2.1 History

It has been suggested that arches and vaults originated in the Middle East about five thousands years ago (Van Beek 1987). Most of ancient and medieval arch barrels are constructed of a number of rough or cut stone voussoirs, positioned in a single ring. These early arches were constructed in horizontal courses, each succeeding stone being corbelled out beyond the one below it. Howe (Howe 1987) believed that Chinese built the first arches. There are many of old arch bridges in China with many of them are still in use. Zhau Zhou is a bridge of 37.0m span, span to rise ratio of 5.3 and ring thickness 1.0m, built about 1400 years ago and is still in use (Ng 1999). Howe also noted that a four-course brick arch, dating from about 1540BC was found in Campbell's tomb in Egypt.

Romans were also great arch builders and many of the ancient bridges that have survived to now are those constructed by Romans. Cloaca Maxima, the earliest Roman arch, was built about 615 BC. One of their largest bridges was built in 105 BC at Alcantra in Spain, it has six arches with main spans of 30.0m. Romans built their arches with stones generally in semicircular shape, but some were segmental and also some were made of brick (Page 1993).

The main period of masonry arch bridge construction in the UK began with the construction of the canals in the second half of the 18<sup>th</sup> century and ended when the railway network was completed during the early part of the 20<sup>th</sup> century (Page 1993). Early builders relied on their experience for arch building and sometimes they had to try several times. For example Pontypridd Bridge was built successfully after 3 times failing.

By the middle of the 19<sup>th</sup> century the use of the masonry arch as a bridge construction material was less prevalent and iron and concrete were soon to be preferred, primarily due to their ability to resist tensile stresses.

At present there are more than 100,000 road bridges in the UK and masonry arches bridge form an important part of them with some 40% of the total bridges. Durability and low maintenance of the masonry arch bridges compared with the steel and concrete bridges, as built today, provides a stimulus for the structural form to be reconsidered as a viable option. When maintenance is taken in to the whole life analysis of these structures they are cheaper than other structures. Cox and Hsall have shown that the whole cost of an 8.0m span arch, 120 years old, is about 12% less than the same arch in concrete or steel (Cox and Hsall 1996). For this reason some masonry bridges are built recently, for instance Ellerbeck Bridge on Carleton road (1987), Monk New Bridge in Lancashire, Prestwood Bridge near to the Stourbridge (1986), Shinafoot Bridge in Tayside Region (1987) and Kimbolton Bridge (Page 1993).

## 2.2 General assumption of masonry arch

The structural elements of a typical masonry arch bridge are shown in Figure 2-1. The figure has the following elements resisting the loading:

- The arch barrel: that is the basic element of the arch.
- Backfill: Generally, transfers load from the pavement to the backfill and is then distributed on to the arch ring. It has been shown that backfill material properties and interaction between arch and fill is a significant parameter in an arch's load capacity (Fairfield and Ponniah 1994a; Royles and Hendry 1991).
- Arch spandrel and wing walls: A series of models tests carried out by Royles and Hendry (Royles and Hendry 1991) indicated that the spandrel and wing walls have a significant role in arch load bearing capacity but traditionally the contribution of spandrel and wing walls to the stiffness and load capacity of the bridges is ignored. This may be reasonable because in many arch bridges the spandrel walls are detached from the barrel during their lifetime (Page 1993).

The masonry elements interact with each other and with the fill under the applied load and the behaviour of arch is influenced by the relative contribution of these

elements. The behaviour of a typical arch bridge is shown in Figure 2-2. In general masonry structures have high strength in compression and low tensile strength, that may be ignored in calculations. Arches are usually made from stone or bricks which cover a high range of material strengths. So the material properties of the masonry structure must be defined carefully, but some material properties are assumed in simple analysis of these structures. Heyman (Heyman 1982) defined the following three basic assumptions for the masonry materials:

- Sliding failure cannot occur as voussoirs are effectively interlocked due to high friction.
- Masonry has no tensile strength; although stone itself has a definite tensile strength the joint between them may be dry or with weak mortar. So this assumption is safe, perhaps too safe, because interlocking between of the stones which prevents sliding also enables tensile forces to be transmitted locally.
- Masonry has an infinite compressive strength; this assumption implies that stresses are so low in a masonry structure that there is no danger of crushing of the material.

According to these assumptions, and some others, basic theoretical work on arch analysis and assessment were suggested which is explained in the next sections.

### **2.3 Analysis and assessment of arch bridge**

For many centuries masonry arch bridges were built by trial and error, using simple rules of thumb. Reviews of the early literature relating to the analysis and design of arch bridges by Hook, de la Hire, Gregory, Couplet, Pippard, Heyman and other researchers has been undertaken by Crisfield and Page (Crisfield and Page 1990) and Page (Page 1993). A review on the UK masonry arch bridge assessment methods was undertaken by Hughes and Blackler (Hughes and Blackler 1997). Analysis of arch bridges generally can be divided in two major groups, elastic methods and plastic methods of analysis. Recently some researchers have tried to analyse arch bridges using FE methods which can be classified under elastic methods. In this section theoretical work on the analysis and assessment method of masonry arch bridge is reviewed.

### 2.3.1 Elastic method

The first work on elastic methods was carried out by Navier (Page 1993). He developed the straight line law for the distribution of pressure across a surface, and demonstrated that the resulting line of force had to be within the middle third of the surface to prevent tension arising. Castigliano (Castigliano 1879) developed an elastic method based on the minimum strain energy. He assumed that provided the line of pressure fell within the middle third of the arch ring, the ring would behave as a continuous elastic rib (Page 1993). Based on Castigliano strain energy Bridle and Hughes developed a computer program as known CTAP (Bridle and Hughes 1990). It is capable to analysing all normal arch geometries under varying loads. The arch ring is treated as a linear elastic material fixed at both ends. The arch ring is discretised into a number of elements and loads are applied to the arch barrel and the resulting member forces determined. These are used to determine the stress state and deformation. The stresses are used to identify the tensile area. This area then has a reduced effective depth of ring. This process is continued until the formation of incipient hinges. This method has an ability to calculate the deformation of arch under load. Soil/masonry interaction is also considered in this analysis by incorporating active and passive pressures around the arch extrados.

Pippard and his co-workers made a significant contribution to the development of using elastic theory in arch assessments. He conducted a series of experiments on model arches and concluded that the voussoir arch behaved elastically within certain limiting loads. He also demonstrated that the collapse of arch bridges was due to the formation of hinges as the result of cracking (Pippard 1951). He derived an expression relating the span, rise, and thickness and fill depth over the crown to vehicle type. This simple approach to assess the arch bridge was used during the Second World War. Pippard ignored the possibility of the formation of the third hinge and analysed the arch as a two-hinged arch. The arch assumed for analysis was parabolic, loaded with a point load  $W$  at the crown and the analysis was confined to the case where the rise at the quarter span was 0.75 times the rise at the half span. Pippard's actual and idealized arch are presented in Figure 2-3 A-B. For the loading shown in the figure the value of the live load thrust  $H_L$  and the corresponding value of bending moment at the crown  $M_L$  are given by:

$$H_l = \frac{25}{128} \left( \frac{Wl}{a} \right) \quad 2-1$$

And

$$M_l = -\frac{7}{128} Wl \quad 2-2$$

Where the negative sign indicates that the thrust line lies above the arch rib (Page 1993). The numerical values resulting from the above equations must be added to the corresponding values for the self weight. A further strain energy analysis then gives values of the dead load thrust and bending moment at the crown as

$$H_D = \frac{\gamma^2 h}{a} \left( \frac{a}{21} + \frac{h+d}{4} \right) \quad 2-3$$

$$M_D = \frac{\gamma L^2 ah}{168} \quad 2-4$$

The combined effect of the dead load and a point live load at the crown of the arch are given by:

$$H = \frac{l}{a} \left[ \gamma h l \left( \frac{a}{21} + \frac{h+d}{4} \right) + \frac{25}{128} W \right] \quad 2-5$$

And

$$M_c = \frac{1}{4} l \left( \frac{lah}{42} \gamma - \frac{7}{32} W \right) \quad 2-6$$

Pippard used the moment equation to derive the rules of assessment. As larger and larger values of W are imposed at the crown of the bridge, the second part of the equation increases and develop tensile stresses. Pippard argued (Page 1993) that a less restrictive criterion might be based on the middle-half rule, in which the limiting value of W would be given by solution of

$$\frac{M_c}{H} = -\frac{d}{4} \quad 2-7$$

Which leads to

$$W_1 = \frac{32\gamma h[2a^2 + 4ad + 21d(h+d)]}{21(28a - 25d)} \quad 2-8$$

Similarly based on the maximum compressive stress criteria for arch ring having a depth  $d$  and effective width of  $2h$

$$f = \frac{H}{2dh} - \frac{3M_c}{hd^2} \quad 2-9$$

Substituting the values of  $H$  and  $M$  gives

$$W_2 = \frac{\frac{256fhd}{l} + 128\gamma h\left(\frac{a}{28d} - \frac{1}{21} - \frac{h+d}{4a}\right)}{\left(\frac{25}{a} + \frac{42}{d}\right)} \quad 2-10$$

Pippard took a range of numerical examples and the full scale tests results undertaken by Building Research Station and he verified the use of equation 2-10. For arches the cover  $h$  is generally less than 0.6m so the effective width is less than 1.2m and the safe axle load  $W_A$  for vehicle of normal arch width may be taken as

$$W_A = 2 W_2 \quad 2-11$$

Pippard constructed tables for single span parabolic arches with a span to rise ratio of 4, with a unit weight of arch ring of  $21.6\text{kN/m}^3$  and the limiting compressive stress of  $1.4\text{N/mm}^2$ .

Equation 2-11 was then modified by the Military Engineering Experimental Establishment (MEXE) in the form a nomogram and is currently recommended by the Department of Transport (Department of Transport 1997a). In the current method the load carrying capacity of the arch is assessed without the effect of the spandrel and wing walls, backfill, abutment condition etc. and then the effect of these elements is added to the

assessed load by using modifying factors. The provisional axle load can be calculated based on geometric data by using the following formula (or nomogram).

$$W_A = \frac{740(d+h)^2}{L^{1.3}} \quad 2-12$$

The geometric data required is:

The span  $L$ (m); the thickness  $d$ (m) of the arch barrel at the crown and the depth  $h$ (m) of fill including the pavement at the crown. This formula can be used for bridges with spans between 1.5m up to 18.0m, (it may be too conservative for spans bigger than 12.0m), and 0.25m to 1.8m for  $d+h$ .

The provisional axle load ( $W_A$ ) is then modified by the following factors (Department of Transport 1997a):

**Span:** rise factor; deep arches are stronger than flats one so it considers  $F_{sr} = 1$  for an arch with span: rise of 4.0 or less, decreasing for span: rise ratios greater than 4.0.

**Profile factor  $F_p$ ;** takes into account arch shape. The ideal arch profile is parabolic and for this shape the rise at the quarter-point is given by  $r_q/r_c = 0.75$ . Any arch profile different of this is modified by this factor.

**Material factor  $F_m$ ;** this factor takes into account the type of backfill and arch ring materials.

**Joint factor  $F_j$ ;** this factor models the effect of joints (size and condition) and the quality of mortar.

**Condition factor  $F_{cm}$ ;** this factor is related to engineering judgement in assessing the arch condition. Zero is applicable to a bridge in poor condition with a lot of defects and 1.0 is chosen for an arch in good condition.

The modified axial load can then be calculated by applying these factors to the previously calculated  $W_A$ .

$$\text{Modified axle load} = F_{sr} F_p F_j F_{cm} W_A \quad 2-13$$

This method is simple and easy to use for assessment engineers but is now considered to be conservative, particularly for longer spans (Crisfield and Page 1990). The method also

relies on experienced judgement and may result in different arch capacities for a unique bridge assessed by different engineers. The method also has no information about stresses or deflections, and is not appropriate for use with repair techniques.

### 2.3.2 Plastic method

The usual assumptions in plastic methods are detailed in section 2.2.1. The method uses ideas of the geometrical properties of the arch and equilibrium, but makes no use of material properties. Pippard (Pippard and Ashby 1939; Pippard and Chitty 1942; Pippard et al. 1936) developed a tabulated mechanism method for the assessment of a single span standard arch of parabolic profile with a span/rise ratio of 4.0. According to Pippard the collapse load  $W$  (Figure 2-4) can be found by statics and is directly related to the weight of the three blocks and has contributions from both the arch ring and the associated fill. Pippard assumed that the hinge B occurred under the load position and D at the far springing. The positions of the other two hinges had to be obtained by trial and error using a tabular method of computation.

Pippard did not use the terminology plastic method directly in his mechanism analysis. Heyman (Heyman 1980; Heyman 1982) related his work to plasticity theory. According to Heyman's work "if a thrust line can be found, for the complete arch, which is in equilibrium with the external loading (including self weight), and which lies everywhere within the masonry of the arch ring, then the arch is safe". He developed an approximate approach, which enabled a quick assessment to be made for the strength of a given bridge. The method computes the load necessary to just transform an arch into a hinged mechanism. Figure 2-5 shows the dimensions of the arch assumed by Heyman. The road surface is assumed horizontal and the fill is assumed to have no strength and to transmit live load  $P$  to the arch ring without any dispersion. The same unit weight of  $\gamma$  is assumed for both the fill and ring. The calculations are normalised with respect to the rise at the crown ( $h_c$ ) so that the parameter  $\alpha = h_q/h_c$  gives the measure of the shape of the arch and  $\beta = h_0/h_c$  gives the measure of the depth of the bridge (fill depth + ring thickness) at the crown and  $\tau = t/h_c$  is a measure of the vertical thickness of the arch ring at the quarter-span. Writing the statical equations of equilibrium gives the value of live load that would just cause the arch to collapse (Heyman 1982).



$$p = 16 \frac{W_2 X_2 [\alpha + (1 - \frac{1}{4} k)\tau] - (W_1 X_1 + \frac{1}{4} W_2) [(1 - \alpha) - (1 + \frac{1}{4} k)\tau]}{(3 - 2\alpha) - (2 + k)\tau} \quad 2-14$$

A further approximation made in order to get equation 2-14 into a form suitable for general application, the weights of  $W_1$  and  $W_2$  are calculated from trapezium, in which the intrados of the bridge has been replaced by a straight line. By considering a unit width of the arch (Heyman 1982) equation 2-14 becomes

$$p = \frac{P}{\frac{1}{6} \gamma L h_c} = \frac{(1 + 3\beta - \alpha) [\alpha + (1 - \frac{1}{4} k)\tau] - (6 + 9\beta - 5\alpha) [(1 - \alpha) - (1 + \frac{1}{4} k)\tau]}{(3 - 2\alpha) - (2 + k)\tau} \quad 2-15$$

The constant  $k$  expressing the vertical thickness of the arch ring at the springing is taken as unity, so that equation 2-15 gives the intensity of the live load necessary to cause collapse, in terms of the  $\alpha$ ,  $\beta$  and  $\tau$ .

Both Heyman and Pippard ignored the effect of fill on load capacity, but later work showed that the fill can have a significant effect on the strength of an arch. Crisfield and Packham (Crisfield and Packham 1987) developed a computer program based on a mechanism method. They used the virtual work equation instead of the static equilibrium equation and had two options for distributing the load through the fill. The first procedure applied a uniform pressure over a horizontal line at the level of intersection with the arch directly under the load. The second had a linearly varying distribution between two points. They used the concept of passive resistance for considering the lateral earth pressure. Their study showed that this assumption of lateral earth pressure may overestimate the collapse load by as much as 25% in some cases, particularly for arches where the soil resistance is important. Harvey (Harvey 1988) used a mechanism method to developed a model, named ARCHIE which is easy to use and is widely used by engineers.

### 2.3.3 Finite element method

The first attempt at application of the FE method to masonry arches was carried out by Towler (Towler 1985; Towler and Sawko 1982) who compared their own numerical solution with experimental results on a series of brickwork model arches. In both works masonry and fill interaction was ignored. Crisfield (Crisfield 1985) showed that, in these circumstances, the FE should give lower collapse loads than the mechanism method. Hence, non-linear springs were used in FE models to simulate the lateral resistance of the backfill (Crisfield and Wills 1986).

Choo et al (Choo et al. 1991) used tapered beam elements in a 2-D model, and in addition to neglecting regions of tensile stress, limited the magnitude of the compressive stress. Horizontal fill elements were used to represent the passive resistance of the soil around the masonry arch. This model resulted in reasonable predictions of the response of full scale tests on masonry arch bridges.

Loo and Yang's procedure (Loo and Yang 1991a) incorporated several additional concepts into a 2-D model. The material cracking in the arch ring was examined in more detail than in previous models. A von Mises failure envelope was developed for 2-D stresses. Stress-strain curves for a variety of failure conditions were used to more accurately represent the state of stress in the arch ring during loading. Rather than distinguishing between individual properties the entire masonry/mortar assembly was used. The horizontal and vertical forces on the arch ring from the fill were found using a second FE model. This model replaces the arch/fill interface with a series of spring supports. The horizontal and vertical reactions found at these supports from the weight of the fill elements can then be applied to the standard FE model of the arch ring.

Boothby et al (Boothby et al. 1998) used ANSYS, a commercial FE package, for studying the service load response of masonry arch bridges. The masonry arch FE mesh used five element types to duplicate the behaviour of a system of discrete blocks under fill. Four-node isoparametric elements were used for the voussoirs, while gap and hinge elements provided the necessary mesh connectivity between blocks. Cable elements were used to simulate the resistance to arch movements provided by the fill. Spring elements were placed at the abutments to control the amount of abutment spread under load. Joints

between voussoirs in a masonry arch were able to transmit negligible tension and form hinges under eccentric thrust. This behaviour was modelled by a combination of gap and hinge elements at the intrados and the extrados. The gap elements transmit compression but not tension. The gap elements, however, do not allow rotation. This shortcoming was overcome by locating a hinge element immediately adjacent to each gap.

Ng et al (Ng et al. 1999) carried out FE analysis using a commercial FE package. Three full scale bridge collapse tests were modelled and the results compared with available field test data. Comparisons were also made with results obtained from other arch bridge assessment methods. Eight-noded quadrilateral elements were used to model the arch, backfill and extrados interface. The behaviour of backfill and interface elements was elasto-plastic with failure defined by a Mohr-Coulomb yield criterion. The arch was simulated by a stress-dependent von Mises constitutive law enabling different tensile and compressive strength material to be specified.

3-D nonlinear FE models of different masonry arch bridges was generated using a commercial FE package (ANSYS) by Boothby, Fanning and others (Boothby and Roberts 2001; Fanning and Boothby 2001b; Fanning et al. 2001). The behaviour of the masonry was replicated by use of a solid element that can have its stiffness modified by the development of cracks and crushing. The fill material was modelled as a Drucker-Prager material, and the interface between the masonry and the fill was characterised as a frictional contact surface. The bridges were modelled under service loads, and the model results compared to the results of a programme of field testing of the structures. It was found that the model of the structure, implemented through a program of the 3-D nonlinear FE analysis enabled good predictions to be made of the actual behaviour of a masonry arch bridge.

The features of a non-linear FE approach suitable for the progressive failure analysis of masonry arch bridges are summarised by Loo (Loo 1995; Loo and Yang 1991b). According to his study from various properties of materials, only the masonry tensile strength and the strain softening parameter  $N$  have a significant influence on the failure behaviour of the arch bridge. Based on the collapse load results of the five full scale bridges tested in Britain, a comparative study was carried out and the best values for these parameters was suggested for both brick and stone bridges. For the cracking and failure analysis of the arch rib, the masonry can be modelled as a strain softening material

and Loo proposed stress-strain relationships for the masonry. At a given point of masonry arch, when the state of stress reaches a certain value, he identified three possible modes of local failure:

- Cracking in both principal stress directions. This occurs when the state of stress is of the biaxial tension-tension type and both the tensile principal stresses are beyond the tensile–failure envelope. In this situation the material loses its tensile strength completely.
- Cracking in one direction occurs when the state of stress is of the tension-compression type and a principal stress exceeds the limiting value prescribed by the tensile–failure surface.
- Crushing occurs when the state of stress is biaxial compression-compression and the stress level is beyond the simplified von Mises failure surface.

According to the above assumptions a FE program was developed by Loo and calibrated, based on five full scale test results. From this calibrated study he was concluded that for a good estimate of the ultimate strength of a stone arch bridge, the masonry tensile strength shall assume a value of 1.6MPa and the strain softening parameter  $N=12$ . The recommended values of the tensile strength and the strain softening parameter for brickwork arches are 0.3MPa and 4 respectively. These values may be used in conjunction with the experimental values of  $E$  and  $\sigma_c$  for the stones or bricks, as appropriate. Since the collapse load computed using the proposed analysis is rather insensitive to  $E$  and  $\sigma_c$ , their estimated values may also be acceptable in the absence of experimental data.

## 2.4 Experimental work on arch bridges

The span, rise, width, arch shape including distortions, arch thickness, depth of fill, arch material including defects, fill material including surface, quality of mortar, thickness of spandrel and wing walls, degree of bond between arch and spandrel walls, strength and stiffness of foundations, and applied load including its position, form and distribution through the fill and surfacing all affect the capacity of an arch. So there is no possibility that experimental works can include all of these parameters and so the test programme has to focus on some of these variations. Literature reviews have shown a lot of experimental work on determining the effect of one or more of these parameters on the

load capacity and assessment of arch bridges. Some of these experiments were carried out on real arches (most of them redundant bridges), some on full scale models, built in a controlled condition in labs, and some carried out on small scale models. An overview of experimental work which has been undertaken in the UK and the influence it has had on our understanding of the behaviour of masonry arch bridge is presented by Melbourne (Melbourne 2001). In following sections, a brief review on experimental works on arch bridges is presented.

#### **2.4.1 Load test on full scale bridges**

The use of load testing to understand the behaviour and assessment of arch bridges is well known. A comprehensive review of load tests on arch bridges was presented by Page (Page 1993). He identified 13 tests on full scale bridges and 77 load tests on model scale bridges. Davey (Davey 1953) at the Building Research Station in Britain carried out a series of 21 serviceability and failure load tests on real arch bridges. In his failure tests he observed the significant effect of backfill on bridge load capacity. For instance he observed for one test the collapse load was 2.5 times higher in the presence of the fill than in its absence. Chettoe and Henderson (Chettoe and Henderson 1957) carried out elastic tests on 13 real bridges in Britain. The maximum applied load was limited to 90 tonnes to avoid any damage. All bridges were in a good condition. The load deflection measurement was elastic, and they concluded that the behaviour of bridges were elastic under the test conditions. The results of these tests showed that the assumption of 45° dispersal of load through the fill down to the level of the arch intrados provide a reasonable approximation to the values estimated from the tests.

In recent years, some tests have been carried out under the direction of the TRL to examine the validity of the MEXE method for the assessment of arch bridge capacity. Eight of these are the TRL tests on redundant bridges (Hendry 1986; Hendry et al. 1985), Page (Page 1987; Page 1988; Page 1989), two laboratory full scale tests (Harvey et al. 1989; Melbourne and Walker 1990) and three of them from the earlier tests that were carried out before the Second World War (Davey 1953). The results of these tests have shown that non-linear behaviour was observed from the very start of loading but in all cases the load at which the first visible sign of damage occurred was recorded which is different for each bridge when compared to the failure load. In some cases this point was near to the failure load (Crisfield and Page 1990).

The problem with the full scale tests (especially on redundant bridges) is that the properties of the components are not well known. Masonry properties (brick, concrete block, stone and mortar) fill materials and the exact geometry of arch may not be available. Also understanding the effect of interaction between the soil and masonry in these tests is impossible. Any attempt to install gauges would have caused a significant disturbance to the fill and changed the initial condition of the bridges. To avoid this problem two full scale model were carried out under the TRL contracts. The first one was a semi-circular arch with a 4.0m span that was built of bricks at the laboratory in University of Dundee (Harvey et al. 1989; Smith 1991; Smith and Harvey 1989). The thickness of barrel was 0.25m and the depth of fill over crown was 0.2m. The soil pressures were measured using 48 pressure cells on the extrados of arch barrel. The results of this test showed that linearity of the output from the cells with respect to the applied load was remarkable. The second arch was a flat arch with a 6m span, 1.0m rise and two ring of brickwork built as a part of the TRL programme in Bolton (Melbourne and Walker 1990). Loading was applied at the quarter span across the full width of the bridge. Test results showed that the arch failed due to the formation of a four-hinge mechanism and the spandrel walls provided a significant restraint to the arch barrel. Ring separation observed at the quarter point under a load of about 30% of the failure load and no ring separation was recorded at the unloaded quarter point until after reaching the maximum load. Fill pressure was recorded by 34 pressure cells. The result showed the backfill did provide a significant lateral resistance to the arch however no passive pressure was recorded. The pressure cells beneath the load increased indicating angles of up to  $45^{\circ}$ , but this depend upon the fill condition at the load stage considered; at fill failure the pressure became more concentrated (Melbourne 1990a). The load deflection response was initially linear until hinging of the barrel.

Fairfield and Ponniah (Fairfield and Ponniah 1994a; Fairfield and Ponniah 1994b) focused on the soil/structure interaction effect, load dispersal angle and lateral soil pressure in arch bridges. They worked with the TRL to install pressure gauges at Kimbolton Bridge during the building period and monitored the pressure in the fill during the building period and after. The arch is a single 8.0m span, 2.0m rise brick arch. The arch was built in four rings with a 440.0mm thickness. Two different types of pressure sensors were used, one to measure the vertical pressure within the soil fill and the second to monitor the interaction between the barrel and soil.

### 2.4.2 Load test on model scale bridges

The literature review has shown that there is a wide range of laboratory tests on scale model arches. A variety of arch spans, span to rise ratios, single or multi ring arches, single or multi spans, square or skew arches with different materials have been tested. A review of these tests has been reported elsewhere (Page 1993). Short reviews of these tests are repeated here. Many models were built without spandrels or wing walls. The results of these tests have been used to calibrate numerical models, but some models were tested as 3-D tests with spandrel walls to understand the behaviour of different parts of an arch under load.

The first significant research work in this area was carried out under the supervision of Professor Pippard (Pippard and Ashby 1939; Pippard and Chitty 1941). A series of segmental model arches were built using steel voussoirs. Hanging equivalent weights at the centre of each voussoir simulated the dead load of the fill. He concluded that a voussoir arch behaves elastically within a limiting load and then fail by a four hinged mechanism. In the second series of Pippard's tests 26 arches with the same geometry, but using mass concrete voussoirs, were built. The results showed that the arches failed in the similar manner by a four hinge mechanism. From these tests Pippard concluded that it was reasonable to analyse an arch as a linear elastic material.

Royles and Hendry (Royles and Hendry 1991) carried out a series of tests on 24 model arch bridges with spans of 1.0m, 2.1m and 2.5m. The object of these tests was to examine the general behaviour of these structures, which had span to rise ratios between 2.0 and 6.4, and in particular to establish the effect on the strength of the arch of the fill and wing-wall masonry. The models were built from masonry materials with sand or gravel fill. The dimensions of the models were selected based on three actual bridges, Bridgemill, Bargower and a bridge across the Carron River in the Highland Region. Each bridge vault was built three times and tested with fill material, the fill material plus the spandrel masonry, the fill material and the spandrel masonry plus the wing walls. One-third scale clay bricks were used for both the vault and the spandrels for Bridgemill. Concrete bricks and 1/3<sup>th</sup> scale clay bricks were used to model the Carron river bridge and finally the Bargower model was built with concrete bricks. The fill material in the models was from sand to 20.0mm crushed stone. The abutments of all models were rigid. Test results showed a significant effect of the components of the bridges on their load capacity. In the Bridgemill models the vault only showed 50% of complete model failure

load, the vaults and fill test showed 59% and the model with spandrel, the unrestrained wall showed 77% of the capacity of the restrained model. For the Carron River arch bridge model, vault, vault plus fill, vault plus fill and unrestrained spandrel, showed 24%, 28% and 41% of the failure capacity of complete arch model (with fill, spandrel and wing walls), respectively. The results of tests on the Bargower arch models also showed the significant effect of the components on the load carrying capacity. The results of all these tests are presented on Table 2-1. The load deflection from these tests showed the non linearity of arches under load, but they might be assumed linear up to about  $1/3^{\text{rd}}$  of the maximum load. Models constructed with different strength bricks failed virtually at the same load, therefore the strength of the material used for the construction of the arch was not critical. The main conclusion from these tests was the significant effect of the spandrel, wing wall and fills. The extent of this effect is greatest in arches with a high ratio of rise to span i.e. in arches approaching a semicircular profile. In this case, the failure load of the complete structure was about twelve times that of the vault only.

Significant research work has been carried out at the Bolton Institute by Melbourne et al (Melbourne et al. 1995; Melbourne and Gilbert 1995; Melbourne and Walker 1988). These tests include of small scale and full scale models. In full scale models he focused on the single and also multi span arch (Melbourne and Wagstaff 1993), the effect of defects, multi ring and skewed arch bridges. Tests results indicated the effect of different components on arch load capacity. In the case of testing arches with defects the results showed a decrease of about 30%-65% due to full ring separation. The pressure measurements during the tests indicated a dispersal angle of up to  $45^{\circ}$  in some cases.

Fairfield and Ponniah (Fairfield and Ponniah 1994a) carried out a series of tests on arch spans of 700mm constructed in timber with 25 voussoirs and a span to rise ratio of 4.0. Polythene film was used to minimise the friction between the fill and sidewall. The fill was medium, uniformly graded dry silica sand with rounded particles. In all 88 tests were carried out, of which 3 were use to establish the end wall boundary condition and 4 on the semicircular arch to determine the regions of fill displacement. Three tests on semicircular arches were carried out with various fill densities. Finally 60 tests were carried out as part of a parametric study of both semicircular and span to rise ratio of 4 arches. Some of the above tests were undertaken twice to check the repeatability of the tests. The results showed a distance of about 33% of the arch span from the springing to



end walls was sufficient. Collapse loads increased 13% for a 3% density increase. They also concluded that the collapse load increased with increasing fill depth. This was caused by, increased load dispersal and dead load. This increased dead loading increases the magnitude of the live load needed to cause collapse and increases the vertical stresses causing increased lateral pressures which prevent arch movement into the fill on the side of arch remote from the load. Generally they concluded that soil/structure interaction contributed significantly to the capacity of the model arches.

## **2.5 Centrifuge Modelling**

### **2.5.1 Principles of centrifuge modelling**

Scale models are used widely in engineering related works. For example mechanical engineers study aircraft and vehicles using wind tunnel modelling and hydraulic engineers use scale models to study the flow in open channel problems related to coastal engineering and many other various studies related to hydraulic engineering. Scale modelling is used most often when the theoretical solutions contain major simplifications and approximations or when numerical solutions are very lengthy, as is often the case in geotechnical engineering. Normally a model and the prototype will be geometrically similar so that all the linear dimensions in a model will be scaled equally, but in some situations, it is impossible to construct a model that behaves exactly the same as the prototype in all aspects. Instead, the model should have similarity with the prototype in the aspects of behaviour under test. For example in river engineering the relationships between water depth and velocities (Froud number) should be the same. Similarity between the model and prototype might be determined by using dimensional analysis. The basic principle is that any particular phenomenon can be described by a dimensionless group made up of the fundamental variables. Models are said to be the similar when the dimensionless group has the same value and then the particular phenomenon will be correctly scaled.

In constructing a geotechnical model the object might be to study collapse, ground movement, loads on buried structures, consolidation or some other phenomenon during the construction or loading sequence. Consequently, the stresses in the model and prototype should be the same at the same corresponding points. The basic scaling law in centrifuge model derives from this point. The scaling laws can be obtained from

dimensional analysis. These laws, shown in Table 2-2 indicate that for a 1/N scale model to replicate its prototype, the density( $\rho$ ) of the material used in the model must be N times bigger than that of the prototype material(Cheney and Fragaszy 1984). In Figure 2-5 the vertical stress on a point in prototype and the corresponding location in the centrifuge model are presented. In the prototype the vertical stress can be determined by:

$$\sigma_p = \rho g h_p \quad 2-16$$

Where

$\rho$  is the density of soil in prototype

$g$  is the gravity acceleration ( $9.81\text{m/s}^2$ )

The stress at the corresponding point in the model can be represented by:

$$\sigma_m = N\rho_m g h_m \quad 2-17$$

Where

$\rho_m$  is the density of soil in model

$h_m = h_p / N$  is the height of the point in the model.

Therefore if the same material is used in the model and prototype the stress at the corresponding point in the model and prototype will be the same and the scale factor (model: prototype) for linear dimensions is 1:N. This enhanced gravity can be achieved by placing the model in a centrifuge and rotating it with an angular velocity of  $\omega$ . When the model rotates with angular velocity of  $\omega$  any point located at distance  $r$  from rotation axis include the centrifugal acceleration.

$$A = r\omega^2 = Ng \quad 2-18$$

Where

$\omega$  is the angular velocity

$r$  is the radius of point and

$N$  is scale factor

Therefore with a known scale factor and the point which exactly needed to be under Ng, the angular velocity can be easily determined.

### 2.5.2 Masonry arch centrifuge modelling

The first attempt at employing a centrifuge model for studying masonry arch bridges masonry was carried out by Taunton (Taunton 1997) at Cardiff University. He tried to assess the viability of modelling soil/brickwork structure interaction problems, at small scale, using a centrifuge. A series of tests that simulated the behaviour of a 3.0m span brickwork arch bridge, at 1/6<sup>th</sup> full scale, at an elevated gravity equivalent to 6g were carried out. The results showed that not only are the overall mechanisms of failure correctly modelled but that the influence of both brickwork and soil strength can be properly investigated (Hughes et al. 1998). Small scale bricks were sawn from full size bricks to the required model dimension and two different mortar mixes of 1:3:12 and 1:2:9 (cement:lime:sand) were used to measure the arch deflections. A local graded limestone was sieved to remove all particles greater than 6mm to provide the model-scale backfill material. The load was provided by a gearbox through a 20kN load cell. The load was applied to the whole width of the arch from the top surface of the backfill and a range of high-resolution linear variable displacement transducers (LVDTs), with full scale deflections of 2-10mm, were used. These were positioned radially, distributed throughout the intrados, measuring movements normal to the barrel. Taunton's study showed that small scale modelling of brickwork arch bridges under increased gravity produces consistent results and replicates all the features of full scale behaviour.

A series of 1/55<sup>th</sup> scale models of William Edwards 43.0m span bridge at Pontypridd was tested in a centrifuge by Sicilia (Sicilia 2001). Different models of the structure were tested, in which the main structural elements i.e. arch, backfill and spandrel/parapet walls, were added one by one. Test results indicated the effect of the backfill and spandrel walls on the arch load capacity. The results were then compared with a 3-D FE model (Sicilia et al. 2001).

A series of 1/12<sup>th</sup> scale model 2-D arches, with a full size span of 6.0m, were built and tested for two principal arch shapes, shallow arches with span to rise ratio of 4.0 and semicircular deep arches, were carried out by Burroughs. He tried to determine the effect

of the parameters that influence the strength of masonry arches bridges using a number of similar tests, six for shallow arches, and four for deep arch geometries (Burroughs 2002). Each arch model was tested under service rolling load first and then up to knife edge failure load. The results obtained were compared to the parametric tests results. The parametric study demonstrated that in general, masonry arches have an inherent strength dependent on their geometry, which is then modified by changing various structural parameters. A three fold increase in backfill depth above the crown was shown to double the arch strength, and header bricks were shown to increase the arch strength by 30% and to prevent ring separation. Some understanding of soil/masonry interaction was developed (Burroughs et al. 2000; Burroughs et al. 2002). The tests results showed a more significant effect of backfill in the deep arch behaviour.

Small scale centrifuge models were also used to identify the effect of applying different repair techniques on masonry arch bridges by Baralos (Baralos 2002). The application of stitching bars, longitudinal steel, extrados concrete and sprayed concrete were investigated as means of restoring the load capacity of under strength and damaged arch structures. Results indicated that the application of repair techniques reduces arch barrel deflections and can delay the formation of traditional failure mechanisms associated with arch bridges. It was shown that the increase in the stiffness and ultimate load capacity of the models correspond with those seen in large scale tests. In previous tests studying the effects of defects on masonry arches it was necessary to induce damage such as ring separation in the models by artificial means such as the inclusion of damp sand between the rings of the arch barrel (Melbourne and Gilbert 1993). The arch models were tested in two stage by Baralos, first loaded up to observe the first sign of failure and then, on the repaired arch model, up to full failure. By using this method the suitable model for repair was provided from the first stage of the tests.

## **2.6 Defects and repair of masonry arch bridges**

In the UK there are about 40,000 masonry arch bridges in daily use in highways, railways and canals. Most of them are an over 100 years and some are over 500 years old. The traffic they are required to carry both in terms of weight and numbers has increased considerably since they were built. It is important that they continue to perform their function because it would be neither practicable nor desirable to replace them. It is

estimated that as many as 350 bridges, representing 1% the UK highway arch bridge stock will require some form of maintenance to be carried out on them every year (Sumon and Ricketts 1995). The costs are enormous so it is important that the cause of deterioration in the structure is clearly understood and the most effective method of repair employed. There are many factors that can cause defects on arch bridges and can influence the choice of repair techniques. In the following section reference is made to the defect problems of arch bridges and some experimental work undertaken in this area.

### 2.6.1 Common defects affecting masonry arch bridges

There are several very common structural defects, which affect masonry arch bridges. Sunley (Sunley 1990) listed them in four categories:

- Construction e.g. results from poor design and workmanship.
- Long-term loading e.g. from ground movement or foundation weakness.
- Transient loading e.g. resulting from traffic loading etc.
- Environment loading e.g. resulting from weathering.

Page (Page 1993; Page 1996) listed the different categories for the most common defects in arch bridges. These included defects in foundations, piers and abutments, arch ring, spandrel walls, wing walls, parapets, fill and road surfacing. The first defect may include settlements and scour. Piers and abutments will be affected by settlement of the foundation, particularly if it is not uniform. This case needs to be identified, particularly if it is active. It may be due to geotechnical factors, material deterioration, or flooding. Scour of foundation is probably the most common cause of collapse of arch bridges. Their foundations are often shallow and susceptible to scour. It has been found from laboratory experiments and field studies that in the main local scour holes develop in the horseshoe vortex region (Page 1993). Arch ring defects include splitting from the spandrel walls, movement of abutments and ring separation. Flexing of the arch ring due to traffic loads will produce shear stresses in the ring where the relatively flexible part, with only fill above it, is stiffened by the spandrel wall, and these stresses may result in cracking. None of the present standard assessment methods take into account the stiffening of spandrel walls. It is however safe to ignore their potential contribution. The effect of abutment movement on arch ring is depended on movement direction. The effect of arch ring defects on load capacity may be assessed when using the MEXE assessment method by using the recommendation condition factors by BA 16/97 (Department of

Transport 1997a) or for more recent methods by basing calculations on the distorted arch shape and by building into the model any pre-existing cracks.

Ring separation is a common problem with multi-ring brick arches and may be due to chemical deterioration of the mortar or may be load included. In order to study ring separation on arch capacity some arches were built with and without ring separation and were tested (Gilbert 1993). Spandrel walls are frequently affected by dead and live load laterals forces from backfill or vehicle impact on the parapet or suffer from weathering changes. The effect may be outward rotation, sliding on the arch ring, or bulging. Wing walls suffer from similar problems to spandrel walls and also from shallow or inadequate foundations.

### **2.6.2 Tests on arch bridges with defect**

In his first attempt to understand the behaviour of arches with defect in them, Melbourne carried out a series of 22 arch model tests. These tests divided in to six different groups and each group had a different geometry. The arches were built with and without spandrel walls, with and without ring bond and with different fills. In addition two skewed and two arch rings (without backfill) were tested in this programme. Tests results indicated that the load capacities of those arches that were built with a mortar joint was about twice of those without ring bond (Melbourne 1990b).

In the next attempt a series of 6 full scale arch bridges were built at Bolton Institute. Two of these bridges had 5.0m spans and four had 3.0m spans. All the bridges had segmental arch barrels with span to rise ratios of 4.0, built with engineering bricks and 1:2:9 (cement:lime:sand) mortar. To understand the effect of different defects some of these arches were built with defect such as, detached spandrel, ring separation, and spandrel detached and ring separation. A knife-edge load was applied at a quarter of the span and each arch was loading up to failure. The test results showed significant decreases in arch load capacity caused by the defects. The 5.0m span bridge with the defect of ring separation carried only 29% of the load carried by the bridge with bonded rings. For the bridges with a 3.0m span built with attached spandrel walls, the bridges with the defect of ring separation carried only 53% of the bridge with the fully bonded ring, whilst of the 3m span bridges built with detached spandrel walls, the bridge with the defect of ring separation carried only 67% of that without ring separation (Melbourne and Gilbert 1993).

One of the usual defects in old arches is spandrel walls detached from the arch barrels. This may cause bulging or tilting of the spandrel walls. The usual solution to prevent movement of arch spandrel is to tie them together. To understand the effect of this repair two 5.0m span arch were built at Bolton Institute with detached spandrel walls. The spandrel walls were then tied together using tie bars. The test result showed that the tie bars had a negligible impact on the stiffness of the bridge under serviceability and higher loads (Melbourne et al. 1995).

### **2.6.3 Test on repaired arch bridge**

To examine the effect of different repair methods on arch load capacity, 5 full scale arch bridge were tested at the TRL (Sumon 1998). The objective of these tests was to examine experimentally the increase in capacity of the arch ring provided by a variety of repair strengthening methods and to use the experimental results to develop a design process for repair and strengthening schemes. To decrease the unknown parameters they were built without spandrel walls. The mortar used had cement: lime: sand ratio of 1:3:12. The arch bridges had 5.0m spans, 2.0m wide and had three brick rings. One arch was tested without any strengthening up to full failure. A 150mm layer of sprayed concrete was applied to the soffit for 28 days before testing the second arch. The same concrete layer was applied to the extrados of the third arch as a second strengthening method. To determine the elastic behaviour of the arch, a series of single 50kN point load was applied to the fill at different positions and the maximum displacement of each arch was recorded. The knife edge load was applied at the full width of the arch at a quarter of the span. The results showed the lowest displacement was in the arch built with sprayed concrete because of the additional stiffening effect. The result from the failure load test showed sprayed concrete increased the strength of the arch 3.7 times compared to the unstrengthened arch whilst the saddle concrete increased the strength by the factor of 2.9. In an elastic test before failure, the maximum displacements of the crown was also reduced considerably.

Two arches were built with ring separation. A layer of wet sand was substituted for mortar between the rings to simulate the effect of ring-separation. The arch was tested to failure then reprofiled and strengthened using Masonry Arch Repair Strengthening (MARS) and tested again. The second arch was strengthened using the Archtec System developed and installed by Cintec International Ltd in partnership with Giffords &

Partners and Rockfield Software. The strengthened arches were tested under knife loading at quarter span. The results showed an increase in load bearing capacity of 38% and 105% respectively compare with an identical unstrengthened arch.

Choo carried out an experimental and numerical investigation on a number of arch bridges at Nottingham University (Choo et al. 1995). Arch models were built with 2.5m spans, span to rise ratios of 4 and ring thickness of 225mm. The test results showed that a 75mm thick layer of concrete, giving a 33% increase in barrel thickness (applied to the inside of arch) increased the collapse load on average by 1.9 times the pre-repair strength. The FE study indicated that depending on the bond condition up to double the load carrying capacity may be expected. The MEXE method suggests the load carrying capacity may increase by 1.4 times. This is significantly more conservative than the results obtained from either the numerical or the experimental results. Comparisons between the two studies at the TRL and Nottingham University show a good correlation in the results.

## **2.7 Repair and strengthening techniques**

Many repair techniques are available for the strengthening of arch bridges. Some of them such as saddling, stitching, repointing and spraying concrete on to the soffit have been used for many years (Melbourne 1991) and some newer ones such as retro-reinforcement have been developed recently. In the case of deterioration it is very important to choose the most effective repair technique. There are a varieties of factors that affect the choice of repair method. Table 2-3 identifies the common faults of arch bridges and the repair and strengthening methods, which may be applied (Page 1996). Garrity (Garrity 2001) listed many parameters for selecting the most appropriate form of strengthening for masonry arch bridge which are in a wide range of structural conditions, cost of the repair method, road accessibility during repair and arch appearance after repair. According the above referenced parameters the most effective strengthening method can be selected from the various methods. Some of the usual repair methods are briefly described in the following sections.

### **2.7.1 Saddling**

Saddling involves removal of the fill and casting an in-situ concrete arch, which may be reinforced, on top of the existing arch. The construction of a saddle can reduce the load



on the arch by improving its distribution throughout the entire structure, and it may carry all of live load or part of the load applied to the structure. The minimum saddle thickness worth considering is about 150mm and it may be necessary to support the arch with centring during the repair works. The reason for arch deterioration must be understood very clearly before choosing saddling. If deterioration is caused by movements of the abutments the additions of the saddle may increase the movement of the abutments and make the problem worse. The survey that was carried out (Ashurst 1992) has shown that saddling is an effective method for strengthening arch bridges.

### **2.7.2 Sprayed concrete**

Sprayed concrete is a mixture of cement, aggregate, water and admixture, projected at a high velocity from a nozzle into place against an existing structure, where it is compacted by its own velocity to form a dense homogeneous mass. It was first used in the early 1900s, and has been used widely for many new and old construction and repair application, including the repair and strengthening of masonry structures (Long 1990). There are many methods for placing concrete on the arch. In the dry method the mixed cement and aggregate are carried by the high velocity air stream to the special nozzle where the operator adds the water required for hydration and workability. In the wet method the cement, aggregate and water are mixed and then are carried by high velocity air stream and are projected into place. There is also the composite process, whereby the cement, aggregate and water are mixed to a suitable consistency, and introduced into a high velocity air stream, which transports them to the discharge nozzle and project them into place.

### **2.7.3 Repointing**

Mortar is a vital constituent of masonry construction and it too may vary in strength and durability. Old lime mortar, particularly, loses its cementitious nature with time and reverts to a sand filled joint; this may be washed out, so destroying the integrity of the structure (Ayres 1990). The repair or replacement of the exposed face of the mortar between masonry units is commonly known as repointing but its value has been largely indeterminate although some work by Burroughs (Burroughs 2002) recently looked at this issue.

#### 2.7.4 Retro-reinforcement of masonry

Retro-reinforcement is a method of reinforcing existing masonry structures. This method first introduced by Dr. Lizzi to strengthen masonry structures damaged during the Second World War. Even though masonry is very brittle and therefore susceptible to cracking, it is often cited as being a very forgiving material, particularly when referring to masonry structures constructed with lime mortar. These structures often have considerable reserves of strength above those predicted using conventional methods of analysis. One type of retro-reinforcement was developed at the University of Bradford from a technique originally devised for the repair and strengthening of masonry buildings (Garrity 1995a; Garrity 1995b; Garrity 2001). It consists of grouting stainless steel reinforcing bars into pre drilled holes or pre-sawn grooves in the exposed near surface zones of the masonry where tensile stresses arising from external loads or settlement effects and are likely to result in cracking. The most appropriate repair and strengthening method for masonry structures of this type therefore appears to be one that improves the tensile strength of the structure and its resistance to cracking without causing a significant change in the fundamental structure behaviour. Recent experiences has shown that installing stainless steel reinforcing bar in the surface zone of existing masonry is an effective and economical means of repairing and strengthening low-rise masonry bridges (Garrity 1995a). In order to identify the effect of retro-reinforcement a series of un-reinforced and reinforced 2m spans clay brick model arches were tested at University of Bradford. Retro reinforcement in the tests was simulated by using thin strips of steel glued to the surface of the brickwork with an epoxy adhesive. The test results showed that reinforcement installed on the intrados strengthened and stiffened the arch by delaying the formation of hinges normally initiated by cracking in an un-reinforced arch. Using surface reinforcement to connect the spandrels and parapets and connect them to the arch ring produced a considerable increase in the strength and stiffness (Garrity 1995a). Near surface reinforcement can only be effective as a strengthening measure if it acts compositely with the existing masonry. To ensure this, the shear connection between the masonry and the grout and the grout and reinforcement must be maximised otherwise premature bond failure at the grout masonry interface or the grout/reinforcement interface may occur. Clearly the selection of a grout material that is compatible with the existing masonry and likely conditions on site is of considerable importance (Garrity 2001).

There is some published research on the analysis of masonry arches with surface or near surface reinforcement. Most research has focused on the development of plastic methods of analysis to predict the collapse load of reinforced arches. Falconer has presented a mechanism analysis (Falconer 1997). The capacity of the arch was estimated from consideration of moment and force equilibrium of the arch barrel at an assumed 4 hinge collapse mechanism with the moment capacity of one of the hinges enhanced by the presence of the intrados reinforcement. A numerical method has been developed to predict the in-service performance of a reinforced arch as well as the collapse load (Chen et al. 2001) and a preliminary investigation of a typical single span masonry arch has been carried out using a 2 stage 3-D FE analysis (Garrity and Toropova 2001).

Tests carried out on a small scale centrifuge single arch by Baralos showed that applying a series of longitudinal steel bars at the intrados of arch barrel can increase the load capacity by 1.05 times compare with an unrepaired arch. While the test on the same arch geometry which was strengthened with longitudinal and transverse steel indicates a 50% increase in arch stiffness no significant increase in arch load capacity was observed compared with the unstrengthened arch (Baralos 2002).

### **2.7.5 Archtec (Cintec Anchor)**

Cintec International Limited with Giffords and Partners and Rockfield Software have developed a system for strengthening masonry arch bridges called Archtec. The system consists of stainless steel reinforcing bars that are inserted and grouted into place within the barrel of the arch. The use of stainless steel and high performance grout ensures that there will be enhanced durability. The bars and grout are contained within a sock which protects the surrounding masonry from being displaced or otherwise damaged by the grouting pressure of 3 to 4 bars (Brookes and Tilly 1999). During inflation, the sock deforms and permits sufficient leakage of grout to develop chemical and mechanical bonding with the masonry resulting in a structural connection. The reinforcement is positioned in the arch barrel in a longitudinal direction and tangential to the curvature. Depending on the connection of the structure, reinforcement may also be positioned in the barrel in a transverse direction. The numbers and precise location of the bars are determined by numerical analysis using ELFEN, a non-linear discrete element program (Brookes and Tilly 1999).

### **2.7.6 MARS (Masonry Arch Repair and Strengthening System)**

The masonry arch repair and strengthening system (MARS) consists of a network of ribbed stainless steel bars that are installed and bonded into the soffit of the arch. The system has been tested at the TRL with a comparison between two full scale arches models were constructed in TRL, one repaired using the MARS system, showing that significant increases can be achieved from this repair method. The repaired arch failure load was increased 38% compared to the identical arch with ring separation (Sumon 1999).

Model	Load at first crack	Load at Failure (kN)	Mean (kN)	Ratio to full bridge =100	Condition
Bridgemill 1	-	4.05	3.9	100	With spandrels restrained
2	1.5	3.75			With spandrels restrained
3	1.0	3.1		77	Spandrel unrestrained
4		2.5	2.3	59	No spandrel with fill
5	2.25	2.3			No spandrel with fill
6		2.15			No spandrel with fill
7	1.25	2	1.95	50	Vault only
8		1.9			Vault only
Carron 1		12	13.5	100	With spandrel+wing walls
2	8	15			With spandrel+wing walls
3	3.5	5.5		41	Spandrel unrestrained
4	2.5	3.5	3.75	28	No spandrel with fill
5		4			No spandrel with fill
6		2.6	3.3	24	Vault only
7	1	4			Vault only
Bargower 1	68	90		100	With spandrel+wing walls
2	56	88		98	With spandrel+wing walls
3		65		72	Spandrel unrestrained
4		32.5	37	41	No spandrel with fill
5		41.5			No spandrel with fill
6	4.5	5.25	7	8	Vault only
7	4	8.75			Vault only
8	32	50			Spandrel with only half width loaded
9		80		89	Spandrels unrestrained rubble masonry

**Table 2-1: Model test results (Royles and Hendry 1991)**

Property	Scale
Linear dimension	$1/N$
Area	$1/N^2$
Volume	$1/N^3$
Force	$1/N^2$
Stress	1
Strain	1
Density	N

**Table 2-2: Centrifuge scaling law (Cheney and Fragaszy 1984)**

Fault	Repair/Strengthening
Deteriorated pointing	Repoint
Deterioration of arch ring material	Masonry Repair Saddle Sprayed concrete to soffit Prefabricated linear soffit Grout arch ring
Arch ring thickness assessed to be inadequate to carry required traffic loads	Saddle Sprayed concrete Prefabricated linear to soffit Replace fill with concrete Steel beam relieving arches Relieving slab
Internal deterioration of mortar (Ring separation in multi ring brick arches)	Grout arch ring Stitch
Foundation movement	Mini piles Grout piers and abutments Underpin
Outward movement of spandrel walls	Tie bars Spreader beams Replace fill with concrete Take down and rebuild Grout fill if it is suitable
Separation of arch ring beneath spandrel walls from rest of arch ring	Stitch

**Table 2-3: Fault, repair and strengthening on arch bridges (Page 1993)**

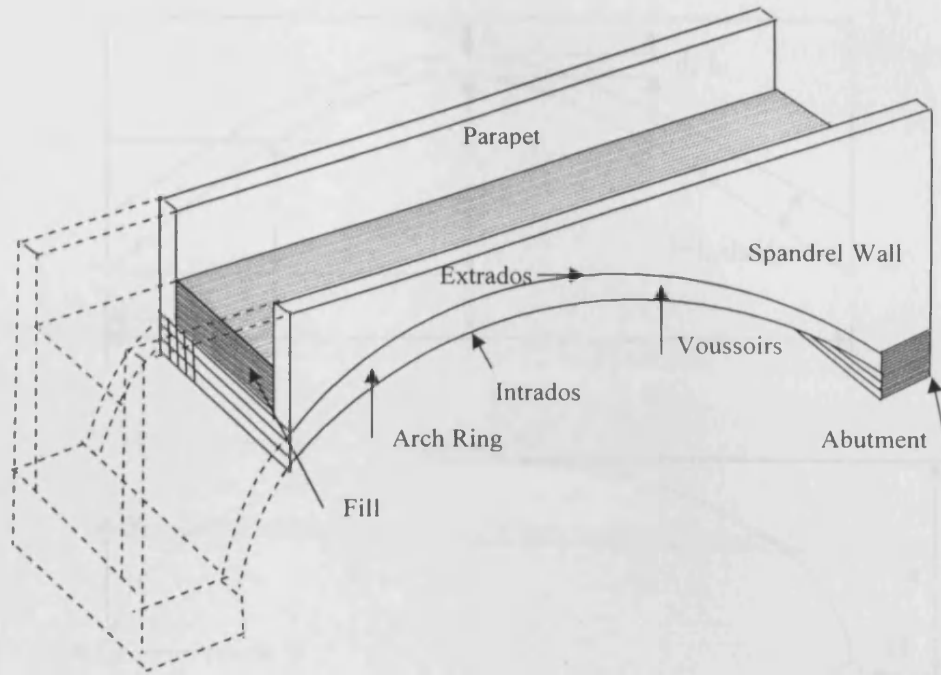


Figure 2-1: Typical masonry arch bridge

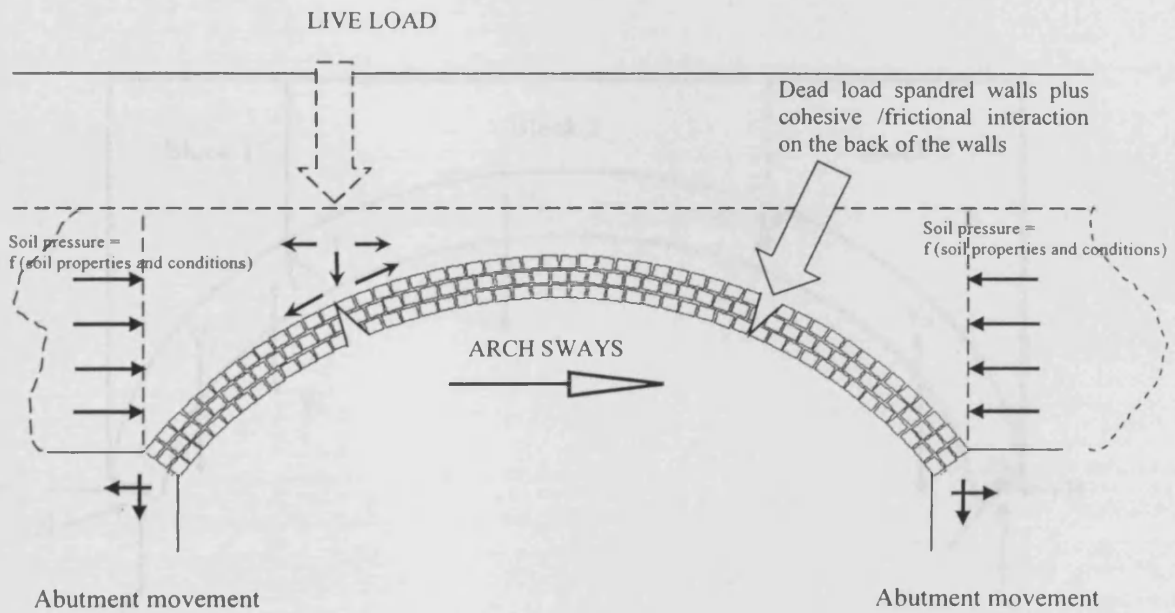


Figure 2-2: Response of arch bridge to applied load



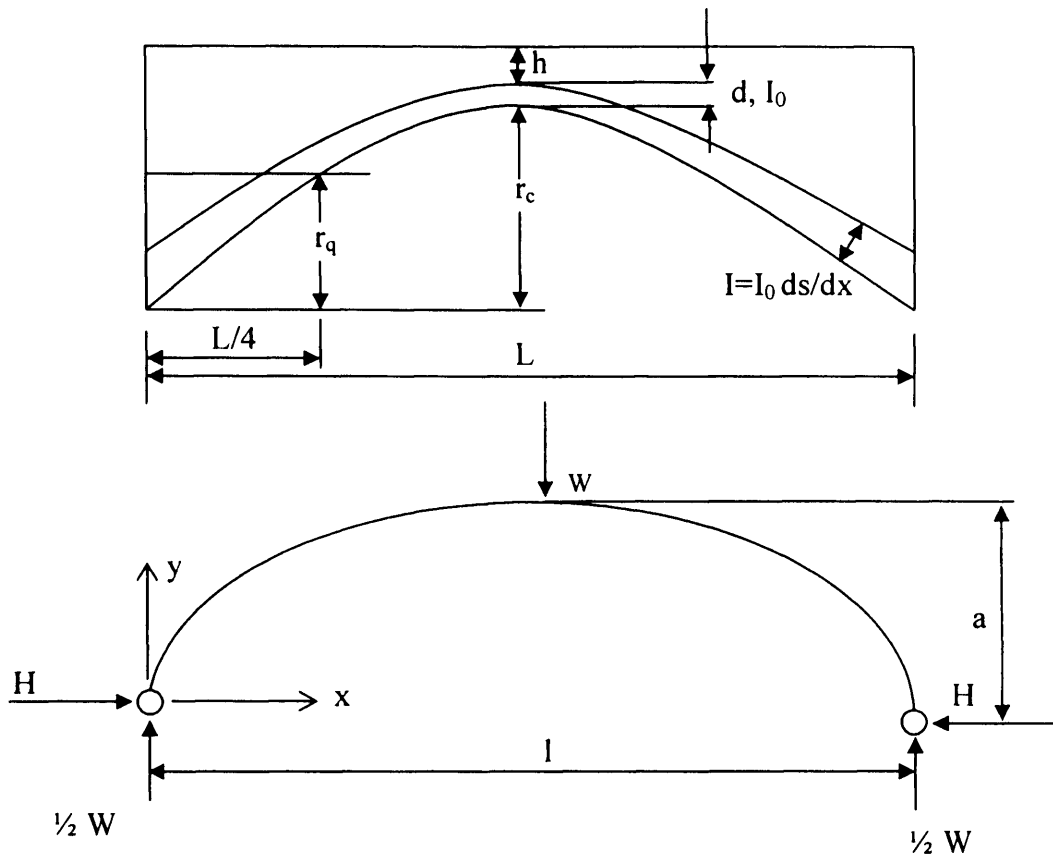


Figure 2-3: Pippard's real and analytical arch model

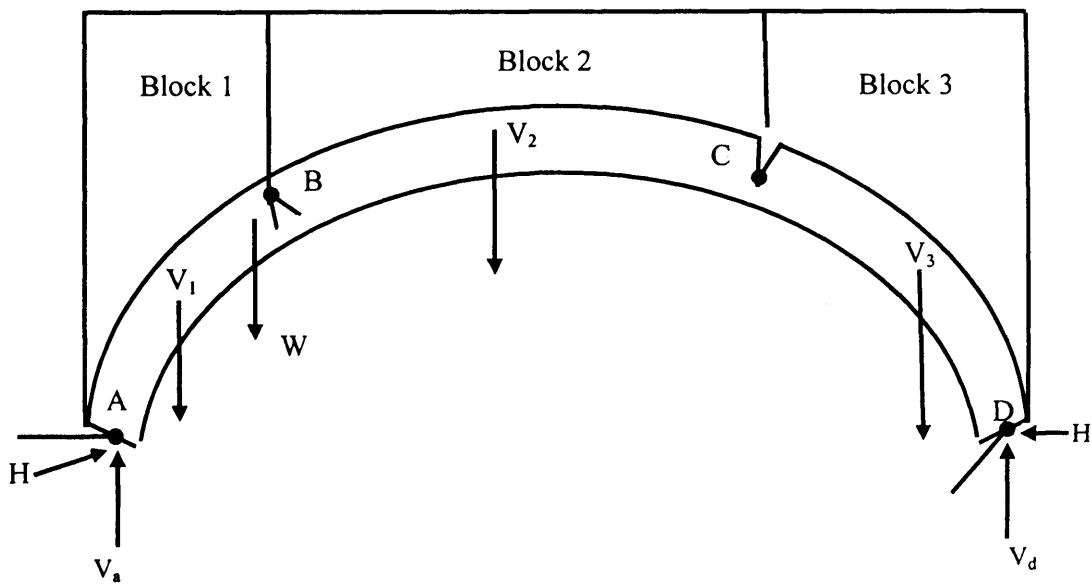


Figure 2-4: Mechanism with equilibrating forces (Page 1993)

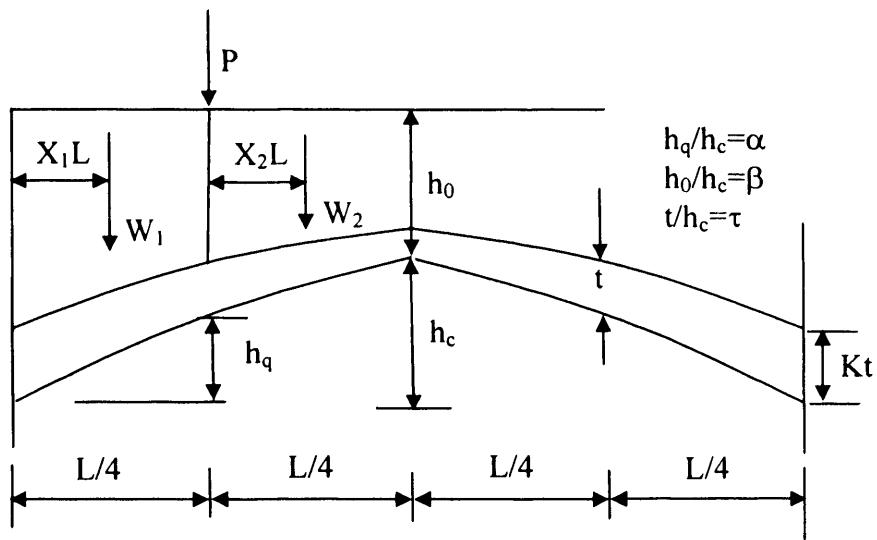


Figure 2-5: Heyman's arch model

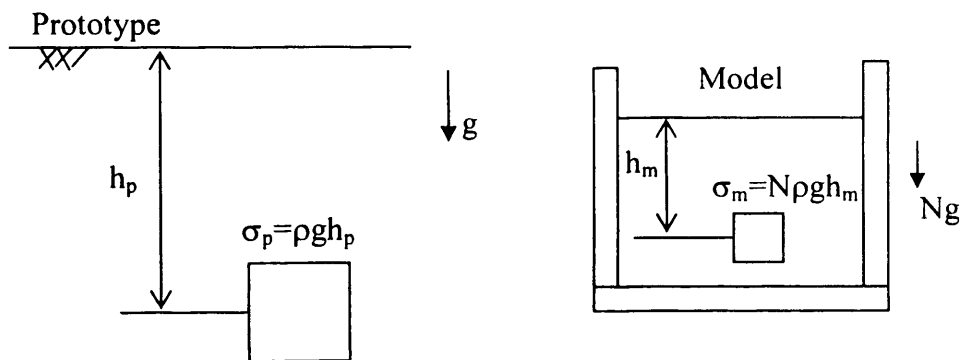


Figure 2-6: Centrifuge scale model

## **3 Material Properties**

### **3.1 Introduction**

A comprehensive series of material tests were carried out to determine the properties of the different materials used in the centrifuge arch models. The objective of these tests was to determine the required input data for the numerical models. The appropriate testing standards were used with small sizes of materials to represent the behaviour of the materials in small scale models. In some cases the differences between the results from small scale and standard size tests are shown during the test programme. All the tests were carried out in normal gravity condition since testing within the centrifuge was impractical. These types of tests were previously successfully used to determine the properties of arch bridge centrifuge models (Sicilia 2001). Because some similar materials were previously used in centrifuge model tests on arch bridges some of the material properties determined from that work are used directly in other parts of this thesis. In this chapter details of the materials tests, the results obtained and discussion of the results are presented.

### **3.2 Mortar tests**

Mortar is one of the main elements which is used in making masonry arch bridges. Therefore it was decided to undertake tests on the mortar to determine its characteristics. The tests were carried out using standard procedures, but in some cases the standards were adapted to better present the real behaviour of mortar in this work. Table 3-1 shows

all the tests were that performed on the mortars with the standard number and specimen dimensions.

There is no specific recommendations for the curing process of lime mortar in the standards therefore samples in all tests were de-moulded after 3 days, due to the slow hardening process of lime mortar and then submerged in water tanks at 20°C until the test time. Because there was some delay on the centrifuge tests, to determine the effect of age on strength of mortar some of tests were performed on 28 and 56 days specimens. The compressive test, the flexural test and the stress strain test were carried out on mortar to determine its characteristics. The tests procedures and results with some discussion are presented in the next sections.

### 3.2.1 Compressive tests

The compressive strength of mortar was determined using compression tests on different sample sizes, age and different curing conditions. Tests were carried out in accordance with the appropriate British Standards. Six 25mm mortar cubes and three 100mm cubes were used to determine the compressive strength of the mortar. Different mortar specimens were tested to determine the size effect on the compressive strength of the mortar. As a result of using thin layers of mortar in the arch model, mortar tests were carried out on small specimen as it seemed more representative of the behaviour of model mortar joints.

To determine the effect of specimen's age on compressive strength tests were under taken at 28 and 56 days. These two ages were selected because the benchmark models were tested normally at 28 days and some repaired tests about 56 days after the arch barrel construction.

### 3.2.2 Specimens and procedures

A typical compression test arrangement and specimen are presented in Plate 3-1. The compressive strength of mortar was determined according to the guidelines of British Standard (BS 4551-1 1998). The British Standard advise 70.7mm and 100mm cubes are used for determining the compressive strength, but these samples seem too large when compared with the 1.5mm thickness of the mortar which is used to join the bricks

together in 1/12<sup>th</sup> scale models. Therefore the compression tests were also carried out on 25mm sample cubes. This type of sample size has recently been used at Cardiff University (Baralos 2002; Sicilia 2001). Mortar was filled and compacted in the mould using the vibrating table. The British Standard suggests applying a uniform load rate in the range of 0.03N/mm<sup>2</sup> per sec. to 0.1N/mm<sup>2</sup> per sec. but a lower loading rate is permitted for weaker mortar. In this case according to the size of the samples and the mortar type the load was applied with a rate of 0.2mm/min until failure occurred. The loads were applied with the same rate on both of sample sizes to obtain comparable results.

### 3.2.3 Tests results and discussion

Tests results on 25mm cubes at different ages detailed in Table 3-2. The mean compressive strength value of 1.7N/mm<sup>2</sup> was obtained from 28 days tests on 25mm cubes, which is significantly larger than the average value of 0.9N/mm<sup>2</sup> achieved from 100mm cubes of the same age. This suggests that in larger size cubes the core of the mortar has hardened less than the mortar on the face. Baralos (Baralos 2002) reported 1.1N/mm<sup>2</sup> and 0.8N/mm<sup>2</sup> as a mean compressive strength on 28 days of 25mm and 100mm cubes respectively for the same mortar mixture. The difference between the results may be due to the differences in the compaction and the curing method. Hendry recommends using values between 0.5N/mm<sup>2</sup> and 1.0N/mm<sup>2</sup> for numerical analysis of lime mortar on old bridges (Hendry 1990). Although these values are recommended for numerical models they are representative of the expected values in old masonry structures and those which required repair. Consistence between the recommended values and the tested values confirms the correct selection of mortar type for the centrifuge models.

The average compressive strengths obtained from tests on the same sample size at different ages have shown little effect of sample age on the compressive strengths of mortar. While the average compressive values of 1.7N/mm<sup>2</sup> was obtained from 28 days tests, the average strengths values of 1.9N/mm<sup>2</sup> was achieved from 56 days tests. This shows an increase of 4% for the 56 days tests. Similar results were reported by Sicilia (Sicilia 2001) from tests on lime mortar with a 1:3 lime: sand mixture and water: lime ratio of 1.2. However as a result of the slow hardening process the effect of the

specimen's age on the compressive strength of the mortar is accepted, the results from the current study on different age specimens (at period of centrifuge tests) shows a negligible age effect on the compressive strength. Because of the small difference between these two tests results the effect of age on the compressive strength of the mortar was neglected later on in this work with the 28 days tests results being used in the numerical models.

The bulk density of hardened mortar was determined using immersion in water. An average value of  $18.0\text{kN/m}^3$  was obtained from four bulk density tests. An average value of  $19.3\text{kN/m}^3$  was reported by Baralos (Baralos 2002) for similar mortar which is consistent with the current results.

### **3.2.4 Flexural tests**

#### **3.2.4.1 Specimens and procedures**

The arrangement for the mortar flexural tests is given in Figure 3-1 and Plate 3-1. The flexural test determines the tensile strength indirectly using a three or four point bending beam and the tests carried out following the British Standards procedure (BS 4551-1 1998). Six  $25\times 25\times 100\text{mm}$  specimens were cast from the same mix using standard moulds. Following the procedure for the compression tests the moulds were filled in two stages and the mortar was compacted using the vibration table. The specimens were de-moulded after three days and immersed in  $20^\circ\text{C}$  water tanks until the time of the test.

The specimens were supported on two 10mm rods at a distance of 75mm between the axes of the roller during the tests and the load was applied by another roller rod midway between the specimen's supports. All three rollers were in direct contact with the cast face of the samples. The maximum applied load in each test was recorded and the modulus of rupture was determined using the standard equation. It is necessary to consider that the modulus of rupture determined corresponds with the maximum tension at mid span at the failure load, while tensile cracking would start before the final failure load but for the purpose of the numerical work in this study the above data seems reasonable.

Some researchers have determined the tensile strength of mortar using the procedure suggested in the RILEM Standard for concrete tests (RILEM 1994). This can be done on cylindrical samples with 100mm diameter and 200mm long, but Sicilia (Sicilia 2001) has shown that these large specimens are not sufficient to determine the tensile strength of lime mortar. Therefore in this work the tensile strength of mortar was determined using the flexural test following the above referenced British Standard.

#### 3.2.4.2 Results and discussion

The results of the flexural tests on mortar are detailed in Table 3-3. The average values of  $0.76\text{N/mm}^2$  and  $0.92\text{N/mm}^2$  were obtained for the 28 and 56 days samples respectively which show a 20% increasing for the older specimens. Sicilia (Sicilia 2001) reported 0.62, 0.65, 0.71 and  $0.68\text{N/mm}^2$  for the samples at 28, 56, 108 and 231 days old on his similar mortar mix. However more effect of mortar age was obtained compared with the Sicilia but the results are acceptable and comparable with his results. In this case no more tests results on the same mortar were found in the literature.

#### 3.2.5 Stress strain

A series of tests carried out to determine the stress strain relationship and Poisson's ratio of mortar following the relevant standards. Tests procedures, the results obtained and their discussion are presented in the next sections. Test arrangement and equipments are presented in Plate 3-1.

##### 3.2.5.1 Specimens and procedures

The stress strain relationship and Poisson's ratio of the mortar were determined following the procedure described in the British Standard for concrete (BS 1881-121 1983) as there was no specific standard found for mortar. The tests were carried out using three  $75\times 75\times 255\text{mm}$  specimens. Vertical and horizontal movements of samples were measured using LVDTs which were attached to the surface of specimens using aluminium holders and plastic padding. Four LVDTs (Two in the vertical and two in the horizontal direction) were used to measure the sample movement in both directions. The load was applied at a rate of  $0.02\text{kN/s}$  up to 33% of the estimated failure load; the applied load was then reduced to zero and then was raised up to 66% of the expected failure load and decreased

again. To avoid any damage to the LVDTs they were removed at this stage and the specimens were loaded up to failure at rate of 0.05kN/s.

### 3.2.5.2 Results and discussion

The average modulus of elasticity and Poisson's ratio of 2,900N/mm<sup>2</sup> and 0.090 respectively were obtained from the tests on mortar. These were achieved from a best fit line between 5% and 35% of the failure load from the second loading branch. Sicilia was reported 1,900N/mm<sup>2</sup> and 0.064 for modulus of elasticity and Poisson's ratio respectively for similar lime mortar using the same size of specimens (Sicilia 2001).

### 3.2.6 Mortar tests results, discussion and conclusions

The main mechanical parameters of the mortar were tested and determined during the current study following British Standards procedures. As a result of the thin layer in the mortar joint in masonry models, compression and flexural tests were carried out on small sample sizes but the modulus of elasticity and Poisson's ratio were determined using the standard sample size for concrete. Reported tests results on prototypes and 1/6<sup>th</sup> scale models of mortar in compression showed no significant effect of modelling scale on mortar properties (Mohammed and Hughes 2005). Tests results carried out indicated that the compressive strength of the 100mm mortar cube was about 4% more than that of the 25mm mortar cube. This is in agreement with the results obtained in the current study. The tensile strength was measured using flexural tests. The results of the mortar tests are summarised in Table 3-4. There are limited results using lime mortar in the literature review, but the results obtained had a good agreement with those found. The results are in a range of suggested values for the lime mortar (Hendry 1990) and also those suggested or used in numerical masonry arch models (Fanning and Boothby 2001b; Fanning et al. 2001).

## 3.3 Brick tests

To obtain the same in-situ stress in the centrifuge models and the prototype it is necessary to use the same materials for the model as for the prototype but at small scale. Accordingly the size of the model bricks will be very small. Some previous researcher



tried to manufacture model bricks using the same procedure that were manufacture in the prototype (Egermann et al. 1991) but the model bricks which were made by this process had no equivalent strength to those used in the prototype. This was because the small scale models were better fired in the manufacturing process and hence were stronger than the prototype. In addition in the manufacturing procedure the small bricks were distorted. For this reason in previous research using centrifuge arch bridge models, bricks were sawn from full size bricks and have been used successfully (Baralos 2002). Following that procedure and to have comparable results it was decided to employ the same method to make the small scale bricks in this work. To determine the bricks properties some tests were undertaken using relevant standards on the full and the small scale bricks. These include the bulk density of the bricks, determination of compressive strength, modulus of elasticity and Poisson's ratio of the bricks which are presented in the following sections.

### 3.3.1 Bulk density and compression tests

To allow calculation of the bulk density of bricks 10 air dried full size samples were measured and weighed and the average bulk density was determined. No specific standard was found to measure the bulk density of bricks. The average value of  $22.1\text{kN/m}^3$  was obtained for the bricks which has good agreement with the  $21.8\text{kN/m}^3$  was reported elsewhere for similar bricks (Burroughs 2002). The bricks dimensions were measured following the procedure described in the British Standard (BS 3921 1985). Twenty-four bricks were selected in accordance with the standard from the batch of bricks and the dimensions were measured.

The compressive strength of the bricks was determined following the procedures of BS 3921. A typical brick specimen under tests is shown in Plate 3-2. The bricks were immersed in water 24 hours before each test and tested immediately after removing from the water. The load was applied according to the standard procedure and the failure load was recorded. To ensure a uniform bearing in each specimen the specimens were placed between plywood sheets to take up irregularities. A compressive strength value of  $96.4\text{N/mm}^2$  was obtained from the tests which is about 1% is greater than the  $95.0\text{N/mm}^2$  which was reported by Burroughs (Burroughs 2002) for the similar bricks.

Baker tests results have shown the effect of specimen's size on compression tests (Baker 1996). He reported about a 10% decrease in the compression strength in 65×65×65mm cubes compared with tests on whole bricks but he reported no significant effect of packing on the compressive strength. Compressive tests on prototype and 1/6<sup>th</sup> scale model of bricks indicate a 60% increase in compressive strengths values of model compare with the prototype values (Mohammed and Hughes 2005).

A report published by the British Railway Research at Derby (Temple and Kennedy 1989) has shown that the bricks found in railway structures range in compressive strength from 10N/mm<sup>2</sup> to 100N/mm<sup>2</sup>. This indicates that the bricks used in this research are in a high range of compressive strength and therefore no increase as a result of scale effect added to the obtained compressive strength value and 96.0N/mm<sup>2</sup> was used as a compressive strength of a unit in later parts of this thesis.

### 3.3.2 Stress strain and Poisson's ratio tests

The 65×65×215mm specimens were used to determinate the stress strain relationship for the bricks. These specimens were sawn from full size bricks and had been used successfully to determine the modulus of elasticity and Poisson's ratio for bricks elsewhere (Baker 1996). The movements were measured using four LVDTs glued to each side of the specimens in both horizontal and vertical directions. The mortar test procedure (Sec.3.2.3) was followed for these tests and the loads were applied to the specimens using two 8mm fibre board. The load was applied to about 33% of the expected failure load with rate of 0.5kN/s and then unloaded to zero with rate of 1.0kN/s, then the load was raised up to 66% of the expected failure load and decreased to zero again with the same rates. The LVDTs were removed in this stage and the specimens were loaded up to failure.

The results are given in Table 3-5. The average values of 30,100N/mm<sup>2</sup> and 0.14 were obtained from the above tests for modulus of elasticity and Poisson's ratio. As with the mortar tests the modulus of elasticity was calculated using a best fit line between 5% and 35% of the failure load in the second branch loading.

### 3.3.3 Bricks test results and discussions

The specimens' condition before and after test are presented in Plate 3-3. The test results and their related specimens are summarised in Table 3-6. Generally the results have shown good agreement with previous results reported for similar materials.

### 3.4 Backfill tests

The backfill material has a significant effect on the arches' strength (Taunton 1997) and therefore selection of a suitable material is very important. For a centrifuge model the bulk density of the model backfill and prototype backfill should be the same. When the scale of model is determined the grading curve of the fill can be determined. In this study there is no identified prototype so there is no limitation on the backfill material selection, but for comparable results with previous work on centrifuge modelling it was decided to use similar materials. The backfill material used was a granular limestone. The material is a 1/6<sup>th</sup> scale of a typical Type 2 road base material. The overall scale of the arch model in this study is 1/12<sup>th</sup>, but this grade size is acceptable because the plan scale of bricks is 1/6<sup>th</sup>. An earlier study showed some differences in repairs because two types of backfill material were used (Baralos 2002). To prevent any change in the material properties during the current study it was decided to purchase sufficient material for all the tests at one time. To determine the backfill property some samples were selected at different times during the study and tested. As a result of the same material and the same supplier generally the same properties were expected but some variation was accepted.

The tests were carried out in accordance with the relevant British Standards (BS1377 1990) to determine the backfill material properties. These included dry sieving, compaction and standard shear box tests. The tests carried out are detailed in Table 3-7. The test procedures and results are detailed and discussed in the next sections.

#### 3.4.1 Particle size distribution and compaction tests

The particle size distribution of the soil was determined using the dry sieving method following the test procedure in British Standard (BS 1377-2 1990) and the results are presented in Figure 3-2. Values of 25.0 and 2.0 are obtained for coefficient of uniformity

and coefficient of curvature respectively and these show that the backfill can be considered a well graded soil.

The compaction tests were conducted on the backfill with various moisture contents using British Standard (BS 1377-4 1990) procedure to determine the maximum bulk density and the corresponding optimum moisture content. The result of compaction tests are presented in Figure 3-3. From this figure the maximum bulk density of  $22.0\text{kN/m}^3$  was obtained at an optimum moisture content of 7.5%. Burroughs (Burroughs 2002) reported  $22.0\text{kN/m}^3$  as a bulk density for similar materials and an optimum moisture content of 9% while the result was obtained by Baralos (Baralos 2002) indicated value of  $23.0\text{kN/m}^3$  at a moisture of content of 8%. As seen the values obtained in the current study have a good agreement with previously reported values. To obtain the optimum moisture content during the tests the backfill material was compacted with a moisture content of about 8% (0.5% bigger than the obtained value) during preparation models.

#### 3.4.2 Shear test

The engineering properties of the fill materials were determined by a series of standard direct shear tests. The tests were conducted following the procedure in British Standard (BS 1377-7 1990). Samples were prepared at about 8% moisture content. The  $100\times 100\text{mm}$  standard shear box was used to determine the angle of friction and cohesion constant under 10, 20, 40 and 60kPa normal stress. Test results are presented in Figure 3-4. From this figure the angle of friction of  $53.0^\circ$  and the cohesion constant of 16.8kPa was obtained for the backfill materials. Values of  $50.0^\circ$  and 10.8kPa were obtained from shear tests on similar materials by Barolos (Baralos 2002). He also reported the values of  $50^\circ$  and 13.6kPa of a series of 70mm drained triaxial tests on similar backfill materials. The triaxial tests on similar materials with the same specimen's size and following the same procedure by Burroughs has shown values of  $47.0^\circ$  and 0.0kPa as an angle of friction and cohesion constant (Burroughs 2002). The results obtained from the shear tests in the current study are similar to the previous values reported from both the shear and the triaxial tests. The other materials properties, specifically Poisson's ratio and modulus of

elasticity, were obtained from the test carried out in the previous works (Baralos 2002; Burroughs 2002) are accepted as suitable for the current material.

### 3.4.3 Backfill tests results and discussion

Backfill materials properties have been obtained from a series of tests carried out following the British Standard procedures. Particle size distribution, compaction test and direct shear box tests have been undertaken in this study and the results were compared with other reported properties for similar materials. As a result of the good consistency between the results obtained in the current study with those reported elsewhere for similar materials no more tests were carried out on the backfill and the other properties obtained from those references were used in the numerical models. The tests results and additional assumed values for backfill materials are presented in Table 3-8.

### 3.5 Micro concrete tests

Micro concrete was used for some of the repair model tests in this study. Concrete usually is a mix of coarse aggregate, sand, cement and water with the relative amounts according to the type and the strength requirement. Models of 1/12<sup>th</sup> were selected for the current study therefore 1/12<sup>th</sup> scale size of concrete with the same material properties as the prototype is needed for this study. No specific code exists to design concrete at small scale. Therefore it was decided to make the small scale size concrete following a previously successful procedure (Baralos 2002). Coarse aggregate was modelled by 2mm aggregate (1/12<sup>th</sup> scale of 25mm aggregate usually used in the prototype). To obtain this, first the 10mm aggregate limestone was crushed using a commercial stone crusher and then the result materials was sieved and the aggregate less than 2mm and bigger than 1.18mm was collected. From 100kg of crushed materials about 10kg of 2mm aggregate was obtained. Chelford 95 silica sand and OPC were used as the fine aggregate and the cement in the micro concrete mixture.

The literature review has shown that there is no specific code to determine the engineering properties of micro concrete, therefore the relevant standards for mortar and concrete were used to determine the micro concrete properties. The tests on the micro concrete and their related standards are detailed in Table 3-9. Compression tests were

carried out on a series of 25.0mm and 70.7mm cubic specimens at 28 and 56 days age samples. Flexural test were undertaken on standard 25×25×100mm moulds for the testing of mortar specimens again at 28 and 56 days. Because some of centrifuge tests were carried out on a model of more than 28 days, 56 days test was carried out to determine the effect the age of models on their strength. Finally the stress strain relationship was determined by testing the 75×75×255mm specimens. The bulk densities of the specimens were determined using the immersion in water method. The tests procedure and results are presented in the next sections.

### 3.5.1 Micro concrete compression tests

The British Standard allows the determination of the compressive strength of concrete by tests on 100mm and 150mm cubes. The nominal maximum size of the aggregate is limited to 20mm for 100mm cubes and 40mm for 150mm cubes. These are seen as very large compared with the size of aggregate and thickness of micro concrete slabs which were used in the centrifuge models. Therefore 25mm cubes were used to determine the compression strength of the micro concrete. These types of specimens were used successfully at Cardiff University to obtain the characteristic of a similar concrete (Baralos 2002). As a comparison and determine the size effect and age of specimens tests were undertaken using 70.7mm standard concrete specimens at 28 and 56 days. Tests were carried out following the procedure of the British Standard (BS 1881-116 1983). Six 25.0mm and three 70.7mm cube specimens were cast from the same batch of micro concrete and tested at the same age. The moulds were filled in two stages and compacted using a vibrating table. The specimens were cured for 24 hours under a plastic sheet to protect their moisture content and then submerged at 20°C in a water tank until the test date.

The load was applied to the samples at a rate of 0.2mm/min until failure. The maximum applied load and types of failure were recorded during each test. The bulk density of the micro concrete was determined using the submerged water method.

### 3.5.2 Test results and discussion

A compression strength average value of 51.3N/mm<sup>2</sup> was obtained at 28 days for the 25mm cubes. The average result from the same batch of concrete at the same age and

curing method for the 70.7mm cubes was  $46.3\text{N/mm}^2$ . Compared to the mortar compression results this shows less effect of the specimen's size effect. Specimen details and test results are presented in Table 3-10. Baralos (Baralos 2002) reported compression values of  $33.8\text{N/mm}^2$  for a similar mixture of micro concrete on 25mm cube which is about 34% weaker than these results. There is no specific reason for this significant difference between the results but it may be due to the different compaction of the concrete in the moulds and curing methods.

### 3.5.3 Flexural tests

Flexural tests on the micro concrete were carried out following the guidelines laid out by RILEM Standard CPC5 (RILEM 1994) on  $25\times 25\times 100\text{mm}$  specimens at 28 days. The specimens were placed on supports with a distance of 75mm between them. The load was applied at the centre of beam at a rate of 0.2mm/min. The test results and details are presented in Table 3-11. The maximum load was recorded and the flexural strength of concrete or the modulus of rupture was determined. An average value of  $7.53\text{N/mm}^2$  was obtained for the micro concrete modulus of rupture which is in a good agreement with the  $7.04\text{N/mm}^2$  reported by Baralos (Baralos 2002) for similar materials using the same specimen size and test procedure.

## 3.6 Masonry tests

The properties of masonry were obtained from a series of tests on masonry assemblies. Triplets and walls were tested under uniaxial compression to obtain elastic and failure characteristic and couplets were used to determine the tensile strength of the masonry bed joint. Samples were built using the same unit which was used to building the arch barrel and spandrel walls in models. Construction and curing conditions followed exactly those on the bridge models. All tests were carried out 28 days after construction. Test procedure and obtained results are detailed in the next sections.

### 3.6.1 Uniaxial compression tests

A series of tests on masonry under uniaxial compression were performed to determine the compressive strength and stress strain properties of masonry. The tests specimens are

shown in Figure 3-5 to 3-6. The tests were undertaken according to the RILEM Standard LUMB1 (RILEM 1994). Two series of triplet and wallette specimens were tested to determine the masonry properties. The triplet specimens were used to determine the modulus of elasticity and compressive strength of the masonry and the wallette specimens were used to measure the Poisson ratio. Due to the small size of the specimens, vertical movements were measured between the top and bottom loading plate in the triplet specimens. To avoid inaccuracies on the reading the samples were built with the two loading plates bonded with mortar joints. A triplet specimen is shown in Plate 3-4 before the test. The load was applied through the loading plate and the vertical movements were recorded using two LVDTs which were installed between the two loading plates. These types of samples have successfully been used at Cardiff University previously (Sicilia 2001; Taunton 1997). The vertical and horizontal movements in the wallette were measured using small masonry clip gauges which were used previously for small scale masonry specimens (Baker 1996; Hughes and Kitching 2000). The gauges and their locations are shown in Figure 3-6 and Plate 3-5.

Test results are presented in Table 3-12. As can be seen from this table, the average values of  $44.4\text{N/mm}^2$  and  $41.5\text{N/mm}^2$  were obtained for the compressive strength from the triplet and wallette specimens respectively. This indicates that the triplets were on average 7% stronger than the wallettes specimens. It appears that the head joints had very little effect on the behaviour of masonry. In terms of the stress strain behaviour the results show that the wallettes were about 13% stiffer than the triplets. Average values of  $4400\text{N/mm}^2$  and  $5050\text{N/mm}^2$  were obtained as a modulus of elasticity for the triplets and the wallettes respectively. In a previous study, in which wallettes (3×5) and triplets were tested, Baker (Baker 1996) found the triplets to be stronger but more flexible than wallettes which is confirmed by the current results. No related values were found in the literature for the same materials but the reported results by Sicilia (Sicilia 2001) indicated the compressive strength and modulus of elasticity of  $31.0\text{N/mm}^2$  and  $4900\text{N/mm}^2$  and respectively for the triplet specimens with the same mortar and the stone unit with the same compressive unit of the current study. The current results are consistent with those reported by Sicilia.



### 3.6.2 Bond tensile strength

The bond tensile strength of masonry was determined following the bond wrench test procedure in the RILEM Standard LUMB3 (RILEM 1994). The tests were performed in couplets as shown in Figure 3-7 using a loading rig which was specially designed for the tests and has previously been used successfully (Sicilia 2001). The test is performed in stroke control at the rate of 0.2mm/sec.

An average tensile bond strength of  $0.27\text{N/mm}^2$  was obtained from the above tests. Results of previous research on masonry brickwork gave an average of  $0.50\text{N/mm}^2$  for brick masonry (Ng 1999) and  $0.17\text{N/mm}^2$  for stone masonry (Sicilia 2001).

### 3.7 Materials tests conclusions

A comprehensive test programme was undertaken in the current study to determine the properties of the materials which were used in the small scale centrifuge models. Relevant British Standards procedures were followed in most cases and where no specific British Standards were found RILEM Standard (RILEM 1994) procedures was used. Compression, flexural, stress-strain relationships and Poisson's ratio tests were conducted using different sizes of specimens at different ages of mortar. Tests results from these tests have indicated a significant effect of the specimen's size but little important effect of age on mortar tests. As a result of the small scale models and the very thin mortar joint used in making arch models the small size test results are preferred and used in the numerical models.

Tests on bricks were undertaken on full size and small scale specimens in the current study. Comparison of the test results with test results reported elsewhere have shown good agreement. Masonry tests were carried out on three brick prisms and five course walls which were built using the spandrel wall centrifuge model bricks. In Table 3-13 the current tests results are compared with the results which were found in the literature review. However the reported test results do not belong to exactly the same materials and same test procedure but all are presented in one table to show a better general idea about the material properties. Brief descriptions about the types of materials under test are presented below the table.



Test	Specimens (mm)	Relative Standard
Compressive strength	100×100×100	BS 4551-1
Compressive strength	25×25×25	BS 4551-1 (adapted)
Flexural strength	25×25×100	BS 4551-1
Stress strain and Poisson ratio	75×75×255	BS 1881-121

**Table 3-1: Mortar tests, specimens and related standards**

Cube No.	Length (mm)	Width (mm)	Age of specimen (day)	Load (N)	Compressive strength (N/mm <sup>2</sup> )
1	26.3	25.6	28	1178.8	1.8
2	25.8	25.7	28	1221.0	1.8
3	26.3	25.5	28	1068.4	1.6
Mean compressive strength (N/mm <sup>2</sup> )					1.7
4	25.5	26.5	56	1259.3	1.9
5	25.4	25.6	56	1243.5	1.9
6	25.5	25.4	56	1189.0	1.8
Mean compressive strength (N/mm <sup>2</sup> )					1.9

**Table 3-2: Engineering properties of mortar (compression strength)**

Sample No.	Height (mm)	Width (mm)	Age of sample (day)	Maximum load (N)	Modulus of rupture (N/mm <sup>2</sup> )
1	25.9	25.8	28	121.0	0.79
2	25.9	26.0	28	112.6	0.72
3	26.0	26.0	28	121.0	0.77
Mean modulus of rupture (N/mm <sup>2</sup> )					0.76
4	25.9	25.7	56	146.2	0.95
5	26.0	25.7	56	136.6	0.88
6	26.0	25.6	56	143.6	0.93
Mean modulus of rupture (N/mm <sup>2</sup> )					0.92

**Table 3-3: Engineering properties of mortar (modulus of rupture)**

Test	Average result
Hardened bulk density ( $\text{kN/m}^3$ )	18.0
25 mm cube compressive strength ( $\text{N/mm}^2$ )	1.70
Flexural strength ( $\text{N/mm}^2$ )	0.76
Modulus of elasticity ( $\text{N/mm}^2$ )	2,900
Poisson's ratio	0.09

Table 3-4: Mortar tests results

Specimens	Compressive strength ( $\text{N/mm}^2$ ) <sup>a</sup>	Compressive strength ( $\text{N/mm}^2$ ) <sup>b</sup>	Modulus of elasticity ( $\text{N/mm}^2$ )	Poisson's ratio
1	92.7	112	30,160	0.14
2	108.7	64.3	30,100	0.14
3	91.9	59.7	30,100	0.14
4	93.7	68.2	30,200	0.14
5	94.1			
6	89.6			
7	84.5			
8	115.5			
9	94.4			
10	99.0			
Average	96.4	76.1	30,100	0.14

a) From compression tests on whole bricks

b) from stress-strain tests

Table 3-5: Modulus of elasticity and Poisson's ratio (bricks)

Test	Specimens	Average Result
Bulk density ( $\text{kN/m}^3$ )	Whole bricks	22.0
Compressive strength ( $\text{N/mm}^2$ )	Whole bricks	96.4
Modulus of elasticity ( $\text{N/mm}^2$ )	65×65×225mm	30,100
Poisson's ratio	65×65×225mm	0.14

Table 3-6: Bricks test results

Test	Size of specimens (mm)	Relative standard
Particle size distribution	N/A	BS 1377-2
Compaction test	N/A	BS 1377-4
Shear test	100×100	BS 1377-7

Table 3-7: Backfill tests

Property	Specimens size	Values
Coefficient of uniformity	N/A	25.0
Coefficient of curvature	N/A	2.0
Bulk density (kN/m <sup>3</sup> )	1 litre mould	22.0
Optimum moisture content (%)	1 litre mould	8.0
Angle of friction (degrees)	100×100 (shear box)	53.0
Cohesion constant (kPa)	100×100 (shear box)	16.8
Modulus of elasticity (N/mm <sup>2</sup> )	70mm drained triaxial	18 <sup>a</sup> - 66 <sup>b</sup>

<sup>a</sup>Under 20 kPa pressure<sup>b</sup>Under 80 kPa pressure**Table 3-8: Backfill materials properties**

Test	Specimens size (mm)	Relevant standard
Compression	25×25×25	BS 1881-116(adopted)
Compression	70.7× 70.7×70.7	BS 1881-116
Flexural	25×25×100	RILEM

**Table 3-9: Micro concrete tests**

Specime n	Length (mm)	Width (mm)	Failure Load (kN)	Compression strength (N/mm <sup>2</sup> )
1	26.1	25.7	34.3	51.1
2	26.4	25.4	34.5	51.5
3	26.4	26.3	36.8	53.0
4	26	26.4	34.6	50.4
5	25.8	25.8	33.9	50.9
6	26.6	26.3	35.7	51.0
Average				51.3
1	70.9	71.1	23.4	46.4
2	70.9	70.8	23.1	45.9
3	71.03	70.9	24.0	46.7
Average				46.3

**Table 3-10: Engineering properties of micro concrete (compression strength)**

Specimen	Length (mm)	Width (mm)	Load (kN)	Modulus of rupture (N/mm <sup>2</sup> )
1	25.3	26.0	1.27	8.58
2	25.9	26.5	1.07	6.73
3	25.7	26.0	1.05	6.85
4	25.5	25.7	1.13	7.57
5	25.0	25.5	1.11	7.86
6	25.8	25.7	1.16	7.65
Mean modulus of rupture				7.53

**Table 3-11: Engineering properties of micro concrete (modulus of rupture)**

Specimen	Compressive strength (N/mm <sup>2</sup> )	Modulus of elasticity (N/mm <sup>2</sup> )	Poisson's ratio
triplet 1	39.8	2,870	N/A
triplet 2	48.9	6,280	N/A
triplet 3	38.7	4,170	N/A
triplet 4	50.0	4,170	N/A
Average triplet	44.4	4,400	N/A
wallette 1	42.6	3,170	0.27
wallette 2	36.0	N/A	N/A
wallette 3	47.5	6,400	0.37
wallette 4	46.2	N/A	N/A
wallette 5	35.1	5,600	0.22
Average wallette	41.5	5,050	0.29

**Table 3-12: Masonry compression strength and modulus of elasticity**

Mortar Properties					
Property Reference	Bulk density (kN/m <sup>3</sup> )	Compressive strength (N/mm <sup>2</sup> )	Flexural strength (N/mm <sup>2</sup> )	Modulus of elasticity (N/mm <sup>2</sup> )	Poisson's ratio
(Baker 1996)	N/A	3.5 <sup>a</sup>	0.25	11,154	0.14
(Sicilia 2001)	15.9	1.4	0.62	1,897	0.064
(Baralos 2002)	19.3 <sup>b</sup>	1.1	N/A	N/A	N/A
(Burroughs 2002)	19.0 <sup>b</sup>	1.1	N/A	N/A	N/A
Current Study	18.0 <sup>b</sup>	1.7	0.76	2,900	0.09
Unit properties					
Property	Compressive strength (N/mm <sup>2</sup> )	Flexural strength (N/mm <sup>2</sup> )	Modulus of Elasticity (N/mm <sup>2</sup> )	Poisson's Ratio	
(Baker 1996)	38.0 <sup>a</sup>	2.75	13,500	0.18	
(Sicilia 2001)	94-108 <sup>b</sup>	6.5-13.6	19,820-22,340	0.14	
(Baralos 2002)	42.0 <sup>c</sup>	N/A	N/A	N/A	
(Burroughs 2002)	95.0 <sup>d</sup>	N/A	N/A	N/A	
Current Study	96.0	N/A	30,100	0.14	
Backfill Properties					
Property	Bulk density (kN/m <sup>3</sup> )	Cohesion (kPa)	Optimum moisture (%)	Modulus of elasticity (N/mm <sup>2</sup> )	Angle of shear
(Sicilia 2001)	23.3	172	7	45	45
(Baralos 2002)	23.1	13.6	8	18-66	50
(Burroughs 2002)	22.0	0.0	9	N/A	47
Current Study	21.9	16.8	8	N/A	53

Table 3-13: Arch bridges material properties

Masonry properties				
Property	Compressive strength (N/mm <sup>2</sup> )	Flexural strength (N/mm <sup>2</sup> )	Modulus of Elasticity (N/mm <sup>2</sup> )	Poisson's Ratio
(Sicilia 2001)	31.0 <sup>a</sup> -33.8 <sup>b</sup>	0.017	4,182 <sup>a</sup> & 4,954 <sup>b</sup>	0.17
(Baker 1996)	13.5 <sup>a</sup> -21.0 <sup>b</sup>	0.065	2,500 <sup>a</sup> -7,000 <sup>b</sup>	0.07
Current Study	41.5 <sup>a</sup> -44.4 <sup>b</sup>	N/A	4,400 <sup>a</sup> -5,050 <sup>b</sup>	0.29

Mortar: <sup>a</sup> Mortar grade III <sup>b</sup> Lime mortar

Bricks: <sup>a</sup> Clay brick <sup>b</sup> Carboniferous sandstone <sup>c</sup> Laybrook Paver <sup>d</sup> Staffordshire blue

Masonry: <sup>a</sup> triplets tests <sup>b</sup> wallettes tests <sup>c</sup> Mortar grade IV & clay bricks

**Table 3-13: Arch bridges material properties (Cont.)**

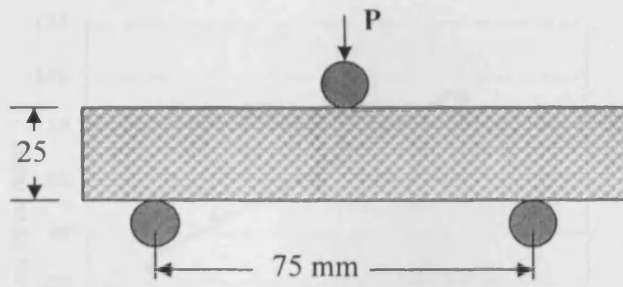


Figure 3-1: Mortar flexural test specimen

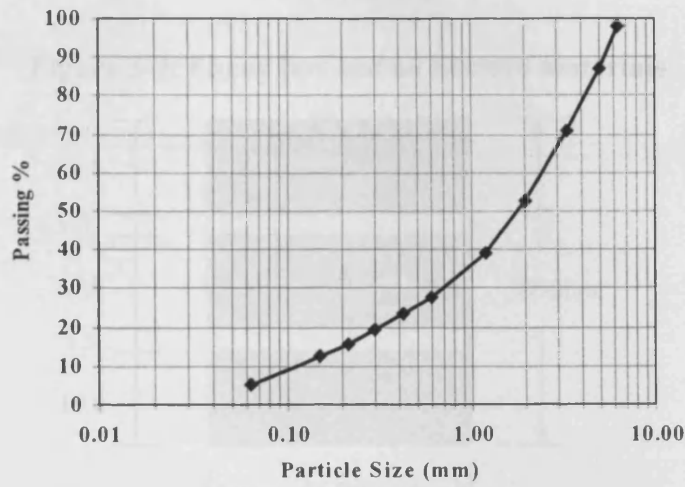


Figure 3-2: Backfill size distribution curve

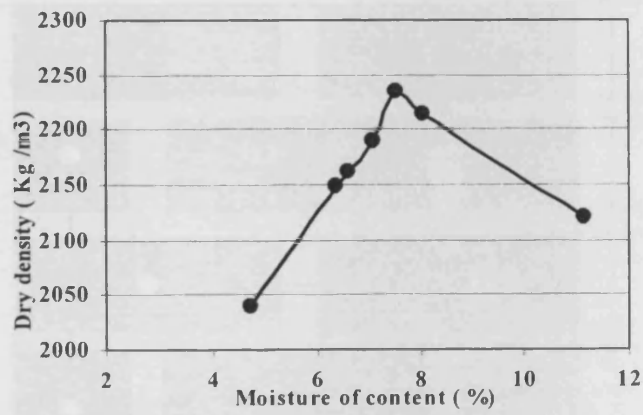


Figure 3-3: Maximum bulk density of limestone backfill



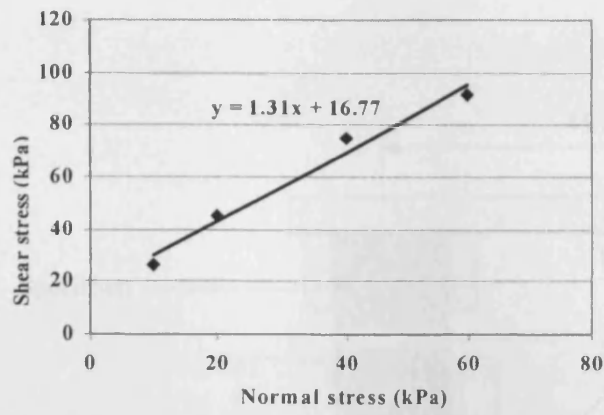


Figure 3-4: Shear box test on backfill materials

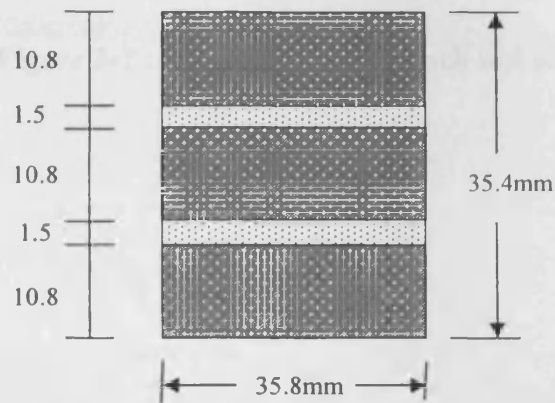


Figure 3-5: Masonry test specimens (triplet)

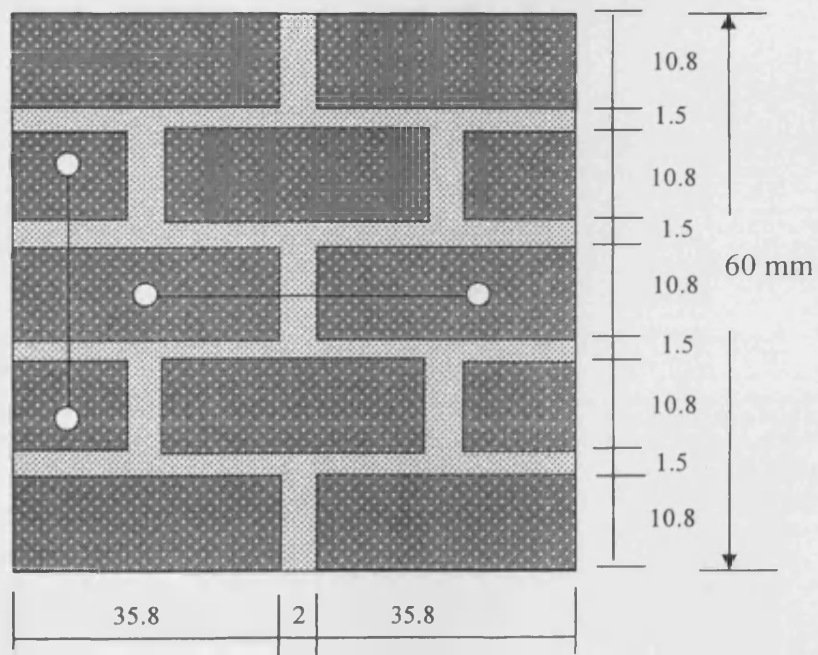
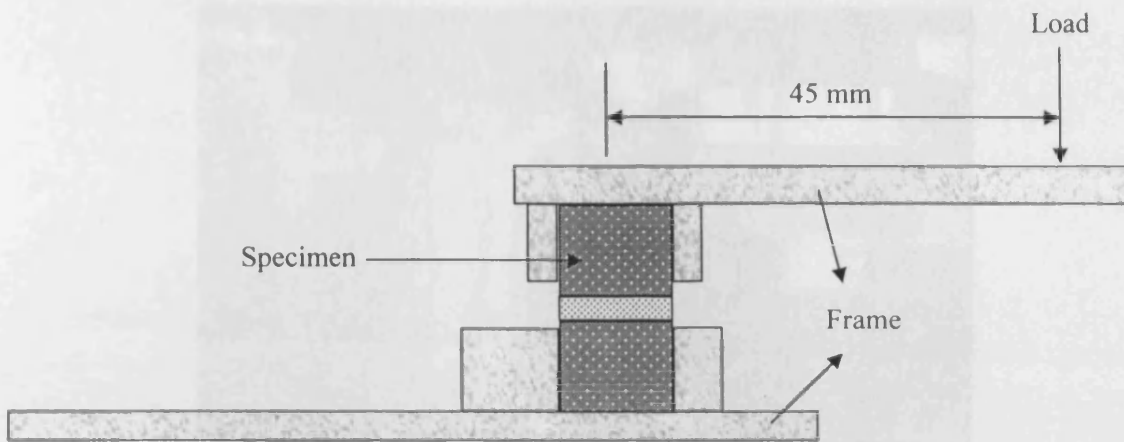


Figure 3-6: Masonry test specimens (wallette)



**Figure 3-7 : Masonry bond wrench test setting**

Plate 3-1: Mortar test

Plate 3-2: Compression bond test

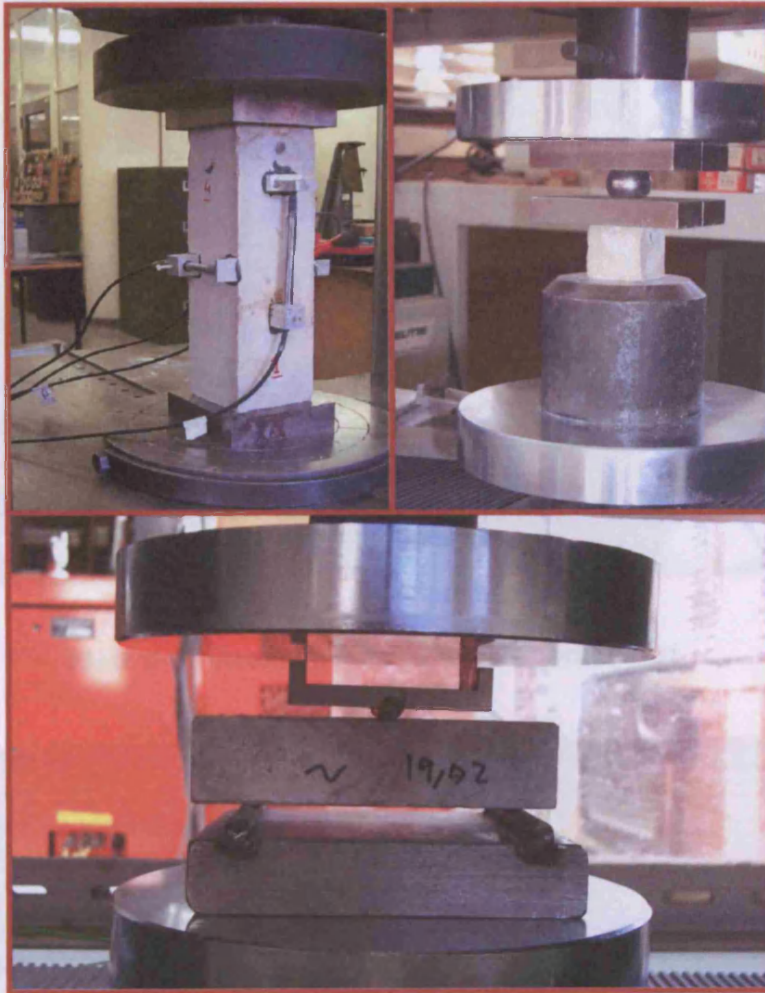


**Plate 3-1: Mortar tests**



**Plate 3-2: Compression bricks test**





**Plate 3-3: Stress strain relationship brick test**

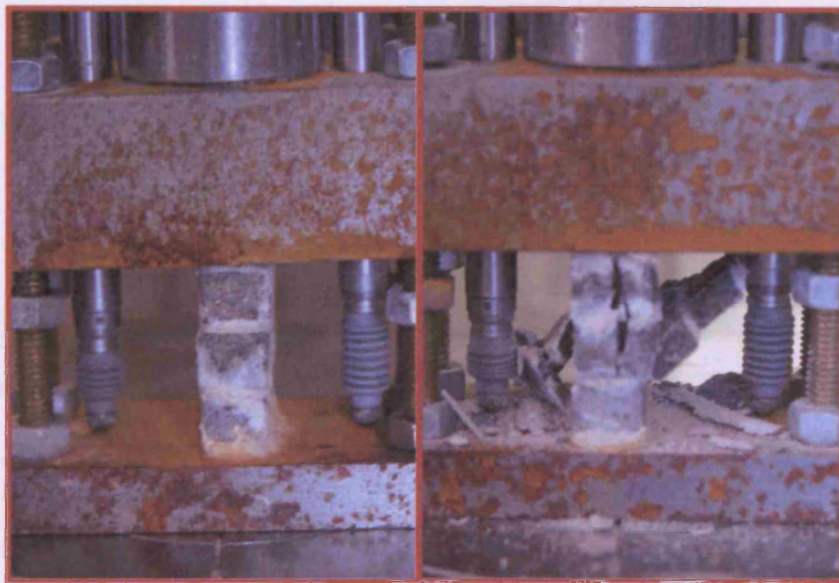


**Plate 3-4: Masonry test (triplet)**



**Plate 3-5: Masonry test (wallette)**

Significant experiments on arches have been reported by Hendry et al. (Hendry et al. 1967), Wadley (Melbourne and Wadley 1990), Hughes et al. (Hughes et al. 1987) and others. All of the early tests on arch bridges and their results were reported by Egan (Egan 1992). An overview of experimental masonry arch bridge research in the 1980s is presented by Melbourne (Melbourne 2001). The majority of these experiments had a primary direction of load application and have provided significant experimental data in terms of these types of structures to static loads. Most of the existing masonry arches remain that a hundred years old and therefore there is significant interest in modern strengthening techniques. In recent years, experimental work has also moved away from assessing masonry largely towards investigations of masonry in concrete systems. The effect of various strengthening methods on full scale masonry was reported by Soudki (Soudki 1990) and Melbourne et al. (Melbourne et al. 1992). Harries (Harries 2002) applied different types of strengthening method to 1922 masonry 2-D single span arch systems. The effects on arch load capacity of applying a composite saddle assessed by small scale centrifuge models are presented by the author elsewhere (Harries and Huggins 2004).

In most of the above referenced work 2-D arch models were studied, however it is known that a significant number of arch bridge defects are due to three-dimensional effects. Lateral earth pressure on spandrels and wing walls tends to cause the overturning of the walls and often causes longitudinal cracks between the spandrel and the arch ring.

## **4 Experimental tests and procedure**

### **4.1 Introduction**

Significant experiments on single arches have been carried out and reported by Hendry et al (Hendry et al. 1985), Page (Page 1988), Melbourne and Walker (Melbourne and Walker 1990), Hughes et al (Hughes et al. 1998) and others. Most of the early tests on arch bridges and their results were reported by Page (Page 1993). An overview of experimental masonry arch bridge research in the UK was also presented by Melbourne (Melbourne 2001). The results of these experiments were initially directed at load assessment and have provided significant understanding on the response of these types of structures to static loads. Most of the existing structures in use are more than a hundred years old and therefore there is significant interest in repair and strengthening techniques. In recent years, experimental work has also moved more from assessing existing capacity towards investigations of methods to increase capacity. The effect of various strengthening methods on full scale arches was reported by Sumon (Sumon 1998) and Melbourne et al (Melbourne et al. 1995). Baralos (Baralos 2002) applied different types of strengthening method to 1/12<sup>th</sup> scale 2-D single span arch models. The effects on arch load capacity of applying a concrete saddle assessed by small scale centrifuge models are presented by the author elsewhere (Miri and Hughes 2004).

In most of the above referenced works 2-D arch models were studied, however it is known that a significant number of arch bridge defects are due to transverse effects. Lateral earth pressure on spandrel and wing walls tends to cause the overturning of the walls and often causes longitudinal cracks between the spandrel and the arch ring.



Longitudinal cracks can also be caused by the lane directionality in the loading but these tend to be on the centreline rather than at the spandrel ring interface. The edge longitudinal cracks may result in the simple separation of the arch barrel and spandrel wall. Additionally the backfill downward pressure due to self weight and traffic loads on the barrel which is restrained in each side between two relatively stiff spandrel walls may cause transverse bending in arch barrel. This suggests that 3-D and spandrel wall effects on these structures should also be considered. The 3-D numerical and experimental works by Fanning and Boothby (Fanning and Boothby 2001b) and Boothby and Roberts (Boothby and Roberts 2001) have shown the bending effects and transverse behaviour of arches under service loads tests. Despite the magnitude of this problem, little research has been carried out on understanding the behaviour of spandrel walls and to the author's knowledge nothing specifically on the effect of strengthened walls on the arch behaviour under service and ultimate loads. It seems more research is still needed especially on 3-D behaviour and strengthening method effects on masonry arch load capacity to overcome the lack of knowledge related to this type of structure and their repair. The 2-D and 3-D models were therefore built and tested under rolling and increasing load. A standard procedure was adopted during the building and test procedure. To make the results comparable with available data from other researchers, similar material properties and procedures were selected. The major materials properties that were used in this study were assessed using related or adapted standards and the programme and test identification are presented in the next sections of this chapter. Different strengthening methods were applied to models in accordance with their conditions after the benchmark tests. Details of the strengthening methods and their application procedure are presented in the last part of this chapter.

## **4.2 Test arrangement**

Because the current study is a part of a larger study investigating the behaviour of small scale centrifuge models, all raw and processed data have been stored on a database, the following reference system was used to identify each test. This identification system covers both the 2-D and 3-D tests. Shallow and deep arches were indicated by S and D prefix while two-dimensional and three-dimensional tests were identified by 2-D and 3-D prefixes respectively. The number of each test followed this prefix and finally repair and

benchmark tests were referenced using the R and B prefix. According to this reference system S2D-3R represent the third 2-D shallow repaired test and D3D-1B indicates the first 3-D benchmark test on a deep arch geometry. The first 2-D shallow arch was tested up to failure at the first stage and had no repair. Therefore, there is no test under the name of S2D-1R in this thesis. Both of the benchmark and repaired arches were tested under rolling and increasing loads. The prefix of R (rolling load) and U (ultimate load) are used to recognise rolling load data from the ultimate load test. Some of the 3-D arch models were applied under different types and positions of the rollers. Prefixes L (lead roller) and S (steel roller) identified the lead and steel rollers respectively in the figures and file names for these tests. Rolling loads were applied to the whole width, centre and front edge line of the arch in some 3-D tests; this was indicated by Load Case 1 to Load Case 3 respectively in the results. The number of pass rollers and movement direction are also presented in figures. Roller movement in forward direction is indicated by F and its backward direction is shown by B in tests results. The number of passes follows this. Therefore, F7 in the results and figures represent the seventh pass roller in the forward direction.

### **4.3 Tests programme**

In all three previous research works (Baralos 2002; Burroughs 2002; Taunton 1997) studying arch behaviour using small scale centrifuge models and many other experimental works (Page 1993) 2-D arches were considered. In the current study both 2-D and 3-D arch models were tested. The arch models were to be initially tested using appropriate rolling loads and were subsequently to be line loaded up to the observation of the first sign of failure. The initial stage of the tests is called the benchmark tests in the current study. Following the benchmark tests, the arches were to be repaired by applying a suitable repair method. The repaired / strengthened arches were subsequently re-tested initially with a rolling load and then up to full failure under increasing load, this is termed the repair tests in the current study.

Fifteen arch models were tested in total during this study; these include eight benchmark and seven repaired arches. Four 2-D arches were built and tested during the study. The repeatability of the tests were checked using the first 2-D test. This arch model



was loaded up to failure using an increasing load after the initial rolling load test. The other three 2-D models were repaired after the initial benchmark tests. One of these tests was carried out on a deep arch geometry and the others on shallow arches. The second 2-D shallow arch was strengthened by applying a layer of plastic mesh at the mid depth of the backfill at the crown of the arch. The mesh was applied to the whole area of the arch model. The third shallow arch model was repaired using a layer of reinforced concrete slab on top of the backfill. As this had a significant effect on the arch load capacity this repair method was repeated on the deep arch geometry. Details of each strengthening method and results are presented in the next parts of this chapter.

Four 3-D arches were built and tested during this study. One of them on a deep arch geometry. The first shallow arch was strengthened using arch barrel stitching and applying reinforcement between the spandrel and top layer of the arch barrel. The use of a partial reinforced concrete slab was selected as a repair method for the second shallow 3-D arch model. The third shallow and the deep arch models were repaired by strengthening the spandrel wall using reinforced concrete. Brief details of the 2-D and 3-D tests and their strengthening methods are given in Tables 4-1 and 4-2. Full details of the test procedures and repair techniques are presented in the next sections.

Arch models were constructed in two different rigid boxes. A black box with dimensions 850×350×500mm (length: width: height) and blue box with dimensions of 920×350×524mm were used. Both boxes were made from steel plate and had two 50mm Perspex side walls. These allow the observation of arch condition during the tests. Plates 4-1 and 4-2 show the arch model construction procedure for the shallow and the deep arches geometries respectively with related boxes used. The 3-D bridge models were built in a rigid box with a width of 450mm and the other dimensions as per the blue box. The wider rigid box allows sufficient free space (20mm) between the box rigid sidewalls and the spandrel walls. The fill and spandrel walls were extended to be restrained to the rigid end of the box at both longitudinal ends, although flexible packing was included to allow in-plane spandrel wall movements. Both 2-D and 3-D arch barrels were built on connected 100mm square rigid steel blocks as abutments.

## 4.4 Arch model geometry and properties

The major geometric parameters of the arches are summarised in Table 4-3. The arches under test were 1/12<sup>th</sup> scale models of a notional 6m single span brickwork arch bridge. They were built with distorted scale bricks; 1:12 scale in the ring depth and 1:6 scale (including joint) as viewed from beneath the intrados. A distorted scale was used because 1/12<sup>th</sup> scale for units in all directions had been shown to be physically too small to facilitate building of an model arch (Taunton 1997). The small scale bricks were manufactured by being diamond cut from whole bricks. Two different arch geometries were tested with span to rise ratios of 4 and 2; which are referred to as the shallow and deep arches in this thesis. The arches were identical in all other respects. The arch barrel was constructed of three rings in all models laid as separate stretcher bonds without any cross bonding headers. The backfill depth at the crown of the arch barrel was 30mm except for those which were repaired by applying the concrete slab on the top surface of the backfill.

General views of the 2-D and 3-D arch models are presented in Figures 4-1 and 4-2. The 2-D arches were made without spandrel and wing walls. The 3-D models include the arch ring, the spandrel wall and the backfill materials; they do not include parapets or wing walls. In the UK with the exception of waterway arches, most brickwork arch bridges are constructed without headers. The spandrel wall were laid on top of the arch barrel at a thickness of 30mm and were constructed from full width single small bricks which simulate block masonry in the prototype.

### 4.4.1 Bricks

The bricks used in the arch model were Staffordshire Blues (215×103×65mm) which were classified as class A in according to the British Standard (BS 3921 1985). Compressive strengths of 96N/mm<sup>2</sup> were achieved from compression tests following the compression strength test procedure according to the above standard. This compression strength value was obtained from the average results of a standard test on 10 full scale bricks (Chapter 3).

Small scale units were provided following the procedure which was developed in previous arch centrifuge model studies (Baralos 2002; Burroughs 2002). In that procedure small scale sized units of 35.8×10.8×8.5mm were sawn from full scale size bricks. Sawn bricks have a smoother surface compared with the full size unit and this might effect the soil masonry friction angle in the small scale models. A series of shear tests were carried out by Taunton to investigate the shear behaviour between the sawn surface bricks and the backfill during a feasibility study (Taunton 1997). No significant friction angle difference between the results obtained from the small scale and full bricks was observed. It was believed that the friction between the arch barrel and backfill is well modelled in the tests. The spandrel walls were constructed of 30mm width using small bricks with dimensions of 35.8×30.0×10.8mm; this simulates blocks in a prototype. Summarised units dimensions and property results are detailed in Table 4-4. More details of properties are presented in Chapter 3.

#### **4.4.2 Mortar**

The main object of this study was to gain an understanding of the behaviour under loading of arch bridges having been repaired using different techniques. It was decided to make these models using arches, which were initially tested to the observation of signs of the onset of failure. The same procedure had been used successfully in previous studies on arch centrifuge models (Baralos 2002). Most of the arches requiring repairs have been made many years ago and some mortar deterioration is observed in them, therefore a weak mortar was selected to make the models. Referring to British Standard (BS 4551-1 1998), the UK mortar type V with a mix content of 1:3:12 (cement: lime: sand) was used as the joint material. Previous studies have shown that a water to cement ratio of 3:1 provides a good workability so the same ratio was selected for this study. As a result of the small scale of the models thin mortar joints are required and therefore very fine sand has to be used in making the mortar. Chelford 95, fine silica sand, was selected and used in this study. This type of fine sand was used in many research projects at Cardiff University and its properties are well known. Ordinary Portland Cement and Hydraulic Lime, according with British Standard (BS 890 1995) were used without issue because their individual particles are fine enough.

Mortar compressive strengths of  $1.7\text{N/mm}^2$  were achieved based on the compression test on 25mm cubic specimens. That size of small test specimens was selected because of the very thin joint thickness in the arch model construction. The nominal width of the mortar joint was 2mm in the longitudinal direction and about 1.5mm in depth direction of the arch barrel. Comprehensive tests on the mortar and the results and discussion were detailed in Chapter 3 and brief results are presented in Table 4-4.

#### 4.4.3 Backfill

The backfill significantly effects arch load capacity and therefore the selection of a suitable backfill is very important in arch modelling. The backfill material used in the arch models was composed of an approximate 1:6 scale granular limestone material. This was suitable as the interaction with the brickwork is at the correct geometric scale and well simulates prototype backfill properties in small scale centrifuge tests (Taunton 1997). The use of  $1/6^{\text{th}}$  scale was considered appropriate since the brick dimension in the plan of the arch is the same.

An average bulk density of  $22\text{kN/m}^3$  was achieved at about a 8% moisture content according to the procedure of British Standard (BS 1377-2 1990) and a friction angle of  $53^\circ$  was measured from the direct shear test. The backfill for all tests was bought at the start of tests to be sure of having constant properties during the tests. Brief tests results on the backfill are presented in Table 4-4.

The backfill depth at the crown of all arch models, except tests S2D-3B and D2D-1B, was 30mm. These two benchmarks models were tested with the backfill depth of 13mm at the crown to readily facilitate the placement of the concrete without overly disturbing the damaged arches. Concrete slab with a depth of 17mm was applied on the top surface of the backfill as a repair technique. The overall depth of construction over the crown of the arch, including the 17mm concrete layer in the strengthened arch, was therefore 30mm to compare with the other tests.

It was important to make all of the arch models by the same method to minimize any side effects of changing parameters in determining the arch load capacity. It was

attempted to build all models with the same laboratory conditions, workmanship and so on. For instance, the number of barrel courses was kept the same at each working time. The same backfill depth layer was selected during backfill compaction and all layers were compacted in the same way.

## **4.5 Instrumentation**

Arch deflection and soil/masonry interaction were measured during each test. The displacements were recorded using Linear Variable Direct Transducers (LVDT) and small Kyowa diaphragm pressure sensors were used to measure the pressures on the extrados of the arch barrel. In the next two sections, these instruments are detailed.

### **4.5.1 Displacement measurement**

Two types of LVDT, D2/100A with a range of  $\pm 2.5\text{mm}$  and D2/200A with a range of 5mm, were used. Two additional LVDTs with a range of 15mm were used to measure the displacement of the load spreader at the two ends. All LVDTs were manufactured by RDP electronics Ltd.

The arch deflections were measured using two rows of displacement transducers during the 2-D tests. One LVDT row was installed along the centreline of the arch and the other row parallel to the first but close to the edge (spandrel) face. The LVDTs were installed normal to the arch barrel to measure the radial deflections of the arches. Three rows of LVDTs were installed under the longitudinal middle line and at both edges of the arches, to record the arch barrel deflections during the 3-D tests. Due to the limited number of available channels, different numbers of LVDTs were installed in these rows.

Output values are converted to the arch displacement using calibration constants. The LVDT calibrations during the previous study have shown little difference between the measured calibration factor and manufactured company factors (Baralos 2002). It was decided to use the modified calibration factors in this study. Manufactured and modified factors are detailed in appendix Table A-1.

#### 4.5.2 Soil/masonry interaction measurement

Subminiature pressure sensors PS-5KA were used to record the pressures on the extrados of the arch barrel. These are special 6mm diameter diaphragm sensors of 0.5mm thickness supplied by Kyowa electronic instrument company Ltd. These sensors have a capacity of 500kPa and a rated output of about 1mV/V with a 3V excitation. They had been used successfully in previous centrifuge works. In the feasibility study, the sensors were taped to the arch extrados, but some operational problems were observed because of fragility of the cells and sensor displacement. In a previous study, the sensors were installed in a machined recess in scale bricks using epoxy resin and used successfully. Installation of the sensors at their correct position could be easily achieved after removing some of the bricks from the extrados of the arch and replacing them with pre-cast sensor bricks.

Calibration of the pressure sensors is very important to insure the pressure on the extrados of the arch is correctly measured. It was attempted in a previous work using many ways. Taunton (Taunton 1997) tried to validate the manufacturer calibration using the self weight of the backfill under enhanced gravity conditions. The bricks were taped with the sensor to the floor of the rigid box and covered with a fine layer of sand. The fine sand layer was covered with 180mm compacted backfill materials. The package was accelerated up to 50g in 5g steps and kept at an unchanged speed in each step to achieve stable condition. The output results had shown good agreement with manufacturer calibration at low pressure, about 100kPa. Baralos used the head of water instead of backfill self weight to calibrate the sensors (Baralos 2002). He also attached the Kyowa sensors to the floor of the rigid box. The sensors were pre installed in small size bricks using epoxy resin and a head of water 0.4m was selected. The package was accelerated up to 60g with a 5g step (approximately 240kPa at 60g) for this calibration test; he concluded that the manufacturer calibrations were underestimating the true pressure by about 10%. According to the results, he used manufacturer calibration data and simply increased the measured pressure by 10%. The same calibration factor was used in the current study. Manufacturer calibration factors for the different Kyowa pressure sensors are presented in appendix Table A-2.

### **4.5.3 Test observation instruments**

Four closed circuit television cameras (CCTV) are installed in the centrifuge pit area. The centrifuge operator should be able to monitor the centrifuge during the tests as a safety rule. Two of these cameras are attached to the arms and monitoring of the arch during the tests is possible using cameras. One of these cameras was attached to the gondola and the other one near to the rotational axis of the gondola. The output from the side view and the plan of the package are viewed via television monitors in the control room. Control of the arch model test is possible using these cameras. The applied load was controlled according to the view from these pictures. A Kodak digital camera model DC260 was also attached to the gondola and took photos of the package every five minutes during most test. Digital photos were taken also before and after each test. Crack patterns and failure modes were identified using these photos. All visible cracks were investigated and recorded before starting and after centrifuge tests.

## **4.6 Loading system**

Most of the equipment and instruments which were used in this study were developed in previous research studies. Although some modifications were needed, especially in the case of the 3-D tests. It was tried to keep the 3-D arch width between the spandrel walls the same as the 2-D tests to be able to use the previous loading system. Therefore the 3-D arch widths increased by twice the spandrel wall thickness and all the previous loading system and devices have been used in the current study. Details of the rolling and increasing load system can be seen in those previous studies (Baralos 2002; Burroughs 2002) and a brief detail of it is presented in the next sections.

### **4.6.1 Rolling load system**

A general view of increasing and rolling load system is presented in Plate 4-3. Three inline hollow rollers simulated the service load during the tests. These included a lead roller and a steel roller with weights of 14.9kg and 11.8kg, respectively. The lead roller simulates 15 tonnes over a 2.5m axle in the prototype and the steel roller models 12 tonnes at full size. These rollers are applied to the whole width of the arch and in some cases half of them were applied to the half widths of the 3-D arch models. Combinations

of these rollers were also applied in some cases. Details of the applied load in each test and procedure are presented in section 4.10.1 of this chapter.

#### **4.6.2 Increasing load system**

The previous developed increasing load system was used during this study. The device is based on a Wykeham Farrance compression testing machine which is fixed to an aluminium frame. Strip footing and load cells were connected to the machine using a loading arm. The load cell is located between the machine and strip footing, therefore the load cell and arm weights are not recorded during the tests. The load cell and arm self weight were added to the reading later. As different distances exist between the backfill top surface and the load system devices different arm lengths were used during the tests.

Two different load cells with capacities of 10kN and 100kN were used during the tests. Both load cells were calibrated using a compression testing machine with a calibration traceable to national standards in a previous study (Burroughs 2002). Calibration factors are presented in appendix Table A-3. The increasing load was applied to the whole width of the arch through the 17.5mm width spreader. A 3mm wood plate with the same strip width was attached to the spreader in the case with the concrete slab on the backfill as a repair technique. This ensured that the load distribution and no point loading on concrete. Two LVDTs were added to the box to record the spreader beam deflection at both ends.

### **4.7 Model construction procedure**

#### **4.7.1 Arch barrel construction**

The building of each 2-D arch barrel normally took about five working days. The vaults were built on steel centering which was rolled with the same radius as the arch barrel. This was fixed to the abutments before starting to build the arch barrel. In order to easily remove the centring from the barrel and to decrease the adhesion between the steel and the intradoses of the arch barrel, the centering was greased before starting. The centering was made from 3.4mm thickness steel plate for the shallow arch and it is stiff enough to support the weight of the barrel during the building period. The deep arches vaults were



made using a semicircular aluminium plate as a centring, which was supported using some stiffener plates to make it stiff enough to carry the arch weight.

For each shallow arch 47, 49 and 50 rows of bricks were required to complete the first, second and third rings of the barrel. While this increased to 64, 66, and 69 respectively for the deep arch. Approximately 1300 bricks were required for the shallow arch and 1800 for the deep arch. In order to save time two arch models were built at the same time. Therefore for the 8 arch models which were tested during the study large numbers of units were required. Preparation of sufficient units, with limited time, is difficult and uneconomic. Recycling bricks was suggested and used during the previous centrifuge model studied to solve this problem (Burroughs 2002). It was decided to follow the same procedure during this study. After each test the bricks were submerged in water for a few days then the sections were broken into individual bricks. Brick cleaning solution (hydraulic acid base), was applied to clean any remaining mortar from the bricks surfaces. The cleaned bricks were subsequently submerged in a water tank. The water was changed regularly to minimize the acid effect. During the tests, reuse and repairing some bricks were lost so new sawn bricks replaced them.

The arch barrels were made symmetrically from both sides to prevent applying any unwanted non-symmetrical self loading. The course was started from one end abutment and continued until the mortar became unworkable. This happened after completing about 12 courses of the barrel for each mortar batch. The bricks were submerged in water 24 hours before using to keep them in a wet condition prior to laying. This limited water suction by the bricks and mortar shrinkage. The additional water on bricks was wiped off prior to their laying.

#### **4.7.2 Spandrel wall construction**

The 3-D arch barrel building takes slightly more time because of the wider arch bridge model compared with the 2-D models. The same procedure as the 2-D arch barrels was followed in the 3-D arches. The same centring, but wider, was used. The completed barrels were wrapped in a damp cloth for a week without any movement for pre hardening of the barrel. After a week the spandrel wall construction was started. Prior to

the spandrel wall construction the model was installed in position in the rigid box. The reported experimental test results of Fairfield and Ponniah (Fairfield and Ponniah 1994a) have shown the effect of the distance between the wall end and springing on the arch load bearing capacity. This is more important in the deep arch geometry. If the end wall is too close, as a result of wall rigidity, the backfill movement is restricted and the lateral pressure on the barrel will be increased. In order to decrease the end wall effect the arch was placed asymmetrically in the rigid box to increase the distance between the remote springing from the increasing applied load and the end wall of the rigid box. Care was taken to install the model in the middle of the rigid box out of plane direction. This allows sufficient free space both sides of the barrel for spandrel wall construction. Then the front sidewall of the rigid box was removed and two vertical support sheets were installed to both sides of the barrel near to the edge. A wood plate was used at the rear of the arch side and Perspex plate at the front side. The wood plate was covered with a thin layer of greased plastic prior to installation to prevent any mortar water being absorbed by the wood. The grease allowed easier removal of the plate at the end of the work. A Perspex support plate at the front of the model made the constructed spandrel wall visible to control the joint and course thickness during construction. Course layer positions were marked on the plate before using it. Re-installing the front side of the rigid box caused some trouble in the first test. To avoid this a Perspex front sidewall was reinstalled after the vertical support fixing and prior to the spandrel wall construction in the later tests. The spandrel walls were laid on top of the barrel on both sides and it was constructed symmetrically in both plan and longitudinal direction. They were constructed from full width single small bricks. The spandrel walls were extended to be restrained to the rigid end of the box at both longitudinal ends, although some flexible packing was included to allow in plane spandrel wall movement. Construction of the arch spandrel walls normally took between 5-7 working days. On completion of the spandrel the model was wrapped in damp cloths for 28 days before backfilling. Arch barrel centring and spandrel wall vertical supports remained in place during all procedures until LVDT installation. Plate 4-4 shows the spandrel wall construction procedure for a typical 3-D shallow arch model. The same procedure was followed for the deep arch geometry.

### 4.7.3 Backfilling procedure

After completion of the arch barrels, the models were wrapped in damp blankets and kept at the same condition for 28 days prior to backfilling and testing to allow the mortar to cure. However it takes a long time especially for lime mortar, to fully harden but tests on walls in previous research work (Sicilia 2001) and in the current study showed there is no significant difference between the tests results at 28 and 56 days specimens. Therefore 28 days was selected as the hardening time for all arch models prior to testing although some tolerance was allowed at weekends and holidays times.

When the sensors had been placed in the barrel, the backfilling was started. To make the backfilling easier the 2-3mm gap between the edge of the barrel and the Perspex wall of the rigid box was plugged using a roll of greased plastic. About 20kg of backfill were mixed with the amount of water needed to achieve the moisture content of approximately 8%. This was achieved from a series of compaction test which were conducted in accordance with guidelines detailed in British Standard (BS 1377-4 1990). The backfill was compacted in 50mm layers using a hammer handle. It was placed in and compacted symmetrically on both sides of the arch at the same time. A standard 2.5kg compaction test drop hammer was used in a feasibility study and cracks were reported resulting in the use of a lighter compaction method especially in the deep arch geometry for this study. Although it was decided to use a lighter hammer for compaction control was also exercised over the number of hammer drops at each point for all tests. Comparison between the results of the density tests taken after some of the tests indicate little difference between the densities of different models which is as expected for this type of problem. Care was taken during the backfill compaction especially close to the barrel and crown of the arch, where the fill thickness is low. The moisture contents of the backfill was determined according to the British Standard (BS 1377-4 1990) in each test during backfilling. No significant changes in moisture content between different tests were identified.

The centring was in place during backfilling to prevent any damage and crack production as a result of the fill compaction. However some minor but observable cracks

were observed after re-centring especially in the deep arch geometry. Similar cracks were reported in a previous arch centrifuge model study (Baralos 2002).

#### **4.8 Instrument installation**

Two different types of instruments were used during this study. The first type was selected to measure the pressures on the extrados of the arch barrel and the second to record the displacement at different positions of the arch model. Instrumentation types and properties are detailed in section 4.5. The installation procedure of these instruments is presented here.

Prior to backfilling the pressure sensors were installed at suitable positions on the arch barrel extrados. Pressure sensors installation were standardised during a feasibility study (Taunton 1997) and during previous research work in the centrifuge (Baralos 2002; Burroughs 2002). In the current study the pressure sensors were pre installed in special brick units following that procedure and then these bricks were installed in the arch extrados. According to the arch geometry and the available number of the pressure sensors, suitable positions were marked on the barrel extrados and those bricks removed from the barrel. The unit with the sensors in were installed in the arch barrel 4-5 days before backfilling. Two pairs of these small sensors were used across the arch at each radial location.

After completion of the backfilling, the front side of the rigid box was removed and the LVDTs installed beneath the arch barrel. Prior to installation of the transducers the centring was carefully removed to prevent any damage to the arch. The LVDTs, were installed in different rows along the arch to measure the radial deflections of the arches. Two aluminium plates were used to fix them to the support which was bolted to the abutments on both ends. LVDTs were fixed to the support plate using plastic holders. The direction of each LVDT and their position was determined and marked on the plates prior to installation. The front sidewall was then replaced and the load system was fixed to the box. The arch barrel, model instrumentation and location for both the shallow and the deep arch geometry are presented in Figure 4-3.

## 4.9 Centrifuge preparation

Once the instrument installation was completed the model package was weighed and the required balance counter weight was determined. There is an exact correspondence in stress between the model and prototype at  $2/3^{\text{rd}}$  of the model depth if the effective centrifuge radius is measured from the central axis to  $1/3^{\text{rd}}$  the depth of the model (Taylor 1995). The required centrifuge speed was then calculated based on an effective radius to one third of the model depth and with 12g as the required acceleration.

The package was placed in the middle of the gondola base and fixed to it using suitable supports. Then all instruments were connected to their relevant channels. Suitable voltage was checked prior to any connection. The data logger was then switched on, the transferred data checked to ensure all instruments worked and sent the data recorded correctly. The position of the roller was measured and the rolling load system switched to the remote control. This allows the control of the rolling load from the control room. The video cameras were turned on at this stage and adjusted to receive a clear picture of the package. Two cameras were installed to show the gondola package position.

## 4.10 Centrifuge tests procedure

Testing was undertaken immediately following backfilling in order to maintain the moisture level in the backfill material. The test procedures are detailed in the next sections.

### 4.10.1 Benchmark tests procedure

After installation of the model in the gondola, instrument connection, checking data recording and adjusting the counter balance load the flight was started. Prior to starting, the centrifuge model condition including any cracks and other faults were investigated and recorded. The rotation speed was increased slowly and steadily up to 3g. At each 3g model acceleration the speed was kept constant until a stabilized condition was achieved and all received data was recorded. Acceleration was increased again and the same process repeated for each step. The centrifuge tests were undertaken at stable 12g acceleration with initially a rolling load being applied to the models.

#### 4.10.1.1 Rolling load

Once the model acceleration was achieved and stabilized at 12g the rolling load was applied. The rolling load is made up of three roller weights which act as a line load across the full width of the arch between the spandrels. The dead load rollers were moved slowly across the arch bridge taking about 15 minutes per pass. The rollers were rolled on the top of the fill from above one abutment to the other. Fourteen passes of the roller were carried out in each test and the position of the roller was recorded and referenced to the other monitoring equipment. In some cases more or less roller passes were applied related to the test type and time. It was required to stop the centrifuge at the end of the working time as a part of safety procedures. Table 4-5 details the type of roller used and the number of passes in each test.

Once completion of the roller loading test the centrifuge was stopped and the roller was replaced, if required. In the case of applying different rolling loads, the heaviest roller was applied on the first day of the test and the second and third roller types in the next working day. The model surface was covered with a damp cloth during the night to keep its moisture constant.

#### 4.10.1.2 Increasing load

After completion the roller loading test, a fixed location increasing load was applied across the whole width of the arch. The load was applied to the arch through a load spreader beam 17.5mm wide. This simulated a load strip width of about 210mm at prototype scale which is appropriate for full size tests. The load was applied at the quarter span point of the arch for both geometries of models from the top of the backfill on all models except D3D-1B and D3D-1R. In these two models the load was applied at 30% of the arch span. It is accepted that the critical position of the applied load is approximately located at that section (Page 1993).

The distance between the strip and backfill surface was adjusted using the load column. Spreader beam position might change in the case of a large distance between the spreader beam and backfill surface. In the case of no distance between the spreader beam and backfill surface the arm and footing self load will be applied to the arch prior to

starting the loading. The increasing load benchmark tests were stopped when the arch exhibited signs of failure behaviour, for example, when any crack was observed in the spandrel or barrels (by camera) or when the load deflection plot started to level off. The centrifuge was stopped at this stage and package was removed from the model. Then the model was investigated and all failure signs were recorded for later comparison.

Some load and reload was applied to the arch before applying the final load cycle. Details of cycle loads, their results and some discussion are presented in the next chapter.

#### **4.10.2 Repaired tests procedure**

The repaired arches were usually tested after 28 days (curing period) under the same rolling and increasing loads as the benchmarks, but the increasing loading was taken up to the full failure at this stage. The same procedure as benchmark tests was followed for repaired models except some changes in the rolling load weights and the load cells. The suitable rolling load and load cell were selected according to the repair method and the expected arch load capacity. Although most of the original backfill was retained during the repair to help support the arch, all the remaining backfill was removed and then replaced with new material immediately before re-testing.

The rationale behind the test/retest procedure, as designed, is that the repair is to be applied to a damaged rather than a “new” arch and that if possible any construction defects in the initially un-strengthened arches are retained in the repaired tests. Since it is difficult to judge when the initial “ultimate” load test is to be stopped, due to concerns over the inability to repair a completely fragmented arch, separate un-strengthened tests were taken to complete collapse (Baralos 2002). The results of the repair can therefore be compared to both the un-strengthened case as well as the average of a series of other benchmark tests.

#### **4.11 Repair techniques**

Models were repaired using different techniques after completion of the benchmark tests. Repair methods were selected according to the benchmark model condition. Three 2-D and three 3-D models were repaired using four different repair methods. In the case of a

significant effect of the repair method in arch load capacity, the repair was repeated to the deep arch geometry. Each model test from the start to the end of the repair test takes about four months. Repair methods and their procedure are detailed in the following sections.

#### **4.11.1 The 2-D repair techniques and applying procedure**

Models were repaired by a suitable repair method after the benchmark tests were completed and a suitable arch to repair was provided. Repair methods were selected in accordance with the nature of the benchmark models and types of fault on them. The first model was repaired using a plastic mesh reinforcement method. The second and third 2-D models with shallow and deep arch geometries were repaired using concrete slab. The concrete slab had a 17mm thickness and it was reinforced using a single layer of 0.8mm mild steel mesh across the full width and length of the saddle. The mesh was placed in the middle of the slab to have enough cover to both sides of it. Repair applying procedures are presented below.

##### **4.11.1.1 Plastic mesh reinforcement**

The second 2-D model (S2D-2R) was repaired with plastic mesh reinforcement. Plate 4-5 shows this strengthening method procedure and details. Two mesh layers of TENAX Promat (TENAX 2002), which was produced by the TENAX UK Limited Company for ground reinforcement and erosion control, were placed in the backfill. After the benchmark test was completed, the model was investigated and photographed. The backfill was removed from the arch barrel and some fill specimens were taken from the soil to determine its moisture content and density. A long crack was observed across the whole width of the arch barrel during the investigation. It was decided to grout this crack with a mix of water/cement. Therefore the bricks along the crack were removed from the extrados of arch, after replacing the centring, and the cement mix was injected into the cracks. It was believed that this filling of the crack has no significant affect on the arch barrel capacity. However, the barrel was placed in a rigid box in a reverse direction and increasing load was applied on the remote side of arch in the repaired test. The arch barrel was kept for two weeks under damped cloths and then replaced into the rigid box. The arch was backfilled using the same method of the benchmark test until about 15mm fill



depth over the crown. Mesh layers of TENAX were spread on the surface of the soil at this level. The mesh layers were placed across the whole width and length of the box and were fixed to the rigid box sidewalls along its length to keep it in a constant position during filling. Then the remaining part of the fill was placed in and compacted over the TENAX layers.

#### **4.11.1.2 Concrete slab repair**

The repair method application is presented in Plate 4-6. Following the initial tests, S2D-3R and D2D-1R the arches were repaired by laying a reinforced concrete slab on top of the backfill. In this case, the un-strengthened tests had a crown backfill depth of 13mm to readily facilitate the placement of the concrete without overly distributing the damaged arches. The overall depth of construction over the crown of the arch, including the 17mm of concrete layer in the strengthened arches, was 30mm. In this sense the initial benchmark tests were different from the standard benchmark which had an overall crown backfill depth of 30mm.

The concrete itself was manufactured with 2.0mm aggregate as the coarse material, Chelford 95 silica sand as the fine aggregate and OPC (BS 12 1991), with mix proportion of 1:1.8:2.8:0.6 (cement: fine: coarse: water) by mass. Compressive strength tests on 25mm concrete cube samples yielded  $56\text{N/mm}^2$  according to British Standard (BS 1881-116 1983). The model concrete was nominally reinforced with a mesh of type 304 manufactured of 0.8mm mild steel at 20mm centres. The same materials had previously been used in other small scale centrifuge models (Baralos 2002). Supports with height of 8mm were placed under the steel mesh to be ensure from the position of the reinforced mesh in the mid depth of the slab. The concrete was vibrated using an Industrial Engraver model 172 which was manufactured by Burgess Power Tools Limited. As a result of the significant increase in model load capacity this method was repeated for the deep arch geometry.

#### **4.11.2 The 3-D repair techniques and applying procedure**

The first 3-D model was repaired by stitching the arch barrel with steel bars between the barrel and the spandrel walls joints. Partial saddle concrete to the extrados of the arch was

employed to repair the second 3-D arch. The third and fourth 3-D arches were repaired with strengthening of their spandrel walls using a reinforced concrete slab. The 3-D arch repair techniques and their procedures are detailed in the next sections.

#### **4.11.2.1 Stitching reinforcement**

Stitching is a traditional method of repairing old arch bridges and increasing their load capacity. A pattern of holes are usually drilled into the barrel and then 10mm to 20mm steel rods inserted into the holes and grouted (Broomhead and Clarke 1995; Ellis 1990). In a previous small scale repair model study stitching was simulated successfully using 2.4mm diameter stainless steel bars type 304 (Baralos 2002). These small diameter bars simulate 30mm prototype scale bars. The bars were grouted in holes using a simple cement grout with cement: water ratio of 2. It was decided to use the same method in the current study. The pattern of holes with an angle of 45 degree were drilled in the arch barrel and bars were placed in them. It was thought that the inclined hole connected more units in a ring compared with perpendicular holes.

Because of the fragile behaviour of the arch barrel, especially after the benchmark test, drilling any hole in the barrel can damage the arch and spandrel walls. The spandrel wall was protected using a 20mm layer of Plaster of Paris to prevent more damage during the repair procedure. Although most of the original backfill was retained during the repair to help support the arch, all the remaining backfill was removed and then replaced with new material immediately before re-testing.

A longitudinal crack and separation of arch barrel and the spandrel wall was observed as a result of the benchmark test. Mild steel bars (0.8mm diameter) which were bent at an angle of 90 degrees were installed to connect the barrel extrados ring to the spandrel walls. Grooves with a depth of 3mm were made in the mortar joints at the extrados of the arch barrel and spandrel walls. Bent steel rods were placed in the groove and they were filled with a mix of cement/water. These rods were used to connect the spandrel walls to the arch barrel extrados and prevent any separation between the barrel and walls under the rolling and the ultimate loads.

#### **4.11.2.2 Partial saddle concrete repair**

As referred to in Chapter 2 use of a concrete saddle on the extrados of arch barrel is an appropriate method of repairing arches. The advantage of this method is that it not only strengthens the arch but also improves load distribution and ties together any cracked sections (Department of Transport 1997a). The method involves removal of the fill and casting an in-situ concrete arch, which can be reinforced, on top of the existing arch (Page 1996). It might sometimes be necessary to install centring beneath the arch to support it during the repair. The new arch can be designed to resist the applied load compositely with the existing arch, in this case good shear connection between the barrel and saddle is required. A stone arch may have a sufficiently rough extrados to provide it, otherwise stainless steel ties are required. If the new arch is designed to carry all of the applied loading it may be de-bonded from the existing barrel. A minimum saddle thickness of about 150mm is usually used and there must be sufficient space at the crown to accommodate it (Page 1996). Ties may also be applied to connect the arch ring to the spandrel walls. Water proofing should be applied to the saddle and any unsymmetrical applied load (due to concrete or backfill weight) should be avoided (Page 1996).

Test results on arch models that were repaired by applying saddle concrete on the extrados and intrados of arch barrel have shown a significant improvement in the ultimate load capacity of the models (Baralos 2002). One of the big issues related to applying saddle concretes on the extrados arch barrel is removing the backfill from the barrel. In addition, the amount of traffic disruption is such that the road should be diverted during the repair work. Traffic control is very difficult and some time is impossible if there is no alternative road available close to the site. To avoid these disadvantages of saddling, it was decided to apply a saddle concrete to some part of the bridge instead of the whole width of the model. A 60mm width of concrete slab was laid on both edge of the arch barrel from one abutment to the other one in the longitudinal direction. The repair procedure is detailed in Plate 4-7. Parts of the saddle concrete are stitched to the spandrel walls to avoid any disconnection between the spandrel and barrel. This was carried out by removing some parts of the mortar joints in the spandrel walls. The depth of removed mortar was selected as 3mm to 4mm in the model scale (approximately 4cm to 5cm in prototype scale) through the spandrel wall. Then the joint was filled by grout and one side

of angled 0.8mm mild steel was placed in the grout. The other side of this reinforced bar was placed in the saddle concrete. It was supposed this system would connect the saddling to the spandrel wall. These bars will prevent movement of bricks and progress in cracks. Two rows of holes with a depth equivalent to one ring were initially drilled to the arch barrel and 2mm steel rods were installed in them using epoxy resin. These rods had an extra length of about 12mm from the hole depth through the saddle and connected the barrel extrados to the saddle concrete. A width of 60mm in model scale (that means 720mm in prototype scale), was used which should be available as a pavement on most of arch bridge or may be provided by restricting a single lane of traffic to a narrow lane. Therefore there should be no requirement for closing the road during the repair period and also because a narrow part of arch barrel will be covered by concrete the quantity of material that should be removed is significantly decreased.

The concrete was reinforced with the same steel mesh as detailed in section 4.11.1.2. Wood plates were used to support the concrete during laying. These plates were sawn with the same radius of arch barrel extrados. The gap between the supports and barrel was filled using plaster to prevent any loss of water and cement from the concrete during the laying.

#### **4.11.2.3 Spandrel wall strengthening method**

Deterioration of the spandrel and parapet is a usual problem in most arch bridges. BA16/97 requires parapets and spandrel walls to be assessed by visual inspection (Department of Transport 1997b). Page (Page 1996) listed the following forms of deterioration for these parts of the structure:

Tilting, bulging or sagging

Lateral movement of parapet or spandrel wall relative to the face of the arch ring

Weathering and lack of pointing

Evidence of vehicle impact

Cracking, splitting and spalling

However there is no suggestion of any strengthening methods for the spandrel or parapet walls in his guidance on repair and strengthening of masonry arches (Page 1996) .

The Author's literature review has shown there is limited research on the effect of strengthening walls on arch load capacities. Retro-reinforcement is suggested as a method of reinforcing existing masonry to increase its ability to resist bending and shear forces. Test results on a series of un-reinforced and reinforced 2m span clay brick model arch bridges, reinforced with 6mm diameter stainless steel bars into grooves up to 75mm deep, have previously indicated improvements in the in-service performance as well as the load carrying capacity of the reinforced arches (Garrity 1995a). A principal feature of retro-reinforcement repairs is that it often results in a change in the appearance of the masonry arch bridge and this is an important issue with many of these aesthetically appealing structures. This method may also not be applicable where the mortar joints are very thin or where un-coursed masonry has been used. Use of tie bars is another method which is frequently used to prevent lateral movement of the spandrel walls relative to the barrel. These repairs mainly involve the installation of steel rods through both the spandrels and the existing fill; the rods extending into some end plate, visible on the spandrel walls, or terminating within some strengthened anchor section of the spandrel wall. This is a low cost method with little effect on traffic flow (Ashurst 1992) but tests on full scale models of a 5m span with and without tie bars have indicated that the tie bars had a negligible impact on the stiffness of the bridges under serviceability and higher loads (Melbourne et al. 1995).

A method used in the UK, sometimes referred to as the "Stratford" method, involves the excavation of a trench parallel, and immediately adjacent, to the spandrel walls that extends downwards to the arch barrel. The trench is backfilled with reinforced concrete placed on the extrados of the arch barrel to which both the spandrel walls and the arch ring can be stitched using structural steel ties. The construction advantages of this method are that it can be undertaken without closing the bridge, being normally restricted to the footpath; it can be constructed without access beneath the structure and, if extended only up to the road surface, it has no external visibility; the concrete itself can also provide a key for enhanced parapet provision, if required.

It was decided to repair one arch model with spandrel wall strengthening. Various stages of this arch repair are shown in Plate 4-8. After completing the benchmark tests, models were repaired by applying reinforced concrete to the inner sides of the spandrel

walls. The location of the concrete was restricted to those parts of the structure that would in normal circumstances be readily accessible for such work. In the present study the vertical extent of the reinforced concrete was restricted to 100mm in depth (about 1.2m in the prototype) this would require only limited support during construction. The concrete was the same as the one used in the concrete slab repair method with the same reinforced mesh. To apply the strengthening method holes with a depth equivalent to one brick course were initially drilled in the barrel and 2mm steel rods were installed in those holes using an epoxy resin. The emphasis in the experiments was the load capacity of the bridge although there was nothing specifically preventing the spandrel walls overturning.

Test ID	Description
S2D-1B	Shallow benchmark
S2D-2B	Shallow benchmark
S2D-2R	Shallow repair with plastic mesh reinforcement
S2D-3B	Shallow benchmark
S2D-3R	Shallow repair using 17mm concrete slab on top surface of backfill
D2D-1B	Deep benchmark
D2D-1R	Repair using 17mm concrete slab on top surface of backfill

**Table 4-1: 2-D arch models and their repair methods**

Test ID	Description
S3D-1B	Shallow benchmark
S3D-1R	Shallow repair with stitching & bar joint between wall and barrel
S3D-2B	Shallow benchmark
S3D-2R	Shallow repair with partially saddle concrete
S3D-3B	Shallow benchmark
S3D-3R	Shallow, spandrel wall strengthened using reinforced concrete
D3D-1B	Deep benchmark
D3D-1R	Deep, spandrel wall strengthened using reinforced concrete

**Table 4-2: 3-D arch models and their repair methods**

Properties	Shallow arch	Deep arch
Span (mm)	500	500
Span/rise	4	2
Ring number	3	3
Ring thickness (mm)	30	30
2-D arch width (mm)	345	345
3-D arch width (mm)	405	405
Depth of the fill at the crown (mm)	30	30

**Table 4-3: Major dimensions of arch models under test**

Properties	Bricks	Mortar	Backfill
Compression strength ( $\text{N/mm}^2$ )	96	1.7	N/A
Flexural strength ( $\text{N/mm}^2$ )	0.76	N/A	N/A
Modulus of elasticity	30,100	2,900	18-66
Bulk density ( $\text{kN/m}^3$ )	22.0	18.0	22.0
Shear resistance angle	N/A	N/A	53.0
Poisson's ratio	0.14	0.09	N/A

**Table 4-4: Material properties of models**

Test identification	Roller type	Roller weight (Kg)	Roller position	Completed pass number
S3D-1B	steel	11.8	whole width	18
S3D-1R	steel	11.8	whole width	14
S3D-2B	steel	11.8	whole width	14
	half lead	7.7	half width (centre)	6
	half lead	7.3	half width (front edge)	6
S3D-2R	steel	11.8	whole width	14
	half lead	7.7	half width (centre)	6
	half lead	7.3	half width (front edge)	6
S3D-3B	lead	14.9	whole width	14
	half lead	7.7	half width (centre)	6
	half lead	7.3	half width (front edge)	6
S3D-3R	lead & steel	12.2	whole width	14
	half lead	7.7	half width (centre)	6
	half steel	5.8	half width (front edge)	6
D3D-1B	lead	14.9	whole width	14
	half lead	7.7	half width (centre)	6
	half lead	7.3	half width (front edge)	6
D3D-1R	lead & steel	12.2	whole width	14
	half lead	7.7	half width (centre)	6
	half steel	5.8	half width (front edge)	6

Table 4-5: 3-D tests applied rolling loads



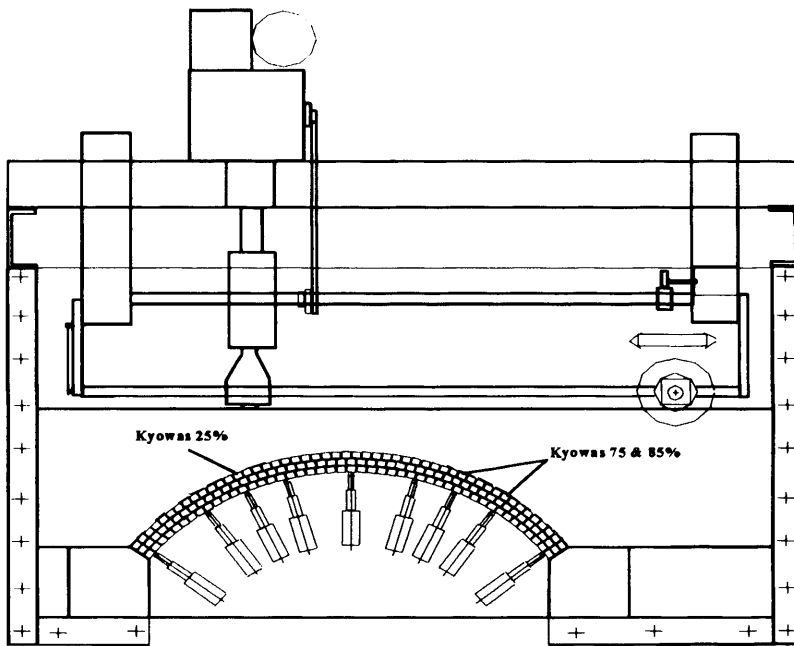


Figure 4-1: General view of 2-D models

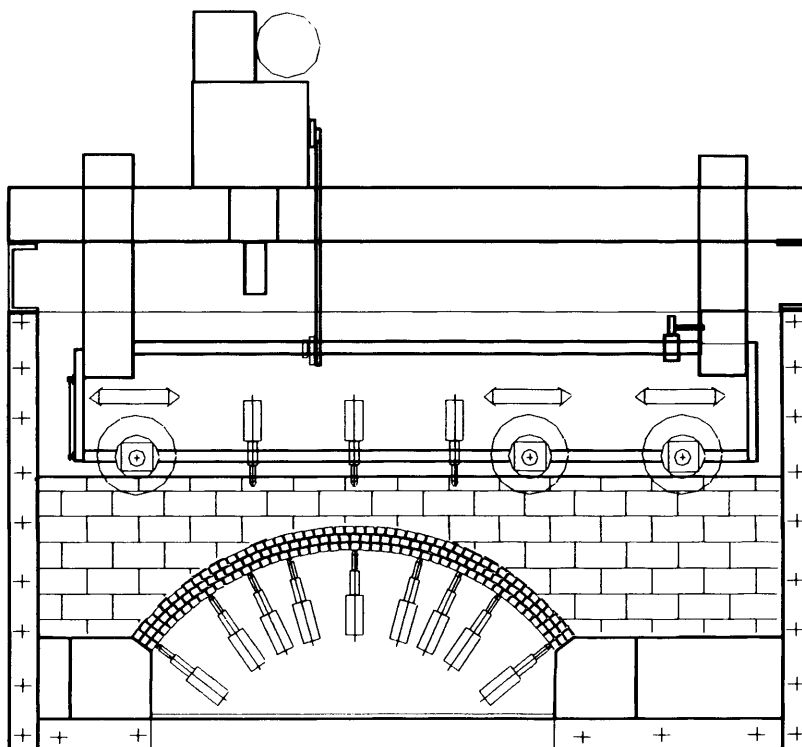
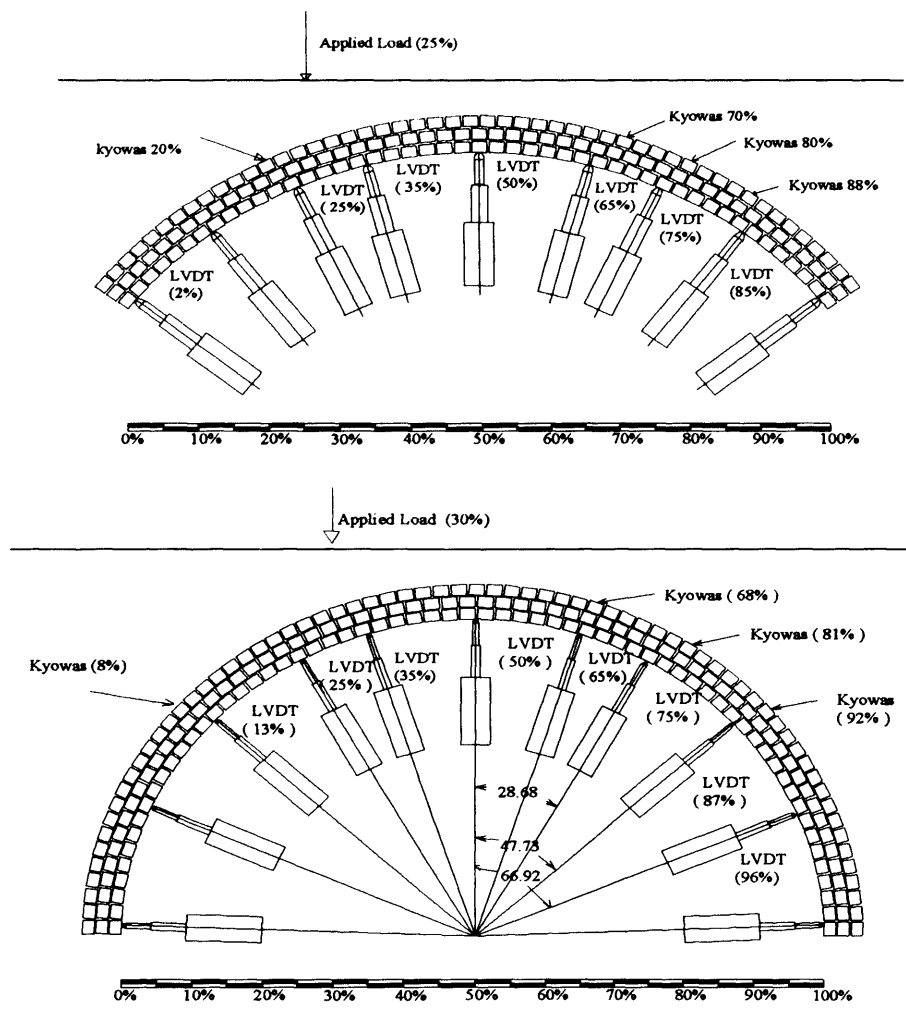


Figure 4-2: General view of 3-D models



**Figure 4-3: Arch barrel and model instruments locations**



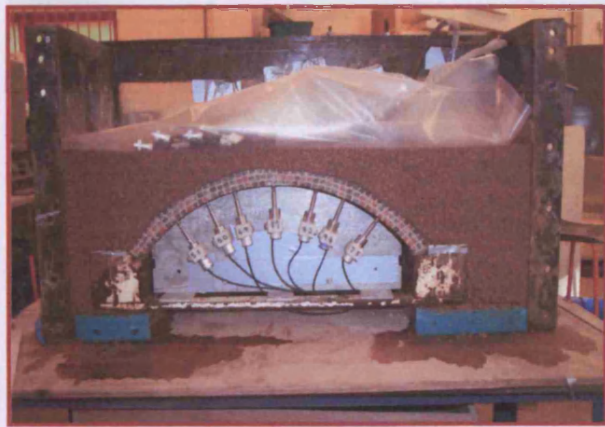
(A)



(B)



(C)



(D)

**Plate 4-1: 2-D shallow arch model construction procedure**

*Faint text: Plate 4-2: 2-D deep arch model construction procedure*





(A)



(B)



(C)



(D)



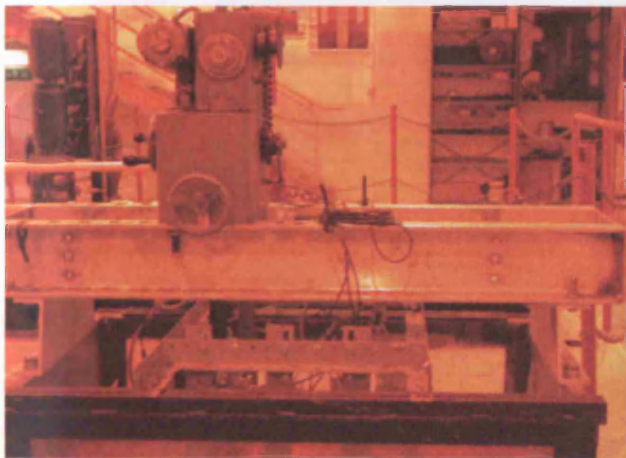
(E)



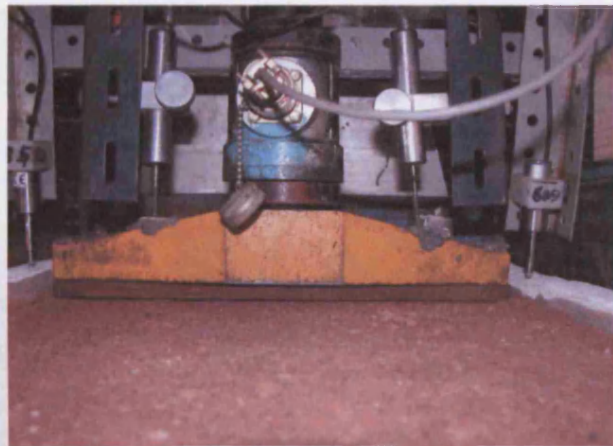
(F)

Plate 4-2: 2-D deep arch model construction procedure





(A)



(B)



(C)



(D)

**Plate 4-3: Load system**

Plate 4-4: 3-D arch model construction procedure





(A)



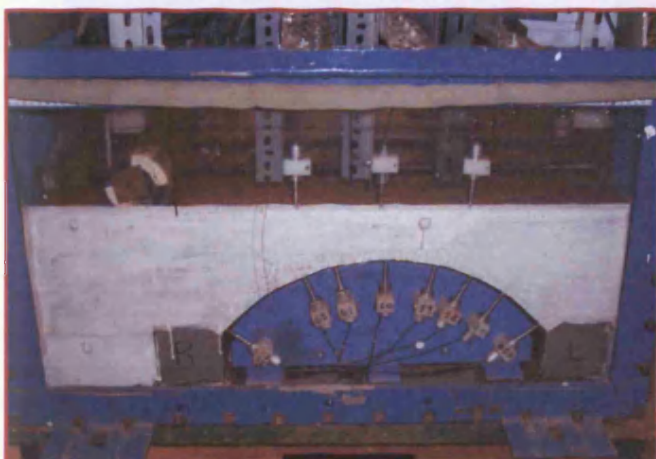
(B)



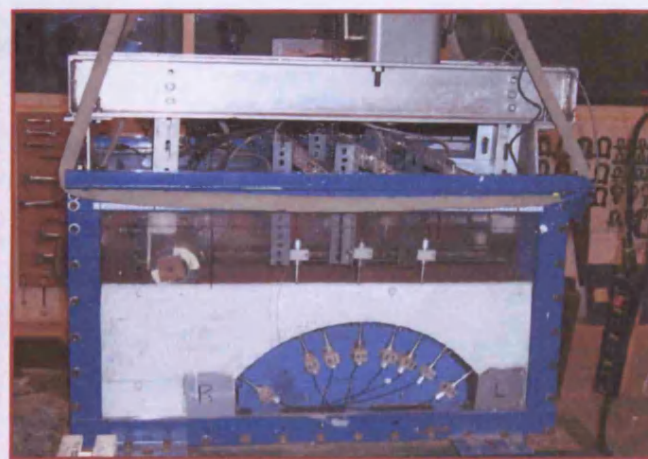
(C)



(D)



(E)



(F)

Plate 4-4: 3-D arch model construction procedure





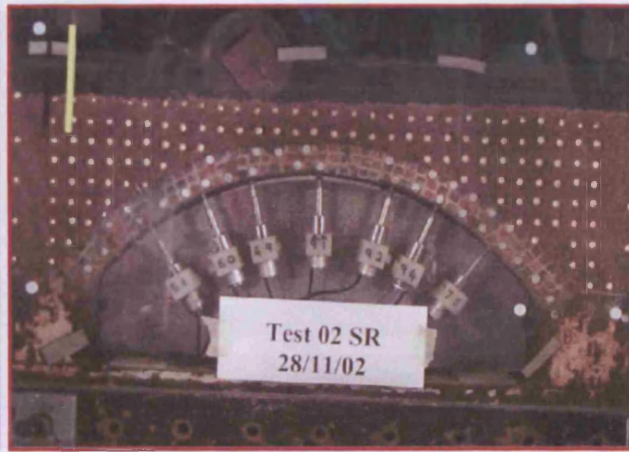
(A)



(B)



(C)



(D)

Plate 4-5: Plastic mesh repair method

Plate 4-6: Concrete slab repair method





(A)



(B)



(C)



(D)



(E)



(F)

Plate 4-6: Concrete slab repair method





(A)



(B)



(C)



(D)



(E)



(F)

Plate 4-6: Spandrel wall strengthening method

Plate 4-7: Partial concrete slab repair method





(A)



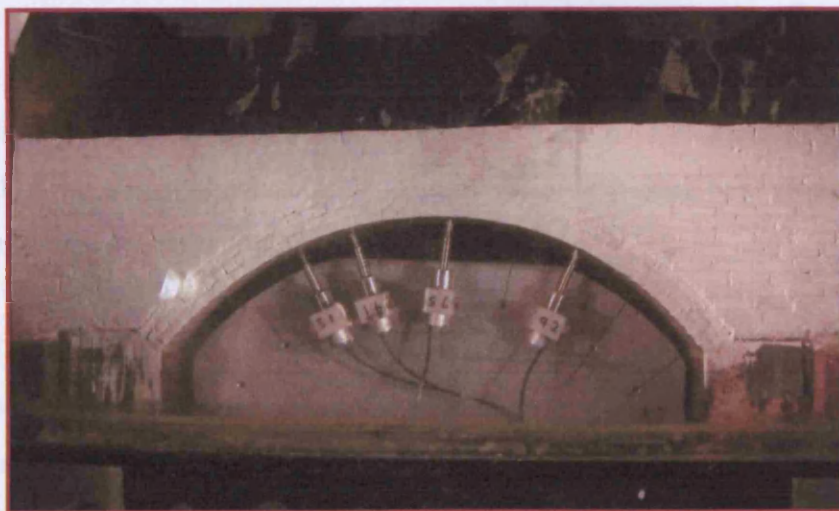
(B)



(C)



(D)



(E)

**Plate 4-8: Spandrel wall strengthening method**

## **5 Benchmark tests and results**

### **5.1 Introduction**

Masonry arch bridges are complex structures and many parameters effects their behaviour and ultimate load capacity. The masonry, backfill and the pavement are the main components and many tests have been carried out to understand the effect of these parameters on arch behaviour. In recent years, experimental work has moved more from assessing existing load capacity towards investigating methods to increase capacity. However most of these experimental tests were carried out on full scale models whilst some small scale tests have been carried out at Cardiff University (Baralos 2002; Burroughs 2002). The main objective of the current study is try to understand the behaviour of repaired masonry arches and study the effect of applying different repair methods. Small scale arch models were tested under the rolling load and increasing load initially to provide suitable models for repair. This stage of tests is called benchmark tests in this thesis. Repaired models were tested with the same roller and increasing load but up to the full failure in the last case. Therefore, arch model behaviour was recorded at benchmark and repaired condition during the tests.

The current study is divided into two major groups of 2-D and 3-D models. Two types of arch geometry models (shallow and deep arch) were tested and significant amounts of data such as deflection of the arches in different sections, pressures on different locations of the arch barrel and quantity of applied load were measured during the tests. This chapter reports the results of both the 2-D and the 3-D benchmark tests. The 2-D and the 3-D arch model results are presented in different sections and in each

section, model details are presented first. Arch model behaviour under the rolling and increasing load is detailed separately in each case.

## 5.2 The 2-D benchmarks tests

Although some researchers built models with artificial faults to make them suitable for repair (Gilbert 1993; Sumon 1997), in a previous study on small scale centrifuge models suitable models for repair were provided by loading them until observation of the first sign of failure (Baralos 2002). In this approach the benchmark test included testing with a rolling loading followed by increased loading up to a significant percentage of the ultimate load. The arch was then repaired and the rolling and increasing load test repeated. In the repair test, full failure was achieved. Therefore, arch response under the roller and a significant part of the increasing load became clear and the repaired arch behaviour is comparable with this data. It was decided to follow this procedure in the current study; models were therefore tested in two stages, which are called benchmark and repair tests in this thesis.

Both benchmark and repaired models were tested with the rolling loads and increasing loads. The rolling load usually included 14 passes of the roller from one side to the other side of the arch in the longitudinal direction. The left inner side of the arch span is indicated by 0% of the arch span and right inner side of the arch is indicated by 100% of span. The roller was usually moved between -5% and 115% of the arch span. After completion the rolling load tests, the roller system was removed and was replaced by the increasing load mechanism. The increasing load was applied to the whole width of the arch from the top surface of the backfill and the amount of the load was recorded during the tests using a load cell. The loading was stopped when the first sign of failure was exhibited. This usually appeared as a visible crack under the load position. In some cases under the applied load region some ring separation between bricklayers was observed. In addition the load deflection results were monitored for signs of impending collapse. Four 2-D arch model tests were carried out, three of them with the shallow and one with the deep arch geometry. Details of models under tests and their instrumentation are given in Table 5-1.

### **5.3 The 2-D benchmark results**

It was decided to build the first 2-D arch model and test it up to collapse to check the instrumentation and repeatability of the tests. This shallow arch test was carried out without any repair to it. The results obtained from this test, which is called S2D-1B, were compared to the average behaviour of the tests that had been carried out previously. All the other 2-D arches were repaired when the benchmark tests were completed. Arch deflections and pressures on different locations of the arch spans were measured during the tests.

#### **5.3.1 Rolling load results**

Two general series of data were recorded during the tests in the current study. The first series were radial deflections of the arches under the rolling and the increasing load and the second series were pressures on the arch barrel extrados at different sections.

In all the benchmark tests the radial deflections under the rolling and the increasing loads were measured using two rows of LVDTs (except test S2D-3B). The first LVDT row was installed beneath the arch barrel along the centre line and the second parallel to it and near to the front side of the barrel. Recorded data is indicated by the prefix M and F for the middle and front edge row in the database and related figures. Because a limited numbers of channels were available to transfer recorded data from the centrifuge pit to the data accusation the numbers of LVDTs installed in the two rows are different. Arch deflections in test S2D-3B and test S2D-3R were measured only along the centreline of the arch because the LVDTs were used on the other tests at the same time.

##### **5.3.1.1 Arch/deflections under the rolling load**

For first 2-D arch fourteen passes of the steel roller were carried out prior to the ultimate load test. In seven of these passes, the roller was moved from the left side to the right and visa versa. Unfortunately, poor results were obtained from the LVDTs which were installed in left side of the arch during this test. This was because of an existing minor gap between the LVDTs and arch barrel at the start of the test in that part of the arch.

Figure 5-1 A-C details arch deflection at 50%, 75%, and 85% of the span under the steel rolling load in test S2D-1B, as typical arch deflections recorded during the tests. The deflections obtained from both middle and front edge LVDTs are given in these figures. Deflections were zeroed prior to the start of moving the roller at a steady 12g. From these figures it can be seen that the maximum deflection was measured at mid section of the arch span when the roller was located directly on top of that section. This confirms the results from the small scale tests carried out by the other researchers (Baralos 2002; Burroughs 2002; Burroughs et al. 2001). This is due to the smaller backfill depth at the crown compared with the other sections. While the major part of the roller load was resisted by the arch barrel when the roller was located on the crown, the roller load was distributed to a bigger area and caused a smaller effect on the arch barrel when it was located remote from the crown. The overall deflections of the arch barrel were inward and progressively larger deflections were recorded over the test periods. This was due to the compaction effect in the earlier passes. Compacted backfill is stiffer and therefore changes in deflection under load was smaller.

Symmetric arch behaviour in the out of plane direction is expected under the rolling load because the roller load was applied symmetrically on the whole width of the arches. Therefore, the same deflection recorded by both LVDTs in each arch section was expected, which was generally confirmed by the test results. The deflections recorded by the middle and the front edge LVDTs at 50% and 75% of arch span are compared in Figure 5-2 A-B for test S2D-1B. Deflections are taken from the final forward roller pass (F7) and were zeroed prior to the roller moving at the start of this pass. Consideration of the results presented in this figure indicate a reasonable consistency between the middle and the front edge recorded deflections. While approximately the same deflections are recorded at the front edge and the middle of the arch at 50% of the span some differences are observed in the values recorded at 75% of the span. The maximum deflections recorded at the front edge is about 10% more than the value measured by the middle LVDT at 75% of the span in test S2D-1B. Approximately the same results were obtained on the other shallow arch models. The arch deformations under the middle and the front edge at 50% and 75% of the span are presented in Figure 5-3 A-B for test D2D-1B at the last forward roller pass. The figure shows that the maximum deflections are located directly under the roller position. Some outward movements were recorded when the

roller was located remotely from the selected LVDT. As with the shallow arches there is good consistency between the measured deflections under the edge and the middle of the arch barrel under the rolling load but more variation between the values recorded on the middle and front edge particularly at 50% of span on the deep arch. While the maximum deflection of 0.13mm was registered by the front edge LVDT at 50% of the span, the maximum value of 0.09mm was recorded at the middle of the arch at the same section. Some differences were registered between the edge and the middle arch deflections on the other sections, but these differences are very small and in general, recorded behaviour from both rows of LVDTs are equal. Unfortunately, there are no recorded deflections on the back edge of the 2-D models and therefore consideration of the out of plane model behaviour is not possible. The middle row results were selected and presented later as an average of the 2-D test results.

As many tests were carried out during this study, the average behaviour of the arches is needed. Arch deflections against the roller location at pass F7 are presented in Figure 5-4 A-C for all tests including the average behaviour. Recorded data from the deep arch tests are also included in this figure but it is not used in the average determination. The deflections at 25%, 50% and 75% of arch span are presented in the figure and the deflections were zeroed prior to starting the roller at the start of the roller passes. As seen from Figure 5-4 A-C maximum deflections were recorded when the roller was located on top of each section and the deflection at 50% of the span were more than at the other sections. Radial deflection at 75% of span is about 70% of arch deflection at mid span, while this ratio is about 40% at 85% of the span when roller is located directly on top of these sections. This can be expected because of the load distribution through the backfill. Rigid abutments at the beginning and the end of the arch span restricted the movement of the arch and recorded deflections at these sections are very small. Inward movements were registered at 25% of spans for all tests when the roller was located on the left side of the arch (0%-50% span) and outward movements were registered when the roller was located on the right part of the span. The inverse is true for recorded movements at 75% of span.

Test results under the rolling load show that the number of passes has an important effect on the recorded arch deflections. Figure 5-5 details the effect of the number of

passes on the arch deflection at 50% of the span for test S2D-1B when the roller is moving in a forward direction. The zero datum was placed at the start of each pass. The plot indicates that with an increasing number of passes the arch deflections decreased but the reduction rate decreased with increasing pass number. The same responses were observed in the other tests. This can be attributed to the increasing pass numbers increasing the fill compaction. As soil becomes more compact, it not only becomes stiffer but its ability to distribute load improves. The rolling load is then distributed over an increasingly large proportion of the arch barrel with each pass and therefore the rate at which the arch deforms was reduced. This is confirmed by the test results on centrifuge arches models reported elsewhere (Burroughs 2002). The other aspect of the soil behaviour also influences outward deformation on remote parts of the arch barrel. As the backfill becomes more compact, its stiffness increases and therefore the resistance to the arch sway provided by the backfill gradually increased, and smaller outward deflections were expected with increasing pass numbers. If sufficient compaction of the soil were achieved due to the passes, the arch deformations would tend to a constant value. The plot indicates these conditions were not completely achieved during the tests, due to the limited time for the test and the possibility of drying backfill no more passes of the roller were carried out during the tests. The behaviour of the arch at the final pass roller is generally presented as the arch behaviour under the rolling load, during the current study.

The average deformations of the shallow arch tests at different positions of the span under the final pass of the roller in the forward direction are presented in Figure 5-6. The zero datum is placed at the start of the forward movement for all positions. The same data for the final pass, but in the backward direction are detailed in Figure 5-7. The deflections were zeroed at the beginning of the backward movement. These figures indicate the effect of pass direction on the arch movements. If there was no effect of pass direction on the arch movements symmetrical behaviour would be expected at mid section of the arch span. However, consideration of Figure 5-6 shows that for an equivalent roller position either side of the crown more deflection was observed in the right part of the arch when the roller moved in the forward direction. The reverse is true for the backward direction. As can be seen from Figure 5-7, more inward deflections were recorded in the left side of the arch in an equivalent roller position in the backward direction. This indicates the effect of pass direction on the arch movements. The effect of movement direction on arch



deformation is better demonstrated through consideration of the deformations recorded at 25% and 75% of the span, when the roller moved in both directions. When the roller was moving in the forward direction the larger inward deflection was recorded at 75% of the span, while the larger deflection is associated with 25% of the span in the backward moving direction. In other words, while the same deflections are expected as a symmetrical arch geometry, larger inward deflections were recorded at the right side of the crown when the roller was moving in the forward direction. The reverse is true in the backward direction and the larger inward movements were registered at left side of the arch. Consideration of these figures indicates that the deflections are a function of the arch condition at the start of each movement. In the other words, the initial condition of the arch at the beginning of each roller movement is different with each subsequent pass. When the roller was located far away from the left abutment, at about 115% of the span at the end of the forward direction, the arch swayed toward the left side and sway under the backward direction was restricted. The same behaviour was true when the roller was located at the end of the backward direction (at about 5%) but this time the arch swayed to the right and more movement in that direction under the forward pass was resisted. To avoid the effect of the initial condition of the arch which is due to lack of fit, the average arch position at the end of each direction was determined and the arch movements were compared to it. The arch movement at the final pass in the forward and backward direction are compared to each other in Figure 5-8. The average arch condition at the end of the forward and backward direction was considered as the initial condition of the arch model in this figure. As seen from this figure, for the same roller location, more inward deflection are obtained at 25% of the span when the roller was moving in the forward direction, while more deflection was obtained at 75% of the span when the roller was moving in the backward direction. This is considered to be because of the existence of the surface shear stress in roller movement (Burroughs 2002). The resultant force acting to cause the local deformation is a combination of the dead weight of the roller and the secondary surface shear forces. When the roller moved in a forward direction the surface shear force acted in a direction which provided a force that was more normal to the arch barrel and consequently the deformations were large. When the roller moved in the backward direction, the additional surface shear force acted in the direction which reduced the resultant force supplied to the arch barrel and with it the magnitude of deflections. When the roller was positioned remotely from the given location on the arch

barrel, the arch generally swayed outwards. Consideration of recorded movement at 25% and 75% of the arch barrel indicated no significant effect of the roller movement direction on arch barrel outward displacement.

### 5.3.1.2 Pressures on the extrados of the arch under the rolling load

Pressures on the extrados of arch barrel were recorded using Kyowa pressure sensors during the tests. Comparisons between the predicted normal pressures under the backfill self weight and observed pressures prior to application of the rolling load are presented in Figure 5-9. The at-rest condition was assumed in the calculation (Poulos and Davis 1974) and measured values were achieved at a 12g steady condition. Test results are identified with their related names in the figure. It was assumed that there was no inward or outward movement of the arch barrel into the soil and the data were zeroed prior to starting the centrifuge. The pressures increase from the crown towards the abutments because of the increasing depth of backfill above the sensors. Consideration of Figure 5-9 shows that the observed pressures generally has good agreement with the theoretical values except for the recorded pressures at 50% and 81% of span at S2D-1R and D2D-1R respectively. In these two cases, the recorded data is significantly higher than the other tests and theoretical values. This might be the result of a concentrated applied load on the sensors, for example a piece of granular stone may be resting on the diaphragm in a point. Recorded raw data have shown (not presented in figure) that the pressure in the S2D-3B and D2D-1B tests were smaller than the other recorded pressures. This is because of the smaller backfill depth at the crown compared with the other tests. In the two tests backfill depths were 13mm. Therefore, recorded pressures were modified by adding the theoretical pressures due to the 17mm layer of the backfill and presented in the figure. Modified pressures show good agreement with the calculated and the other tests results. The average pressure achieved from the previous small scale centrifuge tests (Baralos 2002) are also presented and identified by *B.Av.* in this figure. Good consistency between the current test results and previous recorded data was observed which shows the good repeatability of the tests.

Figure 5-10 shows a typical pressure that was recorded by pressure sensors during the tests as the rolling load traverses across the arch. The presented results are related to

the pressure sensors at 75% of span for tests S2D-1B. The recorded pressures from both the front and back sensors are presented in the figure. Good correspondence was achieved between the pairs of sensors during the tests although some variations between the recorded data were observed which is acceptable for this type of tests. There is no specific reason for those differences but it might be as a result of the behaviour of the backfill bridging over the sensors or applying a concentrated load on a sensor. As can be seen from Figure 5-10 the pressure depends on the pass number, roller position and the rolling load movement direction.

The pressures on the extrados of the arch barrel are affected by the roller dead load and arch movements. When the roller was located on that part of the arch where the sensors were installed the pressures are largely dependent on the roller dead weight, while when the roller was located remotely from the sensors the pressures depends on how the barrel moves relative to the backfill. When the roller is positioned on top of each sensor, the effect of the roller weight was distributed through the backfill and the recorded pressure is affected by the roller weight. Reduction on this effect was observed with increasing the backfill depth. The peak pressures were registered when the roller passed over each pressure sensor. Figure 5-11 presents the peak pressures recorded during the tests under the rolling loads and compares these values with theoretical values. Theoretical values were calculated according to the elastic theory (Poulos and Davis 1974) and the UK practice (Department of Transport 1997b). Elastic theory and the UK practice results are identified by *Elastic* and *Code* respectively in the figure while tests results are indicated with their related names. Elastic theory and the UK code yield very similar results while the benchmark test recorded values which are smaller than both methods. Differences between the recorded data and calculated values are expected because in the elastic method the effect of the arch barrel movement is not considered. No pressures were recorded at 50% of arch span in a previous study on small scale centrifuge arch models (Baralos 2002) but those reported for the other sections of the arches are comparable with the current recorded values. It is suggested that for the arch barrel locations near to the abutments the influence of the roller weight decreased.

When the roller is located remotely from the recorded pressure position, changes in pressures depend on how the arch barrel moved with respect to the backfill. Movement of

the arch away from the backfill mobilises active pressure while movement of the arch towards the soil mobilises the passive pressure. Figure 5-12 A-C details recorded pressures against the roller position for the final forward roller movement for the shallow arch tests. As can be seen from the figures, the peak pressures were registered when the roller was located directly on top of each pressure sensor for all the tests. For those sensors located on the left side of the crown after achievement of the peak pressure a significant reduction in pressure was registered when the roller passed over the sensors. This suggests an effect of the arch moving away from the backfill and a mobilised active pressure condition. However inward movements in the backfill occurred as well, but it is suggested that the rate of the backfill inward deflection is smaller than the arch barrel deflection rate. Therefore an active condition is generated and reduction in pressure is observed when the roller approached the crown. When the roller was located on the left side of the arch and moved in a forward direction small changes in pressure were recorded by remote sensors until the roller passed the crown. When the roller moves onto that part, the arch sways to the backfill on the right side, which is where most of the sensors were installed. This is a mobilised passive pressure condition and increases in the recorded pressure are expected. As Figure 5-6 indicates the arch outward movement is very small and therefore small changes in pressure were observed. A previous study (Burroughs 2002) shows that the maximum passive pressures were recorded when the arch sways about 0.4mm toward the backfill and in this case the arch movement is smaller than that value. When the roller is directly located on top of each sensor position the roller weight is the most significant part of the recorded pressure and therefore a higher pressure is expected. As the roller moves to the right of the sensors this was reversed and a large proportion of load is applied to the backfill and a smaller proportion to the arch barrel therefore a reduction in pressure is expected.

The recorded pressure at each section increased with an increase in the number of passes. Figure 5-13 indicates the recorded pressure at 50% of the arch barrel against the roller position for different pass numbers. The figure shows a high rate of increase in pressure for the first passes and lower rates for the later passes. Consideration of the Figure 5-5, which present the arch deflections against the roller location, indicates that the arch deflection decreased with increasing pass number. Because of the decrease in the deflection due to pass number an increase in the pressure is expected to occur.

The effect of roller pass direction is presented in Figure 5-14 as a typical result. In this figure, the forward and backward roller direction for the final forward and backward passes in test S2D-2B are compared to each other. It can be seen from this figure, that a bigger pressure is recorded when the roller moved in a backward direction. This is thought to be because of the existence of the shear force in movement direction as explained previously.

### 5.3.2 Increasing load results

The increasing load was applied to the whole width of the arch from the surface of the backfill in all the benchmark and repair tests. It was applied to the quarter point of the arch span for both the shallow and the deep arches. To understand the behaviour of arches under cyclic loads, an initial loading and reloading was applied as part of each test. Details of the tests, the load cycle and the peak loads in each test are presented in Table 5-2. This table includes the arch condition and details of any damage to them after each test.

In test S2D-1B the applied load was increased up to 95% of the ultimate load and then completely unloaded. The arch was then loaded up to full failure as there was to be no repair of this model. The ultimate load value of 6.2kN was recorded in this test, which is about 5% more than the average results achieved in a previous study for the same arch geometry (Burroughs 2002). This shows good agreement and indicates the good repeatability of the tests.

In model S2D-2B the first load/unloading was applied at 35% of the peak load. The second and third load cycles were applied at 2.5kN and 3.3kN, which is about 49% and 66% of the peak load for this test. The load system was stopped at 5.0kN because of the high rate of increasing deflection under the load position. It was considered that the arch was suitable for repair at that condition. Inspection after the test showed visible cracks under the applied load position.

Two load cycles at about 49% and 73% of the peak load were applied in test S2D-3B. The first visible crack was observed at 4.6kN beneath the load in this test. No visible ring separation in the arch barrel was observed at this load level.

The applied load was stopped at 4.8kN in test D2D-1B. Two load cycles at about 44% and 60% of peak load were applied in this benchmark test.

### 5.3.2.1 Arch/deflection under the increasing load

The arch deflections at different positions of the span in test S2D-2B are detailed in Figure 5-15 as typical results of the increasing load. The deflections were zeroed at a steady state of 12g, prior to starting the increasing load. Inward and outward deflections under the load side of the arch and remote from the load position are clearly seen in this figure. The load cycle, which was conducted as a part of the benchmark tests, is clearly indicated. In perfectly elastic structures, the structures move back to the original position when the load is removed. Detailed results in Figure 5-15 and the other results obtained from the benchmark tests show that this is not true for the arch models under tests. The results indicate that only a small percentage of the arch deformation was recovered, even at low load levels. The same result was reported by other researchers (Burroughs 2002; Sicilia 2001). This indicates the plastic behaviour of the arch models which might be as a result of the behaviour of backfill materials which effect the overall structural behaviour. Figure 5-15 indicates that at low load levels the deflections induced by re-load are equal to the deflection under the original load. This behaviour was observed in all the benchmark tests where the load/deflection curve was approximately linear.

To have a comparable load/deflection response the load cycles were omitted and the same series of load/deflections for all tests were produced. Figure 5-16 A-C details the load movements at different LVDT locations for all the benchmark tests. Increasing load against arch movement at 25%, 50% and 75% of the arch spans are presented in this figure. The average behaviour for both shallow and deep arch geometries, which was achieved under the load locations of the previous study (Burroughs 2002), is included in this figure. It should be noted that the first arch was loaded up to the full failure and in the other benchmark tests the load was stopped as soon as the first sign of failure was observed. Therefore, the ultimate load was not achieved on these tests and comparison between the previous average ultimate load and these benchmark tests loads is not reasonable.

Consideration of Figure 5-16 indicates that the maximum arch inward deflections were recorded under the load position and at 75% of arch spans the maximum outward deformation were observed. Some variation between the deflections and the stiffness of models are seen and that is reasonable and expected for this type of structure. Good consistency between the tests results were observed and non-linear arch behaviour can be seen from the figure. The first shallow arch (S2D-1B) collapsed at 6.2kN which is about 5% higher than the average benchmark tests results (5.8kN) on a similar arch geometry from the previous study. The maximum inward recorded deflection under the load position was 3.4mm for this test which is comparable with 3.5mm under the same position reported by Burroughs (Burroughs 2002).

Consideration of the results show that the weight of the strip footing varied from about 11% of the maximum load in S2D-1B to 15% of it in test S2D-3B. The average weight of the strip footing is about 13% of the maximum load for the 2-D shallow arch benchmark tests. This value is well within the elastic range of behaviour and is therefore considerable acceptable.

As was noted in section 5.3.1.1, the 2-D tests deflections were recorded using two rows of LVDT which were installed at the front and the middle of the arch barrels. Comparison between the recorded deflections under the middle and the edge are presented in Figures 5-17 and 5-18. In these two figures, the arch deformations under the load position (25% of span) and 75% of spans are detailed as representative inward and outward movements for the deep and the shallow arches. Consideration in these figures indicates that the recorded deflections under the edge and the middle of the arch are approximately the same until about 50% of the peak load for both arch geometries. More deflections were observed in the front edge for the shallow arch while in the deep arch, larger deflections were recorded by the middle LVDT. Smaller deflections under the edge of the arch are might be due to out of plane bending resulting from the existence of some friction between the front rigid wall and the backfill but there is no explanation for the recorded behaviour in the shallow arch. Unfortunately, only one LVDT row was installed in S2D-3B and there is no recorded data under the edge of arch barrel for this test. In order to allow comparison, the results achieved from the middle LVDT row is later used as representative of the 2-D arch behaviour under increasing load.

Arch deformation under increasing load is presented in Figures 5-19 A-D for each test. Consideration of the figure shows that significant movement did not occur until about 50% of the maximum load. In test S2D-2B, 20% of maximum deflection occurred at 50% of the maximum applied load, where in test S2D-3B at 50% of the maximum load just 15% of the ultimate deflection was registered.

### 5.3.2.2 Pressures on extrados of arch under the increasing load

Small scale centrifuge tests on arch bridges, carried out by Taunton (Taunton 1997) showed the significant effect of backfill on arch load capacity. Tests results on small scale models reported by Fairfield and Ponniah (Fairfield and Ponniah 1994a) have also shown soil/structure interaction contributed significantly to the capacity of the model arches. From their research work they have reported that increasing the fill depths at the crown increased the arch load capacity. This increase was made up of contributions from the increased dead load and from the increased live load dispersal. The increase arising from the increased dispersal was considered dominant. Although the significant effect of the backfill on arch masonry load capacity was accepted there was not much quantitative research in this area identified in the literature review.

The soil/masonry interaction was measured in the current study using pairs of pressure sensors which were installed in some sections of the arch barrel. Most of the sensors were positioned remotely from the applied load point to measure the mobilised passive pressure during the tests. A portion of the arch close to the load point can move inward and away from the backfill. This mobilises active pressure condition in this arch region under the increasing load. On the remote side from the applied load position the arch barrel moves towards the backfill and therefore tends to mobilise passive pressure in that zone (Ponniah 1987). The pressures recorded by a pairs of sensors, which were located at 75% of the arch span in S2D-1B, are detailed in Figure 5-20 as typical obtained results under the increasing load. The pressures were zeroed prior to starting the centrifuge. The recorded pressures are therefore pressure under the self-weight and due to the arch movements as well as load. Good consistency between the pairs of sensors are observed and the effect of the cycling of the load on the pressure is clearly seen. As a result of the arch movement away from the backfill, recorded pressures local to the load



position decrease with increasing applied load. The inverse behaviour was recorded on the side of the arch at the remote from the applied load position. The pressures were increased at remote part of the arch until about 4.0kN (about 65% of ultimate load) and after that, the pressures decreased. This may be because of the first sign of the failure at this load level with hinges developing and the resulting change in the arch behaviour at that load level. A similar behaviour was recorded in most of the benchmark tests in a previous study (Baralos 2002).

The response of the sensors monitoring the soil/arch interface pressures for the shallow and deep arch benchmark tests are presented in Figures 5-21 A-D. The sensors were zeroed prior to starting and the load cycle results were omitted for all the tests to make the results clear and comparable. This figure shows that in all the benchmark tests the pressures increased with increasing load in the part of arch remote from the load point. The pressures then decreased when the load approached failure due to changes in the overall arch behaviour. This may be because the backfill acts as blocks and the failure of the backfill blocks has happened before failure in arch barrel. During the backfill failure, the blocks move away from the barrel and therefore the pressures on the arch barrel suddenly decrease. Unlike the other tests the S2D-3B results show an increase in pressure without any drop during the test. This would suggest that passive pressures are still mobilised by the arch and the failure had not occurred when the load was removed.

Consideration in Figure 5-21 shows that a maximum passive pressure of about 20kPa was obtained by sensors which were installed at 75% of the arch span. This value is about 30% of full passive pressure on that section. This indicate that full passive pressure is not developed on the arch extrados and is consistent with the results reported elsewhere (Burroughs et al. 2002).

### **5.3.3 Post test observations**

After completion each benchmark test model was taken out from the gondola and the selected repair technique was applied to the model. Before starting the repair, each model was investigated and any damage and cracks due to the benchmark test were recorded.

Figure 5-22 A-D details the arch conditions after the benchmark test but before repair. As seen from this figure, failure signs was observed under the load position in all the tests.

A mechanism failure occurred in tests S2D-1B and some ring separation was observed beneath the load location. Ring separation appears to start at the load position and progress down towards the abutment. During the post-test inspection four hinges were found in this test as detailed in Figure 5-22A. No mechanism was found on other tests as the load was stopped before full failure.

#### **5.4 The 3-D benchmark tests**

To achieve comparable results to the 2-D tests the width between the spandrel walls of the 3-D arches were to remain unchanged. The thickness of the spandrel walls was selected as 30mm and therefore, a total width of 405mm was used for the 3-D arch models. A new wider rigid box was therefore designed and the 3-D models were tested in this new box. Both shallow and deep 3-D arch geometries were carried out during the current study.

The objective of the 3-D model tests was to try to quantify the difference between the behaviour of the arches with and without spandrel walls under the rolling load and the increasing load. To make the testing easier for comparison between those two types of models the same rolling loads were used in both 2-D and 3-D arches. The 2-D and 3-D arches were built with essentially the same geometry, masonry, mortar and fills. Three tests on 3-D shallow and one on a deep arch geometry were conducted, which are detailed in Table 5-3.

#### **5.5 The 3-D benchmark tests results**

The 3-D test details are presented in Table 5-3. The arch models were tested using the 2-D test procedure but with different types of rolling load cases. The different types of the applied rolling load case are contained in Table 5-4. A general view of the 3-D arches with instrumentation and the applied rolling loads is given in Figure 5-23. Arch deflections were measured via two rows of LVDTs, which were located along the centreline and close to the front face of the arches in S3D-1B. The LVDTs were located

at 2%, 15%, 25%, 35%, 50%, 65%, 75%, 85%, and 98% of the span. In addition, vertical movement on the top of the spandrel walls were similarly measured. Readings were recorded at 6-second intervals throughout both the rolling and increasing load tests. Pairs of soil pressure sensors placed across the arch usually, at 7%, 15%, 65%, 75%, and 85% of the arch span were used for measuring the pressures on extrados of the arch barrel.

After completion of test S3D-1B and processing of the results, it was decided to make some changes in the instrumentation and the rolling load test procedure. This was because of the out of plane observation during the first 3-D test. Therefore in the other 3-D tests the arch deflections were measured using three LVDTs rows beneath the arch. With these measurements, a better representation of the arch 3-D behaviour would be possible. Four LVDTs were usually installed in 25%, 35%, 50% and 75% of arch span in the front and back rows and six LVDTs were placed under the centreline row. Behaviour of the arch under symmetric and unsymmetric rolling loads was tested by applying different rollers at different positions on top of the fill. To prevent any unwanted compaction in some part of the backfill due to unsymmetric loads, the symmetric roller load was first applied on whole width of the backfill. The roller location in each Load Case is presented in Figure 5-23. After the completion of 14 passes of the roller on the whole width of the arch, which is called Load Case 1, the roller was replaced by a half weight roller (half width), which was applied along the centre of arch. Six passes of this roller was applied and then the roller position was changed to the front half width of the arch. These two Load Cases are called Load Case 2 and Load Case 3 in Figure 5-23. The rolling loading was centred about the centre line of the bridge in the Load Case 1 and Load Case 2. In the Load Case 3, the roller was centred about a line 75mm from the centre line of the bridge. The roller weights used and their applied locations for all tests are detailed in Table 5-4.

An increasing load was applied to the whole width of the arch (between spandrel walls) using the same procedure as the 2-D tests and load cycles were applied in each case. Recorded deflections and pressures under the rolling loads and the increasing loads are presented and discussed in the next sections.

## 5.5.1 Rolling load results

### 5.5.1.1 Arch/deflections under the rolling loads

The first 3-D shallow arch benchmark model (S3D-1B) was tested with eighteen passes of the steel rolling load. This load represents 12 tonnes on a 2.5m axle at prototype scale. The arch deflections measured by the LVDTs located at 35%, 50% and 75% of span against the roller positions are plotted in Figure 5-24 A-C as a typical result of the 3-D arch models. The deflections at the edge and the middle of the arch at pass 6, 14 and 18 are compared with each other in this figure. Consideration in this figure shows that the overall behaviour of 3-D arches under the rolling loads is the same as the 2-D models. The maximum inward movement in each section was recorded when the roller located on top of that section and outward movements were recorded when the roller located remotely from the selected LVDT. When the roller traverses the arch the maximum deflection was registered at the mid section of arch locally under the roller. However the recorded deflections decreased with increasing roller pass number but the results show that there were no significant differences between the measured deflections at pass 14 and pass 18. While the maximum inward deflection of 0.08mm was recorded at 50% of the span at pass 6, the maximum value of 0.07mm was measured for both passes 14 and 18 at the same section. Therefore, it was decided to test the other 3-D models with 14 passes of the roller.

The results indicate significant differences between the recorded deflections at the front edge and the middle of the arch in all sections. Consideration of Figure 5-24 shows that the deflections under the middle of the arch are significantly larger than the deflections under the edge at the same section. The registered deflections at the front edge of the arch are about half of the recorded values at the middle for 25% and 75% of the span. The difference at the crown of the arch is larger than this, while the deflection of about 0.08mm was recorded at the middle; the maximum deflection of about 0.03mm was recorded by the front edge LVDT. This confirms 3-D behaviour of the model even under symmetrical and low loads levels (Hughes and Miri 2004). Unfortunately, there was no data recorded on the back edge of this arch.

Consideration of the results from test S3D-2B show big differences between the recorded deflections along the centreline of the arch and the edges even under the symmetrical loads. When the roller was located at 25% of the arch span the recorded deflection by the middle row LVDT is about 1.5 times of the deflection at edges of the arch at that section. Approximately the same deflections values were registered at both edges. This indicates out of plane bending of the arch and the effect of the spandrel walls stiffness on the edges deflection. Unfortunately, there is no recorded data at the crown of the arch span along the edge for this test. It should be noted that all the above presented results are related to the roller Load Case 1, and the effect of other Load Cases are detailed later.

According to the results from all shallow 3-D benchmark tests the average behaviour of 3-D arches was determined. The average deflections of the 3-D benchmarks under rolling Load Case 1 at the final pass of the roller in the forward direction (F7) are presented in Figure 5-25. In this figure, the average arch movements recorded by different LVDT rows at 25%, 50% and 75% of the span are detailed. The movements were zeroed prior to starting the roller for this pass. Larger arch deflections under the centre line were generally observed in all sections compared with the both edges of the arches. This happened for both inward and outwards movements and indicates out of plane bending of the arches even under symmetric low roller loads. The average results show a maximum inward deflection of about 0.08mm and 0.06mm in the middle and the edge of the barrel at the crown, respectively, and that indicates the middle arch deflection is about 35% higher than the edge values at the crown while this ratio is about 80% for 75% of the span.

The results under Load Case 1 confirmed the 3-D behaviour of the arches. To understand the behaviour of the arch models under various roller positions two different roller positions were considered under Load Case 2 and Load Case 3. Recorded deflections at each section of the arch barrel, under the different load cases, show different values in the out of plane direction. The effects of the roller load case and position on the arch deflection are presented in Figure 5-26 A-B. In this figure, recorded deflections under the various load cases measured at 25% and 75% of the arch span in the out of plane direction are detailed. The arch deflections at pass 14 under roller Load

Case 1 and pass 6 on the two other rollers (Load Case 2 and Load Case 3) are presented in these figures. All presented data is related to the forward movement direction. It is considered that sufficient backfill compaction was achieved after applying 14 passes of the roller on the entire width of the arch and the increase in passes at later loads will have no significant additional effect on the arch deflections. Therefore, comparison of the results after 6 passes under the other tests with those results obtained after pass 14 are reasonable. The overall recorded deflections for each LVDT under Load Cases 2 and Load Case 3 are less than the results obtained from the Load Case 1. This is expected because the weight of the roller in Load Cases 2 and 3 is about 60% of the roller weight in Load Case 1.

Comparison between the results obtained from tests under Load Case 1 and Load Case 2 indicate the significant effect of the applied load location. The deflection recorded by the LVDT which was installed in the front edge of the arch at 75% of the span, shows that when the load is directly applied on that side, the deflection is 1.6 times that under the same roller weight when it was applied on the centre line of the arch. This ratio is about 1.2 and 3.3 for the results achieved from those LVDTs which were installed under the middle and back edge of the arch, respectively, and shows the effect of roller position very clearly. The same behaviour was recorded in the other sections of the arch barrel.

The deep arch deflections under the roller at the last pass in the forward direction (F7) at different sections of the arch span are presented in Figure 5-27 A-C for the Load Case 1. The recorded radial deflection under the front edge, back edge and middle at 35%, 75% and 85% of the arch span are compared in this figure. Overall no big differences between the recorded deflection by LVDTs at each section were observed under this symmetric load.

#### **5.5.1.2 Pressures on extrados of arch under the rolling load**

Figure 5-28 presents changes in the pressures on the extrados of the arch barrel at different sections for all the shallow 3-D benchmark tests. All available pressures at 15%, 75%, 81% and 85% of span are compared with each other in this figure. The pressures were zeroed prior to starting the roller and relate to pass F7 for Load Case 1. Good consistency between the results were observed in all the tests and approximately the same

maximum pressures were recorded locally to the roller position at each section. For a given position on the right side of the crown (15% of the span) the pressures increased when the roller approached to the sensors and after achieving peak values the pressures decreased when the roller move away from the sensors. The same behaviour was observed in the 2-D tests (Figure 5-12) but the maximum recorded pressures for the 3-D tests are significantly more than those recorded in the 2-D tests. This is possibly as a result of the arch movement restriction caused by the spandrel walls. In the 3-D tests, the spandrel walls restrict the arch movement and therefore a larger increase in the pressure directly under the roller load might be expected. For any sensors located on the right side of the crown, no significant changes were observed when the roller was located on the left side of the crown. Decreases in pressures were recorded (by those sensors located on the right side) when the roller passed the crown and then the pressures increased when the roller was close to the sensors locations. Burroughs (Burroughs 2002) reported a similar behaviour under the same roller load and reasoned that this behaviour is due to shear stress generation dependent on movement direction. The current results indicate that lower pressure values were registered by the sensors, which were installed at larger arch span points. This is as expected because these sensors are installed at a greater depth in the fill and would expect to show evidence of a greater load dispersal through the fill. Ponniah et al (Ponniah et al. 1997) referred to this but they measured greater values on those sensors which were installed at greater depth in their prototype measurements. They justified those unexpected results as the effect of the rigid pavement. In the present study there are no pavements applied with the load being directly to the top of the fill.

The maximum pressures were usually recorded when the roller was locally located on top of each sensor. The general responses of the sensors in the 3-D tests are the same as the 2-D tests but the maximum recorded pressures in the 3-D tests are more than the 2-D tests. Unfortunately there were no pressures at 81% and 88% of the span in the 2-D tests and no comparisons are possible with 3-D results but at 75% of the span maximum recorded pressures in the 3-D tests are approximately twice those of the 2-D results at the same section. This might be expected as a result of the stiffer behaviour of the 3-D test to the load due to the effect of the spandrel walls.

In test S3D-3B, the roller weight was about 25% larger than the two other tests. The measured peak pressures subsequently increased about 55% and 35% for those pressure sensors, which were installed at 75% and 81% of arch barrel. No effect of the larger load was registered by the sensors which were installed at 88% of the arch span. Ponniah et al (Ponniah et al. 1997) registered an increase of about 30% due to a 20% load increasing in a prototype test, which is in a similar to the results achieved in the current study.

Figure 5-29 A-D details changes in the pressures on the extrados of the arch barrel at different sections for the deep arch 3-D test. The pressures obtained by pairs of the sensors at 8%, 68%, 81% and 92% of arch span are compared in this figure. Reasonable consistency between the pressures recorded by pairs of sensors is observed. The maximum pressures were observed when the roller was located on top of each sensor and the maximum recorded pressures are approximately the same as those that were obtained in the shallow 3-D tests at the same depth. While more effect of the roller weight registered near to the backfill surface (68% arch span), passive pressures are more important in deeper sections (92% of arch span).

The pressure on each point of the arch extrados under the roller load can be estimated using current UK practice (Department of Transport 1997b) and elastic theory (Poulos and Davis 1974). The maximum pressures in each sensor under the rolling load are compared with the UK practice and the elastic theory results in Figure 5-30. Good correlation between the theoretical values and the observed pressures are observed. This provides continued confidence in the use of such pressure sensors in the test programme. It should be noted that the presented maximum pressures for each sensor are obtained from all passes in the forward and backward directions during the rolling load tests and in some cases, it is different from those represented in Figure 5-28 for pass F7.

The last two 3-D shallow arches were tested under a half roller width with different applied locations after the completion of the roller load over the whole width of the arch. When the half roller was applied along the centre line of the arch (Load Case 2) the back sensor was about 70mm outside the width of the loader while the front sensor was approximately under the edge of the roller. The front sensors were almost central to the roller and back sensor was far away from roller in Load Case 3 in the plan direction. This



was reflected in the relative magnitudes of the pressures, where the front sensors recorded higher values under Load Case 3. Figure 5-31 details the average pressures near to the front edge along the arch barrel under the different rolling Load Cases. The same data but near to the back edge of the arch is presented in Figure 5-32. The pressures were zeroed prior to starting the roller for each pass and the presented data are related to the pass F7, F3 and F3 in Load Case 1, 2 and 3 respectively. As it is shown in Figure 5-31, the largest pressure values were recorded under the Load Case 1 at 75% of the arch span by the front pressure sensors. While the general response of the front sensors to all Load Cases are similar the maximum pressures of 21kPa, 18kPa and 9kPa recorded under Load Cases 1, 2 and 3 respectively at this section. The difference between the recorded values at 81% of span is smaller and there is no significant difference in the sensors response to the different Load Cases at 88% of span (Figure 5-31 B & C). This might be because of the more important effect of the roller dead weight at the shallower depth.

The effect of load location can be achieved from comparison between the results obtained from Load Cases 2 and 3. In these two Load Cases the applied roller loads are exactly the same and only their applied location in the plane of the arch are different. The data recorded by the front sensor show larger pressures (about two times at 75% of span) under Load Case 3 when the roller is located on the sensor part of the arch compared with Load Case 2. This is expected because for Load Case 3 the roller is centrally located on top of the front sensor but at Load Case 2 the roller is applied far from the sensor position in plane. When the roller is located remotely from the sensor position the same pressures were recorded under both Load Cases. Consideration of the data recorded at the back edge of the arch (Figure 5-32 A) indicates no change in pressures when the roller is applied to the front edge of the arch as the sensor is some distance from the load location. The applied loads, pressures sensor locations and the UK practice load distribution are shown in Figure 5-33 with sufficient scale. The UK practice load distribution assumes no pressure on the back sensors which agrees with the experimental results. Approximately the same pressures were recorded by both the back and front sensors under Load Case 2 as the roller location is approximately symmetric to both sensors.

### 5.5.2 Increasing load results

The increasing load was applied to the arch backfill surface through the whole width of the arches using a 17.5mm spreader beam after application of the rolling load in all tests following the same procedure as the 2-D models tests. Arch movements and soil/masonry interaction were recorded during the tests with some load cycles being applied.

The first 3-D test was loaded up to 5.7kN. At this load level a large displacement was observed and it was thought the load was approaching the ultimate load. In the second test, the load was increased up to 7.3kN without any increase in load displacement rate but at this load level a sudden drop in load increase was observed in the test and therefore the loading was halted at this level. The behaviour of the model 3 was different from the other tests and greater deflections of the arch were observed under the load. Progressive inward displacement was observed under a constant load of 4.6kN and the applied load was stopped at this level in this test. One deep arch geometry was undertaken during the tests and it was loaded up to 6.9kN. The results obtained from the above referenced tests are detailed in the next sections.

#### 5.5.2.1 Arch/deflection under the increasing loads

The arch/deflections beneath the load (25% span), remote from the load (75% span) and at the crown for all the shallow arches are presented in Figure 5-34 A-C. Inward deflections were observed under the load position and outwards on remote location as expected. The 2-D average load/deflection is included in Figure 5-34 A as a comparison. As can be seen from the figures, overall lower deflections occurred at increasing load application in all the 3-D tests as compared with the 2-D tests. This indicates the effect of the stiff spandrel wall contribution to the load resistance.

Spandrel wall deflections are included to Figure 5-34 in order to get a better overall idea of the arch behaviour. In the first two models, the same movement was recorded at the top of the spandrel walls and beneath of the arch barrel up to about half of the maximum load; after that more deflections were recorded beneath of the arch barrel. This may be because of the progress of the crack between the arch barrel and the spandrel walls. Post test investigations and crack observations in that area confirm this.

In test S3D-3B, the arch deflection is more similar to the 2-D results. This is possibly because the crack progress between the spandrel and barrel during the rolling load test in this model. The difference in the deflections recorded from the start of loadings in this test between the spandrel walls and the arch barrel suggest a discontinuity between the arch barrel and spandrel walls prior to starting the increasing load.

#### 5.5.2.2 Pressures on extrados of arch under increasing loads

When the increasing load is applied to an arch, inward movement under the load position and outward remote from the point of load application are expected. With the increase in load at all sections of the arch progressive increase in pressure is recorded, but during load application at a significant part of the load the arch barrel sways away from the backfill under the load position and a decrease in the pressure on that part of the arch occurred. In this region active soil pressure conditions were generated and therefore a reduction in the pressure is expected. Remote from the load position the arch barrel moves toward the backfill and as a result of the passive pressure generation, increases in pressure in that region are expected. The recorded pressures in those parts of arches, which are presented in Figure 5-35 show this increase very clearly for all tests. With increasing load and its approach to the ultimate load the contribution of the hinges to arch behaviour changed. This is indicated by no further changes in the pressure due to increasing load and even pressure reduction near to the ultimate load.

Maximum pressure values of about 40kPa were observed at 88% of the span in test S3D-2B which is 45% smaller than the 65kPa which was reported by Burroughs (Burroughs 2002) as a result of a series of 2-D tests with the same geometries. This pressure is about 35% of the theoretical full passive pressure at that depth. Recent studies show full theoretical passive pressures were not developed at any location along the arch barrel (Burroughs et al. 2002) which is confirmed by the current results. Maximum pressure values of 25kPa were recorded at 75% of the span for all tests while more variations were observed in the maximum pressures recorded at 81% of the span. While the maximum pressure of about 8kPa was obtained for S3D-2B, the maximum value on that section for both the other tests is about 25kPa at that section. It has been suggested

that it is difficult to reliably measure backfill pressures on a moveable interface (Gilbert 1993; Sicilia 2001), particularly when small pressure sensors are used.

The results show smaller passive pressures in all the extrados arch positions compared with the 2-D arches average tests results which were carried out with the same arch geometries (Burroughs 2002). This is to be expected because in 3-D arches the movements were restricted by the spandrel walls and the smaller arch sway in to the soil as compared with the 2-D tests.

### **5.6 The 2-D and the 3-D test results comparison**

Arch deflections and pressures on the extrados of the arch were measured during the tests for both 2-D and 3-D arch models. The average 2-D and 3-D shallow archs displacements during the final pass of the roller in the forward direction are compared in Figure 5-36. Recorded displacements at 25%, 50% and 75% of the arch span are given in this figure. The deflections were zeroed prior to starting the rolling loads on that pass and modified data were used in the average calculation in cases where different loads were applied to the arch. Consideration of figure shows more deflections under the rolling loads in all sections for the 2-D tests. The results indicated that the average arch deflections under the roller location at 25%, 50% and 75% of span for 2-D tests are approximately 1.30, 1.15 and 1.30 times the 3-D tests under the same rollers.

In terms of soil masonry interaction the recorded pressures at different sections of the arch show good consistency between the obtained results and the UK code (Department of Transport 1997b) for load distribution for both series of tests. Similar behaviour was observed under the rolling loads for both the 2-D and the 3-D tests but the maximum pressures recorded in the 3-D tests are more than the 2-D test values. While an average maximum 2-D pressure of 20kPa was obtained at 75% of the span under the rolling load the mean value of 27kPa obtained from the 3-D tests under the same roller which shows an increase of about 35%. The same behaviour, with larger pressures recorded, occurred under the increasing load for the 3-D tests compared with the 2-D tests. While the maximum value of about 20kPa was recorded under the increasing load the maximum value of 40kPa was recorded for the 3-D tests.

## 5.7 Conclusions

Five 2-D benchmark models tests were carried out during this study. These include four shallow and one deep arch geometry. All models were tested using the roller load first and then increasing load. An increasing load was applied up to the observation of the first sign of failure, except for the first shallow arch model. Arch movements and soil/masonry interaction were measured in different arch section during the tests.

The 3-D arches built with spandrel walls to the same main geometry as the 2-D tests, were tested using the same procedure. Non-symmetrical roller loads were applied to these tests in addition to symmetric rollers and increasing loads.

From the above benchmark tests, the following general conclusions can be drawn:

- As evidenced by similar ultimate load capacity and load/deflections, good repeatability of the tests was observed in comparison with previous tests in the centrifuge for models with the same geometry.
- Non elastic behaviour of the arches was observed even under low load level cycling.
- The load deflection plots are approximately linear up to about 50% of the ultimate loads.
- It is seen that a substantial part of the ultimate load carrying capacity of the arch was resisted prior to the observation of the first sign of failure.
- Test results in conjunction with materials tests properties (Chapter 3) provide a useful databank for numerical models, especially in terms of soil/masonry pressures.
- Recorded soil/masonry interaction pressures have good consistency with the UK load distribution practice and theoretical elastic distribution. This confirms the usefulness of small sensors in soil-masonry interface pressure measurements.

The following conclusions can be drawn specifically from the 3-D arch tests.

- Three dimensional arch model tests show out of plane bending of arches even under symmetrical low load (at about 25% of maximum loads) application.
- The spandrel wall's effect on the arch response in terms of displacement shows arch movements decreasing and arch stiffness increasing.
- Tests results show that the applied load location has a significant effect on the arch behaviour. Non-symmetrical behaviour was observed when loads were applied on some part of the arches.
- The 3-D arch displacements show smaller values compared with the 2-D tests with the same geometry and under the same applied loads. This confirms spandrel wall effect on the control of arch movements.
- More variation under increasing loads was observed in the 3-D arches compared with the 2-D tests. This might be as a result of more complex behaviour of the 3-D arches and more variable spandrel wall interaction.

Test ID.	S2D-1B	S2D-2B	S2D-3B	D2D-1B
Date	27-29/07/02	1-4/10/02	10-11/03/03	26-28/06/03
Intrados span(mm)	500	500	500	500
Width (mm)	345	345	345	345
Span to rise ratio	4	4	4	2
Arch ring thickness(mm)	30	30	30	30
Scale	1:12	1:12	1:12	1:12
Mortar mix.	1:3:12	1:3:12	1:3:12	1:3:12
Courses	47:48:50	47:49:50	47:49:50	64:66:69
Fill depth at crown(mm)	30	30	13	13
Rigid box	black	black	blue	black
No. Kyowa sensors	12	9	10	8
No. middle LVDT	7	7	8	7
No. edge LVDT	6	6	0	7
No. rolling passes	14	14	14	14
Load cell (kN)	10	10	10	10
Load position (% span)	25	25	25	25
Repair	No	Yes	Yes	Yes
Max. load (kN)	6.2	5.0	4.6	4.8

Table 5-1: 2-D benchmark model details

Test ID.	Max. load (kN)	First cycle		Second cycle		Third cycle		Arch description
		Load	%	Load	%	Load	%	
S2D-1B	6.2	5.9	95	6.2	100			Full failure
S2D-2B	5.0	1.7	35	2.5	49	3.3	66	Crack under load location
S2D-3B	4.6	2.3	49	3.4	73			Cracks under load location and spring
D2D-1B	4.8	2.1	44	2.9	60			Crack under load location

Table 5-2: Load cycle and arch condition after each test

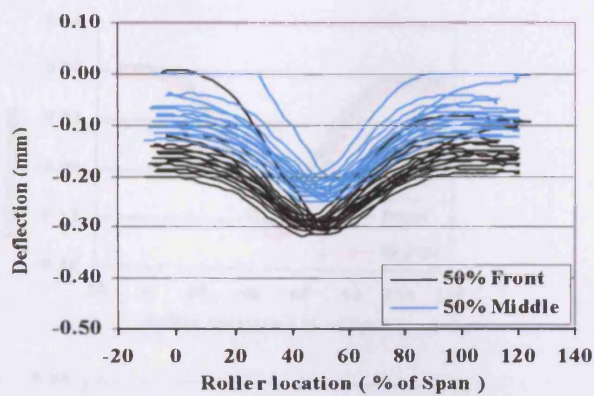
Test ID	S3D-1B	S3D-2B	S3D-3B	D3D-1B
Span to rise ratio	4	4	4	2
Width (mm)	405	405	405	405
No. Kyowa cells	8	8	8	8
No. front LVDT	7	3	4	4
No. middle LVDT	7	9 (rolling load) 7 (increasing load)	8 (rolling load)	6 (rolling load)
No. back LVDT	0	3	4	4
Spandrel wall LVDT( front)	3 (25, 50, 75%)	3 (25,50& 75% span)	3 (25,50& 75% span )	3 (25,50& 75% span)
Spandrel wall LVDT (back)	1 (25% span)	1 (25% span)	1 (25% span)	1 (25% span)
Rolling load	Load Case 1 (18 Pass)	Load Case 1 (14 pass) Load Case 2 (6 pass) Load Case 3 (6 pass)	Load Case 1 (14 pass) Load Case 2 (6 pass) Load Case 3 (6 pass)	Load Case 1 (14 pass) Load Case 2 (6 pass) Load Case 3 (6 pass)
Load cell (kN)	10	10	10	10
Increasing load position (% span)	25	25	25	30
Repair	Yes	Yes	Yes	Yes
Max. increasing load (kN)	5.7	7.4	4.7	6.9

Table 5-3: 3-D benchmark model details

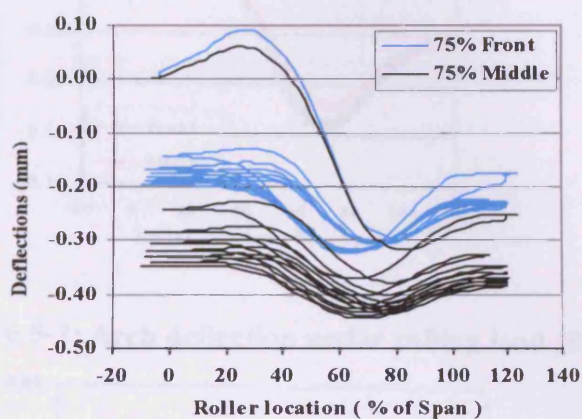
Test ID	Load Case 1	Load Case 2	Load Case 3
S3D-1B	11.8	N/A	N/A
S3D-2B	11.8	7.7	7.3
S3D-3B	14.9	7.7	7.3
D3D-1B	14.9	7.7	7.3

Table 5-4: Roller weight (kg) for load cases for 3-D tests

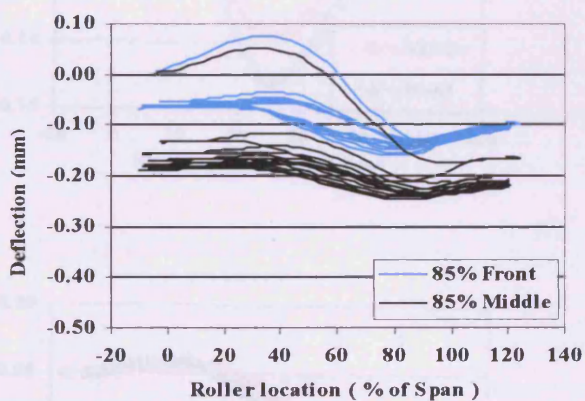




A) 50% arch span

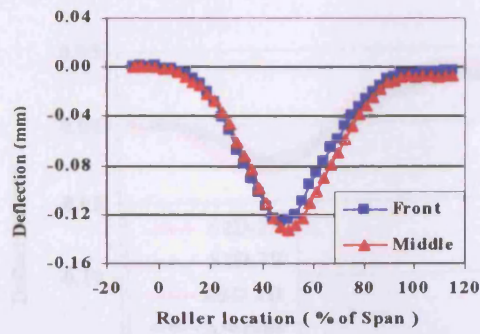


B) 75% arch span

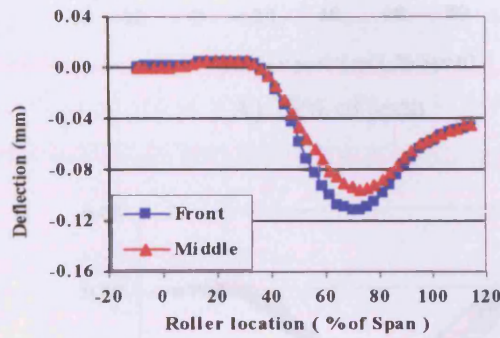


C) 85% Arch Span

Figure 5-1: Typical arch deflection under rolling load (S2D-1B)

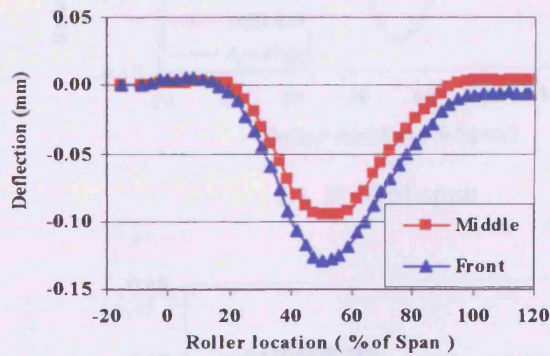


A) 50% span

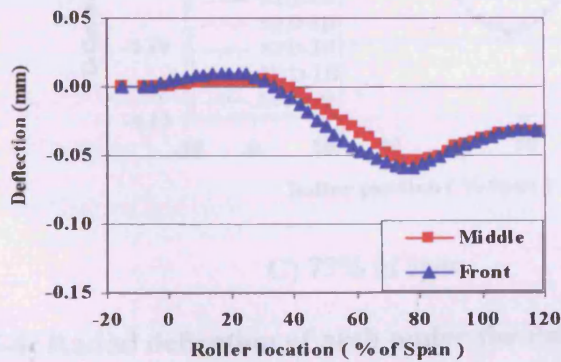


B) 75% span

Figure 5-2: Arch deflection under rolling load (S2D-1B)



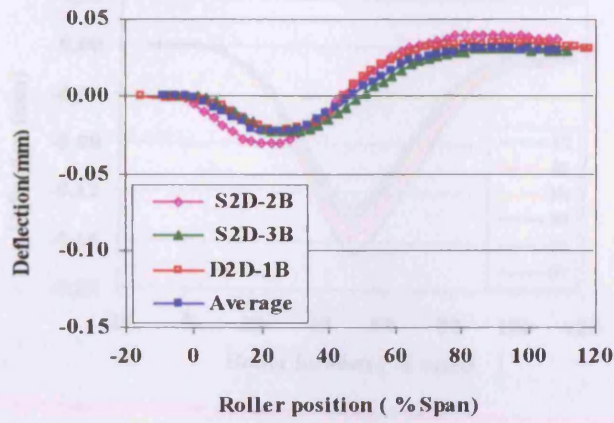
A) 50% span



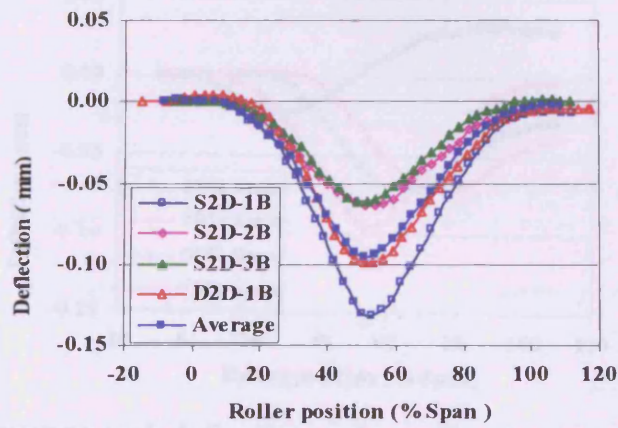
B) 75% span

Figure 5-3: Arch deflection under the rolling load (D2D-1B)

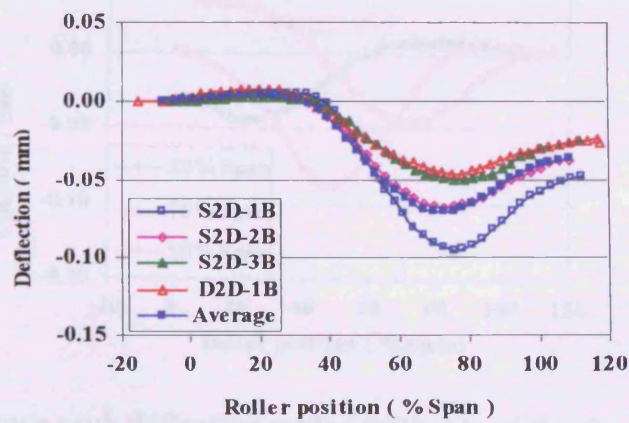




A) 25% of span



B) 50% of span



C) 75% of span

Figure 5-4: Radial deflection of arch under the rolling load (2-D tests)

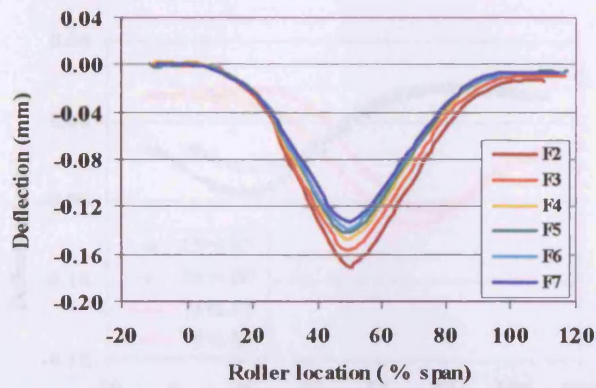


Figure 5-5: Pass number effect on arch deflection (S2D-1B, 50% span)

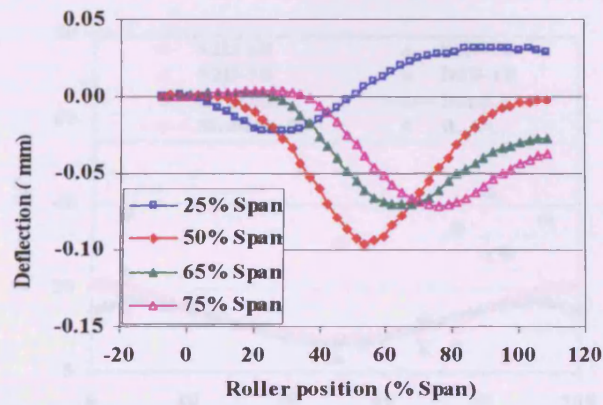


Figure 5-6: Average arch deflection under rolling load (forward direction)

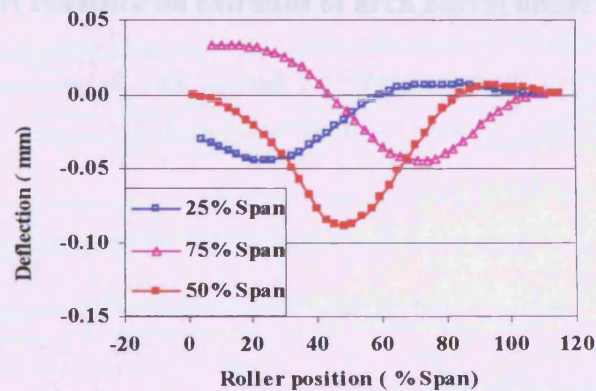


Figure 5-7: Average arch deflection under rolling load (backward direction)



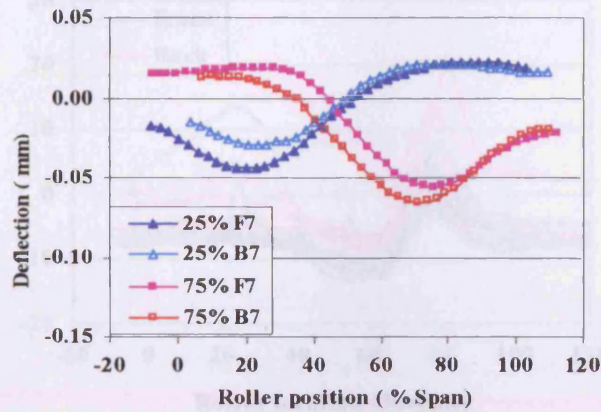


Figure 5-8: Arch response to the roller load in forward and backward movement

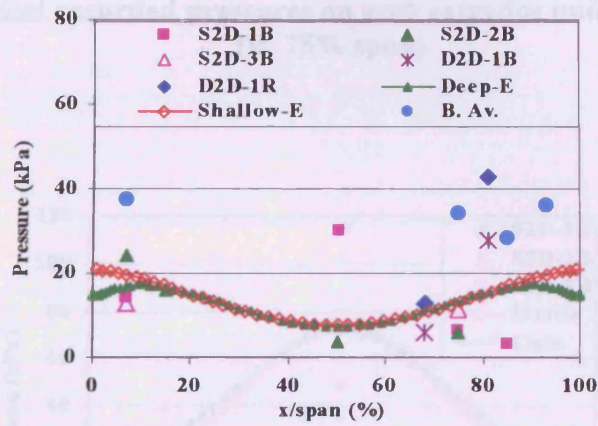


Figure 5-9: Pressure on extrados of arch barrel under self weight

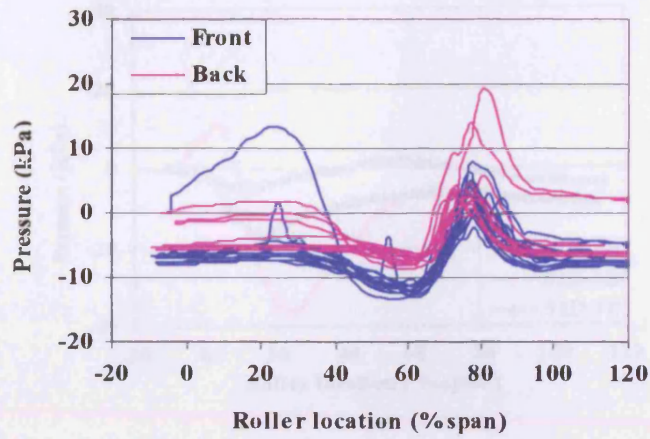


Figure 5-10: Typical recorded pressures on arch extrados under rolling load (S2D-1B, 75% span)

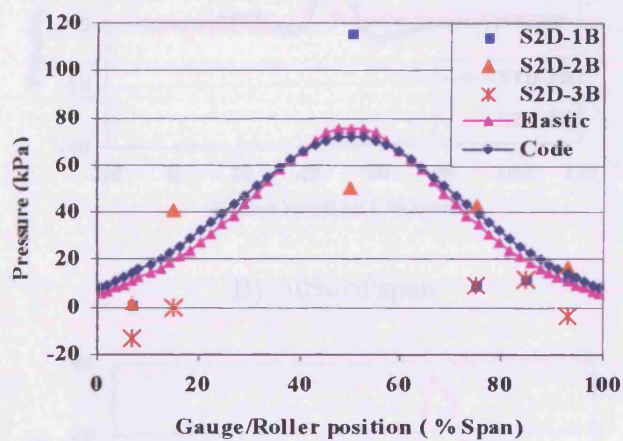
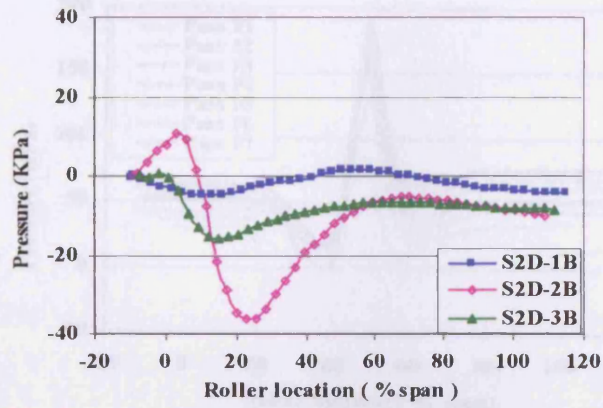
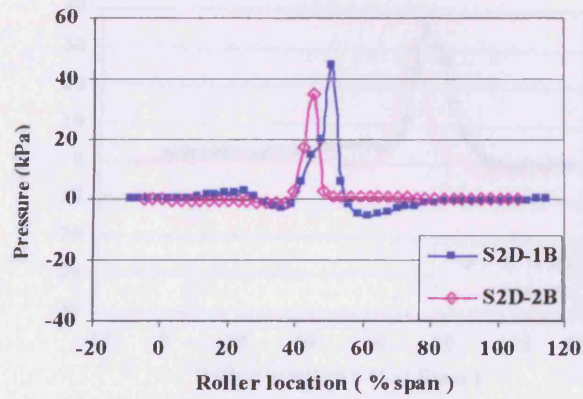


Figure 5-11: Comparison of the theoretical and measured values (shallow arches)

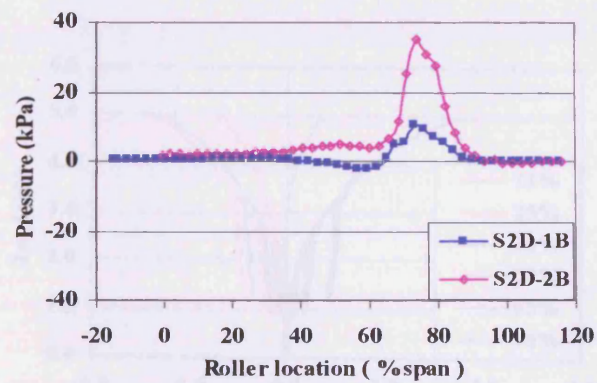




A) 7% of span



B) 50% of span



C) 75% of span

Figure 5-12: Change in pressure under rolling load (2-D tests)

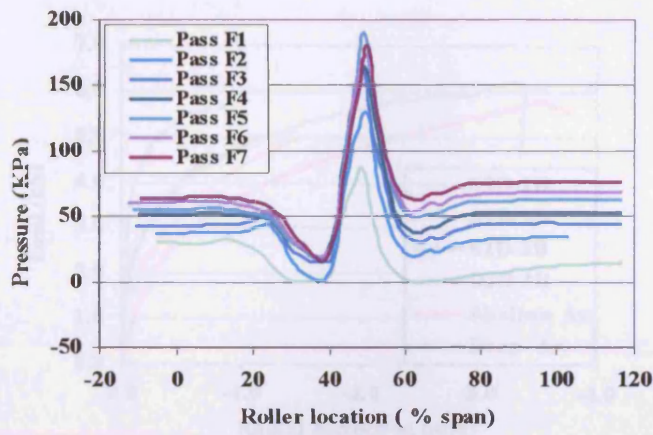


Figure 5-13: Pass number effect on soil/ masonry interaction (S2D-1B)

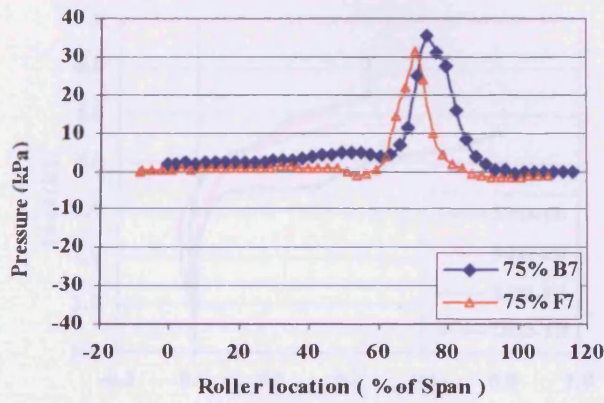


Figure 5-14: Effect of roller movement direction on soil/masonry interaction (S2D-2B)

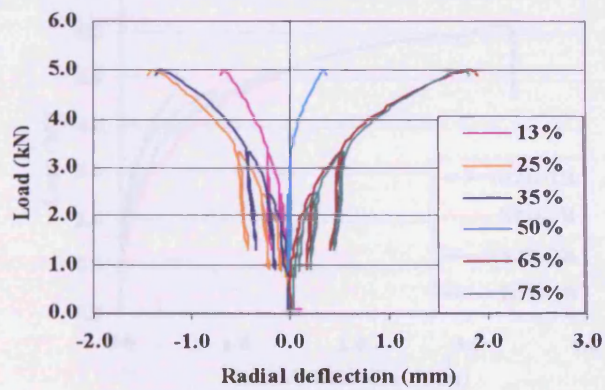
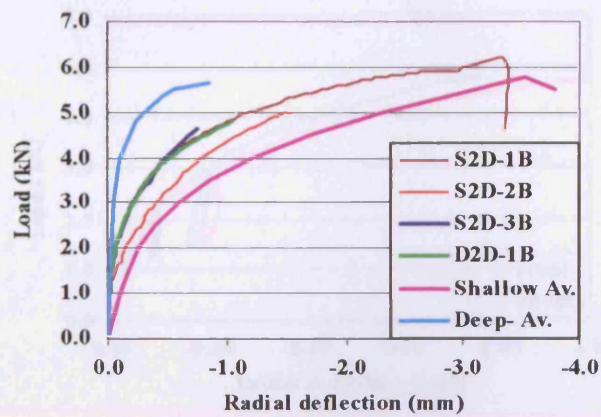
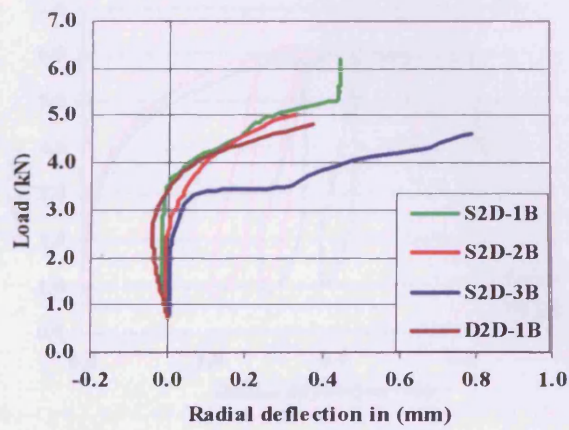


Figure 5-15: Load/deflection at different span positions (S2D-2B)

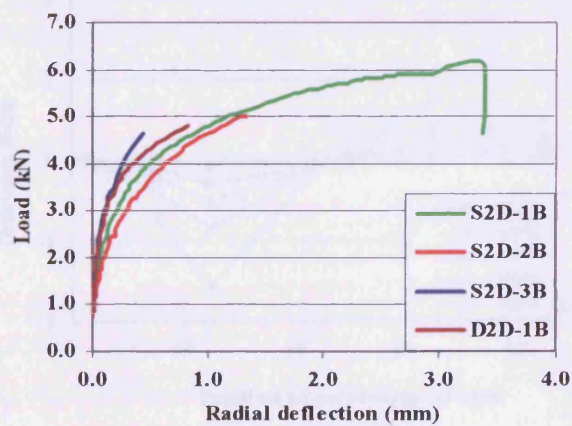




A) 25% of span



B) 50% of span



C) 75% of span

Figure 5-16: Load/deflection at different sections

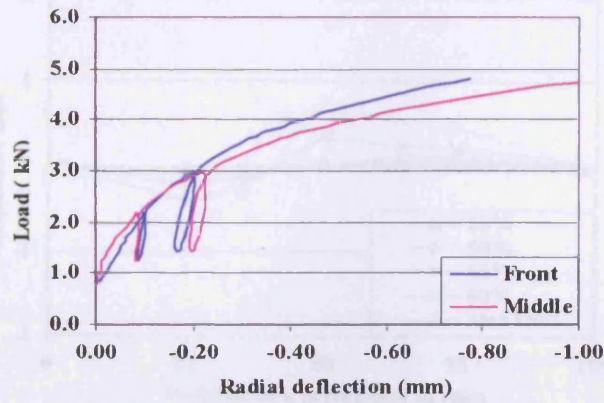


Figure 5-17: Load/deflection at front and middle of arch (D2D-1B, 25% span)

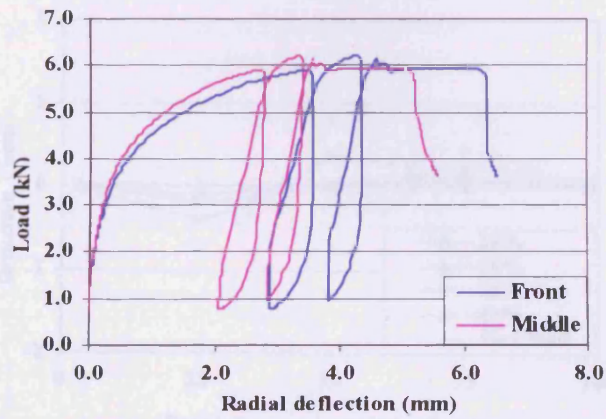
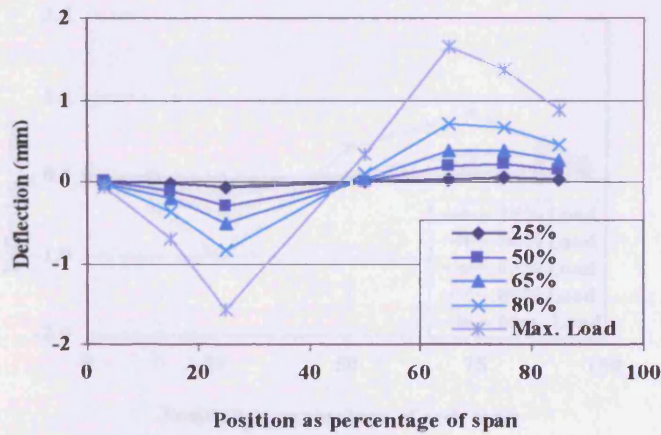


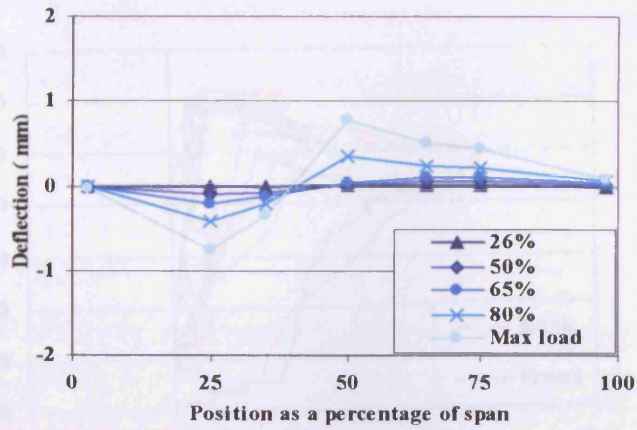
Figure 5-18: Load/deflection at front and middle of arch (S2D-1B, 75% span)



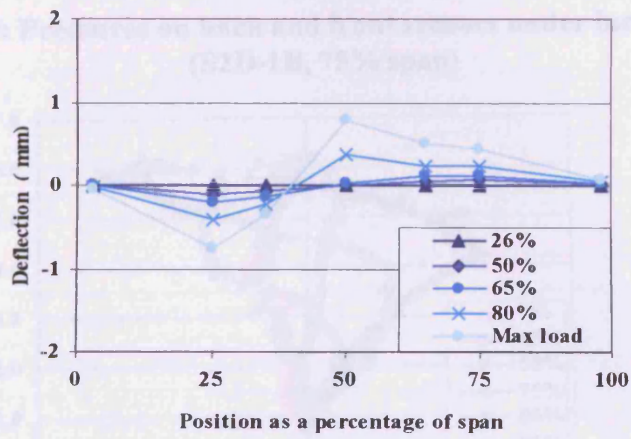
A) Test S2D-1B

Figure 5-19: Arch deflection under the increasing load

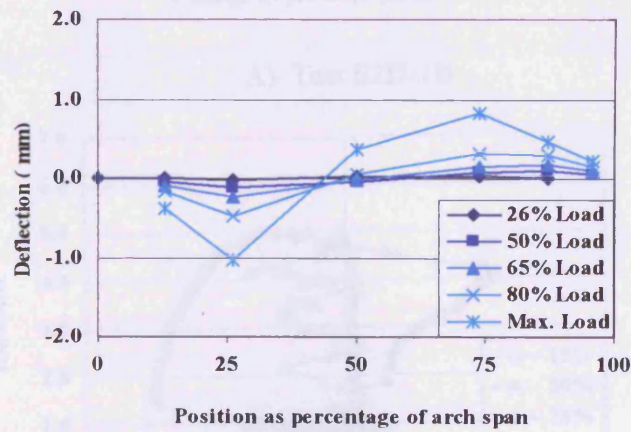




B) Test S2D-2B



C) Test S2D-3B



D) Test D3D-1B

Figure 5-19: Arch deflection under the increasing load (Cont.)

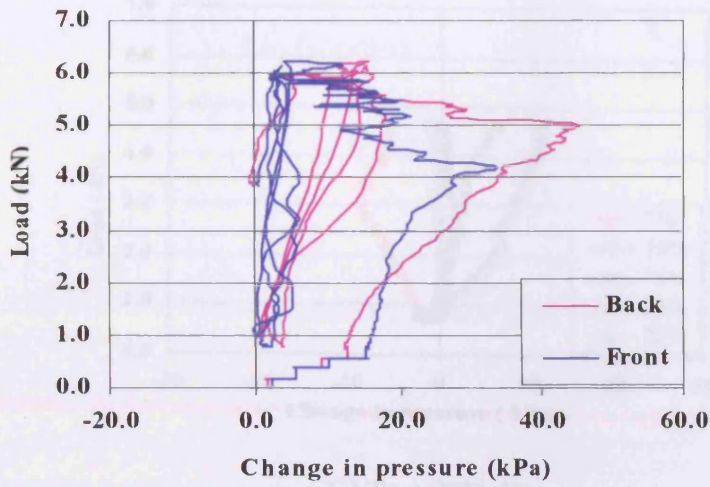
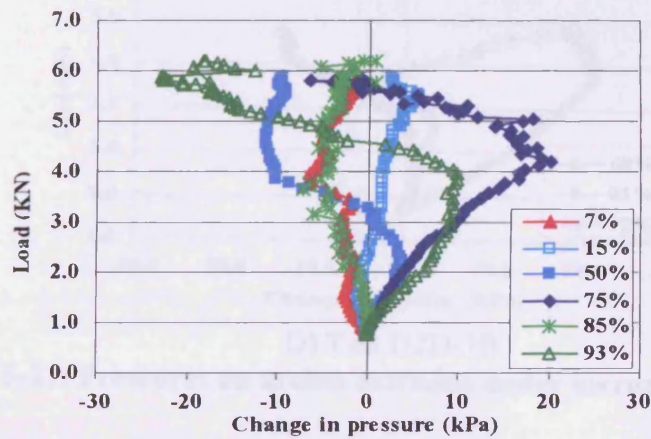
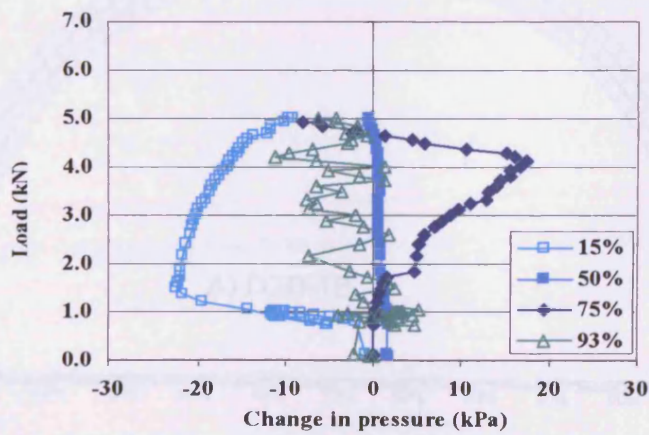


Figure 5-20: Pressures on back and front sensors under increasing load (S2D-1B, 75% span)



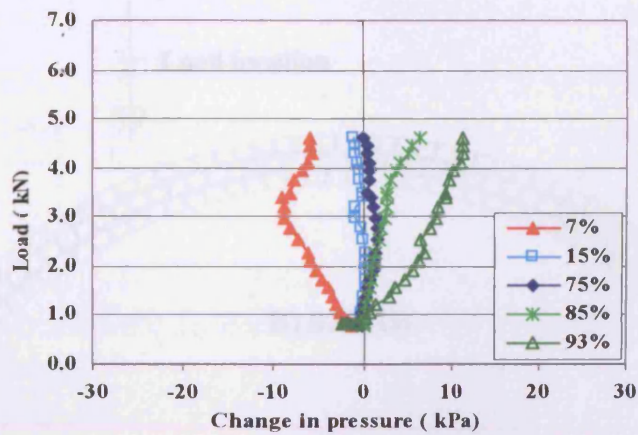
A) Test S2D-1B



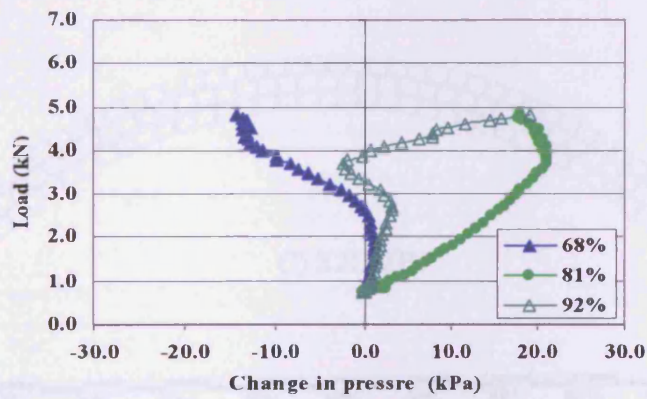
B) Test S2D-2B

Figure 5-21: Pressures on arch extrados under increasing load





C) Test S2D-3B



D) Test D2D-1B

Figure 5-21: Pressures on arches extrados under increasing load (Cont.)

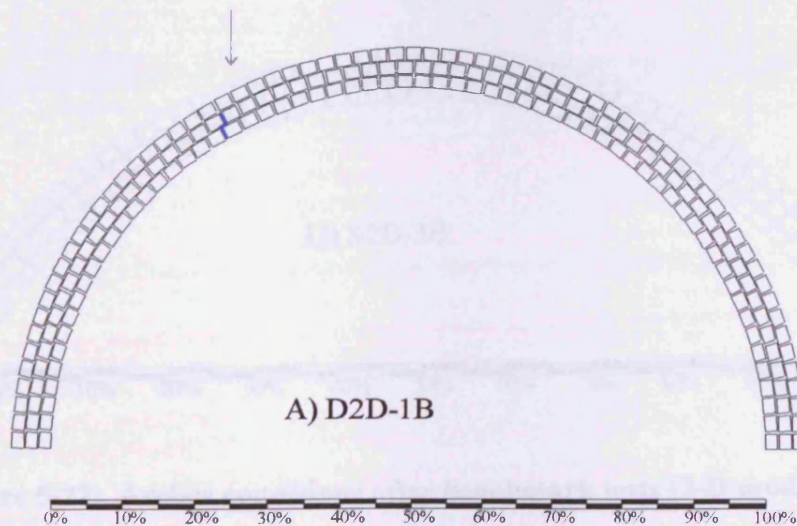


Figure 5-22: Arch condition after benchmark tests (2-D models)

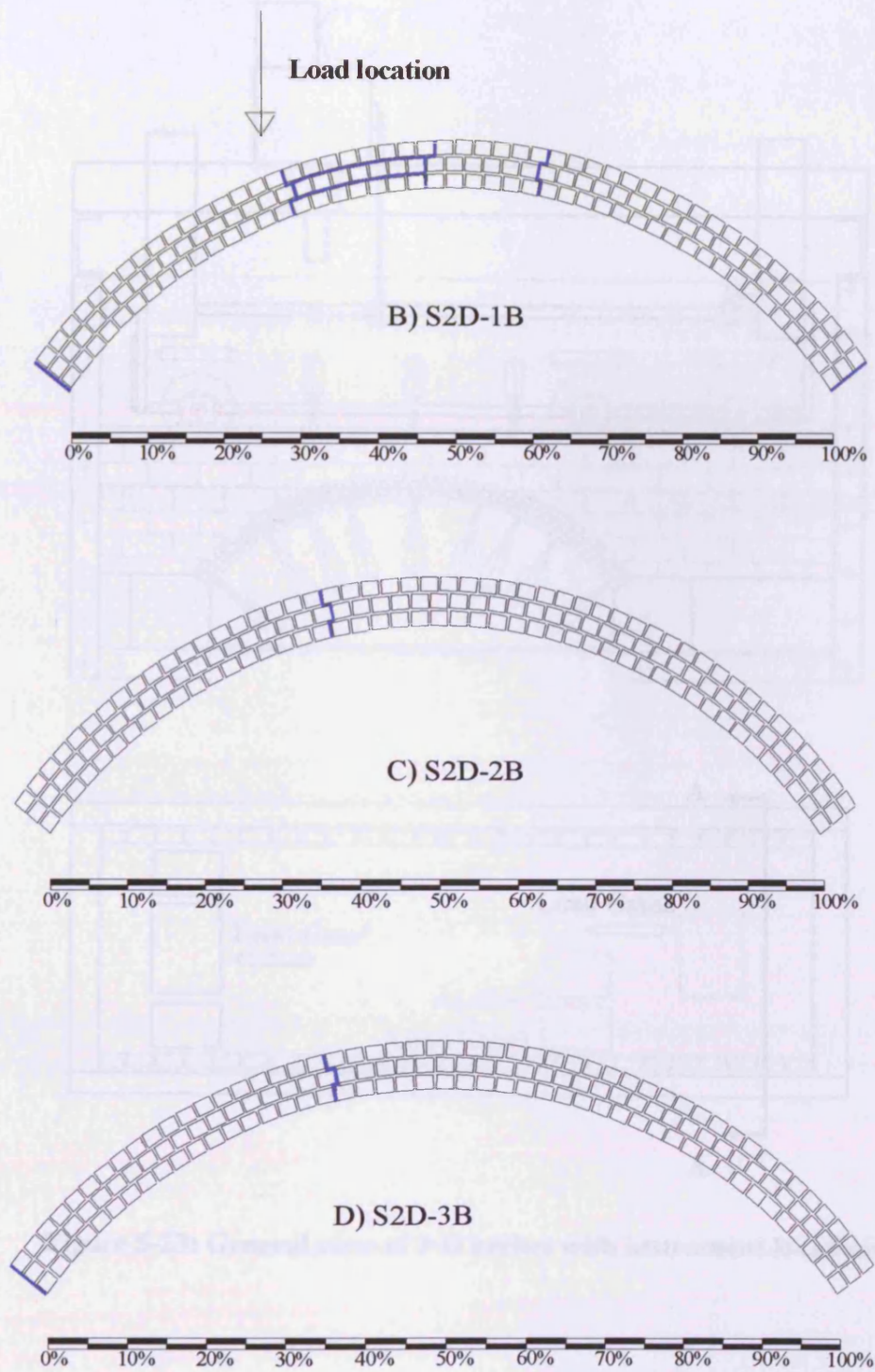
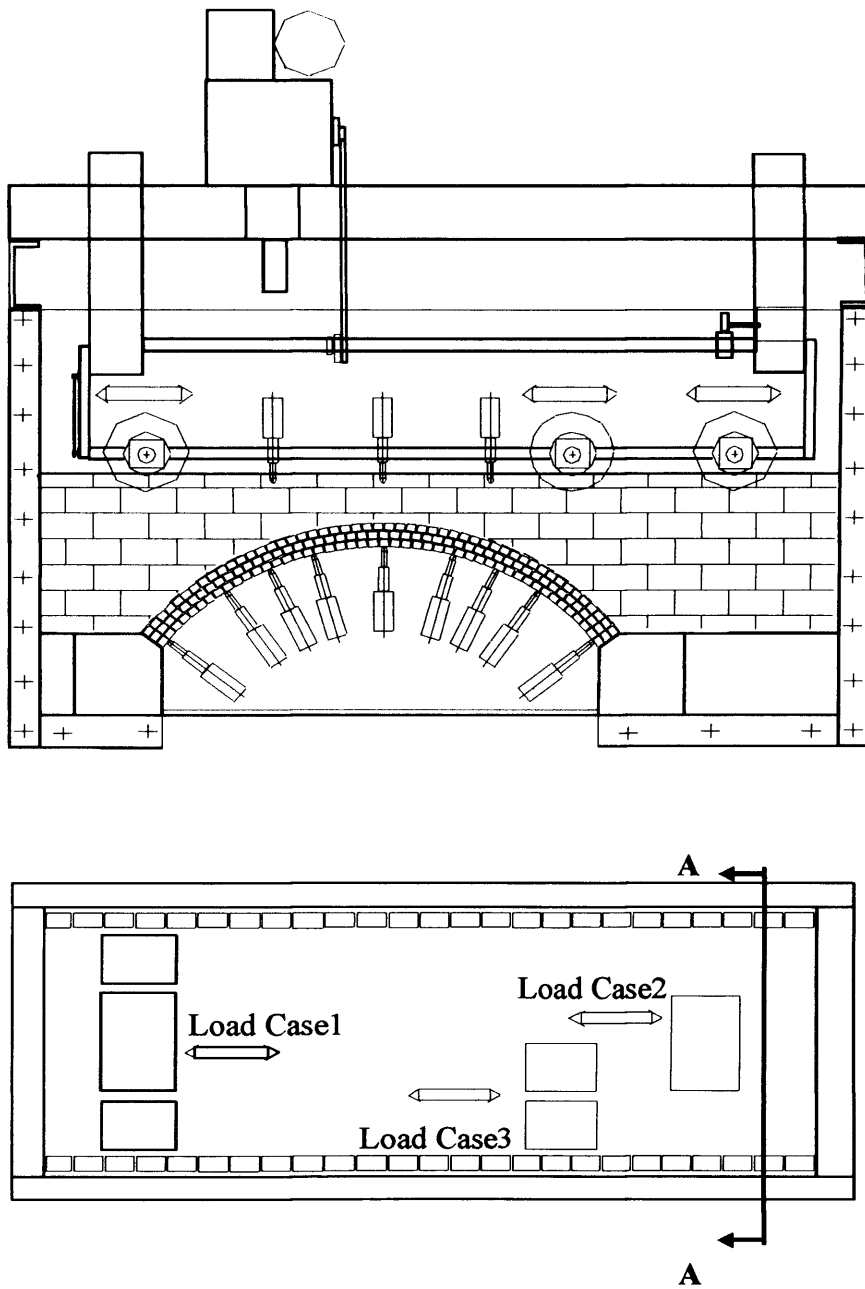


Figure 5-22: Arches conditions after benchmark tests (2-D models, Cont.)



**Figure 5-23: General view of 3-D arches with instrument locations**

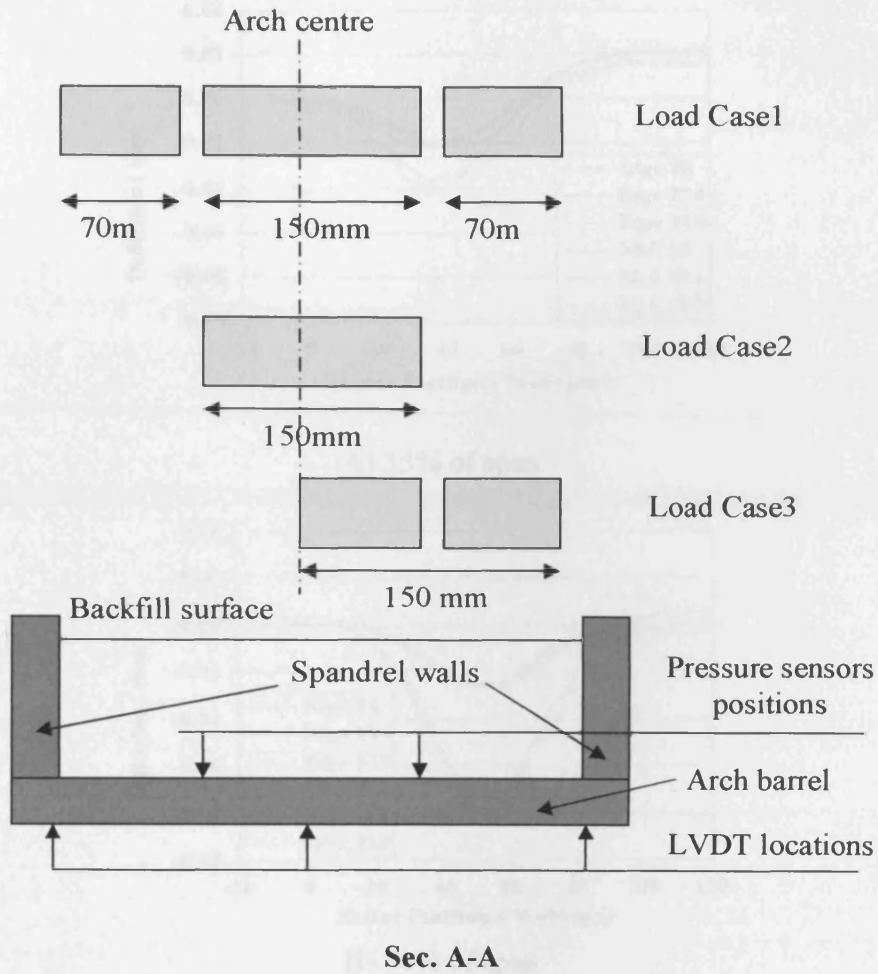
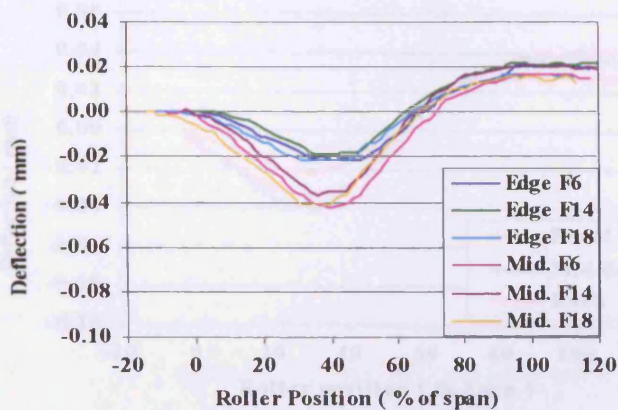
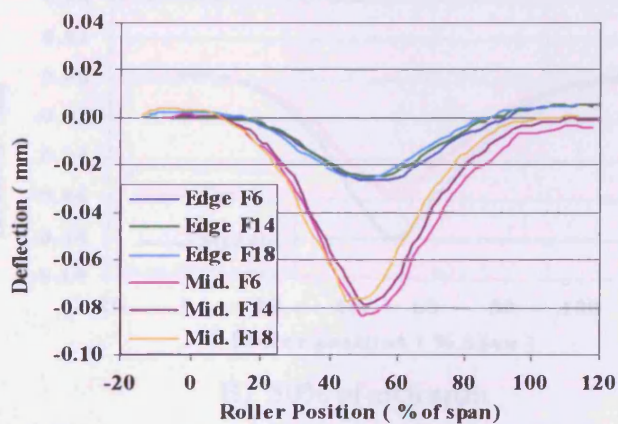


Figure 5-23: General view of 3-D arches with instrument locations (Cont.)

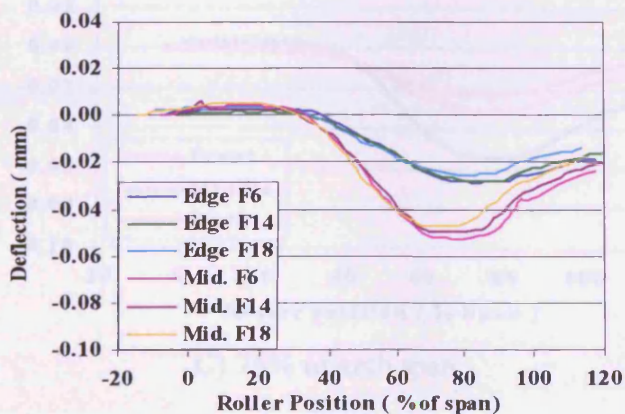




A) 35% of span

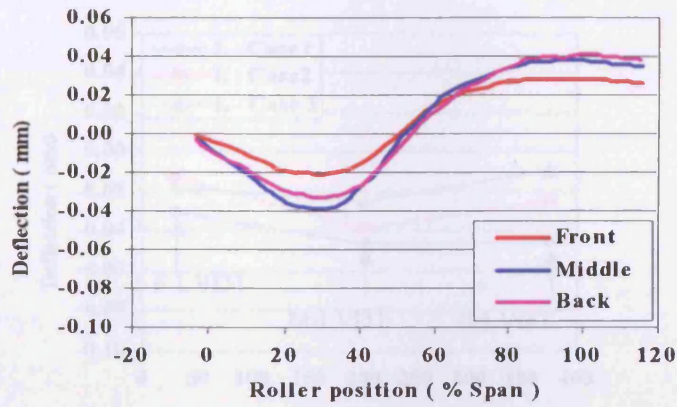


B) 50% of span

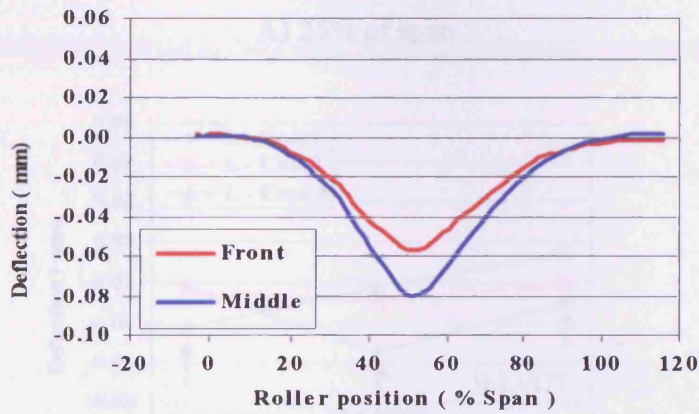


C) 75% of span

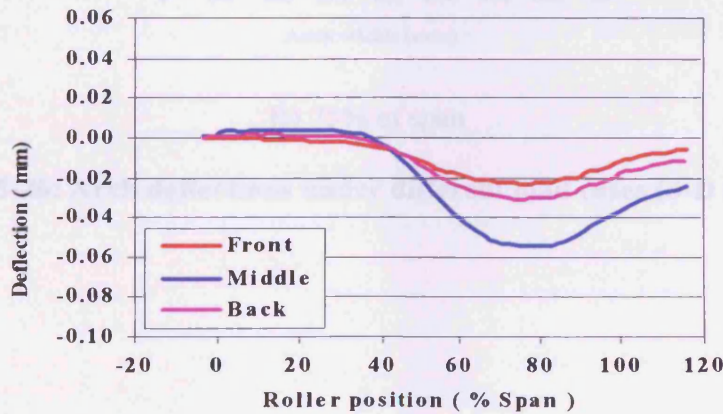
Figure 5-24: Arch deflection at different sections under the rolling load (S3D-1B)



A) 25% of the arch span



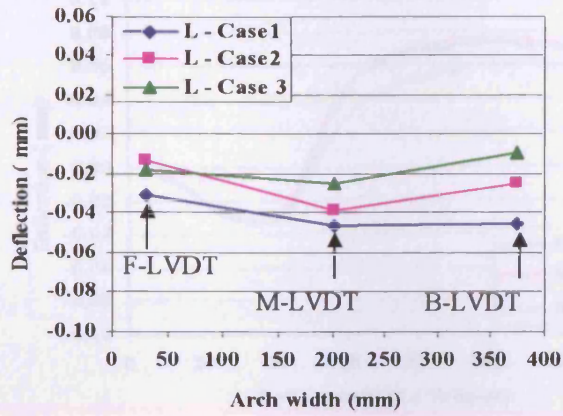
B) 50% of arch span



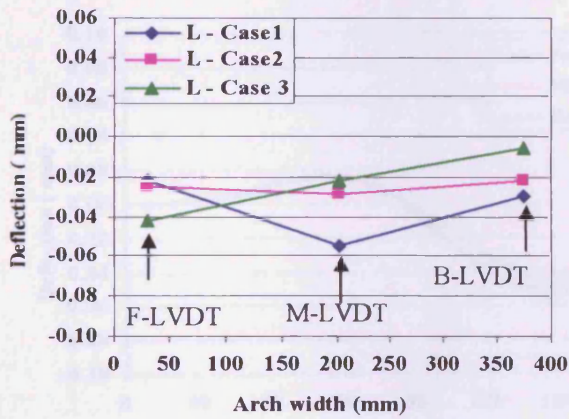
C) 75% of arch span

Figure 5-25: Average 3-D shallow arch deflections under the rolling load (pass F7)



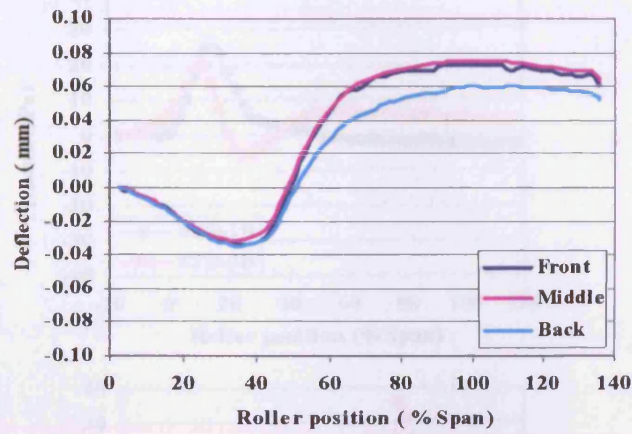


A) 25% of span

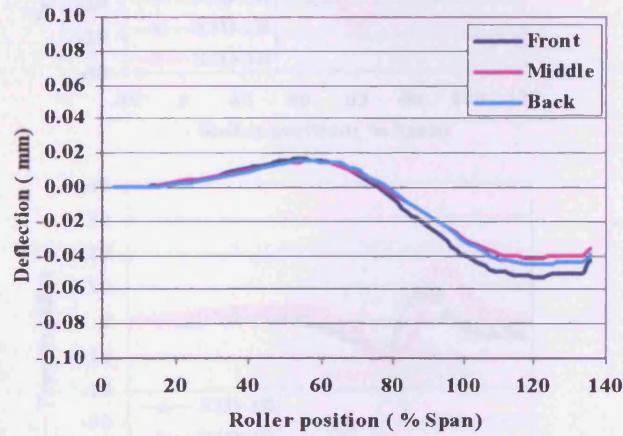


B) 75% of span

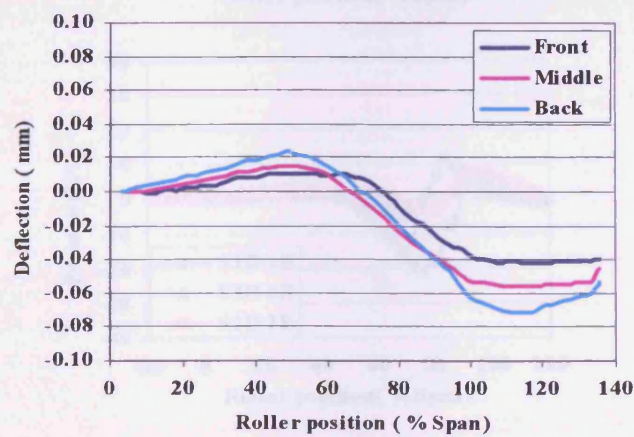
Figure 5-26: Arch deflections under different load cases (3-D shallow)



A) LVDTs at 35% of arch span



B) LVDTs at 75% of arch span



C) LVDTs at 85% of arch span

Figure 5-27: 3-D deep arch deflection under the rolling load (pass F7)



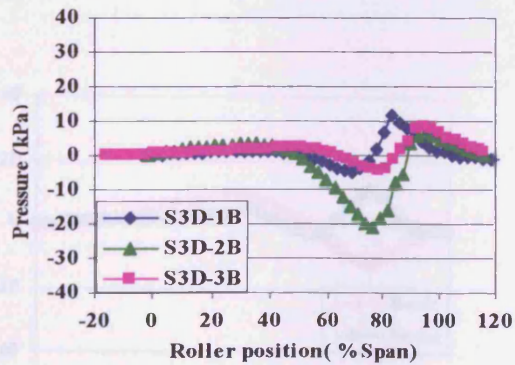
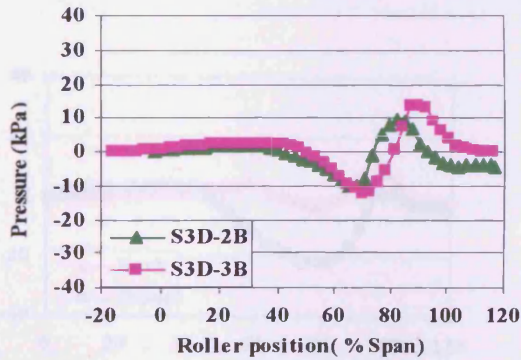
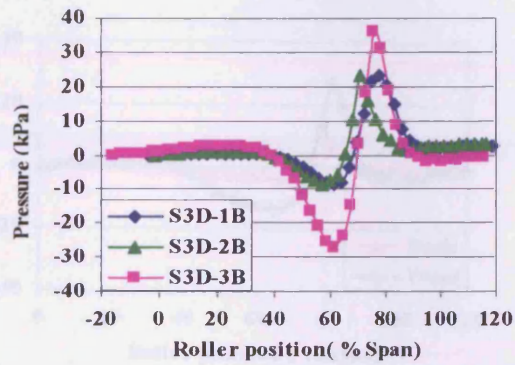
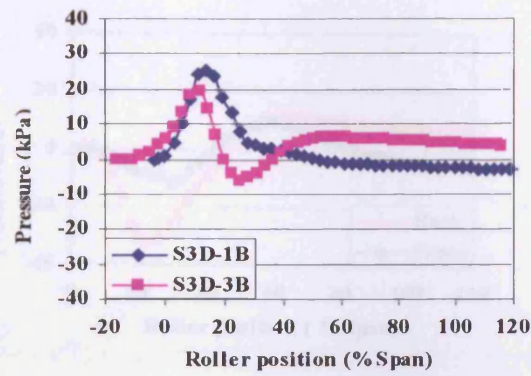
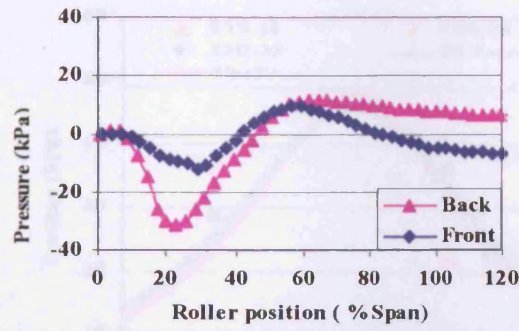
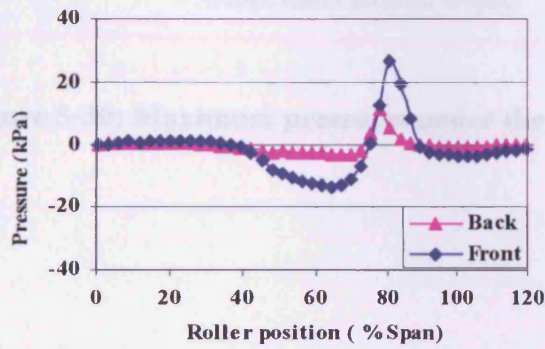


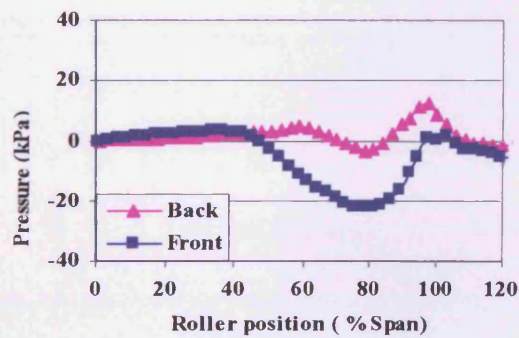
Figure 5-28: Pressure under rolling load at different sections (3-D, pass F7)



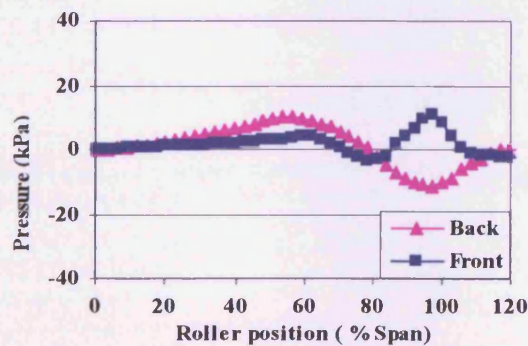
A) 8% span



B) 68% span



C) 81% span



D) 92% span

Figure 5-29: Change in pressure under rolling load (deep arch pass F6)



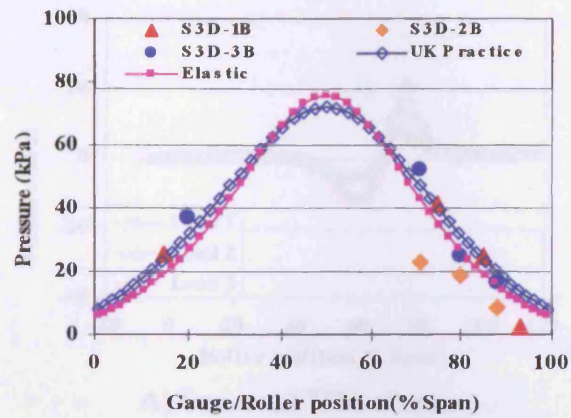


Figure 5-30: Maximum pressures under the rolling load

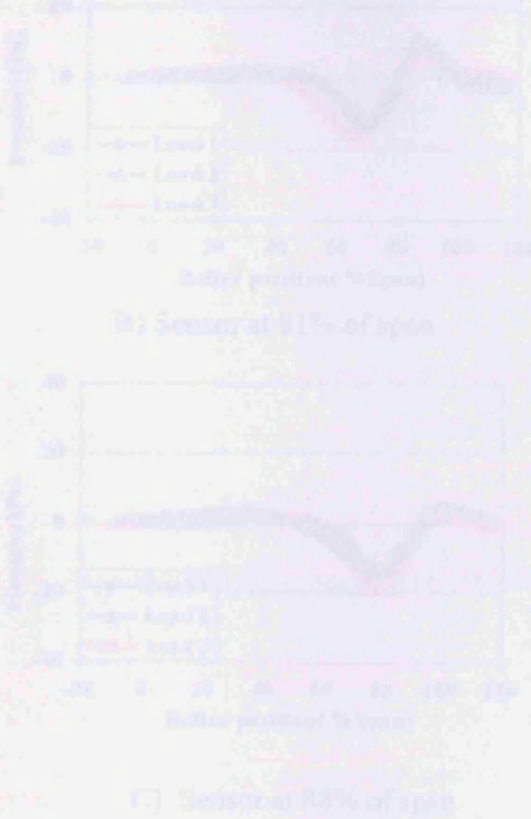
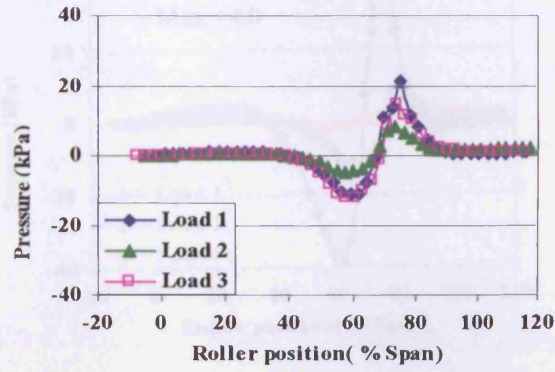
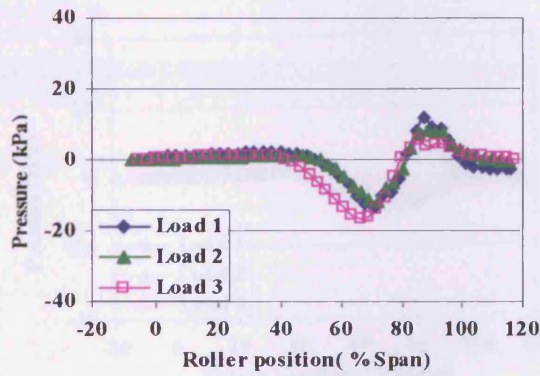


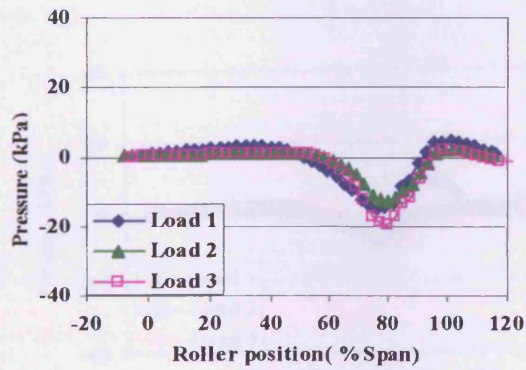
Figure 5-31: Cross section average pressures under the different rolling load cases



A) Sensor at 75% of span



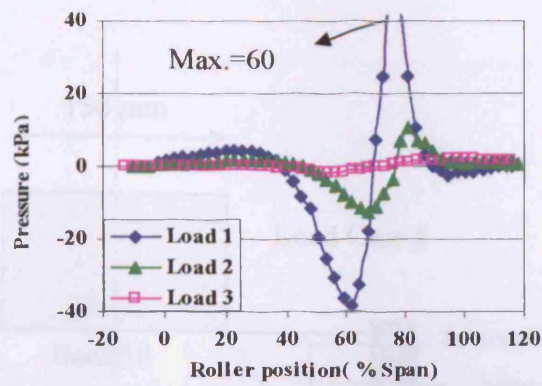
B) Sensor at 81% of span



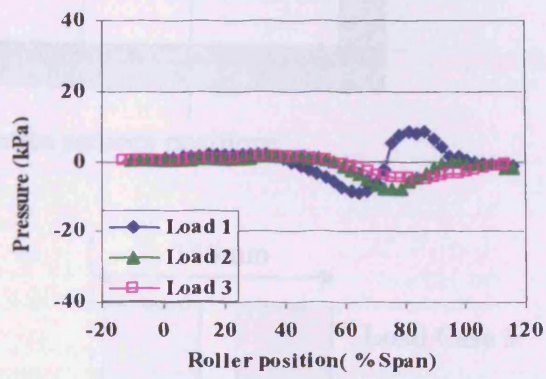
C) Sensor at 88% of span

Figure 5-31: Front edge average pressures under the different rolling load cases

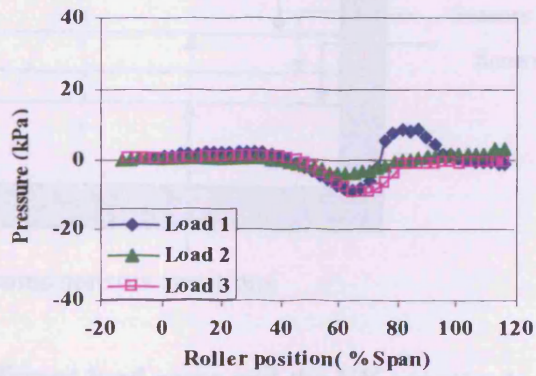




A) Sensor at 75% of the span



B) Sensor at 81% of the span



C) Sensor locate at 88% of the span

Figure 5-32: Back edge average pressures under the different rolling load cases

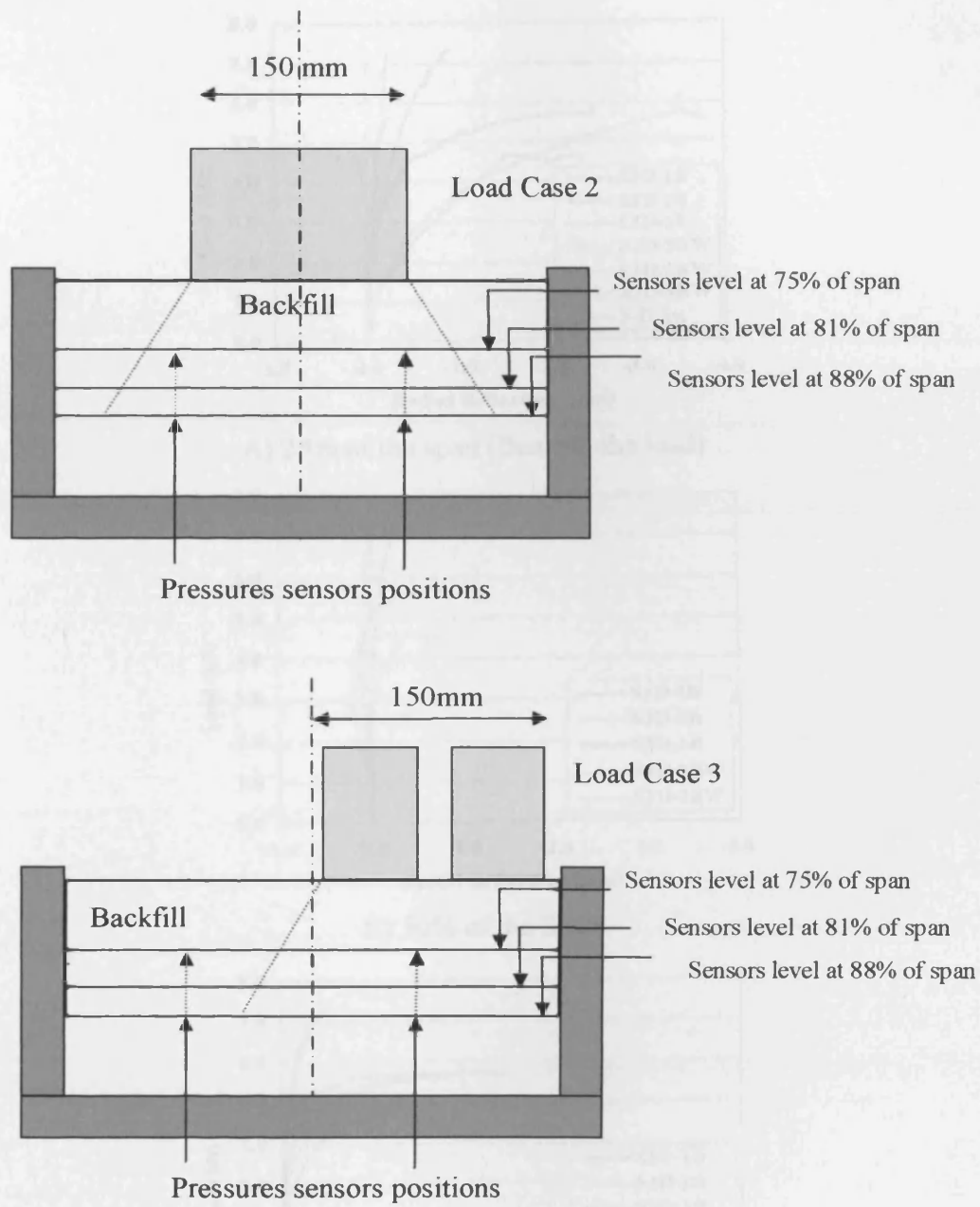
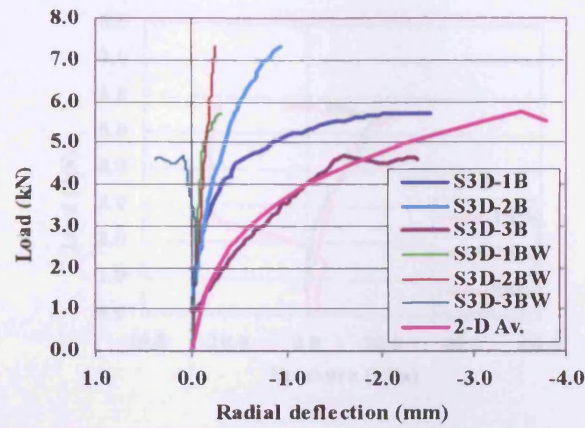
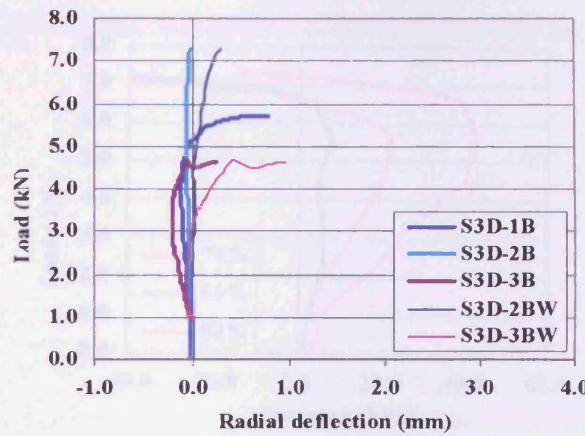


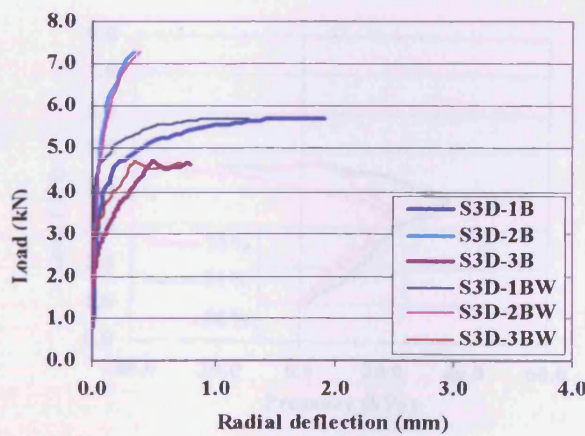
Figure 5-33: Different load cases and the UK practice load distribution



A) 25% of the span (Beneath the load)



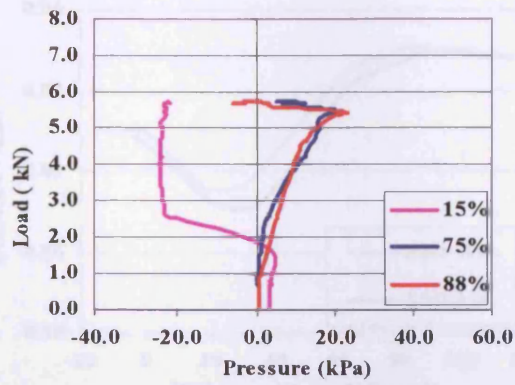
B) 50% of the Span



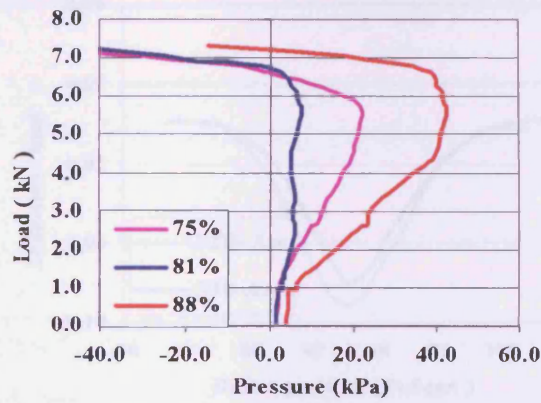
C) 75% of the span

Figure 5-34: Arch deflections under increasing load (3-D tests)

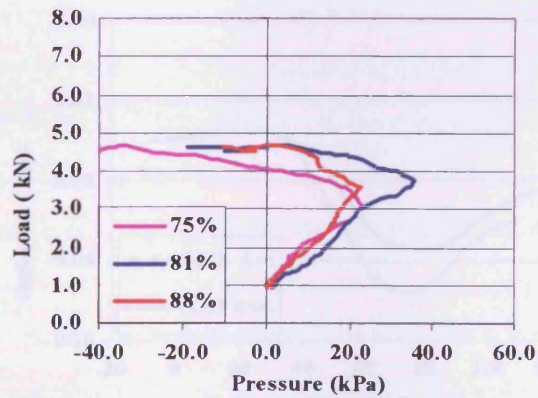




A) Test S3D-1B

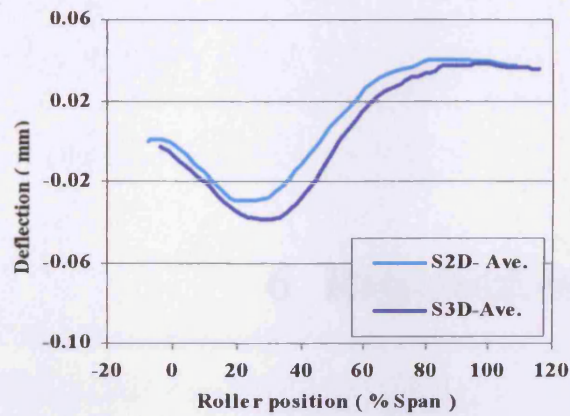


B) Test S3D-2B

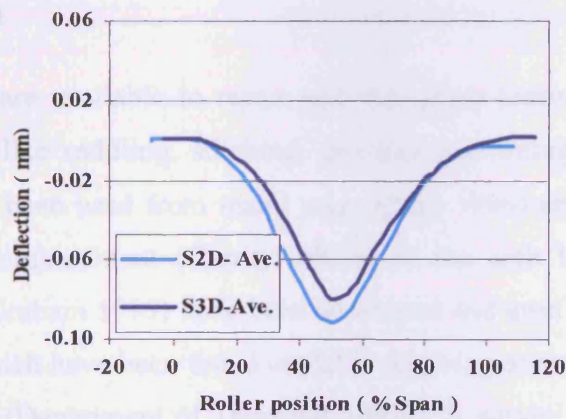


C) Test S3D-3B

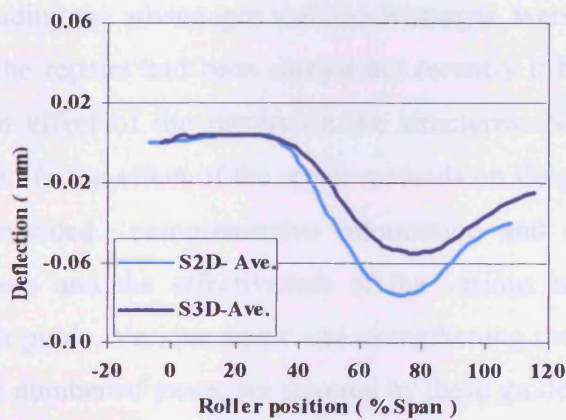
Figure 5-35: Pressures on the arch extrados under increasing load (3-D tests)



A) LVDT at 25% of the span



B) LVDT at 50% of the span



C) LVDT at 75% of the span

**Figure 5-36: 2-D and 3-D average arch displacements under rolling load**

## 6 Repaired tests and results

### 6.1 Introduction

Various techniques are available to repair and strengthen masonry arch bridges. Some traditional methods like saddling, stitching, grouting, repointing and spraying concrete onto the soffit have been used from many years (Page 1996) and some new techniques such as the retro-reinforcement (Garrity 1995a) of the arch barrels and other novel methods (Carl and Graham 1999) have been developed and used in recently years. Some of the techniques which have been found useful in repairing or strengthening arch bridges are listed elsewhere (Department of Transport 1997a). A survey of 50 repaired masonry arch road bridges was carried out by Ashurst (Ashurst 1992) and the effect of various repair methods, including the advantages and disadvantages, were detailed in this survey. As the majority of the repairs had been carried out recently it has not been possible to assess the long term effect of the repairs on the structures. No attempt was made in Ashurst study to identify the effect of the repair methods on the arch load capacity. Page (Page 1996) has provided comprehensive information and advice on present best practice, relative costs and the effectiveness of the various repair and strengthening methods in his repair guide. Various repair and strengthening methods, which have been in common use for a number of years, are covered by these guidelines. Again, no tests on the effect of the arch repair on load capacity are reported.

Works on full and small scale models of repaired masonry arches are also reported elsewhere (Baralos 2002; Melbourne and Gilbert 1993; Sumon 1998). Arch behaviour following the application of various repair/strengthening methods to the small scale

centrifuge models are presented in this chapter. This includes all the repaired 2-D and 3-D arches under the rolling loads and ultimate load tests. For each repair method, the repair details are presented first and then tests results are detailed and discussed. Test and full repair application procedures were detailed in Chapter 4.

## 6.2 Repaired tests and results

The repaired arch models were tested using the same procedures as the benchmark models. The models were tested under the rolling load first and then with an increasing load to failure. The 2-D arch models were usually tested with 14 passes of the rolling load over the whole width of the arch but the 3-D arch models had different rolling load cases applied to them. These included an applied load over the whole width of the arch and over half of it (in two positions) in a similar way to the benchmark test. The same rollers were used in both the benchmarks and repaired models except Load Case 3 in models S3D-3R and D3D-1R. In these two models as a result of the repair condition the roller width was changed to a smaller width.

Increasing loads were applied in the same manner as the benchmark tests with some load cycles during the tests. A larger range load cell was used during the repair tests because higher load carrying capacities were expected. Full test details for the repaired arch model tests are given in Table 6-1 and Table 6-2 for the 2-D and 3-D tests respectively. The first 2-D arch model was tested up to full failure without applying any repair to it. The second 2-D shallow arch model was repaired by application of a layer of plastic reinforced mesh at mid backfill depth (at the crown). The third 2-D shallow arch and first 2-D deep arch were repaired using relieving concrete on top of the backfill.

A stitching repaired method was used to repair the first 3-D shallow arch model. The stitching bar was used to repair the arch barrel in addition it provided a connection between the spandrel walls and the extrados barrel ring. The second 3-D shallow arch model was repaired using a partial saddle concrete. The concrete was applied to the extrados of the arch barrel to the front and rear of the arch in plan. Finally the third shallow 3-D arch and first 3-D deep arch were repaired by applying reinforced concrete to



part of the inside of the spandrel walls. All the 2-D and the 3-D repair tests details and results are presented in the next sections.

## **6.3 Plastic mesh**

### **6.3.1 Repair details**

Masonry arches are simple in appearance but complex in structural behaviour. The load is applied to the masonry through the pavement and backfill. The backfill increases the arch load capacity by distributing the applied load and restricting the arch movements when the arch moves towards it. The soil effect on the arch load capacity and its interaction behaviour has been investigated in model and real bridges (Fairfield and Ponniah 1994a; Ponniah 1987; Ponniah et al. 1997). The soil stress and soil masonry interaction in small scale centrifuge models was investigated and reported by Burroughs (Burroughs et al. 2000; Burroughs et al. 2002). In all the above referenced work a significant effect of the backfill on the load distribution and the arch load capacity were observed. Following the centrifuge small scale test models on soil masonry interaction it was decided to try and test soil reinforcing as a repair method. It was considered that changes in the load distribution will effect the arch load capacity, therefore a layer of plastic mesh reinforcement was used in the mid backfill depth (at the crown) across the entire arch. The reinforced mesh used was a scale version of a typical mesh layer which is usually applied to stabilize soil slopes. A general view of the mesh reinforcement is given in Plate 6-1. More details of the repair procedure were presented in Chapter 4 and the results obtained are detailed in the next sections.

### **6.3.2 Rolling load results**

The response of the LVDT, which was installed at 50% of the span, for different roller locations is given in Figure 6-1 for both the benchmark and the repaired arch. Deflection comparison between the repaired and the benchmark arch indicate an increase of about 50% for the repaired arch. Similar results were recorded by the other LVDTs. Comparison between measured deflections under the roller load when it was locally located at 75% of the arch span indicates an increase of about 175% in the repaired arch

compared with the benchmark test. This suggests that the arch stiffness was reduced following application of the plastic reinforcement mesh into the backfill.

Recorded pressures at 75% of the arch span are compared for the repaired and the benchmark test in Figure 6-2. Comparisons between the recorded pressures show a significant reduction in the recorded pressures for the repaired arch. Unfortunately, a poor response was observed in some of the sensors in the benchmark test but the recorded pressures in the repaired arch are also significantly smaller than the other available benchmark test results. The arch barrel stiffness may have been reduced as a result of ring separation during the benchmark test and this repair method made no attempt to repair it. The smaller recorded pressures in the repaired arch may have been due to more load distribution from the plastic mesh. However, the smaller stiffness of the repaired arch and the larger deflection under the roller most probably caused some reduction in pressures.

### 6.3.3 Ultimate load results

The load deflection plot for the benchmark and the repaired tests (S2D-2B & S2-D-2R) are given in Figure 6-3. The arch deflection beneath the applied load for these tests are compared to the average from previous shallow arch benchmarks tests (Burroughs 2002) which is indicated by 'Shallow' in the figure. The repaired arch model failed at 6.1kN, which shows an increase of about 10% compared with the average shallow arch load capacity. The arch load deflection curves for the repaired arch and the post test investigation show that the failure load was not achieved in the benchmark test and a direct comparison between the arch capacity in the benchmark test and the repaired test is not possible.

Arch behaviour indicates no significant change in arch stiffness and the arch deflections under increasing load are approximately the same as previous tests. There were no significant changes in the arch stiffness under increasing load before and after the repair indicating that the backfill was well compacted under the roller test and there was no separation between the soil layer on top and below the mesh. Soil/masonry interactions under increasing load are detailed in Figure 6-4. Also, included in this figure are the benchmark test results as a comparison. The results show no significant changes in the

recorded pressures after applying the plastic mesh reinforcement layer. The pressures are in the range of the benchmark results and therefore the plastic mesh does not appear to have any significant effect on the redistribution of the loading.

#### 6.3.4 Post test observations

The position of the hinges and ring separation after the benchmark and the repair test for S2D-2R are presented in Figure 6-5 and Plate 6-2. Post test investigation indicated that the applied load was stopped after forming the first hinge in the benchmark test. The failure mechanism was formed in the repair test with the clear formation of four hinges and ring separation in the part of the arch remote from the applied load between the 3<sup>rd</sup> and 4<sup>th</sup> hinges.

### 6.4 Relieving slab

A relieving slab is a flat reinforced concrete slab placed on top of the fill. It generally acts by improving the live load distribution on to the arch (Page 1996). The load capacity of an arch bridge as calculated by the MEXE method can be increased by increasing the value of  $(d+h)$  after applying the slab. This can be achieved by increasing the depth of the road surface (Page 1996). It should be noted that BD 21/97 does not recommend use of the MEXE method if the depth of fill is greater than the arch ring thickness at the crown (Department of Transport 1997a). One shallow and one deep 2-D arch were repaired by applying concrete slab on top of the surface of the backfill. The results and comparison between the benchmark and the repaired arch behaviours are presented below.

#### 6.4.1 Rolling load results

Comparisons of the measured deflections at 25%, 50% and 75% of the arch span for the shallow benchmark and the repair tests (S2D-3B and S2D-3R) are presented in Figure 6-6 A-C. The measured deflections at the last roller pass in the forward direction for both tests are detailed in this figure and the presented deflections were zeroed prior to starting the roller on that pass. Consideration of the recorded deflections of the repaired arch indicate a similar behaviour to the benchmark model under the rolling load. The results show, as expected, that the maximum radial deflection occurs at mid span of the arch when the rollers are directly located above. The slightly non symmetric nature of the

deflections is to do with the direction of movement of the roller. Recorded deflections in the repaired arch are significantly less than those obtained in the benchmark model at the same sections. The measured deflection value at 50% of the arch span for the benchmark test when the roller was locally located on that section is about four times the recorded deflection beneath the arch, at the same section, in the repaired test. This ratio is about 2.5 at 75% of the arch span. The bigger ratio at 50% of arch span (smaller backfill depth) indicates the localised effect of load distribution by the concrete slab.

Maximum outward displacements were recorded by the LVDT installed at 25% of the arch span when the roller was located at about 80% of the span in both the benchmark and the repair test. An average outward displacement of about 40% of the benchmark test was recorded in the repaired arch. The comparison between the maximum inward and outward deflections at 25% of the arch barrel indicates more effect of the relieving slab on inward deflections. This suggest no direct effect of the concrete slab on the arch deflection particularly arch displacement away from the load position. While the inward deflection is directly affected by the applied load which was redistributed by the concrete slab, the outward deflections appear to be more effected by the backfill behaviour near to the arch extrados. The later behaviour is more related to the backfill stiffness which allows the barrel to move into it and therefore the slab on top of that section does not have a significant effect on the outward deflections. If the same slab were to be applied to the extrados of the arch barrel a more significant effect of the concrete slab on the outward arch deflection would be expected. This is because the slab is significantly stiffer than the masonry and therefore significant displacement reduction would be expected. This is confirmed by the reported test results of Baralos (Baralos 2002). His test results indicate that applying the same saddle reinforced concrete on the extrados of the same geometry arch reduced outward deflection of the arch to 5% of the benchmark test which is 8 times smaller than the results achieved in this study when applying the slab on top of the backfill.

The benchmark and repaired arch deflections for the deep arch geometry under the rolling loads are presented in Figure 6-7. Consideration in this figure indicates the similar significant reduction in the arch deflections due to the relieving slab of concrete on top of the backfill of the deep arch geometry. Comparison between the recorded deflections in

the shallow and the deep arch geometry show that the deep arch deflections are reduced more than those for the shallow arch following application of the concrete slab. Larger reductions in the deflections in the deep arch geometry might be as a result of the greater effect of the backfill on this geometry of arch. The deflections of the deep arch at 50% of the span, when the roller was located directly above that section, decreased to about 10% of their previous values.

The at-rest soil pressures at different locations along the arch barrel under the dead load (at a stable stage of acceleration of 12g) are detailed in Figure 6-8. Each test result is indicated with its related name and the calculated pressures in the at-rest condition are indicated with the index *E* in this figure. The average pressure values that were obtained from a series of tests carried out with the same arch geometries by Burroughs (Burroughs 2002) are also presented in the figure as *S2D.Av.* and *D2D.Av.* for shallow and deep geometries, as a comparison. Given the natural vagaries in the determination of the at-rest pressures the results are generally considered to be appropriate and in reasonable agreement with those obtained from simple half space elastic theory (Poulos and Davis 1974). There is little apparent effect of the additional weight of the concrete on the repaired models.

The effect of the reinforced concrete slab on top of the backfill on the pressures generated by the rolling load are detailed in Figures 6-9 for the shallow arch. In this figure pressures recorded at different sections of the arch before and after applying the concrete slab are compared to each other. Pressures calculated according to UK practice for each section under the rolling load are included in the figure as a comparison. In the UK practice for load distribution the effect of movement direction and the stiffness of boundary conditions are not considered and differences between predicted and measured values are expected. As expected, recorded pressures under the rolling load in the repaired arch are significantly smaller than the benchmark test. While the maximum value of 23kPa was registered by the sensor at 75% of the span in the benchmark arch, the maximum pressure under the same roller condition is 7kPa for the repaired arch. It should be noted that the concrete slab depth (17mm) was added to the backfill depth (13mm) in the repair test and therefore smaller pressure values are expected as a result of this increasing backfill depth. Tests on the same arch geometry with an increase backfill depth

of 60mm have been carried out in a previous study (Burroughs 2002) and have indicated pressure reduction values of 12kPa at the same section which is smaller than the 16kPa reduction which is obtained in this test.

The load distribution analysis carried out using the codified method showed higher stresses in the extrados of the arches compared with the measured values. The codified method assumes that the applied load on the road surface is distributed, at extrados level, over the total width of the applied stress plus half the distance from the road surface to the extrados (Department of Transport 1997a). This suggests that a conservative applied load dispersal is achieved using the codified method. The conservatism of the codified dispersal method has been demonstrated experimentally by Fairfield (Fairfield and Ponniah 1993; Fairfield and Ponniah 1994b; Fairfield and Ponniah 1996).

The effects of pass numbers and roller movement direction for the repaired shallow arch (Test S2D-3R) are presented in Figure 6-10. Recorded pressures from the sensors at 75% of the span at pass numbers 2 and 7 in the forward direction are compared to each other in this figure. As the pass numbers increase no reduction in peak pressure was observed, similar to the benchmark tests. This may be due to sufficient compaction during the benchmark test and no significant change in the backfill condition after the repair. The backward movement effect of the roller in the last pass included in that figure as a comparison shows no significant effect of movement direction on the recorded pressures.

The responses of the sensors before and after the application of the concrete slab to the deep arch geometry are compared in Figure 6-11. Consideration on this figure indicates a significant reduction in the pressures after applying the concrete slab. No reduction in the recorded pressure was observed with increasing number of passes which is a similar result to the shallow arch.

### 6.4.2 Ultimate load results

Following the rolling loading the ultimate loading was applied at the quarter span location for each test. Some load cycles were applied similar to the benchmark tests. The load cycles and arch condition after applying the ultimate loads are detailed in Table 6-3. The resulting load deflection responses are presented in Figure 6-12 and Figure 6-13 for the shallow and deep arches geometries, respectively. The results show significant improvement in the arch load capacity after applying the concrete slab to both arch geometries. The maximum increasing load of the shallow repaired model was 3.4 times that of the benchmark model and 2.7 times the average benchmark maximum load. Included in Figure 6-12 (beneath load position), for comparison, are the previous results (Baralos 2002) obtained using a concrete saddle as a repair method on the same arch geometry. Saddle concrete on the extrados of the arch barrel with the same geometry increased the ultimate load capacity 2.6 times compared to the average benchmark tests results; this indicates a similar ultimate load increase to that obtained with a concrete relieving slab on top of the backfill surface. The same ultimate load increase for saddling and for the relieving concrete slab indicates a great advantage of the later repair method due to less labour work and disruption in traffic for a similar end result. Consideration of Figure 6-12 shows approximately the same response for both the repaired arch using a relieving slab and for saddling. At about 14kN of the applied load a significant change in arch deflection under the load position is observed for the repaired arch. This might be as a result of the concrete slab collapse. The arch deflection at failure was about twice as large in the load line location as in the repaired arch model, as that compared with the benchmark average deflection.

An initial stiffness value of 19kN/mm was obtained for the benchmark arch for the serviceability loads (between 15-40% maximum loads) which increased up to 57kN/mm for the same range of values for the repaired arch. This shows an increase in the stiffness by a factor of 3.0 following repair. At between 80-95% of the maximum load, the stiffness of the repaired arch relative to the benchmark was increased by a factor of 10 (see Table 6-5 for values). A previous study (Baralos 2002) showed that applying a saddle concrete to the extrados of the arch barrel increased the stiffness by a factor of 7 and 30 respectively for those load ranges. The increase in stiffness reduces the arch sway



remote from the applied load location. Whilst an arch swayed about 0.75mm at 4.6kN (maximum load) in the benchmark test, this arch displacement was observed at about 12kN in the repaired arch.

The increase in the arch load capacity due to the relieving slab can be partially estimated using the MEXE method. At a model fill depth of 13mm in the benchmark test (S2D-3B) the MEXE modified axle load was 11.6 tonnes (for an equivalent prototype 6m single span arch), increasing to 23.2 tonnes at a fill depth 30mm. This represents a doubling of capacity. Repaired tests results give a single allowable axle load of 63 tonnes which is 4.2 times the 11.6 tonnes (according to the 13mm backfill depth). This indicates an increase in the load capacity of more than twice compared with the estimated increase using the MEXE method. It should be noted that the MEXE method cannot distinguish between the addition of extra fill and the addition of extra cover by means of a stiffer reinforced concrete slab overlay. The reported results from research work by Fairfield and Ponniah (Fairfield and Ponniah 1996) have shown an increase of about 60% in the arch load capacity due to apply a 0.10m overlay for a particular deep arch geometry with backfill depth of 0.15m at the crown.

The deep arch ultimate load capacity was increased 3.7 and 3.2 times compared to the specific benchmark and average benchmark respectively. This is comparable with the improvement of the arch load capacity when the arch was strengthened with a layer of concrete with the same dimensions to the intrados or extrados of the arch barrel (Baralos 2002). Previous results have shown a 4.0 times improvement in ultimate load capacity for a deep arch geometry which was repaired using a similar concrete slab to the intrados of the model. It should be mentioned that in the case of the addition of concrete to the intrados of the model this reduces the effective arch span and therefore an additional ultimate load improvement is expected. The results of full scale tests at the TRL indicated that a layer of 150mm of sprayed concrete and a concrete saddle increased the ultimate capacity by factors of 3.7 and 2.9 respectively (Sumon 1999; Sumon and Ricketts 1995) and this has reasonable agreement with the results achieved from the small scale centrifuge tests in the current study.

Figure 6-13 contains the load deflection results at 3 locations along the span for the repaired and the benchmark deep arches. Included in Figure 6-13 are the previous results obtained by applying a similarly dimensioned and reinforced concrete slab to the intrados of the arch barrel. The stiffness values of 110kN/mm for the repaired arch model at 15-40% of the maximum load increased by a factor of 5.5 compared with about 22kN/mm which was obtained for the benchmark arch. At 80-95% of peak load this factor has increased to 12.5. Little or no deflection was observed at the crown of the arch close to the failure load level, but after that upward displacement was observed up to arch failure.

Numerical studies (Choo et al. 1995) indicate that whether non reinforced or reinforced concrete is used in repair, the location of the concrete on the extrados or intrados of the arch is relatively insignificant in determining of the ultimate load capacity. While the current study shows that for small scale tests with the same geometry being repaired using a relieving slab on top of the backfill represents the same response as applying the sprayed concrete to the intrados of the arch barrel.

The response of the pressure sensors under the increasing loads for all available sections of the repaired arches are presented in Figure 6-14 and Figure 6-15 for the shallow and deep arches geometries. Included in Figure 6-14 are the pressures at 7% and 75% of the span obtained from the benchmark test as a comparison. This figure shows a progressive increase in pressure recorded at the remote part of the arch under an increasing load. A significant reduction was registered near to the collapse load. This behaviour was observed in all the sensors. Consideration of this figure indicates that the recorded pressures in the benchmark test are slightly more than in the repaired arch at 75% of span. Figure 6-12 indicates significantly smaller arch sway in the repaired model compared with the benchmark test and therefore smaller pressures on the extrados of the arch barrel are expected. Recorded pressure under the load location showed an increase in pressure up to about half of the ultimate load and then reduction in pressure after that for the repaired arch. This is consistent with some part of the applied load being resisted by the reinforced slab with therefore a smaller part of the applied load being resisted by the arch barrel. With increasing applied load more of the load appeared to be distributed to the arch barrel and this resulted in inward displacement under the load location.

With increasing load the sway movements of the arch barrel were smaller than other similar arches although more pressure was recorded. This might be because the remote part of the backfill was restricted by the concrete slab from above. Therefore the backfill cannot readily move which is possible for other tests and therefore more pressures were generated. This is confirmed by Figure 6-15. As can be seen from this figure after the achievement of the peak pressure of 20kPa, on the arch extrados at 80% of span under the applied load of 4.0kN, the pressure suddenly decreased with an increasing load, which indicates the moving away of a block of backfill from the barrel. At the same position under the same load level for the repaired arch the pressure of 10kPa (half of the benchmark value) was recorded which is due to the effect of the smaller barrel movement towards the backfill. With increasing load, an increase in pressure was observed, the inverse to the benchmark, because the movement of the backfill blocks away from the barrel was restricted by the slab.

#### 6.4.3 Post test investigation

The failure modes of the repaired arch barrels are given in Figure 6-16 and Figure 6-17 for both the shallow and the deep arch geometry respectively. Also the arches' condition after the tests are shown in Plate 6-3 and Plate 6-4. The shallow arch repaired model failed after developing ring separation on the loaded side of the model between the springing and the arch crown. No hinge formation was identified after the test. Consideration of the arch condition after the benchmark test showed a hinge developing between the load location and crown of the arch. In the repaired arch no more hinges developed and ring separation was observed in most parts of the barrel. Two hinges under the load application and on the top of the crown of the arch were developed in the concrete slab for the shallow arch. Separation between the slab and the backfill surface was observed near to both ends of the arch. Four hinges were developed in the arch barrel for test D2D-1R with some ring separation occurring during the test, this separation formed between the load location and the arch crown. Three hinges were formed in the slab during the test, one of them was located under the load position and one above the hinge formed in the arch barrel just above the crown.

## 6.5 Stitching

After the completion of the 2-D tests, the 3-D tests were undertaken and the first 3-D shallow arch was repaired using a stitching method. The repaired arch was tested under a similar rolling load to the benchmark tests with a full width roller. Repair details and test results are presented in the next section.

### 6.5.1 Stitching repair details

Ring separation is a common defect in multi ring arch masonry bridges and is associated with loss of bond between the rings. A survey of 98 bridges by Page (Page et al. 1991) indicated that 19 bridges had some cracks in their rings and 41 bridges had an arch ring defect of some kind. The effect of ring separation on ultimate arch load capacity has been investigated by Melbourne (Melbourne and Gilbert 1993; Melbourne and Gilbert 1995). Reported results by Melbourne have shown that ring separation caused a reduction of between 30% to 60% in the ultimate load capacity of the model and full scale arch bridges. Stitching was applied to the shallow arch geometry in a previous 2-D test (Baralos 2002) using steel rods normal to the barrel. In most of the above referenced tests 2-D models were considered and no effect of stitching in combination of the spandrel walls were investigated. For the current study it was decided to apply the rods at an inclined angle and also using some thin steel bars as a shear connection to connect the spandrel and extrados barrel to each other.

### 6.5.2 Rolling load results

The arch repaired using a stitching method was tested under 14 passes of the roller load, which was applied to the whole width of the arch. Comparison between the measured deflections at 50% of the span along the centre line and the front edge of the arch with roller movement are given in Figure 6-18 as a typical recorded deflection for this test. Deflections under both the mid width and the front edge of the arches are presented in this figure. As can be seen the repaired arch deflections were reduced in comparison with the benchmark arch probably due to the higher stiffness of the repaired arch and a greater contribution of the spandrel walls to the load resistance. A maximum recorded deflection of 0.08mm for benchmark model, was reduced to 0.055mm in the repaired arch, which

indicates a reduction of about 30% in arch deflection under rolling load due to applied stitching. The arch was restricted by the stiffer spandrel wall and smaller deflections are expected at the edge of arch compared with the mid width and this can be seen in the figure. This suggests out of plane arch bending even under the rolling loads, particularly in the repaired arch where the spandrel wall was connected to the ring using the shear connection steel bars.

Comparison of the pressures measured in the benchmark and the repaired arch show that increases in the pressures are seen in some of the sensors for the repaired arch. The increases lie however within the range of the results which were recorded for the shallow arch benchmarks. This indicates no significant effect of applying stitching on the pressure at the extrados of the arch barrel. A similar result has been recorded by Baralos (Baralos 2002) after applying a stitching repair method on the same shallow arch geometry but in a 2-D arch model test.

### 6.5.3 Ultimate load results

Comparison of the load/deflection results for tests S3D-1B and S3D-1R are given in Figure 6-19. Consideration of the load deflection plot indicates no significant difference in arch stiffness between the repaired and the benchmark arch up to about 80% of the benchmark peak load. When the applied load reached 6kN the arch stiffness was significantly increased until 8kN and after that a significant increase in deflection was observed with a small increase in load. This re-strengthening response of the arch barrel might be due to more contribution of the spandrel walls in load resistance. It should be noted that a small separation crack was noticed during the preparation time of benchmark test and therefore arch deflection was not fully restricted during that test. In the repaired arch model the spandrel walls were connected to the extrados ring layer and therefore a fuller response of the walls due to load is expected. Post test investigation with no observation of cracks between the spandrel walls and the arch barrel confirm this.

An ultimate load capacity of 8.6kN was obtained in the repaired arch model test which is about 50% bigger than the benchmark test. The obtained results showed no increase in repaired arch load capacity compared with mean benchmark results when

stitching was used to repair the same shallow arch geometry in a previous 2-D model tests (Baralos 2002). As explained above the greater effect of the repair method for this test might be as a result of the spandrel wall effect on the load carrying capacity. Tests results on a 2m wide and 5m span full scale arch carried out at TRL (Sumon 1999), which was repaired using a network of 6mm diameter stainless steel bars indicated a similar load capacity improvement in that particular test. In that test stainless steel bars were bonded into rebates cut into the soffit on both faces of the arch. The repaired arch load capacity was increased 38% above the un-strengthened model for that particular arch. No stitching was applied to that arch. Consideration of the results indicates that the increase in the repaired arch load capacity might be as a result of the addition of stainless steel bars between the barrel and the spandrel walls. On the other hand stitching bars have no effect on increasing of arch load capacity. This is supported by the previous test results on small scale centrifuge models (Baralos 2002) and the post test result observation.

Application of a novel system to a similar arch geometry have previously indicated a significant improvement (of about 200%) in the arch load capacity compared with an un-strengthened arch (Carl and Graham 1999). In that system the bars and grout were contained within a sock, which protects the surrounding masonry from being displaced or otherwise damaged by the grouting pressure. During inflation, the socks deform and permits sufficient leakage of the grout to develop a chemical and mechanical bond with the masonry. At small scale model test 2mm rods with a cement mortar were placed in pre-installed holes in the masonry. Post test investigation of test S3D-1R showed a poor connection between the mortar and masonry and separation under the loading even in the area of the bars. This might be as a result of shrinkage of mortar during mortar curing. In addition smooth rods were used for stitching which might not be as effective for the test propose.

Recorded pressures on the extrados of the arch barrel under the increasing load for the repaired arch are compared to the same locations in the benchmark test in Figure 6-20. A similar behaviour was recorded in both the benchmark and the repaired arch tests. Greater pressures were recorded on the remote part of repaired arch which is not expected as there were smaller movements of the arch towards the backfill.

#### **6.5.4 Post test investigation**

The overall failure mechanism that developed during the repair test is shown in Figure 6-21. The arch condition after the test indicated that ring separation development was not prevented by application of the stitching to the arch barrel particularly under the loaded part of the arch. A previous study (Baralos 2002) on 2-D shallow arches with the same geometry showed that the application of stitching bars did prevent the development of ring separation. In the previous tests no increase in load capacity was observed and the repaired arch collapsed under a smaller load compared with the benchmark tests. No separation between the spandrel wall and arch barrel was observed during the current test and this indicates that the steel bars successfully connected the arch barrel to the spandrel walls. Crack investigation in the spandrel walls indicated the walls moved as a block. The separation between the blocks are clearly visible under the load location. Cracks positions and arch condition after benchmark and repair tests are shown in Plates 6-5 and 6-6.

### **6.6 Partially saddled concrete**

Partially saddled concrete was used to repair the second 3-D test. This repair method was applied to the shallow arch geometry and the model was tested to the same roller loading and ultimate loads as the benchmark tests. Details of the repair method and the test results are presented in next sections.

#### **6.6.1 Repair details**

As referred to in the previous sections the use of a concrete saddle on the extrados of an arch barrel is a popular method of strengthening arches. Saddling concrete usually requires a road closure or one way working if the saddle is to be built half at a time. Traffic control is often difficult and sometimes it is impossible to build if there is no alternative road available near the site. In addition this method involves significant excavation and a considerable volume of material must be removed from site and replaced. This increases the cost of the repair method by a considerable amount. To try to avoid these disadvantages of saddling it was decided to try concrete saddling some parts of bridge instead of the whole width; these parts of saddle concrete to be stitched to the spandrel walls to avoid any separation between the spandrel and barrel. More details of



the repair method were presented previously in Chapter 4 and the results obtained from the test and discussion are presented here.

### 6.6.2 Rolling load results

The repaired arch model was tested with initially 14 passes of the steel roller which was applied first to the whole width of the arch (Load Case 1) and then to 6 passes of half the lead roller which was applied through a half width along the centre line (Load Case 2) and subsequently the front edge (Load Case 3) of the arch. The roller weight for each Load Case are detailed in Table 6-4. Recorded arch deflections under the rolling loads at 25% and 50% of the span are presented in Figure 6-22 for the Load Case 1. Also included in this figure are the benchmark arch deflections under the same roller load as a comparison. Arch deflections are significantly decreased in the repaired arch model. While the maximum recorded repaired arch deflection at 50% of the span is 0.08mm, the maximum values of 0.03mm was recorded by the same LVDT under the same roller load for the benchmark test. With the rolling load at the critical load position, the measured deflections were reduced to approximately 30% of the benchmark deflection following application of the concrete. Saddling with concrete to the whole width of the barrel on the same arch geometry reduced the repaired arch deflections to 20% of the benchmark test (Baralos 2002) which appears consistent with the results obtained from the current application of partial concrete.

The repaired arch deflection showed larger deflections along the middle row compared with the outer rows. This is expected and shows that adding the saddle edge concrete restricts the arch deflections to both edges significantly. Difference in arch deflections under the middle and edges is more important when the unsymmetrical roller loading (Load Case 3) is applied to the arch. The effect of the roller load location on the arch deflection is presented in Table 6-6. Recorded deflections under the middle and front edge of the arch at 25%, 50% and 75% of the span under the different load locations are detailed in this table. The deflections recorded by the middle transducer are larger than those recorded at the edge under Load Case 1 and 2 for both the benchmark and the repaired tests but the difference between the middle and the edges are larger in the repaired test. While the arch deflection at 25% of the span at both edges of the benchmark

arch is about 60% of the deflection along the centreline of the barrel, this ratio reduced to 20% for the repaired arch. This indicates the deflection is being restricted by the application of the saddling in addition to the spandrel wall restriction in the repaired model. A study of a 1.25m segmental arch with a span to rise ratio of 4.0 by Begimgil (Begimgil 1995) found larger deflection values mid width of the arch barrel. In that study during loading, deflections were measured at the edge of the barrel were about 70% of deflection at mid width. This confirmed that the spandrel walls offered a stiffer restraint to barrel movement than the soil. Also, these results are comparable with those which were obtained during the benchmark test under the same rolling load.

Consideration of pressures registered during the rolling load repair test shows a significant effect of the roller load position. Pressures recorded by the front and back sensors at 20% of the arch span under Load Case 2 and Load Case 3 are compared to each other in Figure 6-23 A-B for the repaired arch. When the roller was applied along the centre line of the arch approximately the same values registered by both sensors while applying the roller near to the front edge of the arch cause significantly larger pressures in the front sensor compared with the back sensor. Similar results were recorded on the other sections of the arch barrel.

Comparison of the pressures obtained from the benchmark and the repaired arch, recorded by the same sensors are shown in Figure 6-24. As indicated in Table 6-6 the repaired arch deflections are significantly less than the benchmark test under the same roller load, therefore larger pressures would be expected to be generated in the repaired arch; this is confirmed by the measured values. Consideration of the figure indicates higher pressures recorded by most of the sensors in the repaired arch, as expected, except at 75% of arch span. When the roller is located remotely from the sensors passive pressure were recorded by the sensors in the benchmark test but no response was recorded by those sensors in the repaired arch. This is as expected because following application of the saddle concrete on the extrados of the arch barrel, the barrel displacements were significantly reduced and thus limited passive pressures were expected. Large differences were recorded in all sections when the roller passed the crown and prior to reaching the sensors. A large reduction in benchmark test pressures was observed when the roller passed the crown as a result of the moving away of the barrel from the backfill and the

existence of a surface shear force in the roller movement direction which was explained in Chapter 5. Although the same behaviour was observed in the repaired arch consideration of the figures indicate a smaller reduction in the repaired model due to the barrel movement restriction. While a reduction of pressure of about 10kPa was observed in the benchmark test a reduction of about 5kPa was registered in the repaired model.

### 6.6.3 Ultimate load results

The load deflection at mid width of the arch for both the benchmark and repaired arch for test S3D-2R is given in Figure 6-25. Also included is the recorded deflection from transducers on top of the spandrel wall, for both tests. The figure indicates a significant improvement in both the arch stiffness and ultimate load capacity. At a load level of about 15.8kN a significant increase in the deflection occurred without any increase in the applied load. After reaching 16.1kN the load was generally reduced and this shows the full failure of the arch.

The load was increased up to 9.5kN and then reloaded to 2.5kN as a first load cycle in S3D-2R. The second load cycle was applied when the load increased up to 11.5kN and the applied load was reduced again. The arch deflection was not recovered during the load cycles which shows the plastic behaviour of the repaired arch. It should be noted that a similar response was observed during the benchmark test. The arch stiffness determined from both load cycles is approximately 47kN/mm. The initial stiffness of the 2-D repaired arches using saddling concrete on whole width of the barrel was reported to be about 50% of this value (Baralos 2002). This indicates the addition of the spandrel walls (3-D model) provided additional stiffness to the arch.

The arch collapsed at an ultimate load of 16.1kN which is about 2.2 times compared with the benchmark test. The peak load attained by the arch with the same geometry (2-D model) repaired with the extrados concrete was 14.9kN (Baralos 2002) which is slightly smaller than obtained here. A larger collapse load is expected when the concrete is applied to the whole width of the barrel extrados but it should be noted that the effect of spandrel walls to the ultimate load should also be considered, particularly in this case where the spandrel wall was well connected to the arch barrel. A study of three,

1.5m semi-circular arches by Melbourne & Walker (Melbourne and Walker 1988) found, for their particular bridge geometry, that the presence of spandrel walls increased the ultimate strength of the bridge by 70%. Also reported test results on a wide range of arch geometries by Royles & Hendry (Royles and Hendry 1991) indicated the significant effect of the spandrel walls contribution on arch load capacity. Considering the effect of the spandrel walls on improvements in the arch load capacity, there is a good consistency between the current results with those reported by Baralos (Baralos 2002).

Recorded pressures at different sections of the arch barrel are given in Figure 6-26 for test S3D-2R. The results are similar to the other arches with the recorded pressures increasing with increasing applied load at the remote part of the arch barrel as a result of passive pressure conditions. The pressures registered by those gauges that were installed beneath the load line were reduced because of the active pressure generated on that part. The pressures indicate smaller values under the same applied load for the repaired arch, as expected. The arch movements are restricted following application of the repair and significantly smaller displacements were measured under the same load values in the repaired arch (Figure 6-25). Therefore smaller pressures on the extrados of the arch are expected which was confirmed during the test. While the maximum pressure of 45kPa was recorded under the applied load of 6kN in benchmark test, the value of about 12kPa was registered by the same sensor at the same load in the repair test.

Good consistency was achieved between those results recorded by pairs of sensors in each section. Recorded pressures by the pair of sensors which were installed at 75% of span are detailed in Figure 6-27 as typical results.

#### **6.6.4 Post test investigation**

Plates 6-7 and 6-8 show the arch after the benchmark and the repair tests respectively. The arch conditions are also given in Figure 6-28. The cracks that occurred in both the front and back side of the arch are presented in this figure. Fortunately no cracks occurred during construction and before the benchmark test. The arch failed due to the development of ring separations in the barrel under the load location. Steel shear bars prevented any cracks development between the barrel extrados and spandrel walls. The

spandrel walls failed parallel to the steel bars and the benchmark cracks were not followed in the repaired arch. No separation between the concrete and barrel was observed and this indicates a good connection between the arch barrel and the saddle concrete.

## 6.7 Spandrel walls strengthening

Deterioration of the spandrels and parapets is a frequent problem in most arch bridges. BD 21/97 (Department of Transport 1997b) requires parapets and spandrel walls to be assessed by visual inspection. Page (Page 1996) listed some forms of deterioration for these parts of the structure without any detail of strengthening methods for the spandrel and parapet walls in this guidance. The traditional means of repairing walls that were deforming, tilting or sliding off the barrel was to tie both walls together with rods and large spreader plates on the outside of the bridges (Department of Transport 1997a).

In most assessment methods for masonry arch bridges which are used in the UK the effect of the parapets and spandrel walls are ignored. Royles (Royles and Hendry 1991) studies on a series of 1 metre span arch bridges show a significant effect of the spandrel walls. Their results have shown that arch load capacity with spandrel walls are about 30% higher than the same arch without spandrels. Melbourne's (Melbourne et al. 1995) studies confirmed the effect of the spandrel walls on arch load capacity but this study showed that there is no significant difference between the load capacity of arches with or without tied spandrel walls. The literature review has shown there is little research on the effect of strengthening spandrel walls on arch load capacities. It was decided to repair some of the arch models with spandrel wall strengthening in the current study but from the inside of the walls. After completing the benchmark tests the models were repaired by applying reinforced concrete to the inner sides of the spandrel walls. The location of the concrete was restricted to those parts of the structure that would in normal circumstances be readily accessible for such work. The test procedure and repair application method are detailed in Chapter 4. The results obtained and the effect of using this strengthening method on arch load capacity are presented here. The repair method was applied to both shallow and deep arch geometries.

### 6.7.1 Rolling load results

Both arch models (shallow and deep arches) were applied with the same benchmark rolling load except in Load Case 3. In this load case a smaller roller width was used because the total width of the arch between the spandrel walls was decreased after applying the reinforced concrete. The applied roller weight in this load case was decreased to 5.8kgs compared with the 7.3kgs which was applied to the benchmark tests.

Arch deflections during the tests were measured using three rows, the same as the last 3-D test. Figure 6-29 details arch deflections at 35% and 75% of arch span under Load Case 1. The deflections show the out of plane bending of the arch even under symmetric low load levels (about 30% of the benchmark peak load). While approximately the same displacements were registered in the front and back edge of the arch barrel, the middle values are about twice of the edges values when the roller is located locally on top of each section. This is expected because the reinforced spandrel wall stiffness is significantly higher than the arch barrel and restricts the arch deflections at the edges. In comparison with the benchmark tests significantly smaller arch deflections were measured in all the sections. While a maximum deflection values of 0.10mm was recorded at mid section of the arch when the roller was locally located on top of that section the recorded values for the repaired arch for the same LVDT was 0.05mm, which is a reduction of about 50%. Benchmark arch deflections under the same roller are included in Figure 6-29 as a comparison. Consideration on this figure shows that sway movement was recorded when the roller was located remote from the LVDT position in the benchmark model but in the repaired arch, no or very little sway movement was observed. In the benchmark arch barrel there is no major shear connection between the barrel and spandrel walls and in some sections (Figure 6-30 B) large deflections were recorded at the edges of the arches. This might be as a result of crack propagation and separation between the walls and barrel even under low load levels. In the repaired arch model no crack propagation is possible, at least under the rolling load, and therefore the high stiffness spandrel walls restricted any sway movement of the arch barrel when the roller were located remotely from the LVDT.

Crown arch deflections under the different types of rolling load cases, when positioned at the crown, for the shallow arch are detailed in Table 6-6. The results are for both a full width load of 15kgs and a half width load of 7.5kgs (there are slight differences between the original and repaired loading but the deflections have been ratioed to suit). The shallow benchmark deflections are approximately the same under both the edge and the middle of the arch for the full width load, these reduce, as expected, when the load remains symmetric but of reduced width (and weight); there is also some indication of transverse bending. This effect is repeated with rolling Load Case 3 with the edge under the load now deflecting more than the arch middle. The repaired arch indicates a significantly stiffer response, especially at the edges (where the concrete was placed); the back reading is an anomaly.

The deep arch deflections at the third point of the span are also presented in Table 6-6 for different rolling loads positioned at the third point. The deep arch appears stiffer than the shallow arch but deflections at the one third points would anyway be less. The transverse bending is also less apparent for both centre and edge loading. However the overall effect of the repair appears to produce a similar increase in stiffness over the benchmark arch.

### 6.7.2 Ultimate load results

The load/deflection plots for the shallow arch tests for both the benchmark and repaired arches are presented in Figure 6-30. The results show the deflections at the front edge, middle and back edge of the arch at the quarter point, immediately under the applied increasing load. The first index in each data series indicate the benchmark or repaired model while the second index refer to the LVDT row position in this figure. The results show the 2-D behaviour (this will be affected by the rigid nature of the loading beam) but more importantly the significant increase in both strength and stiffness whilst maintaining the ductility of the overall behaviour. The result of the benchmark test also shows that the test was indeed taken up to the ultimate load capacity (without arch destruction). This is a very satisfying initial outcome. The ultimate load of 11.8kN was obtained for the repaired arch which is 250% larger than the 4.6kN peak load in the benchmark test.



The pressure sensor responses to the applied load are presented for both benchmark and repaired shallow arches in Figure 6-31. The pressures increased with increasing load at sensors remote from the applied load as a passive pressure condition. Comparison between the recorded pressures in the benchmark and repaired model show more change in the pressures in the benchmark test which is due to the larger arch movement in that test.

The effect of arch movement and developed passive pressure for the shallow arch are detailed in Figure 6-32, as determined from the ultimate load tests. The recorded pressure was zeroed before the start of the loading for this figure so as to represent the change in pressure solely as a result of the effect of the live load. Under increasing applied load on the far side of the arch barrel (75% of span) the arch initially moved towards the backfill and due to this movement the passive pressure was mobilised. The benchmark arches indicate slightly higher pressures as the strengthened spandrel wall restricts the arch barrel movement and therefore the change in pressure on the repaired arch is less than the benchmark test. This effect can be seen up to a deflection of about 0.1mm. Following this the hinges are starting to form and the overall kinematics of blocks of arch (and soil) cause the soil to move away faster than the arch resulting in less pressures at these locations. The maximum change in pressure was recorded at 75% of the arch span under a movement of about 0.15mm. The same change in pressure was reported by Burroughs (Burroughs et al. 2002) under a movement of about 0.25mm at the same section for a 2-D arch.

For the deep arch benchmark the increasing load was increased to 6.9kN. At this load level some cracks in the spandrel walls were observed and the test was stopped to avoid a collapse and make an un-repairable arch. Arch deflections at 75% of the span for the benchmark and the repaired arch recorded by the different rows of LVDTs are presented in Figure 6-33. Also included in Figure 6-33 is the deflection of the repaired wall front face. The repaired arch attained an ultimate load of 14.0kN giving just over a 100% increase over the benchmark (un-failed) initial test. The figure shows a largely 2-D response and a very significant increase in the stiffness. Deflection of the repaired arch at an applied load of 14.0kN is about 55% of the benchmark arch at the same position under half of that load.

Soil/ interaction at different positions in the extrados of the deep arch barrel due to increasing load are detailed in Figure 6-34 for the benchmark and repaired arch. The post load peak soil pressures have been removed for clarity. For the benchmark arch the result at 8% (close and to the left of the applied load) show an initial increase in pressure, likely under the direct influence of the applied load, followed by a reduction as the live load pushes the barrel away from the soil, leaving it behind. For the same test the pressure at 81% of the arch span shows a progressive increase associated with the normal development of passive pressures. For the repaired arches there is a similar response at 8% of the span but there is a more gradual reduction in pressure (active pressure) as the arch moves away. At 68% there is little effect as there is little soil to develop any normal pressures. At 92% the effect is significant but is limited by the proximity of the rigid abutment. The maximum pressures develop at 81% of the span where the movement is significant and there is sufficient depth of soil to develop significant vertical pressures.

### 6.7.3 Post test results

Arch conditions before the benchmark test, after the test and after the repaired ultimate load test are presented in Figures 6-35 and 6-36 for both the shallow and deep arch geometries. Propagation of cracks were observed during construction for both arches which are presented in Part A of these figures. Benchmark tests were stopped after observing the first sign of failure (cracks formation) in spandrel walls for both geometries.

The arches failed because of the formation of ring separation under the load position, the formation of the fourth hinge (most remote from the applied load) was not observed in either of the tests. It appears that the strengthened spandrel wall restrained the arch barrel very well. No cracks were occurred between the walls and barrel under ultimate load in the repaired arches. The observation after the tests have shown no separation between the spandrel and barrel or disconnection of the steel rod connectors during either test. In Plates 6-9 and 6-10 more details of arch before and after test are compared with each other for the shallow arch geometry.

## 6.8 Conclusions

Laboratory experiments have successfully been carried out on two different geometries of 1/12<sup>th</sup> scale single span centrifuge arch models. The experiments provided useful information on the effectiveness of the tested repair methods on the failure mechanism and particularly on the service and ultimate load capacity of the arches. Final comparisons of all the repaired arches are presented in Figure 6-37 and Figure 6-38 for the 2-D and 3-D model tests. Consideration on these figures indicate the greatest effect of the relieving concrete slab and partially concrete slab repair methods for the 2-D and 3-D models respectively. The results have been discussed individually in the previous sections and the general conclusions are:-

- The use of plastic mesh reinforcement, test S2D-2R, had no significant effect on arch load capacity and pressure distribution under applied loads.
- The relieving concrete slab on top of the backfill significantly increased the ultimate arch load capacity for both shallow and deep arch geometries. The results indicate a significant improvement in the ultimate load capacity of the repaired arch over the benchmark arch. The load at failure of the shallow strengthened model was 3.4 times that of the benchmark model and 2.7 of the average benchmark. The results for the repaired deep arch were, respectively, 3.7 and 3.2 times as strong as the benchmark arch. The application of the slab to the surface appears to be at least equivalent to application directly to the arch intrados and extrados. A concrete slab on top of the fill distributes the pressure and decreases the recorded pressure on the arch barrel significantly. A significant decrease in arch barrel deflection was observed under rolling loads.
- The first shallow 3-D arch was repaired using stainless steel stitching bars applied to the arch barrel to connect the extrados ring and spandrel walls to each other. Test results showed no prevention of ring separation by the stitching bars but an increase of 50% in the ultimate arch load capacity following application of this method.
- Applying a partial saddle concrete on part of the arch barrel in addition to steel bar connection of the concrete to the spandrel increased the arch load capacity and the stiffness of the arch. The arch load capacity was improved by about 215% for the

repaired arch, which is comparable with applying the same concrete on top and beneath the barrel in the 2-D arch model tests.

- Two arches were repaired by applying a 17mm reinforced slab of micro-concrete on part of the inside of the spandrel walls. The extent of the repair was limited to that reasonably attainable in the field. Separation between the barrel and spandrel wall observed under low load level and outward movements of the spandrel walls occurred in the benchmark tests especially in the deep arch geometry. Tests results indicate a significant improvement in the load capacity of the repaired arch. The loads at the failure of the repaired models were approximately twice the benchmark for both the shallow and the deep arch geometries. At a low level of applied increasing load and under rolling loads the repaired arch demonstrated a much stiffer behaviour compared with the benchmark arch. The strengthened spandrel walls were seen to restrain the arch barrel and the recorded change in pressure on the extrados of arch barrel due to barrel movement was smaller than that of the benchmark arch.

Test ID	S2D-2R	S2D-3R	D2D-1R
Mortar mix.	1:3:12	1:3:12	1:3:12
Backfill	Granular limestone	Granular limestone	Granular limestone
Rolling load	14 pass steel roller	14 pass steel roller	14 pass steel roller
Load cell (kN)	10	100	100
Load position	25% span	25% span	25% span
Repair method	Plastic mesh reinforcement	Partially concrete slab	Partially concrete slab
Ultimate load (kN)	6.2	15.9	18.1

**Table 6-1: 2-D tests details and repair methods**

Test ID	S3D-1R	S3D-2R	S3D-2R	D3D-1R
Repair techniques	Stitching + spandrel walls connection	Partially saddle concrete	Spandrel wall strengthening	Spandrel wall strengthening
Rolling load	14 Passes L.C.1	14 passes L.C.1 6 passes L.C.2 6 passes L.C.3	14 passes L.C.1 6 passes L.C.2 6 passes L.C.3	14 passes L.C.1 6 passes L.C.2 6 passes L.C.3
Load cell (kN)	100	100	100	100
Load position	25 % span	25 % span	25 % span	30% span
Ultimate load (kN)	8.6	16.1	11.8	14.0

**Table 6-2: 3-D tests details and repair methods**

Test ID.	Max. load (kN)	First cycle		Second cycle		Third cycle		Arch description at failure
		Load	%	Load	%	Load	%	
S2D-2R	6.2	1.5	25	2.1	35	3.9	63	Mechanism failure+ four hinge formation
S2D-3R	15.9	7.5	47	10.6	67			Failure under ring separation at load location
D2D-1R	18.1	9.9	55	16.1	89			Ring separation under load location + three hinge formation

**Table 6-3: Load cycle and arch condition after each test**

Test ID	Load Case 1 (kg)	Load Case 2 (kg)	Load Case 3 (kg)
S3D-1R	11.8	N/A	N/A
S3D-2R	11.8	7.7	7.3
S3D-3R	12.2	7.7	5.8
D3D-1R	12.2	7.7	5.8

**Table 6-4: Roller weight for load cases for 3-D repair tests**

Test No.	Un-cracked stiffness(kN/mm) <sup>a</sup>	Cracked stiffness(kN/mm) <sup>b</sup>	Maximum applied load (kN)
S2D-1B	16	1	6.2
S2D-2B	8	2	5.0
S2D-2R	9	3	6.2
S2D-3B	19	3	4.6
S2D-3R	57	30	16.0
D2D-1B	20	2	4.8
D2D-1R	110	23	18.1
S3D-1B	22	1	5.7
S3D-1R	42	4	8.6
S3D-2B	23	7	7.4
S3D-2R	47	6	16.1
S3D-3B	4	2	4.7
S3D-3R	10	4	11.8
D3D-1B	17	7	6.9
D3D-1R	58	18	14.0

- a) the ratio of applied load to the radial deflection of the arch under load position calculated where the load, 15-40% peak load
- b) the ratio of applied load to the radial deflection of the arch under load position calculated where the load, 80-95% peak load

**Table 6-5: Arch model stiffness and ultimate load**



Test ID	LVDT location	Load Case 1	Load Case 2	Load Case 3
S3D-2B (25%Span)	Front	-.020	N/A	N/A
	Middle	-.032	-.016	-.013
	Back	-.020	-.009	-.004
S3D-2B (50%Span)	Front	N/A	N/A	N/A
	Middle	-.077	N/A	N/A
	Back	N/A	N/A	N/A
S3D-2B (75%Span)	Front	-.061	-.021	-.035
	Middle	-.062	-.028	-.024
	Back	-.069	-.021	-.006
S3D-2R (25%Span)	Front	-.002	-.001	-.004
	Middle	-.009	-.005	-.003
	Back	-.002	-.001	-.003
S3D-2R (50%Span)	Front	-.008	-.004	-.011
	Middle	-.027	-.022	-.011
	Back	-.008	-.004	.000
S3D-2R (75%Span)	Front	-.015	-.002	-.012
	Middle	-.02	-.012	-.007
	Back	-.008	-.008	N/A
S3D-3B (50%Span)	Front	-	-0.04	-0.07
	Middle	-0.10	-0.06	-0.03
	Back	-0.11	-	-
S3D-3R (50%Span)	Front	-0.02	-0.01	-0.03
	Middle	-0.05	-0.03	-0.03
	Back	-	-	-0.11
D3D-1B (35%Span)	Front	-0.03	-0.01	-0.02
	Middle	-0.03	-0.01	-0.02
	Back	-0.03	-0.01	-0.00
D3D-1R (35%Span)	Front	-	-	-
	Middle	-0.02	-0.01	-0.01
	Back	-0.01	-0.00	-

Load Case1: rolling load applied to the whole width of model

Load Case2: half width rolling load applied along the middle of the model width

Load Case3: half width rolling load applied to the front edge of the model

**Table 6-6: Arch deflections (mm) under the different load cases**

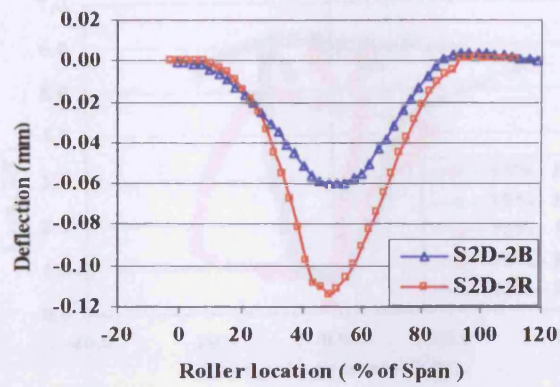


Figure 6-1: Arch deflection for different roller positions at 50% of the span

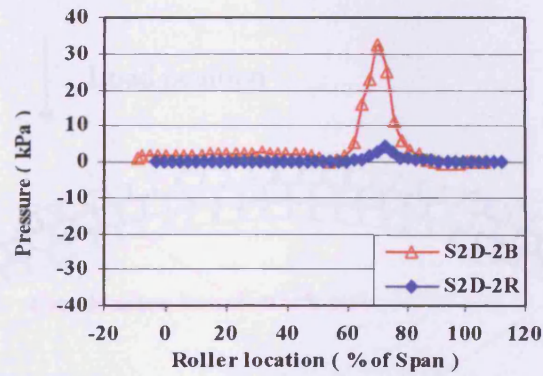


Figure 6-2: Pressures on arch extrados at 75% of the span

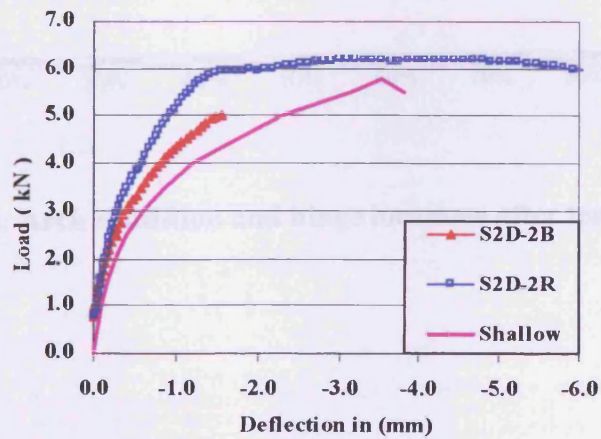


Figure 6-3: Load deflection curve under load position

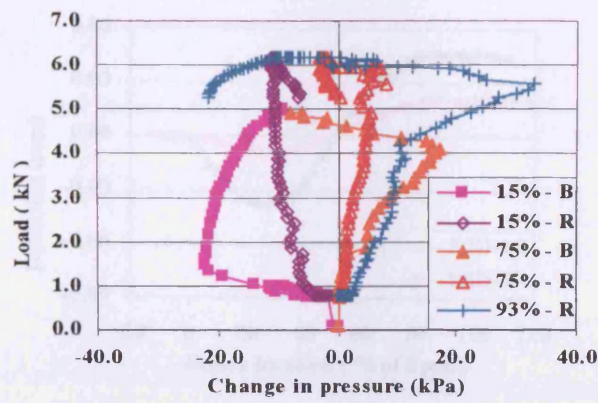


Figure 6-4: Pressures on different locations of the arch barrel (S2D-2B & S2D-2R)

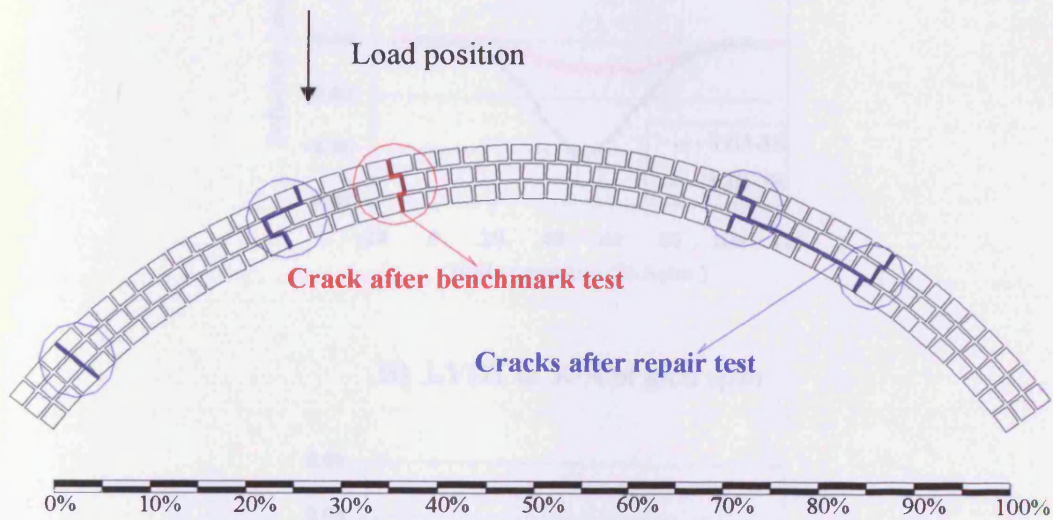
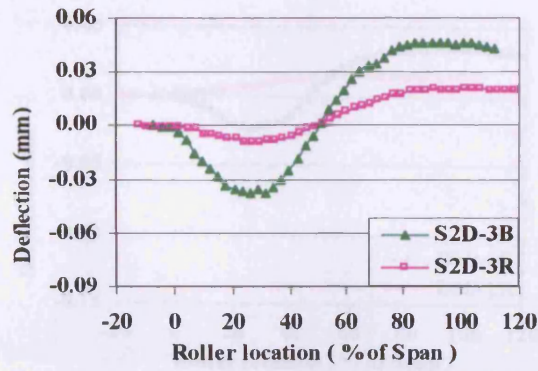
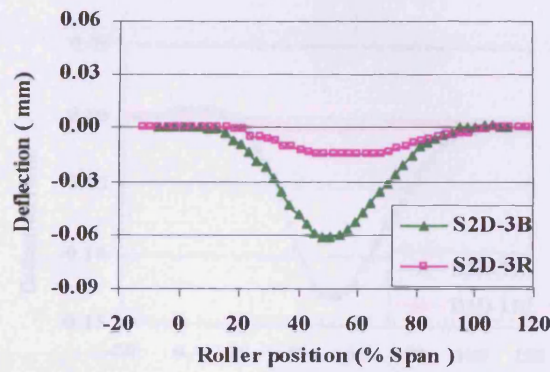


Figure 6-5: Arch condition and hinge locations after test (S2D-2R)

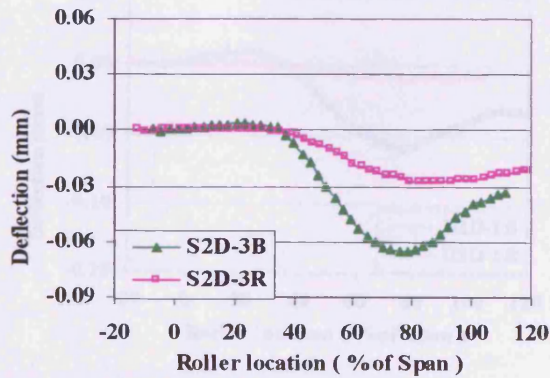




A) LVDT at 25% of arch span

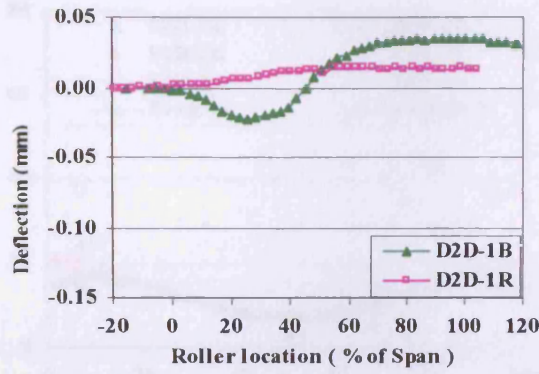


B) LVDT at 50% of arch span

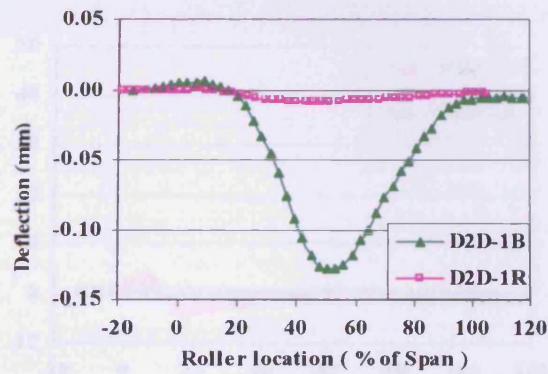


C) LVDT at 75% of arch span

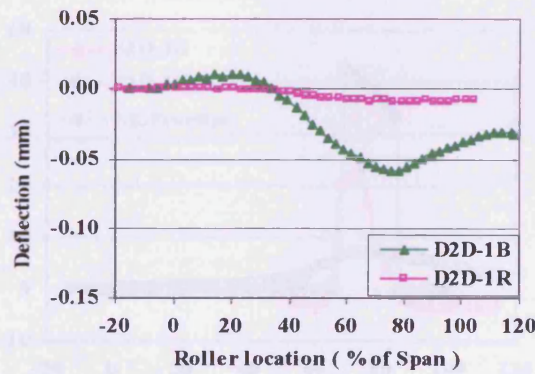
Figure 6-6: Shallow arch deflections under the rolling load



A) LVDT at 25% of arch span



B) LVDT at 50% of arch span



C) LVDT at 75% of arch span

Figure 6-7: Deep arch deflections under the rolling load

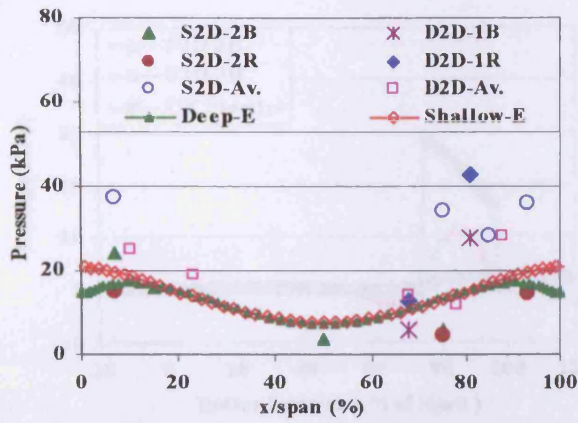
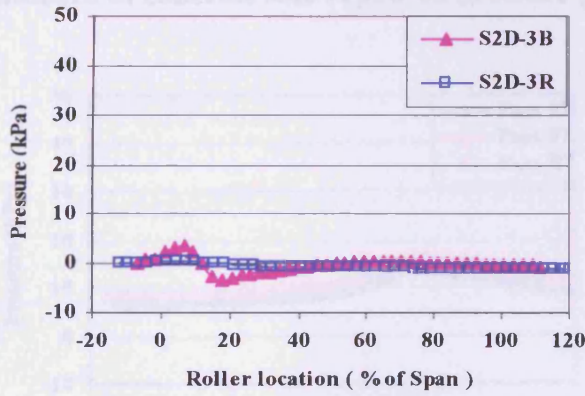
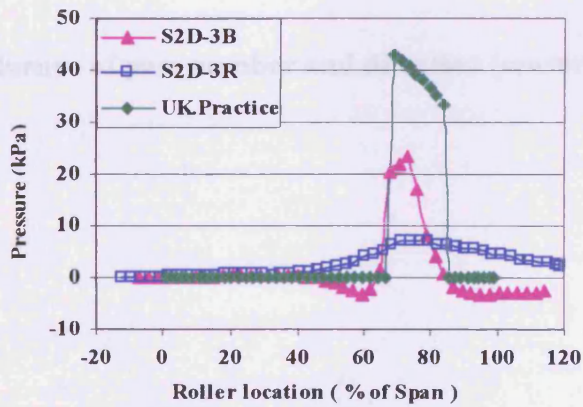


Figure 6-8: At-rest pressures at different locations of the arch barrel



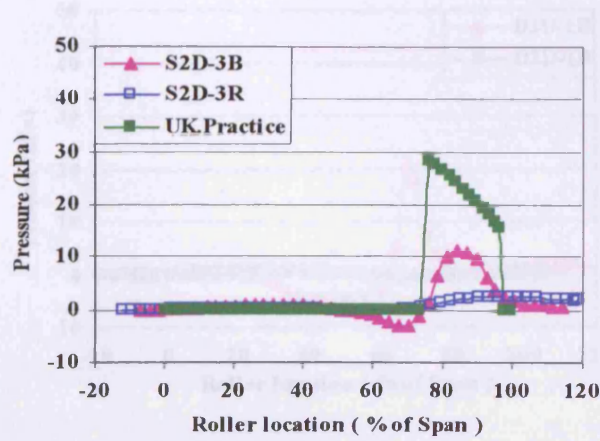
A) Kyowa at 15% span



B) Kyowa at 75% of span

Figure 6-9: Influence of concrete slab repair on pressure (shallow arch)





C) Kyowa at 85% of span

Figure 6-9: Influence of concrete slab repair on pressure (shallow arch, Cont.)

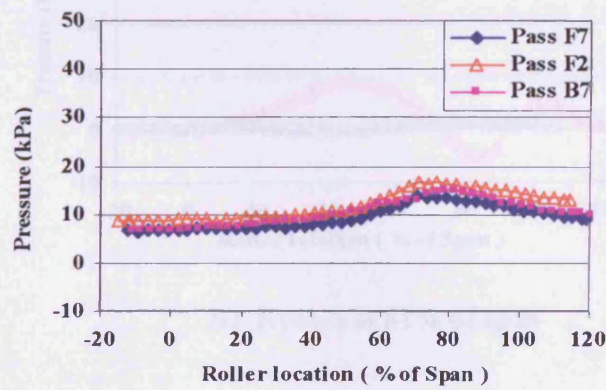
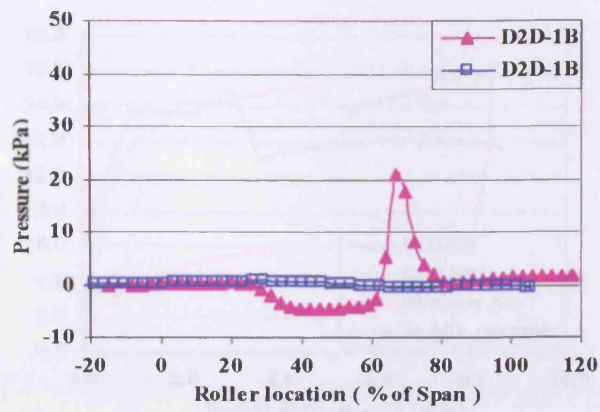
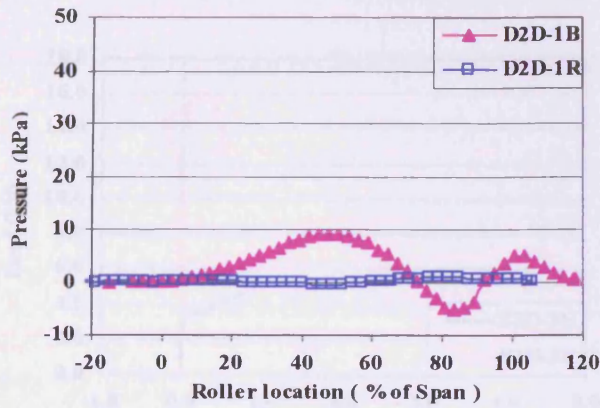


Figure 6-10: Influence of pass number and direction (sensor at 75% span, S2D-3R)

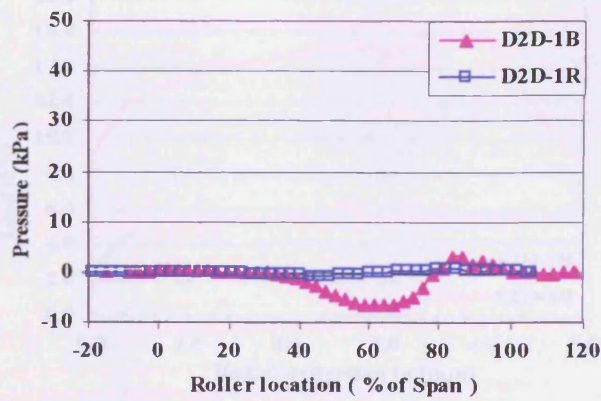




A) Kyowa at 68% of span

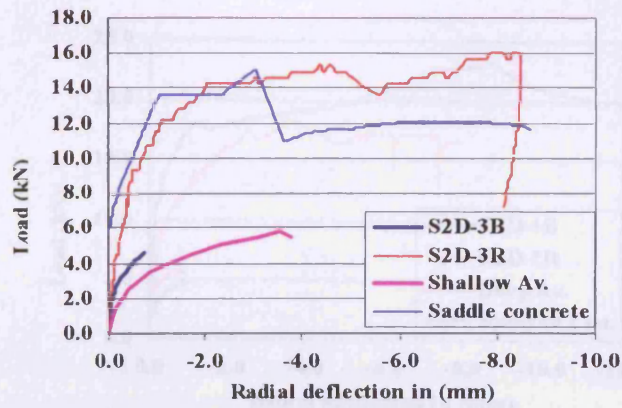


B) Kyowa at 81% of span

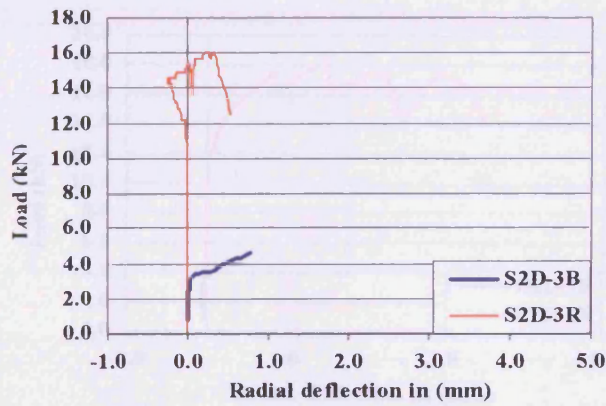


C) Kyowa at 92% of span

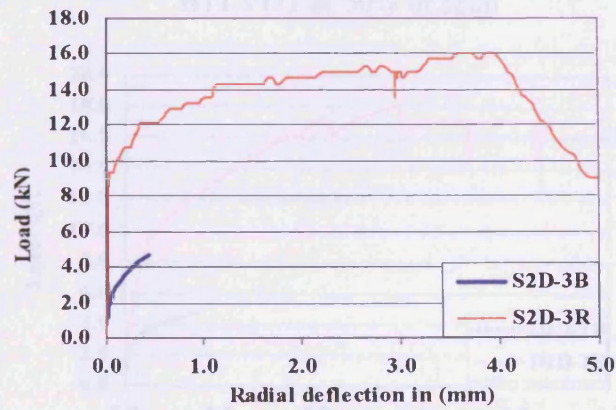
Figure 6-11: Influence of concrete slab repair on pressure (deep arch)



A) LVDT at 25% of span (beneath the load)



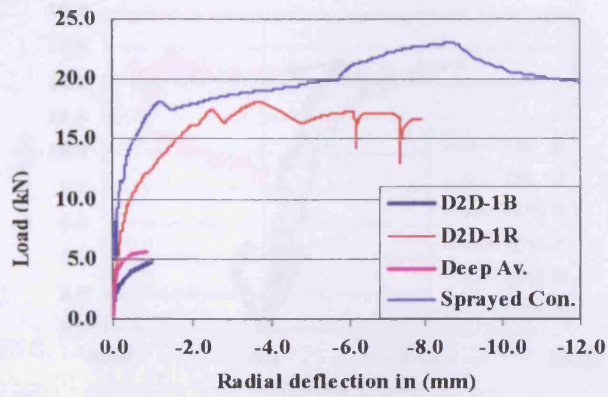
B) LVDT at 50% of span



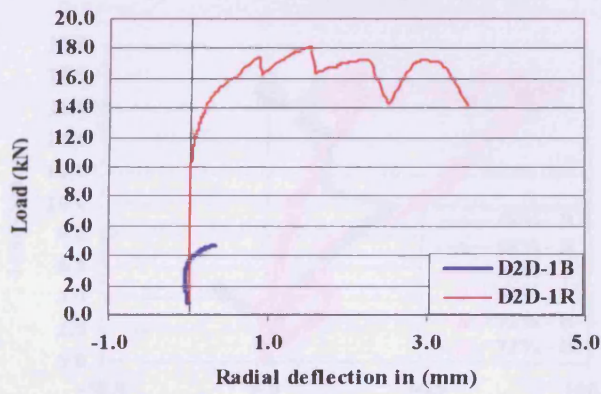
C) LVDT at 75% of span

Figure 6-12: Arch load deflections at different sections (shallow arch)

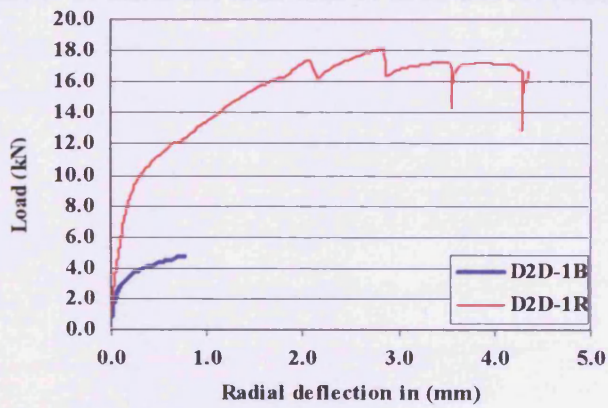




A) LVDT at 25% of span (beneath the load)



B) LVDT at 50% of span



C) LVDT at 75% of span

Figure 6-13: Arch load deflections at different sections (deep arch)

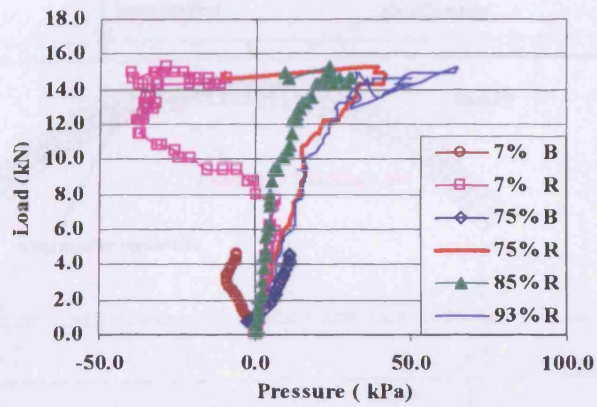


Figure 6-14: Pressures at different locations of arch barrel (S2D-3B & S2D-3R)

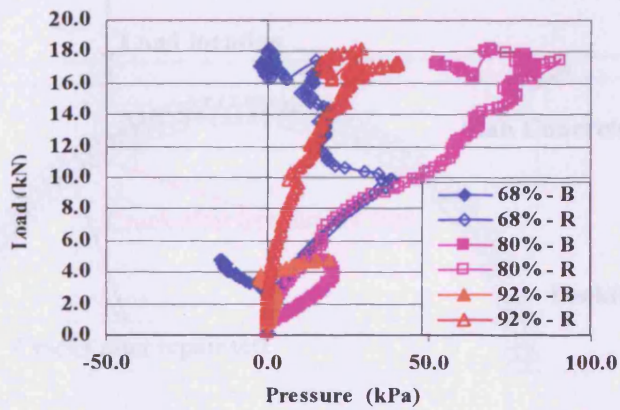


Figure 6-15: Pressures at different locations of arch barrel (D2D-1B & D2D-1R)

Figure 6-17: Arch condition after test (D2D-1R)

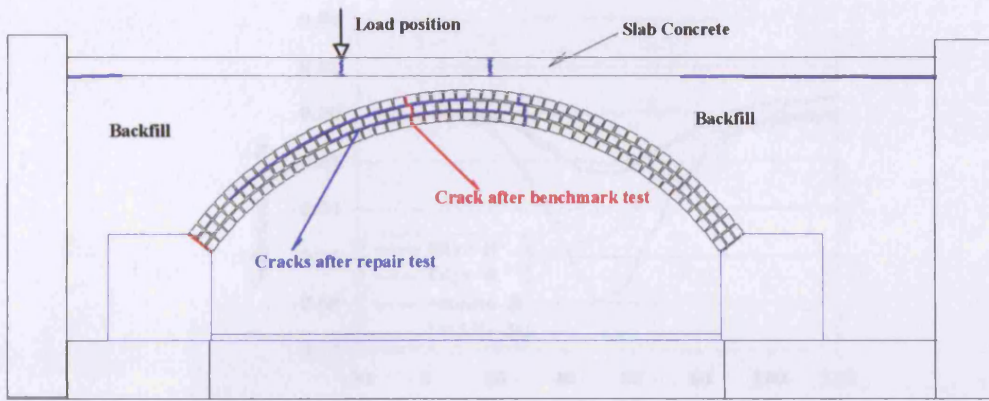


Figure 6-16: Arch condition after test (S2D-3R)

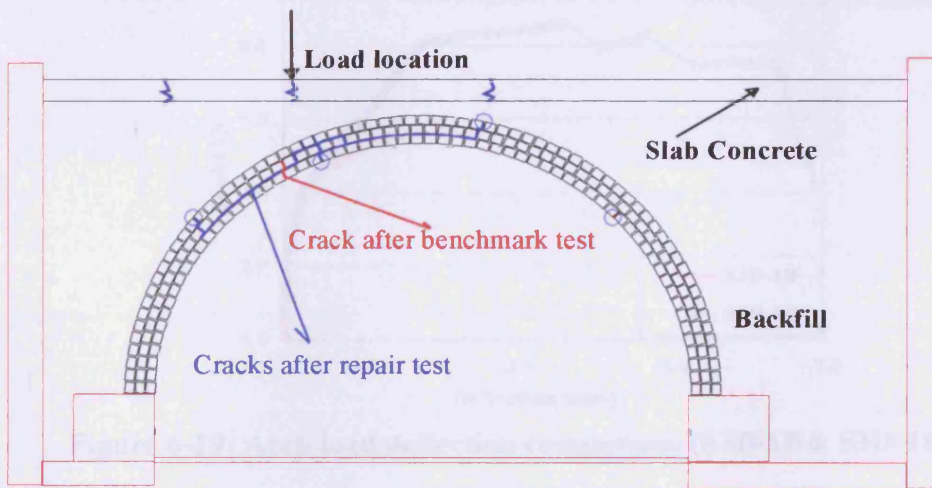


Figure 6-17: Arch condition after test (D2D-1R)



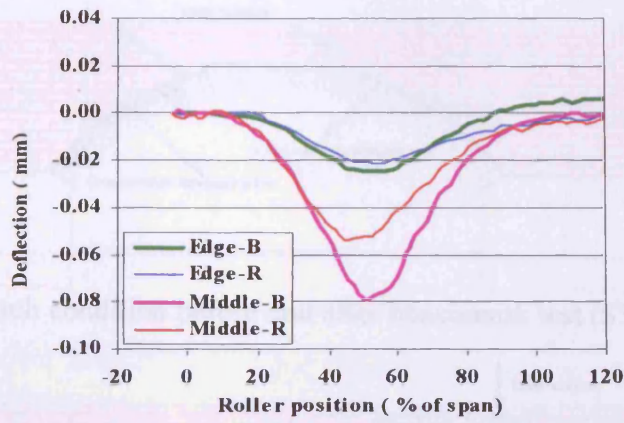


Figure 6-18: Deflections under the rolling load at 50% of span (S3D-1B & S3D-1R)

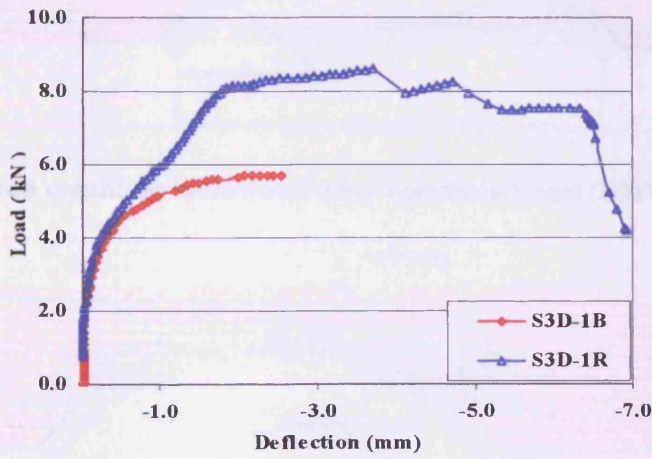


Figure 6-19: Arch load deflection comparison (S3D-1B& S3D-1R)

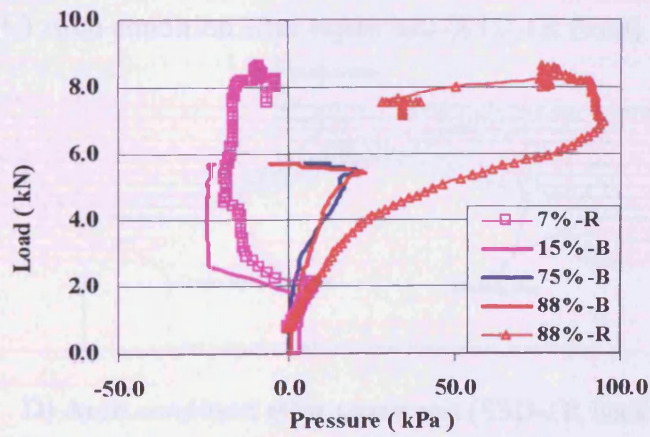
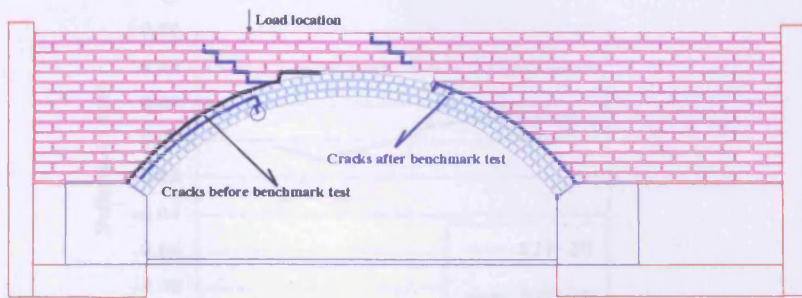
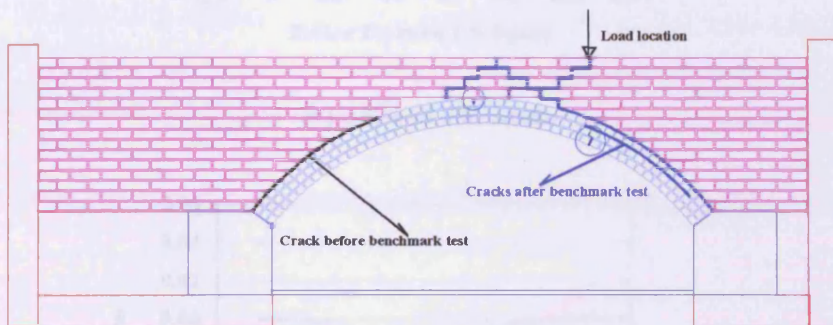


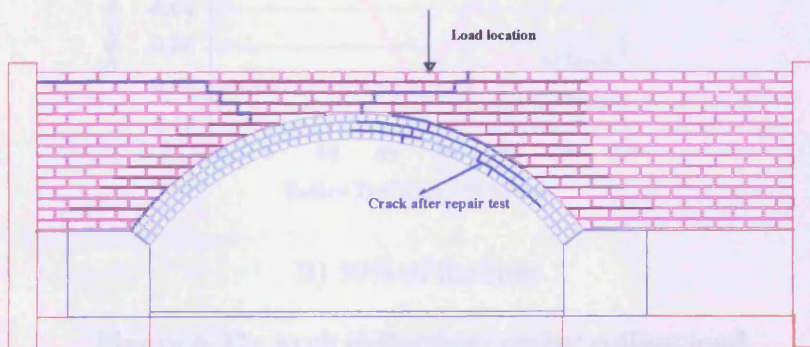
Figure 6-20: Soil/arch interface pressure comparison (S3D-1B & S3D-1R)



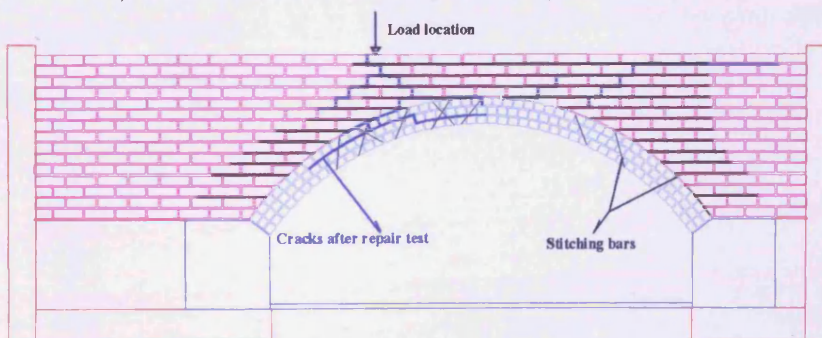
A) Arch condition before and after benchmark test (S3D-1B front)



B) Arch condition before and after benchmark test (S3D-1B back)



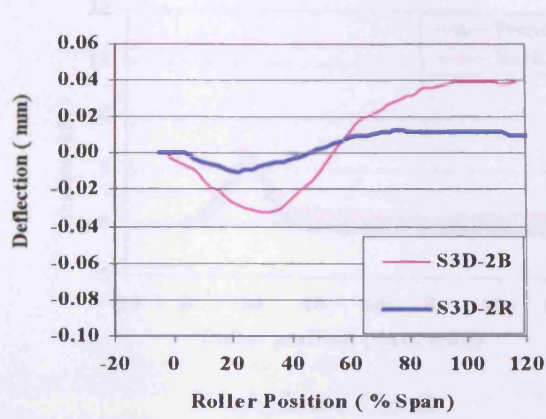
C) Arch condition after repair test (S3D-1R front)



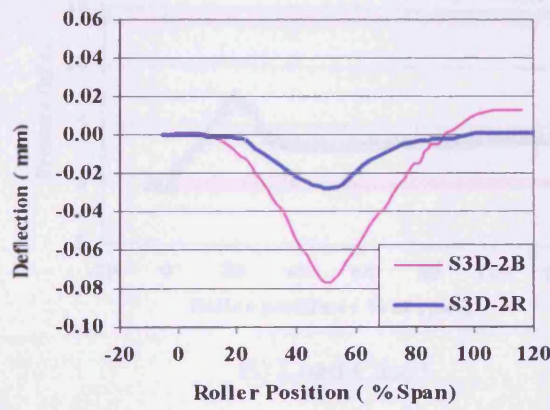
D) Arch condition after repair test (S3D-1R back)

Figure 6-21: Arch condition after test (S3D-1B & S3D-1R)



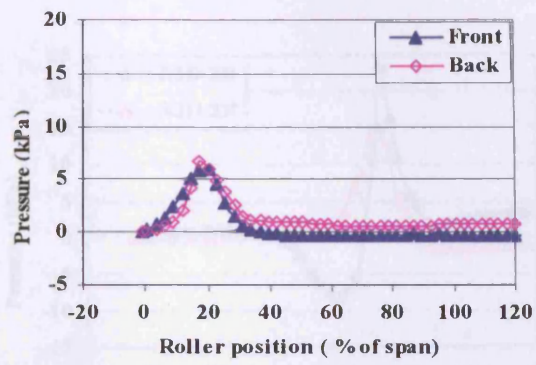


A) 25% of the span

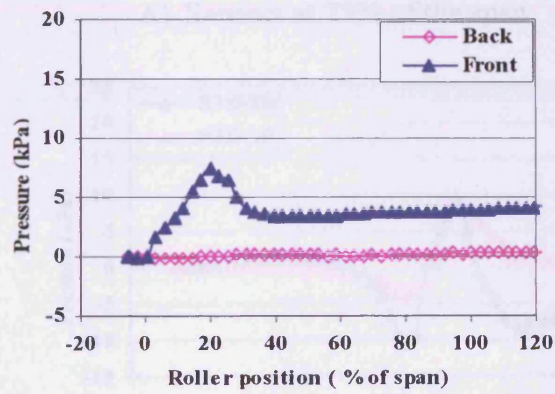


B) 50% of the span

Figure 6-22: Arch deflections under rolling load

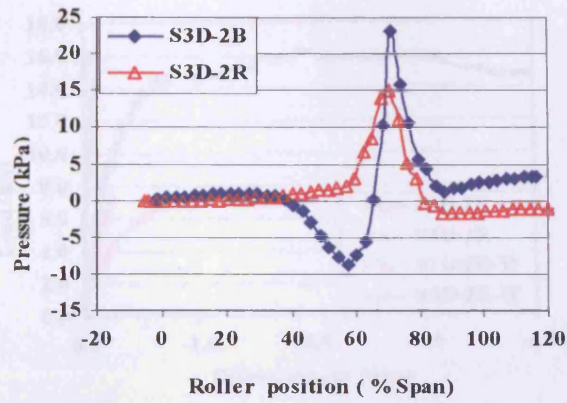


A) Load Case2

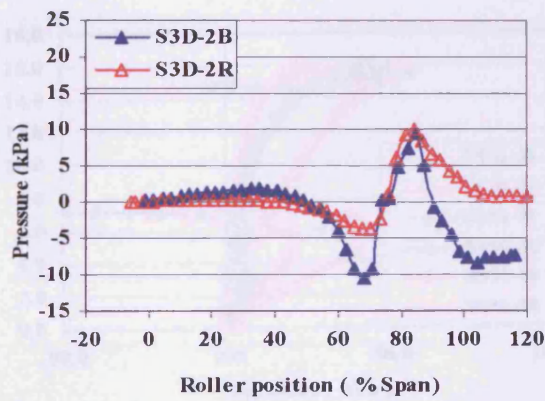


B) Load Case3

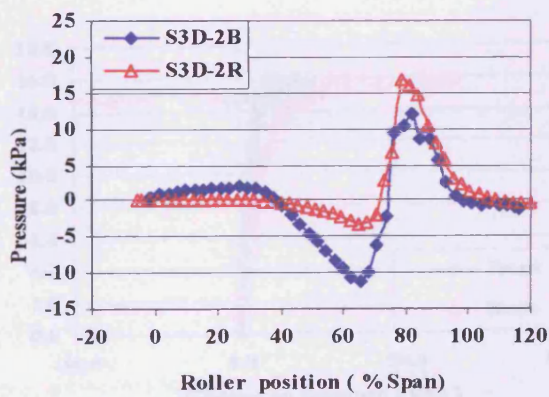
Figure 6-23: Pressures under different rolling loads at 20% of the span (S3D-2R)



A) Sensors at 75% of the span



B) Sensors at 81% of the span



C) Sensors at 88% of the span

Figure 6-24: Pressures at different locations of the arch barrel under the rolling Load Case1



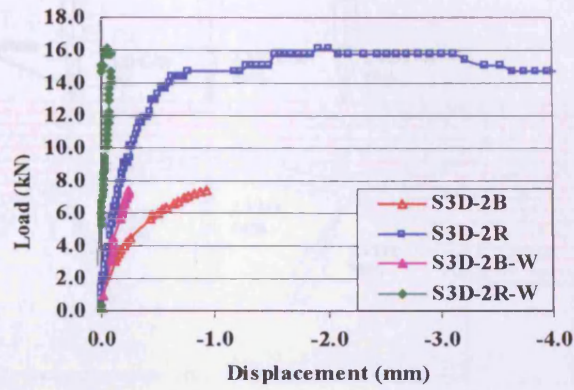


Figure 6-25: Arches deflections under increasing load

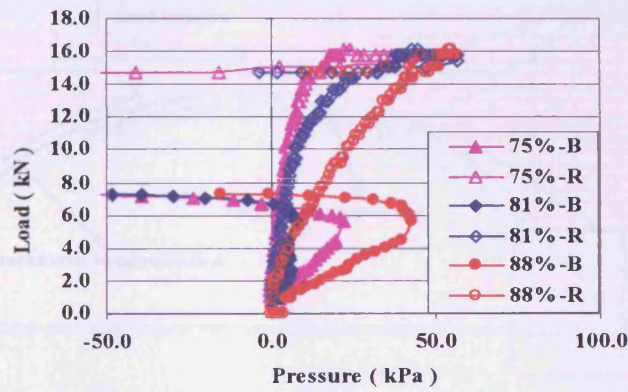


Figure 6-26: Soil/arch interface pressure comparison (S3D-2B & S3D-2R)

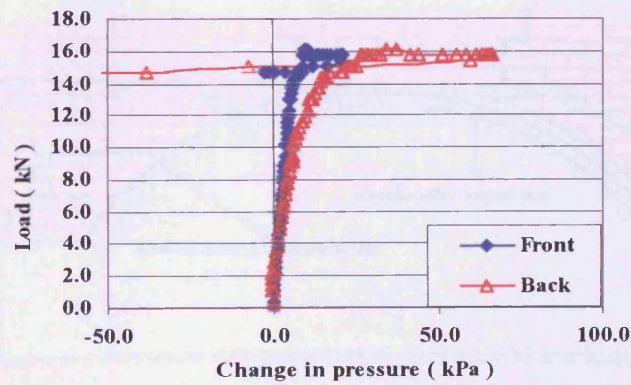
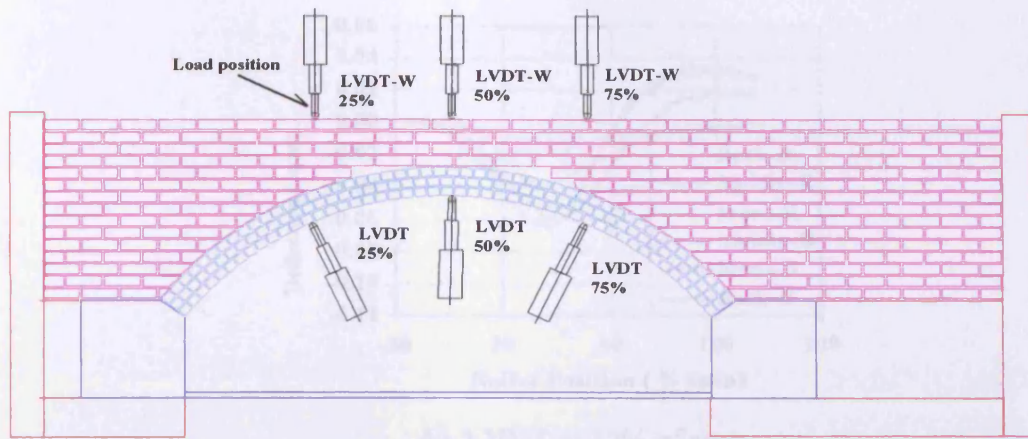
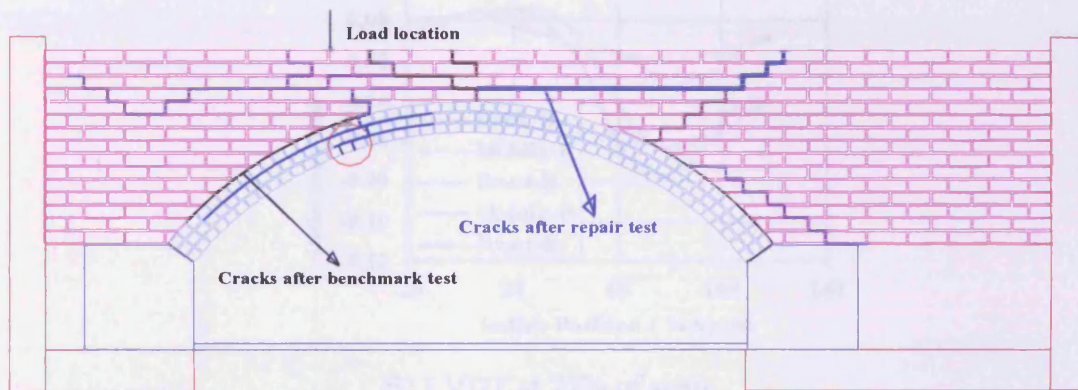


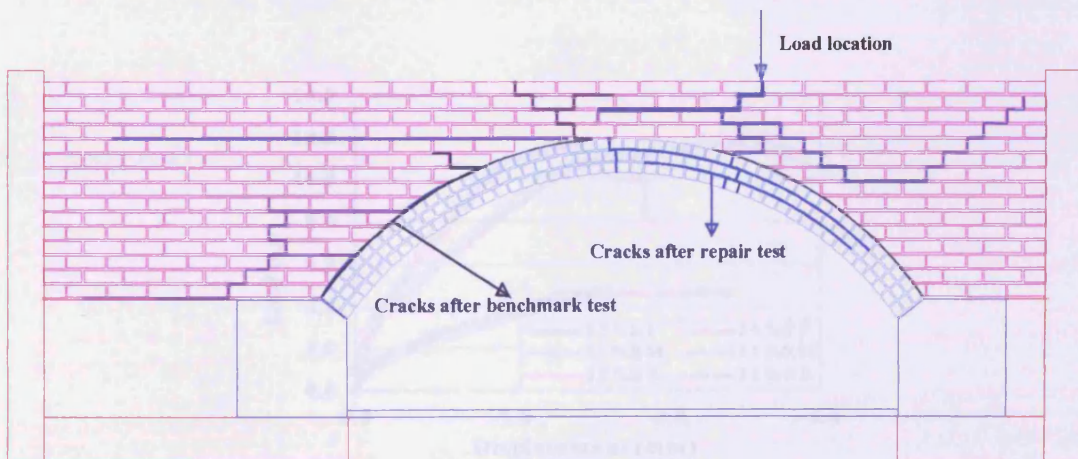
Figure 6-27: Pressures recorded by pairs of sensors at 75% of the span (S3D-2R)



A) Before benchmark test



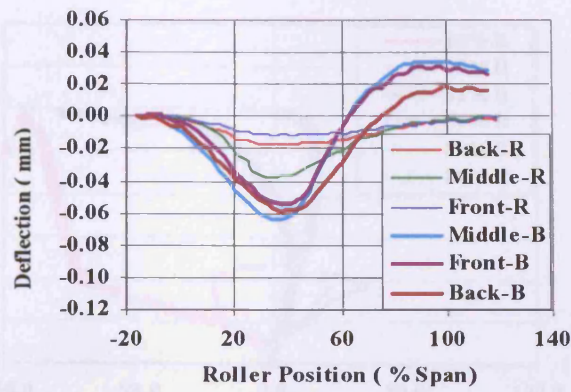
B) Front side cracks (before and after repair test)



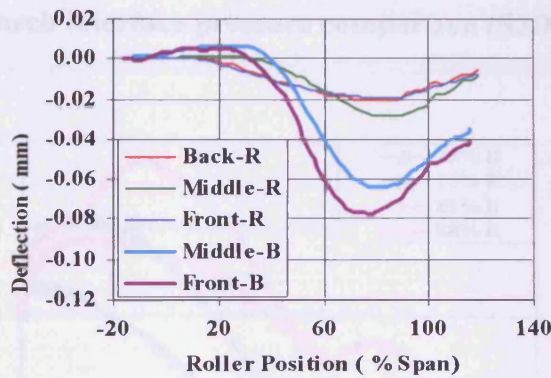
B) Back side cracks (before and after repair test)

Figure 6-28: Arch condition after tests (S3D-2B & S3D-2R)





A) LVDT at 35% of span



B) LVDT at 75% of span

Figure 6-29: Arch deflection under rolling load (S3D-3R & S3D-3B)

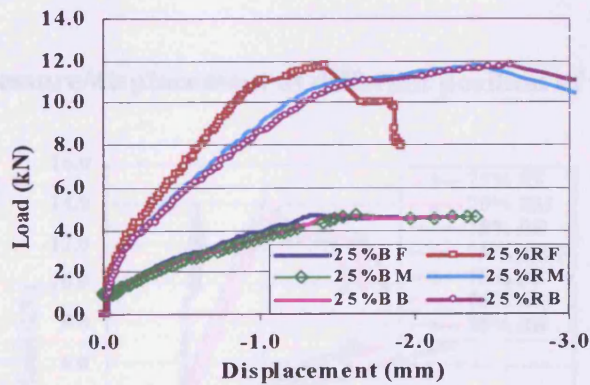


Figure 6-30: Load/deflection comparison (S3D-3B & S3D-3R)

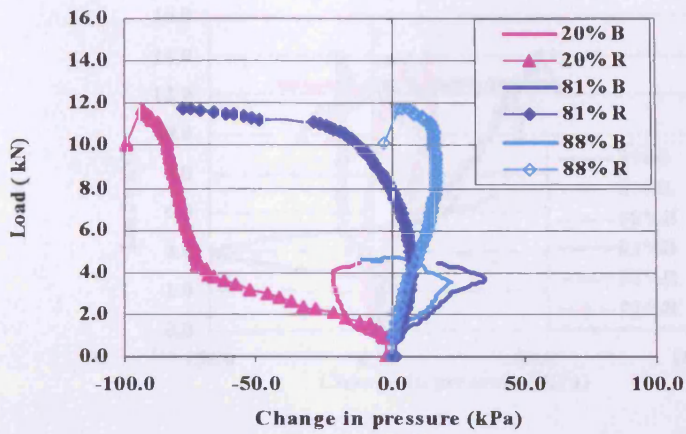


Figure 6-31: Soil/arch interface pressure comparison (S3D-3B & S3D-3R)

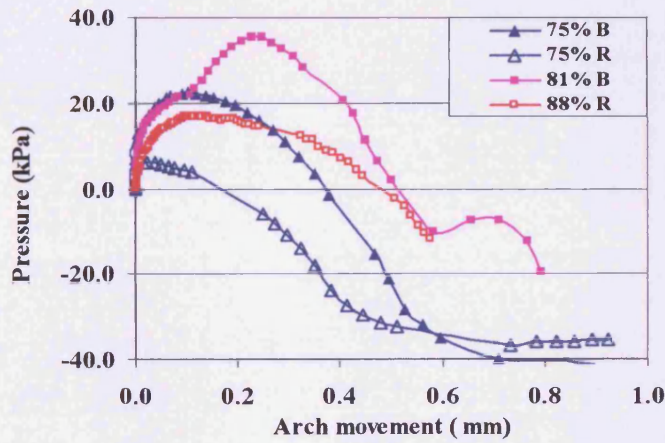


Figure 6-32: Pressure/displacement at different position of the shallow arch

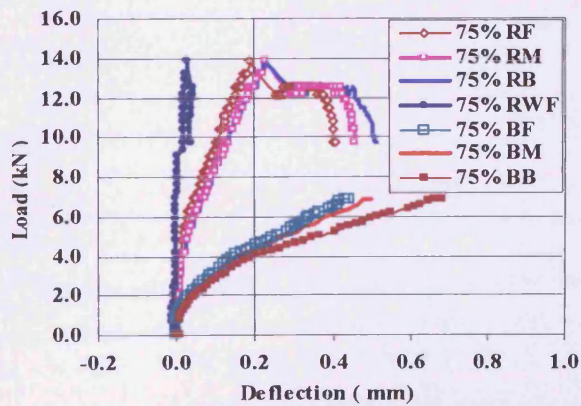


Figure 6-33: Load/deflection comparison (D3D-1B, D3D-1R)



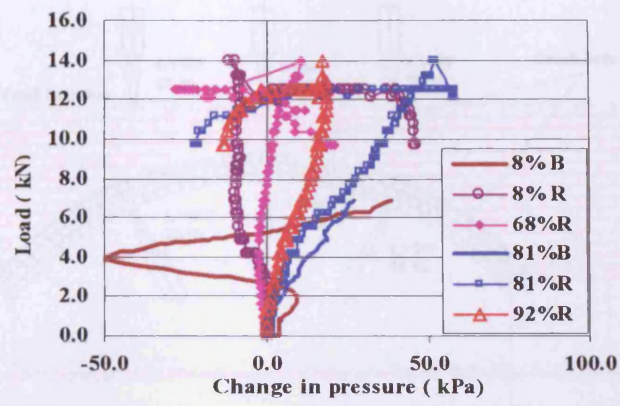


Figure 6-34: Soil/arch interface pressure comparison (D3D-1B & D3D-1R)

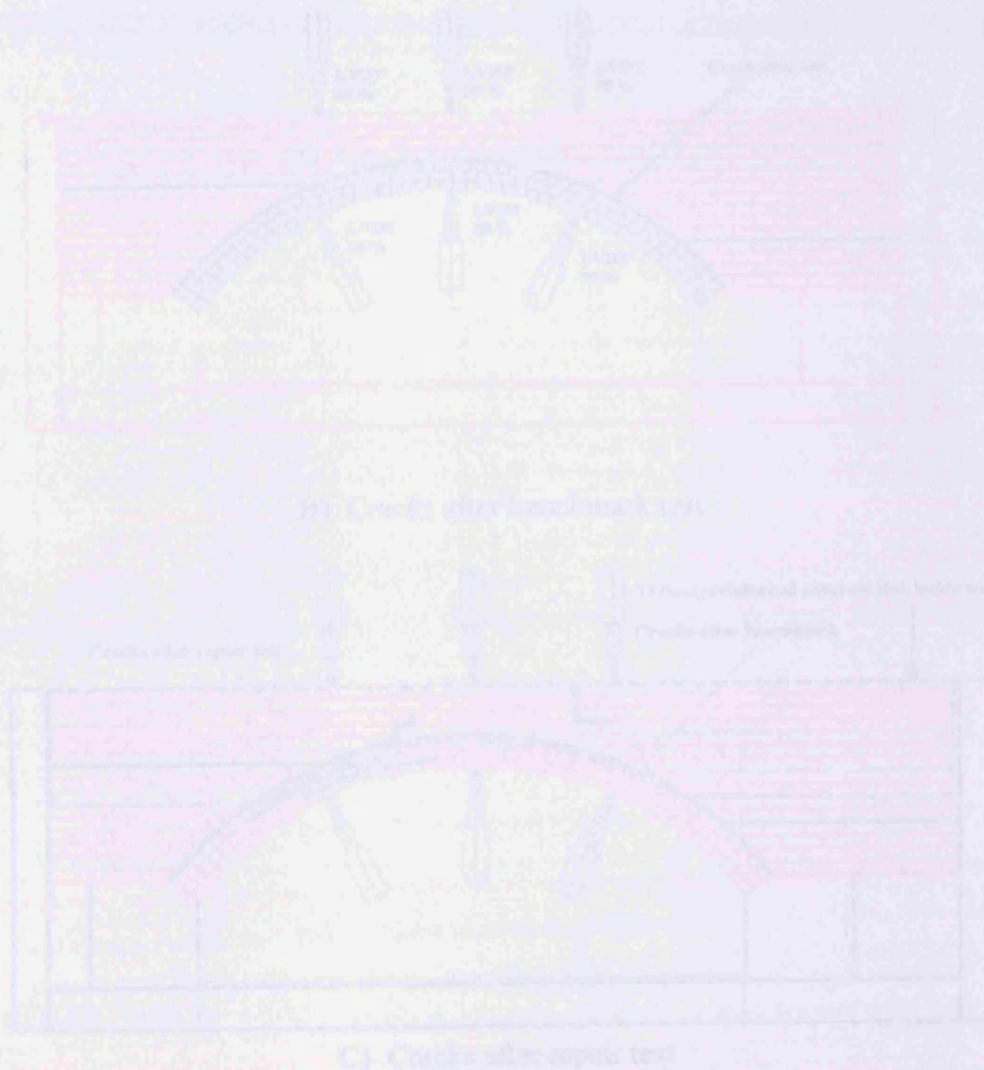
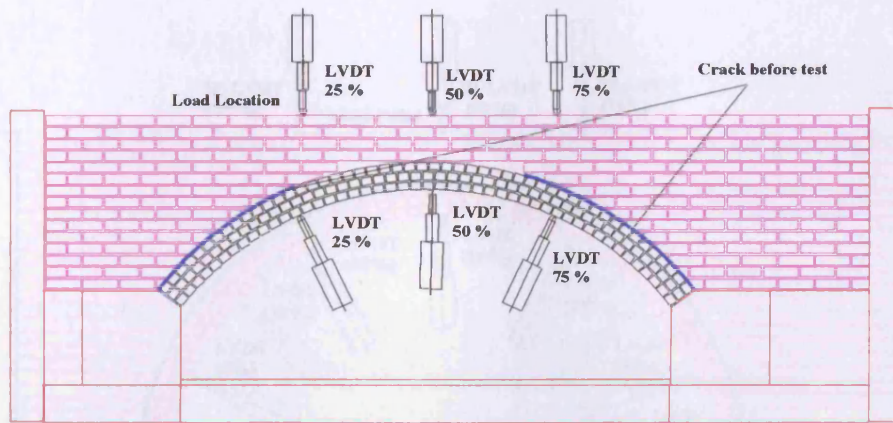
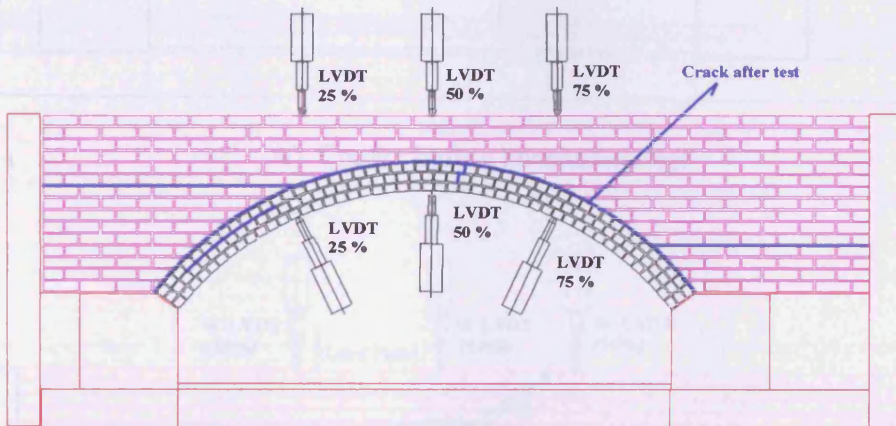


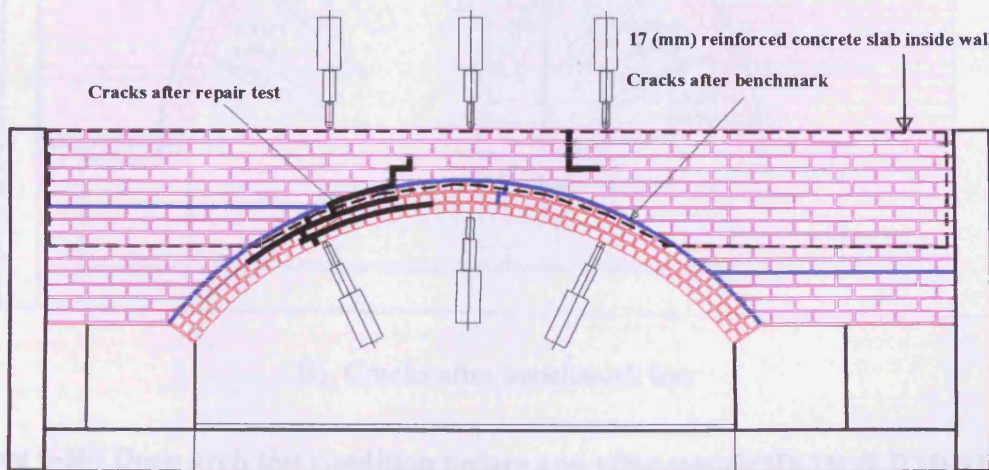
Figure 6-35: Shallow arch test condition before and after test (D3D-1B & D3D-1R)



A) Cracks before benchmark test



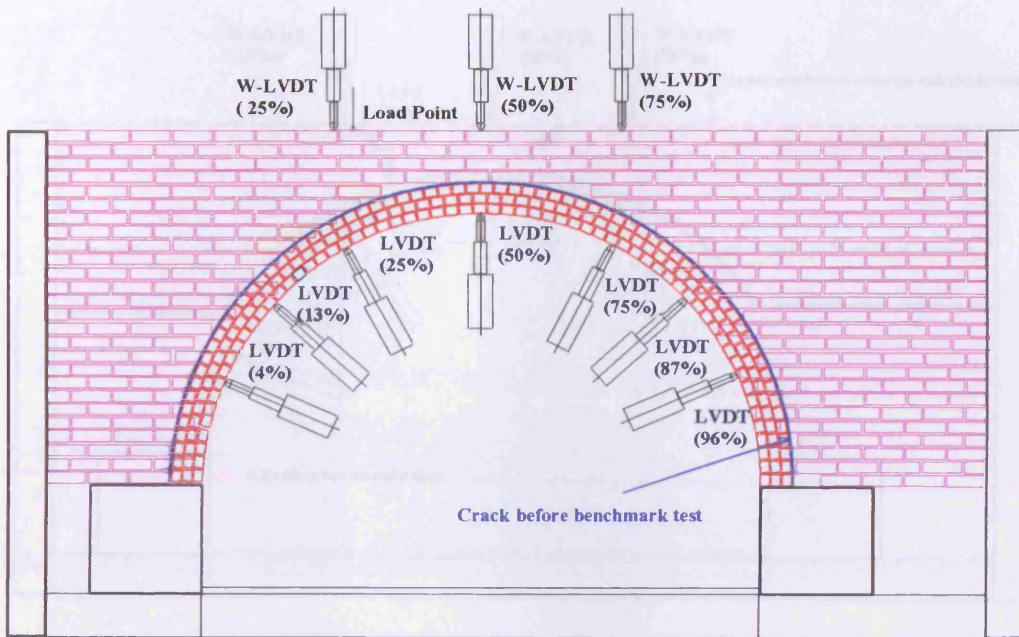
B) Cracks after benchmark test



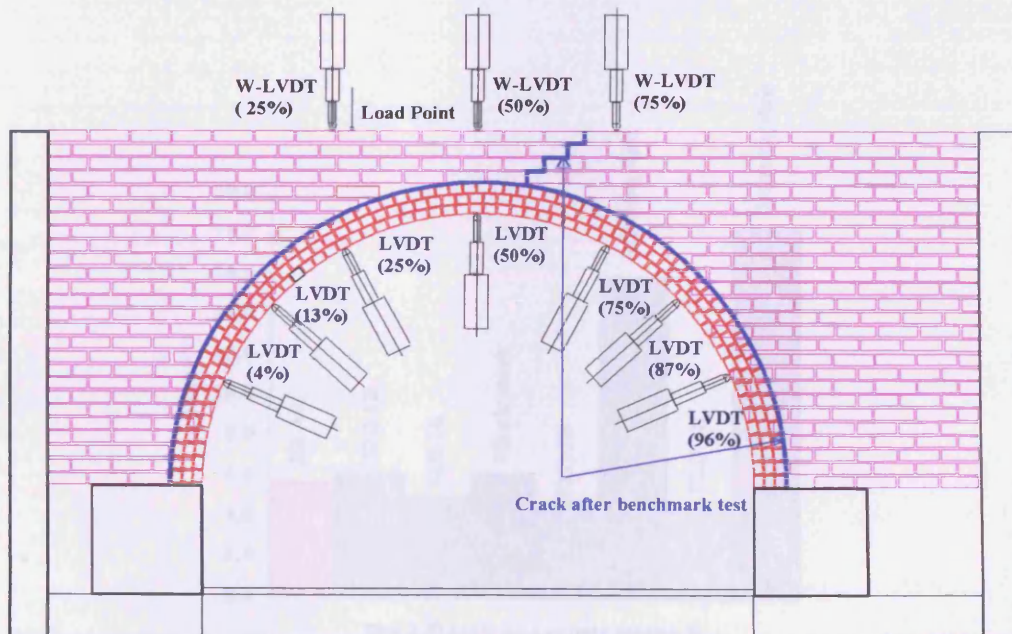
C) Cracks after repair test

Figure 6-35: Shallow arch test condition before and after test (S3D-3B & S3D-3R)



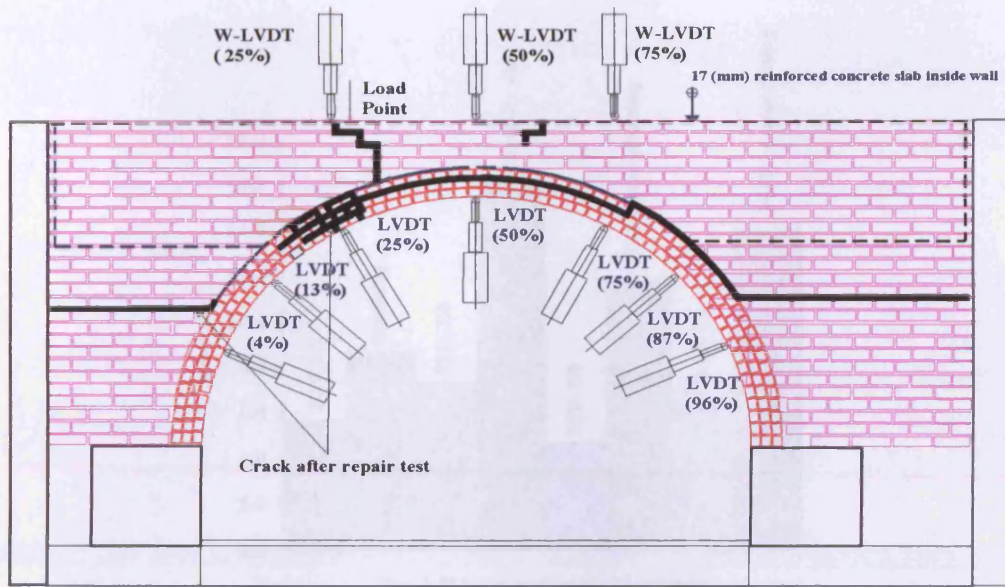


A) Cracks before benchmark test



B) Cracks after benchmark test

Figure 6-36: Deep arch test condition before and after test (D3D-1B & D3D-1R)



C) Cracks after repair test

Figure 6-36: Deep arch test condition before and after test (D3D-1B & D3D-1R, Cont.)

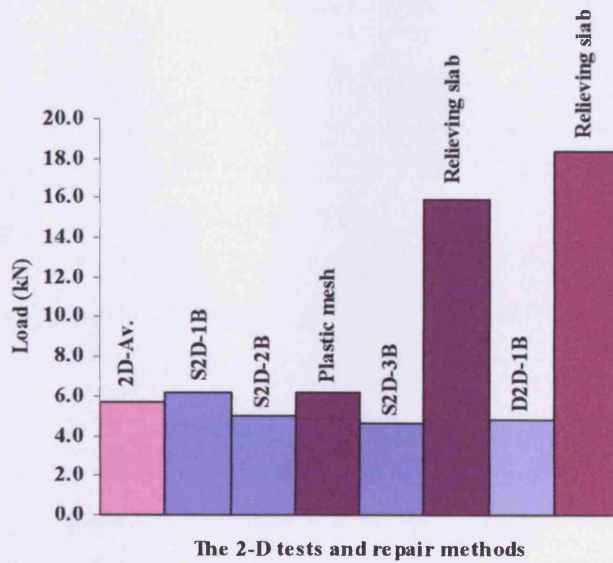


Figure 6-37: 2-D arch ultimate load capacity



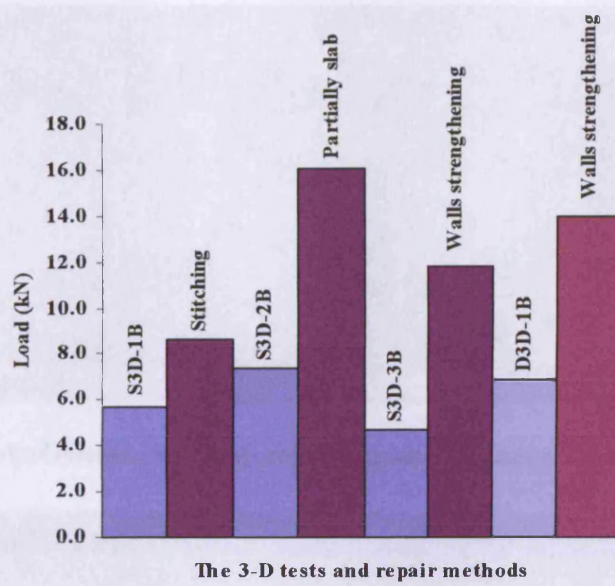


Figure 6-38: 3-D arch ultimate load capacity

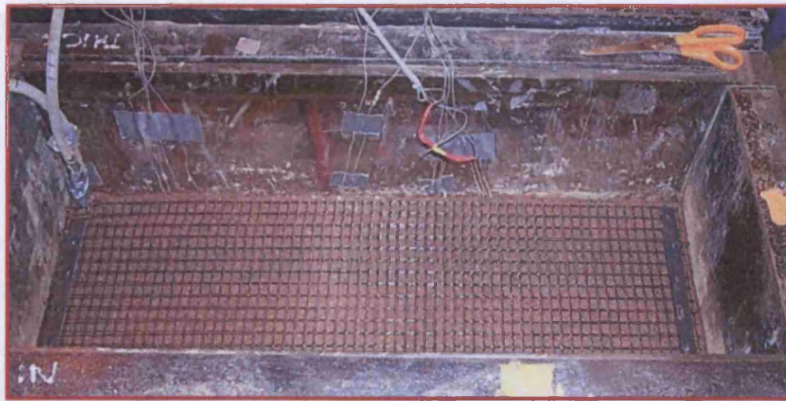


Plate 6-1: General view of plastic mesh reinforcement (S2D-2R)

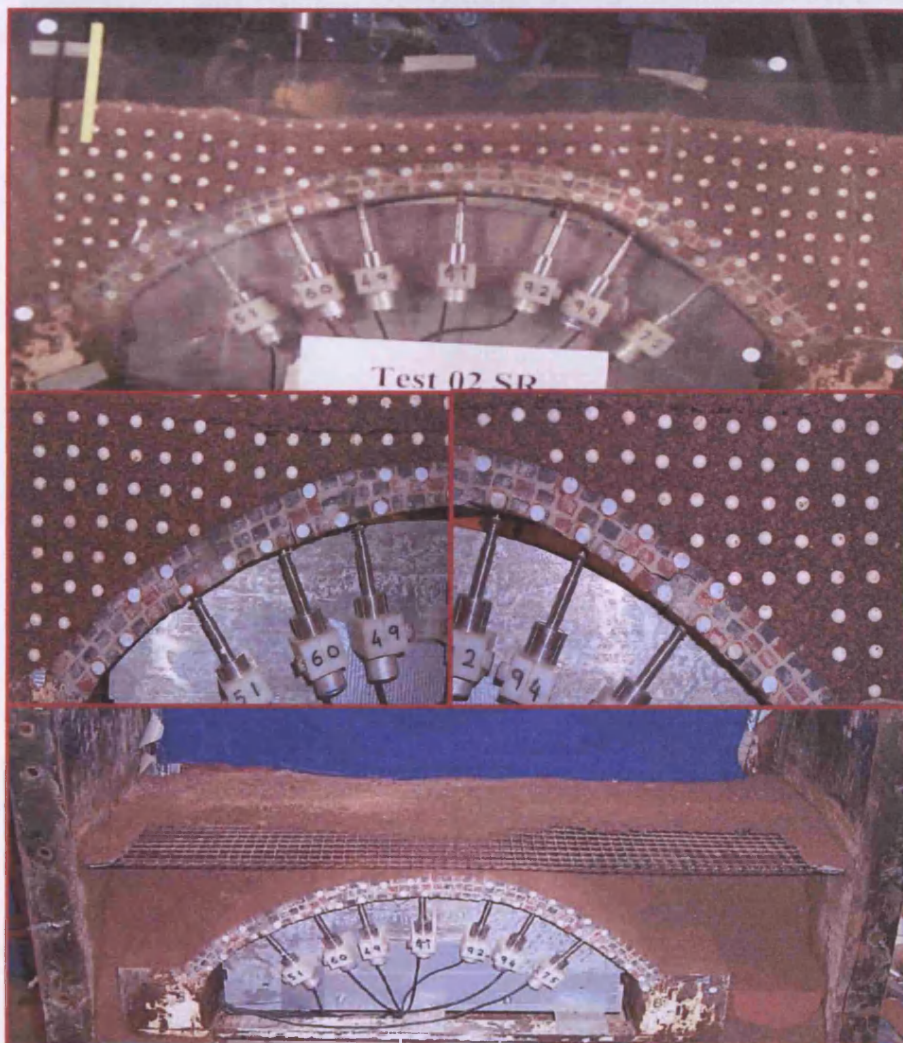


Plate 6-2: Arch condition after test (S2D-2R)



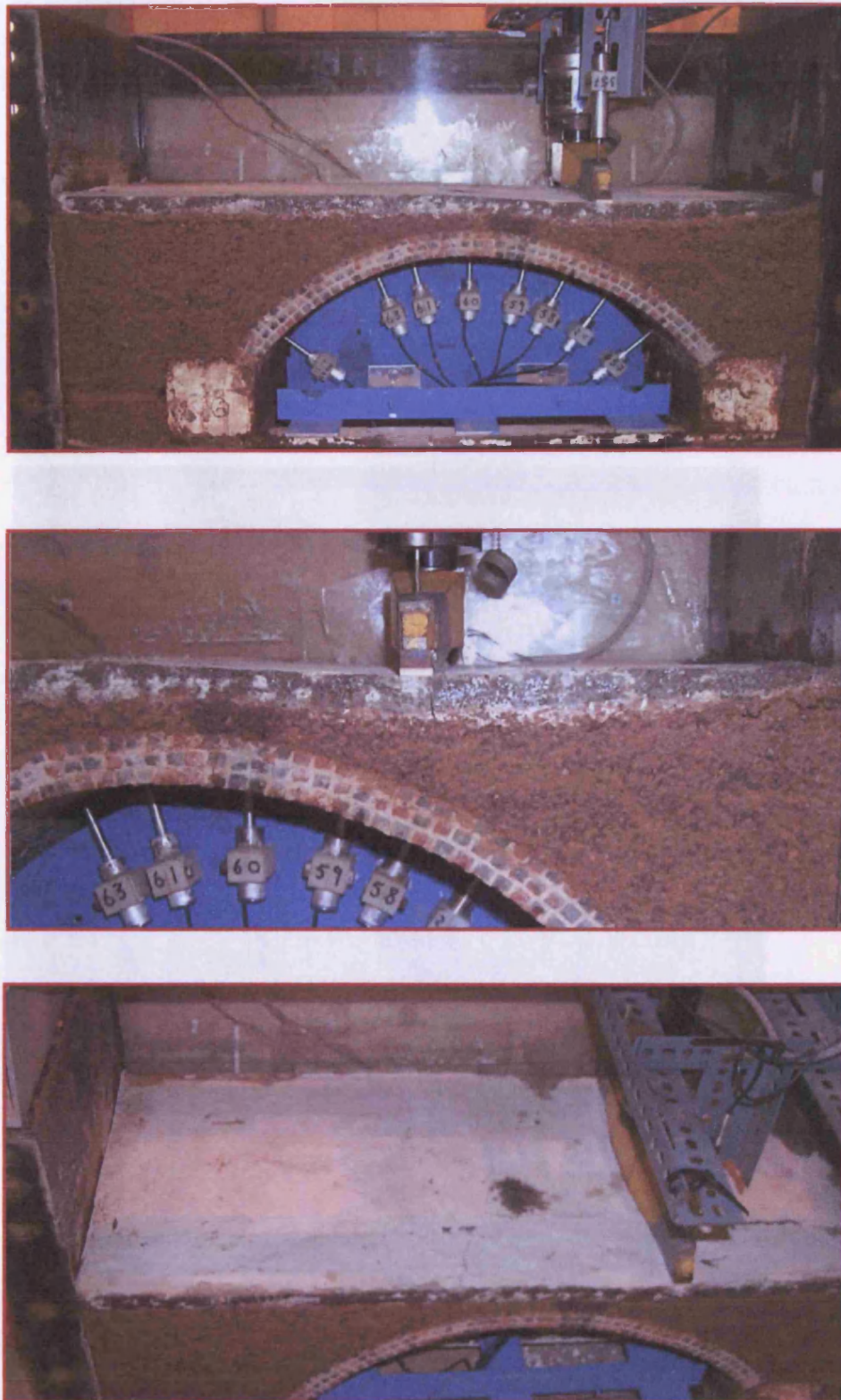
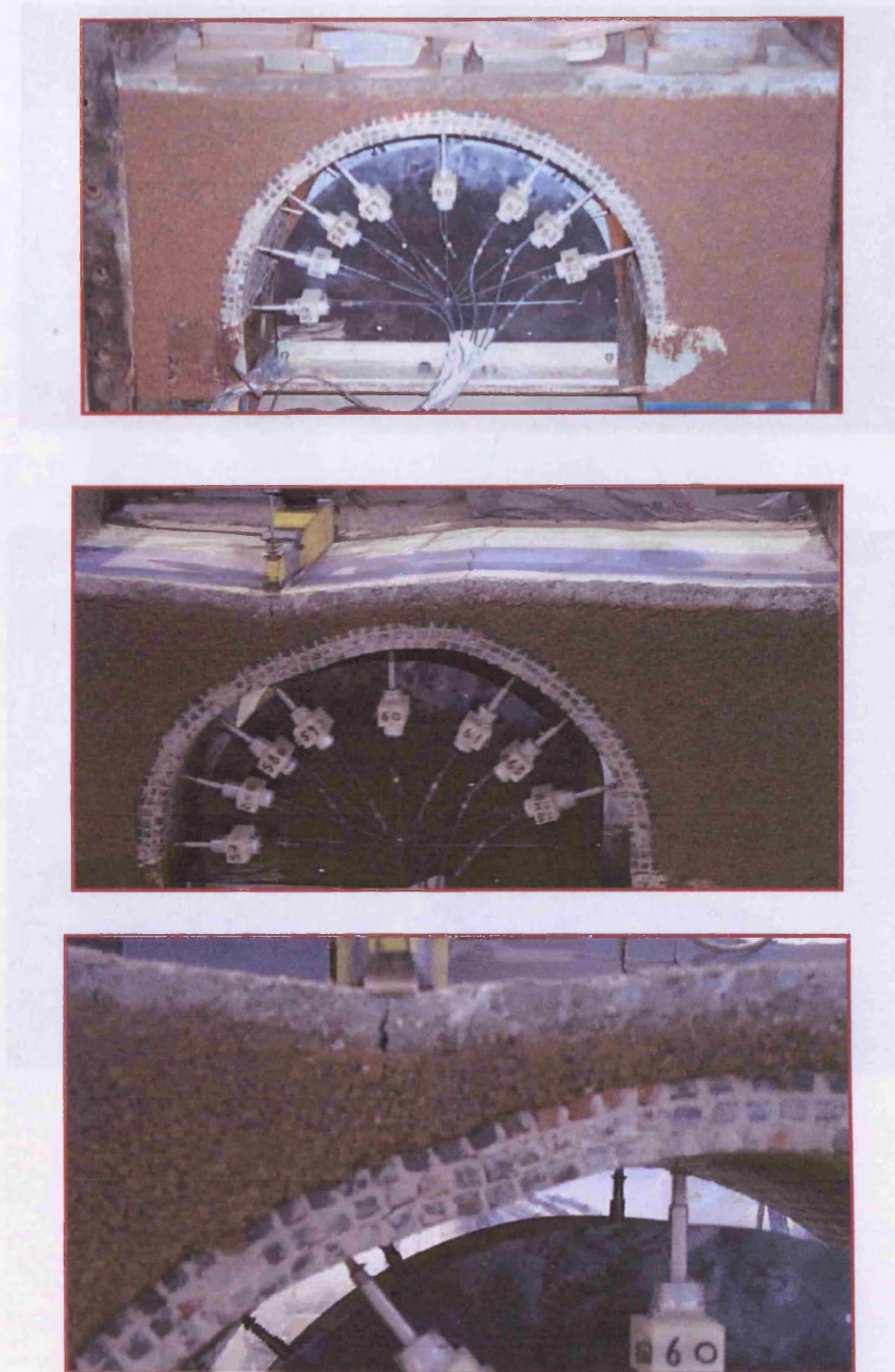
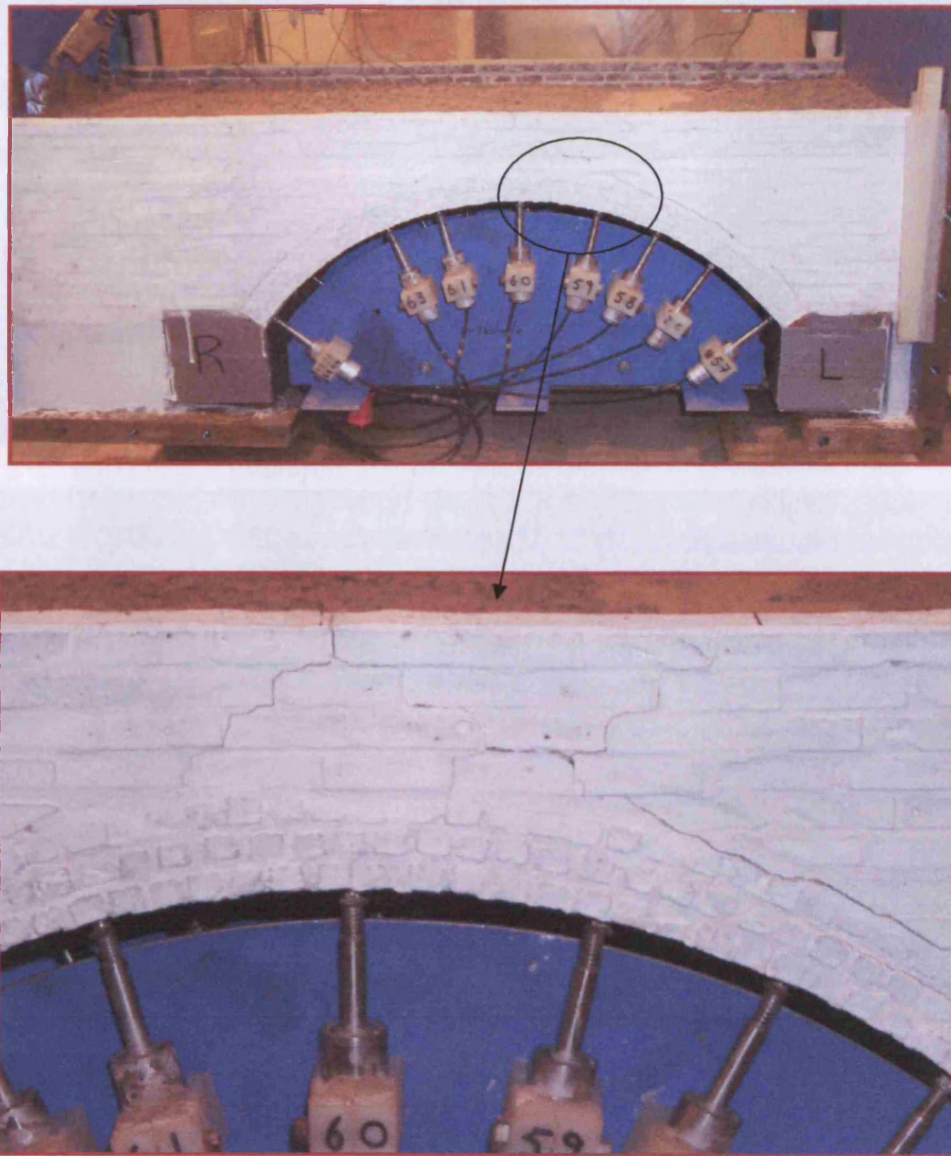


Plate 6-3: Arch condition after test (S2D-3R)



**Plate 6-4: Arch condition after test (D2D-1R)**





**Plate 6-5: Arch condition after benchmark test (S2D-1B)**

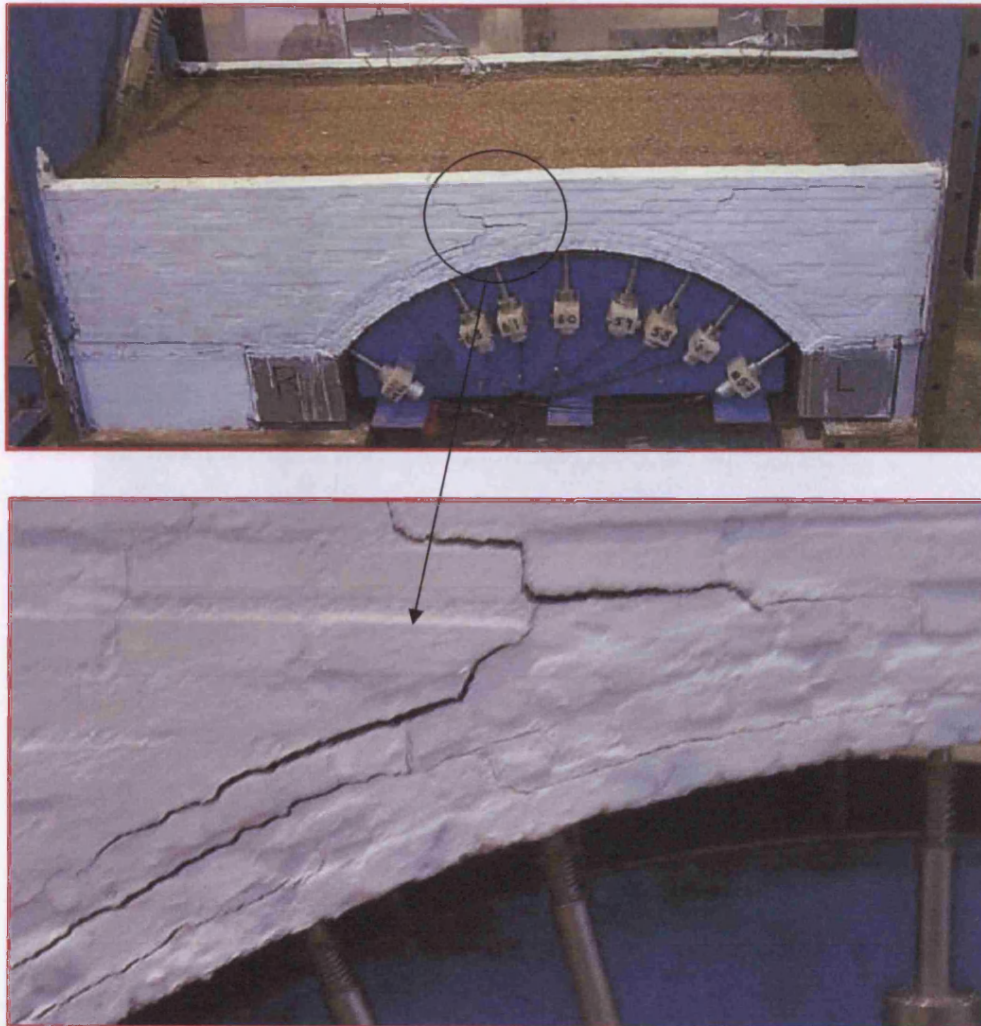


**Plate 6-6: Arch condition after repair test (S3D-1R)**



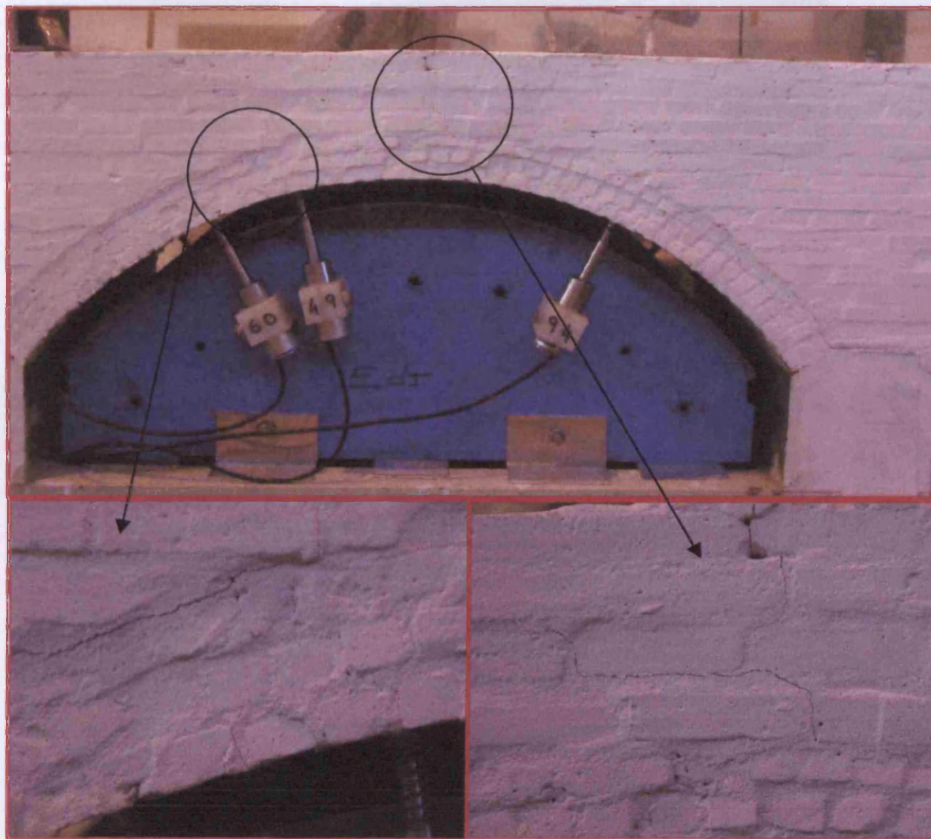


**Plate 6-7: Arch condition after benchmark (S3D-2B)**

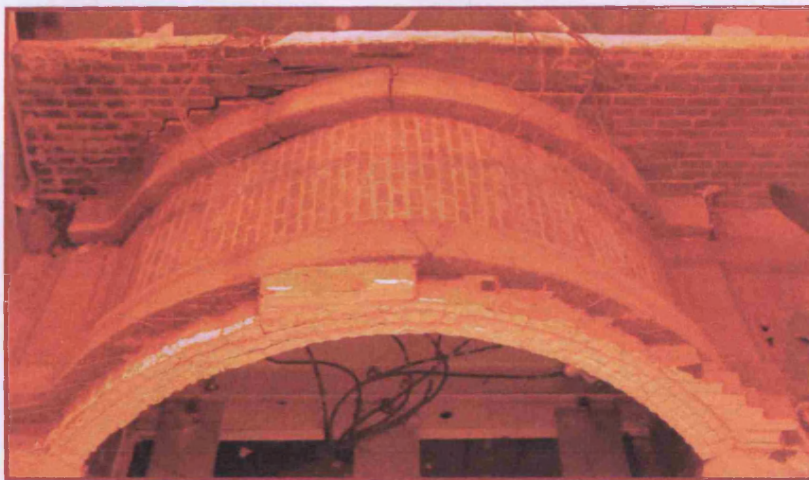
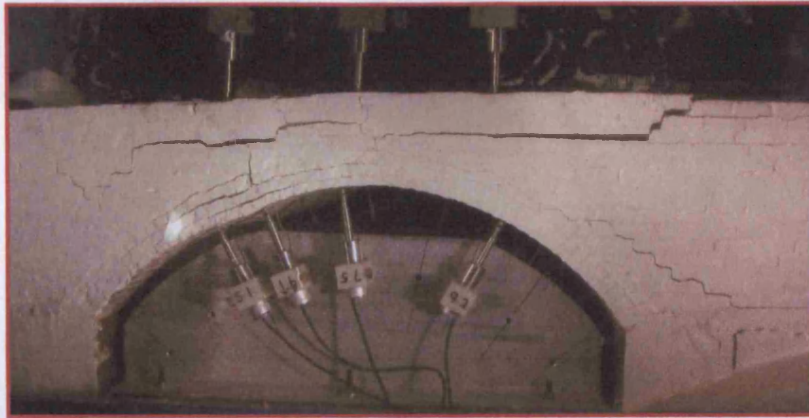


**Plate 6-8: Arch condition after test (S3D-2R)**



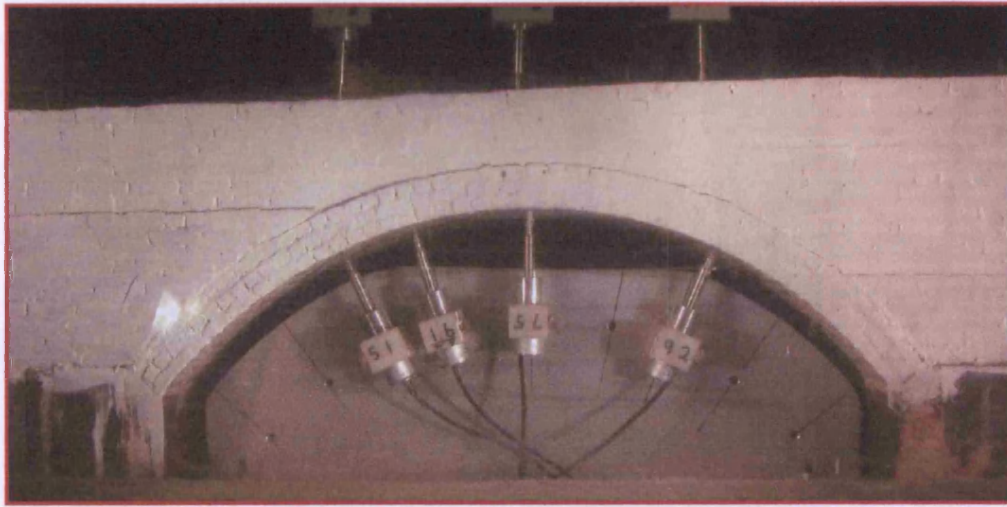


**Plate 6-9: Arch condition after benchmark test (S3D-3B)**

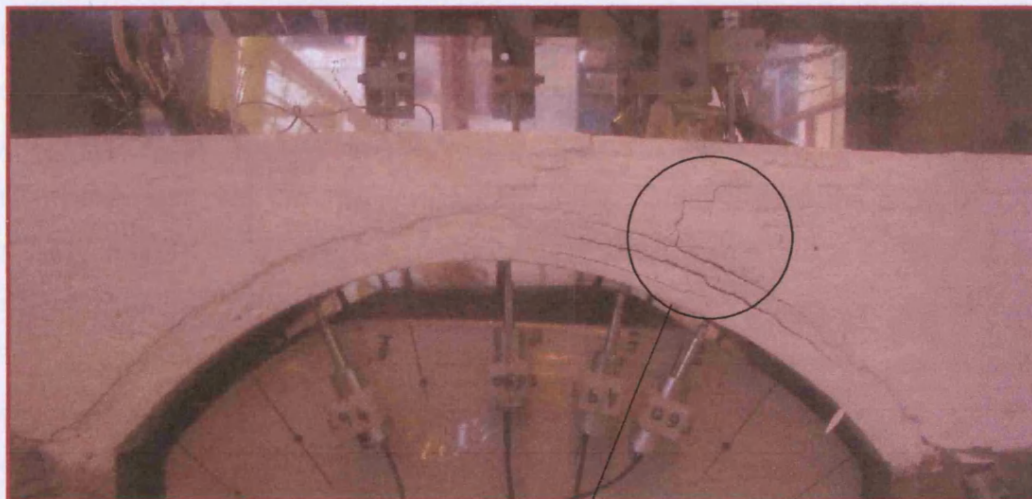


**Plate 6-10: Arch condition after test (S3D-3R)**

## **7 Finite Element model**

### **7.1 Introduction**

Linear and non-linear arch behaviour is modelled with FE at two different stages in the current study. Numerical results are compared with those obtained from the experimental works that are presented in Chapters 5 and 6. In the first part of this chapter the elastic behaviour of the arch is modelled. The FE model was constructed using an available commercial FE package (LUSAS). Materials were initially assumed isotropic, elastic and homogenised and their properties were initially obtained from the material property tests (Chapter 3). Material properties were then adjusted to achieve the best agreement between the numerical and the centrifuge models results. The pressures on the extrados of the arch barrel and the arch deformation at different locations were predicted using the FE model under self weight and rolling loads. These are compared with the experimental results and in some cases with the results were obtained from other theoretical method.

In the second part of this chapter the arch failure behaviour is studied using a non-linear FE model. In initial studies different materials failure criteria, available in LUSAS were tested and the best model was selected for further studies. The arch barrel (without backfill) was studied first and backfill material was then added to it.

The repaired arch model behaviour was studied using the non-linear FE model. A concrete slab with the same depth as the centrifuge tests was added to the FE model and the response under the rolling and the increasing load were obtained. In all cases, both the shallow and the deep arch geometries are studied.

## 7.2 Linear elastic FE model

The FE model of the arch bridge was constructed using the LUSAS commercial package version 13.4 and its modeller program was used for the pre and post processing of the data. Eight-node quadrilateral 2-D plane strain elements were used to model the arch barrel and the backfill materials. Due to the effect of the rigid side walls of the box during the centrifuge tests it was deemed that the backfill above the arch barrel was in a plane strain condition and this condition was assumed in the FE model. A parametric study of plane strain and plane stress showed no important difference between these two models and similar results were achieved from both models at this initial stage. Twenty two elements with  $2 \times 2$  Gauss points were used in the longitudinal direction of the arch barrel, and 3 elements with  $2 \times 2$  Gauss points (FEA Ltd 2001a) were used to simulate the arch barrel thickness. A previous study (Sicilia 2001) showed that 6 elements are sufficient to simulate the crack propagation in the arch barrel but initial studies indicate 3 elements are sufficient for simulation of barrel behaviour in this stage. Different sizes of mesh were used to simulate the backfill materials. A fine mesh was used under the load position and near to the crown of the arch and a coarse mesh used far away from the applied load location and crown. A layer of thin interface elements was generated between the arch ring and the backfill to help account for the soil/arch interaction.

The main material properties of the arch barrel, backfill and arch/fill interface are presented in Table 7-1. Material properties were initially selected from the material test properties, which were presented in Chapter 3. In some cases the material properties were adjusted following the initial studies to fit the centrifuge model conditions. In the case of no measured material properties, the values were assumed according to values found in the literature review. All materials used to simulate the arch model behaviour in this stage were assumed to be linear elastic, homogeneous and isotropic. Series of parametric studies with various material properties were carried out in this study and are presented in the next sections of this chapter.

Figure 7-1 and 7-2 show the general view of the shallow and the deep arch models, with meshes and support conditions for the linear elastic FE model. The arch barrel was fixed in both the horizontal and the vertical direction to simulate the rigid arch

abutments during the centrifuge tests. No barrel movement at the abutments in the centrifuge tests confirm this type of support selection. The backfill was fixed horizontally at both vertical ends and fixed vertically in the base of the model.

Due to no particular arch prototype being considered in the centrifuge models the same scale and units of the centrifuge models were used in the numerical models and no attempt was conducted to use the FE at full scale. Therefore comparison between the numerical and centrifuge will be straightforward. The arches response under self weight was obtained using the above described FE model.

### **7.3 Stress analysis under self weight**

The self weight was applied to the numerical model in the same way as the centrifuge test procedure. As was explained in the experimental procedure, the centrifuge acceleration was increased in the arch model in three stages up to 12g. At each stage the model acceleration was increased 3g and the next acceleration was applied to the model after achieving a constant state condition in the prior stage. To simulate the centrifuge acceleration in the FE model the self load was applied to the model using an automatic incremental body force. The self load was applied to the arch model by assigning the body force to all the elements.

Both shallow and deep arch geometries were considered and the results obtained from the numerical and geostatic classic methods are compared with the relevant measured data from the centrifuge tests. Previous relevant data from the same geometry test are considered and presented. Stress on the extrados of the arch at an acceleration of 12g was considered in both the numerical and experimental and compared to each other. In the following sections, the normal stresses obtained on the extrados of the arch barrel from the centrifuge tests and numerical models are also detailed.

#### **7.3.1 Pressures on the arch extrados**

Normal stress on the extrados of the arch barrel was measured using the Kyowa pressure sensors in the centrifuge tests but the stress component in global directions was obtained

using the FE program. To have comparable results, these stresses are transferred to the normal and tangential direction of the arch barrel using the following equations.

$$\sigma_n = \frac{1}{2}[\sigma_x + \sigma_y] + \frac{1}{2}[\sigma_x - \sigma_y]\cos 2\theta + \tau_{xy} \sin 2\theta \quad 7-1$$

$$\tau = \frac{1}{2}[\sigma_y - \sigma_x]\sin 2\theta + \tau_{xy} \cos 2\theta \quad 7-2$$

The sign conventions of these equations is presented in Figure 7-3.

Geostatic pressures due to the action of self weight were determined using the relationship given in equations 7-3 and 7-4 for vertical and horizontal stresses respectively. The coefficient of earth pressure at rest,  $K_0$ , was assumed to be 0.67.

$$\sigma_y = \gamma y \quad 7-3$$

$$\sigma_x = K_0 \sigma_y \quad 7-4$$

The normal stresses on the extrados of the arch barrel that were obtained from the FE model and geostatic classic method are detailed in Figure 7-4 and 7-5 for the shallow and the deep arch geometries, respectively. Measured stresses from the centrifuge models are also included in these figures. These include the data from the three shallow benchmark arches and one deep arch geometry. The FE models results with both plane stress and plane strain conditions are included in Figure 7-4, where indicated. Consideration of the figures indicate the smallest values of pressure at the arch crown and increasing pressures with increasing backfill depth for far sections. The normal stresses from both the FE and geostatic methods are very close to each other in the middle part of the arch span in the region over the crown. This covers a larger part of the arch barrel at the shallow arch compared with the deep geometry. For the first and last 20% of the end part of the arch span the difference between the two results is more significant with the FE method showing greater pressures. For the geostatic method it is assumed that the point considered is far enough from the boundary conditions and there is no significant effect from the arch barrel on the soil pressure which is a significant assumption for this

condition with the FE results being more realistic. Differences between the results obtained from the two methods are more significant in the deep arch geometry. This may be because of the much steeper slope of the barrel in the deep arch geometry. A similar result was obtained by Ng from an FE study on a semicircular arch model (Ng 1999).

In general, both methods show reasonable consistency with the data obtained from the centrifuge tests results, except the pressures measured at 50% for the S2D-1B and the 75% of the average recorded pressures by Burroughs (Burroughs 2002). There is no clear explanation for such a big difference between the recorded pressures and the predicted values.

Shear stresses that were obtained from both the geostatic and FE methods along the arch extrados are presented in Figure 7-6. The geostatic method results show a zero value on the crown and near to the springing when the arch barrel is horizontal or vertical. Similar results were obtained from the FE method at the crown and the shear stresses obtained are symmetrical about mid span, as expected. The maximum shear stress value of 26kPa was obtained at about 5% of the arch span in the deep arch geometry. Maximum shear stresses at the same locations is predicted by the geostatic method for the same arch geometry but with a smaller value of 10kPa. A maximum shear stress value of 16kPa was obtained from the shallow arch geometry near to the springing. From the shear to the normal stress ratio the angle of shearing resistance on the soil masonry interface can be determined. A maximum shearing angle resistance of 42 degree at 82% of the span was predicted by FE for the deep arch while the maximum value of 21 degree at 96% of arch span was obtained in the shallow arch model. These values are smaller than the 53 degree which was obtained from the direct shear tests on the backfill materials. Therefore, no shearing is predicted on the soil/arch interface due to the self weight.

### **7.3.2 Stress in the arch barrel**

Figures 7-7 and 7-8 detail the normal and shear stresses in the shallow arch barrel predicted by the FE model. The stresses in the three layers inside of the arch barrel are detailed in these figures. The first and third layers are located at 8% of the ring from inside and outside respectively. The second layer is located in the mid depth of the arch barrel. From Figure 7-7 it can be seen that the entire arch barrel is under compression and



no tension was predicted due to the self load. The maximum normal stress was predicted inside of both springing and at the crown section of the arch barrel. The same results were reported by Ng et al (Ng et al. 1999). Maximum normal stresses of 530kPa and 200kPa were obtained at the inside of the springings and crown of the arch while the maximum value of 140kPa and 160kPa were predicted at the outside of those sections. Figure 7-8 shows that there is no significant difference between the shear stresses at the inside and outside layer of the arch barrel. No shear stress was obtained at the crown of the arch barrel and the maximum value was predicted at the springings, as expected, as a result of the steep arch slope at the abutments. Unfortunately, it is difficult to measure the shear stresses during the centrifuge tests and no comparison between the numerical and the experimental results is possible.

### 7.3.3 Parametric studies

As detailed most of the material properties that were used in the FE model were obtained directly from the material test properties but some of them were assumed according to the literature review. In this section, the influence of material properties on the model response is examined. The study was carried out by varying the backfill modulus of elasticity. Figure 7-9 presents the effect of various modulus of elasticity on pressures on the arch barrel extrados. The pressures along the arch barrel for three different values of modulus of elasticity are detailed in this figure. By increasing the modulus of the backfill from 5,000N/mm<sup>2</sup> to 100,000N/mm<sup>2</sup>, the normal stresses decreased from 21kPa to 17kPa at about 20% and 80% of arch span. This can be attributed to the ability of the stiffer backfill to distribute the load over a larger area.

The backfill was restricted between two sides wall in the rigid box during the centrifuge test therefore assuming plane strain condition seems appropriate to simulate the backfill behaviour. Numerical studies with different plane strain and plane stress condition confirm no significant effect of this assumption. The influence of different stress conditions on the extrados pressures for the shallow arch model are presented in Figure 7-4. The initial studies of the model support conditions indicate no significant effects of support conditions on the arch response; this might be because the boundary was sufficiently far away from the arch.

## 7.4 Non-linear FE model

The non-linear FE arch model was carried out in two stages. In the first stage the arch barrel model was constructed and the backfill was then added to it in the second stage. Different material properties and failure modes were tested to simulate the centrifuge model, for both the barrel and the barrel-backfill models. Some common procedures which were used for both models are presented next.

### 7.4.1 Analysis procedure

Formation of a mechanism failure in a masonry arch barrel implies complete loss of stiffness at failure. It is difficult to reach the point of collapse with conventional FE procedures and other ways are needed to assess when the failure is about to occur. Several ways of defining failure of an arch are possible. A visual inspection of the FE results model can be carried out with failure deemed to occur when the fourth hinges appears to begin forming. A predefined displacement can also be used to define failure, although this is difficult to carry over between different sized bridges.

An alternative way of defining failure is to link it to non-convergence of the solution. When using incremental/iterative solution algorithms, a measure of the convergence of the solution is required to define when equilibrium has been achieved. There are many ways of monitoring convergence in LUSAS but two of them, residual norm and displacement norm, were used in the current study to identifying the failure load. The residual force norm  $\gamma_\psi$  is the sum of the squares of all the residual forces as a percentage of the sum of the squares of all the external forces and is written as

$$\gamma_\psi = \frac{\|\psi\|_2}{\|R\|_2} \times 100 \quad 7-5$$

Where R contains the external loads and reactions (FEA Ltd 2001c).

For a problem involving predominantly geometric nonlinearity, a tolerance of

$$\gamma_\psi < 0.1$$

is suggested. Where plasticity predominates, a more flexible tolerance of

$$0.1 < \gamma_{\psi} < 5.0$$

is suggested. The displacement norm  $\gamma_d$  is the sum of the squares of all the iterative displacements as a percentage of the sum of the squares total displacements and is a useful measure of how much the structure has moved during an iteration and is written as

$$\gamma_d = \frac{\|\delta a\|_2}{\|a\|_2} \times 100 \quad 7-6$$

Typical values of

$$0.1 < \gamma_d < 5.0$$

are reasonable.

#### 7.4.2 Load application

To trace the structural response of materially or geometrically nonlinear problems, a time or load stepping procedure must be used. If a significant degree of nonlinearity occurs during a load step, the stresses integrated through the volume of the structure will not satisfy equilibrium with the external forces. Consequently, a residual force will remain. Therefore, a correction procedure is required to restore equilibrium. A modified Newton-Raphson procedure is used to deal with these nonlinearities in LUSAS (FEA Ltd 2001c).

Two methods of load application, the constant load level incrementation and modified arc length incrementation, are available in LUSAS. With the constant load level the load is applied in a fixed increment and the chosen iterative algorithm is utilised to obtain convergence of the solution at each level. Two load increment options, manual and automatic, are available for each load case in LUSAS. Both manual and automatic controls were used to apply the load in the current study. When arc length control is used

the loading varies during the iterations according to either of the two arc-length methods, Crisfield's or Rheinboldt's (FEA Ltd 2001c).

### 7.5 Modelling of failure of arch barrel

A 2-D plane strain model of an arch barrel is developed in this section. The barrel was divided into 22 segmental surfaces. Three divisions in arch radial direction and two in the other direction were selected to make an appropriate mesh on each surface. Analysis of the arch barrel by doubling the mesh size indicated no significant effect of using the finer mesh on the results.

Figure 7-10 presents the shallow arch barrel with the selected mesh, support conditions and the applied increasing load on it. The increasing load was applied to the arch barrel as a concentrated load at 25% of the span for the shallow geometry and at 30% of the span for the deep arch. The self weight was applied to the models as a body force for both geometries. The self weight was applied using manual increments in one step loading and the automatic incrementation was used to apply the increasing load. By this way of switching from manual to automatic control, any loading input under the manual control is remembered and held constant, while the automatic procedure is operating.

Elasto-plastic behaviour was defined for the arch barrel material. The main material properties used in the barrel model are given in Table 7-2. The plastic behaviour of the material was simulated using a concrete crack model which is available as a predefined model in LUSAS (FEA Ltd 2001b). This model assumes that, at any one point in the material, there are a defined number of permissible cracking directions. The model assumes that the material can soften and eventually lose strength in positive loading. The softening follows an exponential curve defined by the tensile strength and the strain at the end of the softening curve. To ensure the softening function is a valid shape the following restriction should be used:

Strain at end of softening curve  $> 1.5 \times \text{tensile strength} / \text{Young's modulus}$

Fracture energy per unit area (to fully open the crack) needs to be specified (instead of the strain at the end of the softening curve) when defining a localised fracture rather than a distributed fracture. Use of the fracture energy is recommended instead of the strain definition for concrete without reinforcement in the LUSAS theory manual (FEA Ltd 2001c).

### 7.5.1 Arch barrel model results

The arch FE model defined by the material properties described above terminated at a load level of 3.45kN. At this load level four hinges had occurred in the barrel and therefore it can be accepted as the arch failure load. Figure 7-11 shows crack positions under this load level. The first cracks occurred under the load location and propagated through the ring depth with increasing applied load. Two hinges were formed near to the springings and one hinge was formed at about three quarters of the arch span. In most of the centrifuge tests the hinges were formed at these locations.

As stated in section 7.4.1 two norms, force residual and displacement norm, effect convergence and the load level at termination. The failure load value of 3.45kN was obtained with input data values of 1.0 and 0.5 for the residual force norm and displacement force norm, respectively. Therefore, some changes in this load level were expected with changes in these two norms. The effects of changing these parameters on the failure load are presented in Figure 7-12 and 7-13 as guidance. These figures indicate the great effect of the force residual norm on the termination load level. Consideration of Figure 7-12 indicates an increase of 20% in the terminated load level for a residual force norm of 1 to 5. According to the LUSAS theory manual (FEA Ltd 2001c) and the initial studies on the effect of changing these norms on the failure load, crack positions and the crack propagation observed, it is considered that the suggested norms are reasonable. The failure load definition criteria for the numerical model of the arch barrel with the backfill are determined later. Unfortunately, no centrifuge tests were carried out on the arch barrel alone and therefore no comparison between the FE model and the centrifuge tests are possible.

### 7.5.2 Parametric study

The effect of changes in some of the material parameter values was tested during the numerical studies and the results are detailed in this section. The failure loads and arch deflection variation with different values of arch barrel modulus of elasticity are detailed in Table 7-2. While a change in the modulus of elasticity from  $2,000\text{N/mm}^2$  to  $50,000\text{N/mm}^2$  for the barrel has no significant effect on the failure load obtained the arch displacement under the load position is significantly higher for smaller values of modulus of elasticity. It seems that reasonable results were obtained using the experimentally obtained value of the barrel modulus and therefore no adjustment in the modulus of elasticity was needed. Poisson's ratio of 0.29 was obtained from the material tests on walette specimens which seems to represent the masonry behaviour in the arch barrel and there was no reason to adjust it during the numerical studies, a Poisson's ratio of 0.3 was therefore used in all the numerical models. Initial studies indicated no significant effect of Poisson's ratio on the results. In addition similar values are recommended for use in arch masonry numerical models by other researchers(Boothby et al. 2004; Fanning and Boothby 2001b; Forde et al. 2003; Ng et al. 1999).

The tensile strength value is the most important input data in relation to its effect on the arch failure load. A tensile strength value of  $0.27\text{N/mm}^2$  was obtained from the material tests properties in the current study. Using this value resulted in a failure load of 3.45kN for the shallow arch barrel which is about 60% of the average failure load of the centrifuge tests and seems a reasonable value compared with the centrifuge experimental values obtained. The effect of different tensile strength value on arch barrel failure loads are given in Table 7-3. The failure loads of 2.62kN and 4.49kN were obtained for tensile strengths of  $0.20\text{N/mm}^2$  and  $0.50\text{N/mm}^2$  respectively. Using a tensile strength of  $0.50\text{N/mm}^2$  resulted in a failure load of 4.49kN which is higher than the expected load for the arch barrel alone.

No experimental values were found for the fracture energy of masonry specimens in the literature review. The research carried out by Baker (Baker 1996) identified values of 0.03N/mm and 0.02N/mm for mortar and bricks respectively. These values related to 1:1:6 mortar mix with a compressive strength of  $12.2\text{N/mm}^2$  and bricks with a compressive strength of  $38.0\text{N/mm}^2$ . He used the same values of mortar for verification



of a cracking concrete model in LUSAS for analysing masonry specimens. The same value was used in the current study for the arch barrel but it should be noted that larger values of strain energy result in larger failure loads. The values of 0.05N/mm and 0.08N/mm resulted in the failure loads of 3.8kN and 4.1kN respectively.

## 7.6 Modelling arches with backfill

The effect of backfill in increasing masonry arch bridge failure loads is accepted (Fairfield and Ponniah 1994a; Fairfield and Ponniah 1994b; Royles and Hendry 1991). The presence of the backfill distributes concentrated load from the surface over the bridge and also its self-weight increases stability by inducing greater initial compression in the arch prior to live loading. The backfill was added to the FE model after completion of the arch barrel studies. Elasto plastic conditions was assumed for the backfill. The modulus of elasticity, Poisson's ratio and mass density was used to identify the elastic behaviour and a Mohr-Coulomb yield criteria was used to model backfill behaviour. The Mohr-Coulomb yield criterion requires three material parameters: the cohesion,  $C$ , the angle of internal friction,  $\phi$ , and the angle of dilation (FEA Ltd 2001c). Most of these parameters were obtained directly from the material tests properties (Chapter 3) and some of them were assumed according to the recommendations of previous research into FE models of masonry arches (Fanning and Boothby 2001a; Fanning and Boothby 2001b; Forde et al. 2003; Ng et al. 1999). The main material properties which were assigned to the model are given in Table 7-4. Determination of the Young's modulus values for soil is difficult as stiffness depends on the stress history, density and moisture condition. The values of 15N/mm<sup>2</sup> and 0.4 were assumed for modulus of elasticity and Poisson's ratios for both the shallow and the deep arch model in the current study. The same values were used in most of the previous FE models of masonry arches. A friction angle of 53 degree and cohesion of 0.02N/mm<sup>2</sup> were obtained from material tests directly and used in the non linear model.

An interface layer of 1.5mm thickness with the same elements as backfill was used to model the soil masonry interaction behaviour. The behaviour of the interface elements were elasto-plastic with a failure defined by a Mohr-Coulomb yield criterion. Similar properties to the backfill was used for these interface elements. The friction

values for the arch/fill interface were taken as 75% of the fill friction. This reduction has been used successfully by Thavalingam and et al (Thavalingam et al. 2001) to simulate soil interaction behaviour on a semi-circular arch.

A general view of the FE meshes for both the shallow and the deep arch with backfill are presented in Figures 7-14 and 7-15. Following the studies on the arch barrel alone the ring was assumed to be rigidly fixed to its abutments. All soil elements in contact with vertical rigid face on both end of the model were assumed fixed in the horizontal direction and those which were in contact with the bottom surface of model were fixed in both vertical and horizontal directions. Initial sensitivity studies indicated that changes in these boundary conditions has no significant effect on the arch failure load.

The loading on a masonry arch bridge is a combination of self weight loading and traffic loading. The proportion of loading due to the self weight is significant and indeed much of the strength of these bridges is due to the stresses induced in the masonry material due to self weight effects. In modelling this type of bridge an initial gravity-loading step is applied to generate the in-situ stresses to which the bridge is subjected. Subsequent loading events, such as the passing of a truck over the bridge, use the stresses from the gravitational load step as a set of initial conditions. In the current model the self load was applied to the model as a body force with a load factor of 12 to simulate the centrifuge acceleration conditions. The rolling load was applied to the model from the backfill surface at selected positions and increments of applied load were used to model the increasing load. The load application procedure was explained in section 7.4.2.

## **7.7 Results of arch model with backfill**

The initial results obtained from the numerical model indicate the failure values are dependent on the convergence criteria and norm values which was explained in section 7.4. Increasing the norms increased the load non convergence level without any significant changes in the arch condition. The four hinges form at lower load levels but none of them propagated fully until the non convergence stopped the calculation. That means that full propagation of a crack along a section through the arch ring, which was

defined as a failure criteria of arch by Ng and Fairfield (Ng and Fairfield 1999), seems not to have happened. Therefore according to the centrifuge test observations and initial FE model results the failure load was assumed to occur when the fourth hinge formed in the arch and the cracks on the fourth hinge propagated up to 50% of the ring thickness.

The failure loads of the arch model using the above criteria with different tensile strengths are given in Table 7-5. The failure load increased with increasing the tensile strength of the arch barrel materials as is expected. Comparison of the numerical results obtained with the experimental centrifuge test results indicated the best failure load was obtained when the tensile strength of the masonry material was adjusted to  $0.2\text{N/mm}^2$ . Assumed strength values of around this value are usual in the numerical models of masonry arch bridges. Ng was used a tensile strength of  $0.4\text{N/mm}^2$  to model a semicircular single span arch which was built using 1:1:6 (cement: lime: sand) mortar mix (Ng and Fairfield 1999). Fanning and Boothby used a tensile strength between  $0.2\text{N/mm}^2$  to  $0.5\text{N/mm}^2$  to model different single span stone arch bridges (Fanning and Boothby 2001b).

### 7.7.1 Failure load results

Using the above failure definition, failure loads of 5.8kN and 6.2kN are predicted for the shallow and the deep arch geometries, respectively. These results indicate good agreement with failure loads that were obtained from the centrifuge tests. In case of the deep arch, the predicted failure load is about 10% more than the average centrifuge results for the same geometry while there is no significant difference between the predicted and experimental values for the shallow arch.

The deformed arch under failure loads for both the shallow and deep arch geometries are presented in Figures 7-16 and 7-17. The deformed mesh was multiplied by a scale of 5 to indicate more detail. The yielding points which indicate the cracks opening positions are also included in these figures. These figures show four hinge formations for both geometries. In the shallow arch two hinges locations are near to the springings but in the deep arch the left hand hinge moved up the arch from the springings. In both arches the first hinge occurs under the load location.

In Figure 7-18 the FE predicted load deflection for the shallow arch is compared with those obtained from the current study benchmarks tests and the average load deflection from the previous study on small scale arch model with the same geometry (Burroughs 2002). The numerical and experimental results are generally in good agreement with the numerical model being significantly stiffer than the experimental one. While maximum deflection of 3.5mm was obtained from the experimental tests under the load location the numerical model predicts a maximum deflection of 0.58mm under the failure load for the shallow arch which is significantly less than the experimental results. The results obtained by Ng in his simulation of a single span experimental arch model (Ng 1999) indicate a similar stiffer predicted behaviour using the FE model. This is also confirmed by the comparison between experimental and numerical results which was presented in appendix-E of the design manual for roads and bridge (Department of Transport 1997a). Although using smaller values of the modulus of elasticity in the numerical model would result in larger deflections using very small values is unrealistic. It should be noted that the predicted results do not represent the experimental arch behaviour particularly well near to the failure load level. The same arch deflection results for the deep arch are detailed in Figure 7-19.

The soil arch interface pressures were measured at various positions of the arch extrados in the small scale models. The calculated pressures values at the same positions under increasing load are compared to those values in Figure 7-20 A-C at 3 locations for the shallow arch. Consideration of the figures shows that the predicted pressures are in the range of the registered pressures. In the experimental tests after achievement of a particular part of the failure load there is a significant decrease in the pressures registered but in the numerical method the pressures continue to increase up to the failure load. At 75% of the arch span, the registered pressures varied between  $2.0\text{N/mm}^2$  to  $20.0\text{N/mm}^2$  and the maximum pressure of  $10.0\text{N/mm}^2$  was predicted by the numerical method. Good consistency was achieved between the calculated and pressures predicted for S2D-3B. Poor results was obtained from test S2D-1B and finally about half of the maximum pressures registered at 93% of the span was predicted by the FE model. The numerical pressures predicted at 68%, 81%, and 92% of the span for deep arch geometry are compared with the respected registered values from the centrifuge test in Figure 7-21. The figure shows that the numerical pressures calculated at 93% of arch span are more than

the other two sections under an increasing load while the maximum pressure recorded by pressure gauge is at 81% of the span.

### 7.7.2 Rolling load results

The rolling load was applied to the whole width of the arch barrel in the 2-D centrifuge model tests. The roller was moved across the arch and the deflections and pressures were recorded at different locations of the arch span. To simulate the roller movement after application the self weight different load cases were applied to the numerical model. These load cases are of the same magnitude and were applied on the top surface of the backfill at different arch span positions. The same procedure was used as for the increasing load, the self weight was applied using manual incrementation and the other load cases (roller loads) was applied using automatic incrementation. Therefore the self weight effect was remembered by the model and the roller load effect was added to it (FEA Ltd 2001b). By switching from each load case to the other, the effect of the previous load case was deleted and the new load case was added to the self weight.

Predicted arch deflections at 50% and 75% of the arch span with various roller locations (different load case) are detailed in Figure 7-22 A-B for the shallow arch. The related deflections under the same roller, registered by the LVDTs at the same sections are included in the figure as a comparison. Consideration of the figure indicates that in both the sections the numerical model well predicted the arch deflections when the roller load was applied locally on top of the considered sections. At the mid section of the arch the FE calculated deflections are smaller than those obtained in the centrifuge tests. In the mid section, a deflection of 0.06mm was predicted by the FE model, which is about 30% smaller than the average tests results of 0.09mm. Some difference, but not significant, was observed between the experimentally recorded deflections and the numerical model in the far position of the applied load. Considering calculated deflections at 65% and 75% of the span, when the roller was located on the far part of the arch (0%-50% span) indicate some outward deflections. While the maximum outward movement of 0.02mm (Figure 7-22 B) was obtained from numerical model an insignificant movement was recorded in the experimental tests. This might be as a result of the roller movement direction in the experiments which is not considered in the numerical model.

The pressures on the extrados of the arch barrel are one of the other parameters which were measured in some locations in the experimental work. Calculated pressures at the same positions were taken from the FE model and compared with experiments in Figure 7-23 A-B. The numerical model indicates that the general behaviour of arch was simulated with good consistency but the maximum pressures values in the FE model are significantly more than the experimental data. While a maximum pressure of about 40kPa was measured under the roller at 50% of the arch span in the experimental tests, a maximum pressure of 88.0kPa was obtained from the FE model at the same position. Approximately the same results were obtained at the other sections. There is no explanation for such a significant difference between the results. However higher predicted pressures are expected as a result of the stiffer response of the numerical model. Comparison between the pressures which were obtained using the UK code, which is included in figures, indicates approximately the same results as the FE model.

Figure 7-24 shows the deep arch deflection at mid section against the roller position. The predicted arch deflections from the numerical model for the same load cases are included as a comparison. The numerical results are in good general agreement with the experimental results when the roller is located on most parts of the arch span. A small difference between the two results is observed when the roller is located far away from the mid section.

### **7.8 Backfill depth effect**

The effect of changes in the material properties for both barrel model and barrel with backfill was explained in the last section. To understand the effect of backfill depth on the arch model response two FE models with a backfill depth of 13mm (about half of the benchmark backfill depth) and 90mm (three times of the backfill depth) were constructed. The effect of backfill depth on the rolling load and increasing load were studied and the results are presented in this section.

Larger failure loads are expected for models with deeper backfill through the provision of increased dead load and through the increased dispersal of the applied live load. Previous centrifuge modelling of the masonry arch behaviour (Burroughs 2002)



indicated that a three-fold increase in backfill depth above the crown, for a deep arch, yielded a 125% increase in arch strength, whilst a similar increase in fill depth for a shallow geometry, yielded a 72% increase in the load carrying capacity. That work also indicated that the increased dispersal of the load provides the biggest contribution to increasing the carrying capacity of the arches. Failure loads of 13.1kN and 15.5kN are predicted by the FE model for shallow and deep arches geometries with 90mm backfill depth. This indicates an increase of 130% and 167% for the shallow and deep arch for a 3 times increase in backfill depth. As with the centrifuge tests more effect of the deeper backfill was observed in the deep arch. For both geometries, the predicted failure loads are more than that measured in the experiments.

The results indicate that a three-fold increase in the backfill depth reduces the maximum deflection by about 13% and 16% at mid section for the shallow and deep arch respectively under the rolling load which is significantly less than the 40% reduction recorded for the same deeper backfill in previous study for both geometries (Burroughs 2002). This effect can be attributed to the better distribution of the load through the deeper backfill and the enhanced stiffness and restraint provided by the additional backfill. Decreasing the backfill depth to half the standard value had no significant effect on the predicted deflections. Figure 7-25 details the change in radial deflections against the rolling load position at 75% of the deep arch span as typical of the predicted results. As can be seen from this figure a reduction in the deflections is predicted with increasing the backfill depth under the load position but this decrease is not significant. More effect of the backfill depth was predicted when the rolling load was applied away from the selected section. Outward deflections of 0.03mm, 0.04mm and 0.05mm were predicted by the FE model for the deep arch geometry with 90mm, 30mm and 13mm backfill depth at the crown. More backfill depth and therefore more self weight better restrict the outward movement of the arch barrel and this might be one of the reasons for the lower movement with a greater backfill depth.

Figure 7-26 presents the extrados pressure against the roller position predicted at 68% of the span for the models with different backfill depths at the crown. The results indicate for each pressure sensor that the extrados pressure recorded in the deeper backfill arch was significantly smaller than was observed in the other two tests. The maximum

pressures of  $35.0\text{N/mm}^2$ ,  $81.0\text{N/mm}^2$  and  $104.0\text{N/mm}^2$  for backfill depths of 90mm, 30mm and 13mm was calculated at that section. While increasing the backfill depth up to 3 times decreased the pressure by up to 55%, halving of the backfill depth increased the pressure by 30% and demonstrates the non-linear relationship of pressure with backfill depth. The roller load effect was registered on a wider area for the model with a deeper backfill depth as is seen from the figure. This effect can be attributed to the better distribution of the load through the deeper backfill and therefore the smaller registered pressures. A simple assessment of the extrados pressures directly below the roller can be made using elastic theory (Poulos and Davis 1974) . The results indicate values of  $30.0\text{N/mm}^2$ ,  $67.0\text{N/mm}^2$  and  $99.0\text{N/mm}^2$  for backfill depth of 90mm, 30mm and 13mm respectively, these are smaller values when compared with the numerical results. This might be the result of the lateral stresses, which are not accounted for in the elastic calculation. Both the FE model and the elastic calculation results are significantly higher than the measured values in the current study.

### **7.9 Arch model with repair**

One shallow and one deep arch were repaired by applying a 17mm concrete slab on the top surface of the backfill in the experimental studies. It was decided to study the effect of this repair method using the FE model. Therefore a concrete slab was added to the barrel and backfill model. A plane strain condition was assumed for the concrete and the same 8 noded quadrilateral elements were used. Modulus of elasticity, Poisson's ratio and mass density was used to identify the elastic behaviour of the backfill and the same barrel material cracking concrete model was used to simulate the concrete behaviour at failure. Modulus of elasticity of  $10,000\text{N/mm}^2$ , Poisson's ratio of 0.2 and a tensile strength of  $2.0\text{N/mm}^2$  were assumed for the concrete. Load application and all other procedures remained the same as for the FE model without repair.

### **7.10 Repair model results**

The repaired arch model conditions at failure for both geometries are presented in Figure 7-27 and 7-28. The opening crack positions are included in these figures. The crack positions obtained from the related centrifuge tests are also included in the figures. As can be seen from these figures at the failure load, cracks were propagated in four regions in

both models in the concrete slab. Comparison between the experimental and numerical results indicate that the numerical model simulates the general behaviour of the arch model well and predicted crack positions are consistent with the experimental results particularly for the deep arch. The shallow arch model failed due to ring separation during the tests with just two hinges being formed and in this model can be seen that the FE model predicted their location very well.

Failure loads of 15.2kN and 14.6kN for the shallow and deep repaired arch geometries were obtained using the FE models described above. The predicted failure load for the shallow arch is approximately the same as the experimental result but in the case of the deep arch the value predicted by the FE model is about 12% less than the experimental result. Load arch deflection curves for both the shallow and the deep arches are presented in Figures 7-29 and 7-30. Consideration of these figures indicates significantly higher deflection in the experimental results. However the FE model simulates the arches behaviour with a reasonable accuracy up to about 50% of the failure load but at the higher loads the experimentally obtained deflections are significantly more than the FE models. This shows that the FE model did not predict the arch response well under high load level particularly near to the failure loads.

In Figures 7-29 and 7-30 the arch barrel extrados pressures at different locations are compared with the numerical results for the same sections under increasing loads. In Figure 7-30 the pressures at 75% and 85% of the arch span obtained from S2D-3R are compared with the calculated values from the FE model. In both the experimental and the numerical models an increase in pressure was obtained with increasing load. In both the sections there is good consistency between two methods. However, the calculated pressures on the extrados of the deep arch barrel are in the range of the measured values but the FE model results are slightly larger, for 92% of span, and less, for 68% of span, than the experimental pressure sensor data.

## 7.11 Conclusions

A 2-D FE model was constructed and tested under rolling and increasing loads. The results obtained were compared with related experimental data for both the shallow and

the deep arch geometries. From the FE results and the comparison with experimental data the following conclusions can be drawn.

- The 2-D FE model can simulate the general behaviour of an arch with good consistency. The comparisons between the experimental and numerical results indicate that FE predicted the hinge locations well.
- The FE arch models failed due to the formation of four hinges, while in the experimental models some tests failed through ring separation propagation. More detailed definition of the shear joints along the ring need to be added to the FE model to simulate this behaviour.
- In terms of the value of failure load, the FE model predicted the arch failure loads for both geometries well but in terms of deflections the FE model is significantly stiffer than the experimental models.
- The pressures on the extrados of the arch barrel determined using the FE model are in good agreement with those obtained from the centrifuge tests however some differences were observed particularly near to the failure loads.
- The arch behaviour under rolling load can be simulated by the FE model with reasonable accuracy. The general behaviour obtained is consistent with the experimental results.
- The arch deflections under the rolling loads were predicted well but the calculated pressures are significantly more than the obtained values experimentally.
- The FE model can be used to simulate the repaired arch model. The repaired FE failure loads, predicted the hinges positions well and general behaviour of the arch at failure loads. The FE failure loads are approximately the same as those obtained from both test geometries.

Property	Arch barrel	Backfill	Interface
Modulus of elasticity (N/mm <sup>2</sup> )	4,000	15	5
Poisson's ratio	0.3	0.4	0.4
Bulk density (kN/m <sup>3</sup> )	21	20.5	20.5

**Table 7-1: Material properties, linear elastic FE model**

Modulus of elasticity (N/mm <sup>2</sup> )	Failure load (kN)	Maximum displacement (mm)
2,000	3.22	-1.04
4,000	3.48	-0.45
10,000	3.55	-0.21
50,000	3.69	-0.04

**Table 7-2: Failure load with different modulus of elasticity**

Tensile strength (N/mm <sup>2</sup> )	Failure load (kN)	Deflection under load position (mm)
0.1	1.75	-0.22
0.2	2.62	-0.39
0.3	3.45	-0.45
0.5	4.49	-0.72

**Table 7-3: Failure load with different tensile strength**

Property	Arch barrel	Backfill	Interface
Modulus of elasticity (N/mm <sup>2</sup> )	4,000	15	5
Poisson's ratio	0.3	0.4	0.4
Bulk density (kN/m <sup>3</sup> )	21	20.5	20.5
Tensile strength (N/mm <sup>2</sup> )	0.3		
Friction angle (degree)		53	40
Cohesion (N/mm <sup>2</sup> )		0.02	0.02
Fracture energy (N/mm)	0.03		

**Table 7-4: Material properties, non-linear FE model**

Arch geometry	Shallow				Deep
	$\sigma_t = 0.08$	$\sigma_t = 0.1$	$\sigma_t = 0.2$	$\sigma_t = 0.4$	$\sigma_t = 0.2$
Tensile strength (N/mm <sup>2</sup> )					
Third hinge formation	2.1	2.2	2.7	4.3	3.5
Fourth hinge formation	2.4	2.8	3.5	4.8	3.8
Forth hinge propagation to 50% ring	4.5	4.8	5.8	7.9	6.2
Forth hinge propagation to 75% ring	5.5	5.8	7.2	N/A	N/A

**Table 7-5: Numerical arch failure load with different tensile strength of barrel material**



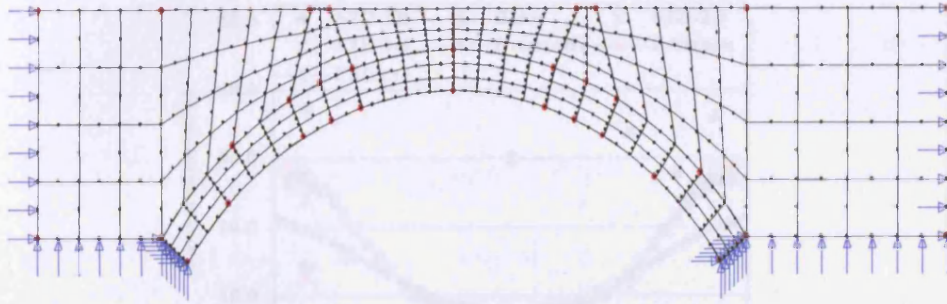


Figure 7-1: General view of 2-D shallow arch FE model

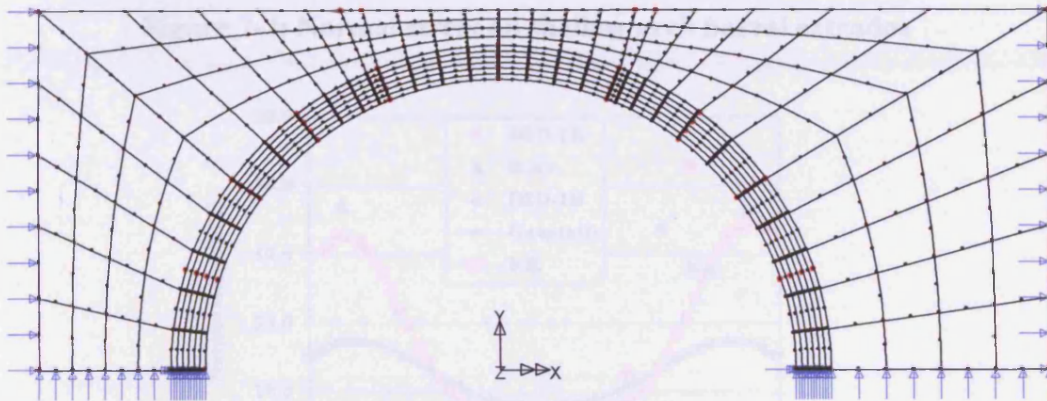


Figure 7-2: General view of 2-D deep arch FE model

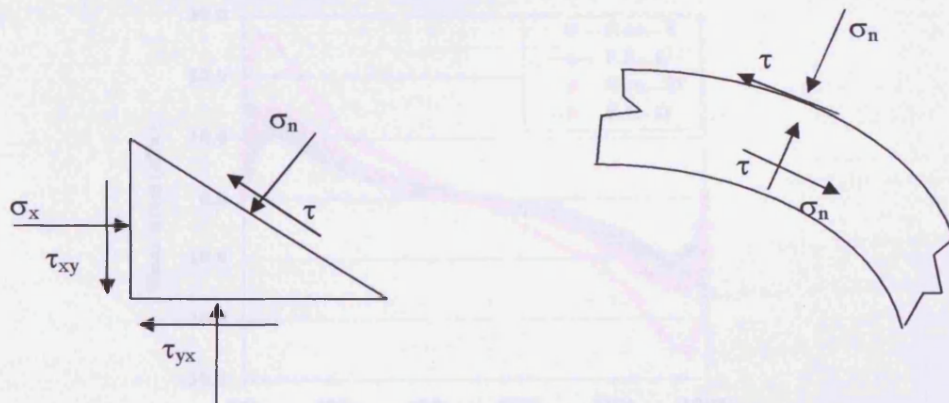


Figure 7-3: Direction of stresses

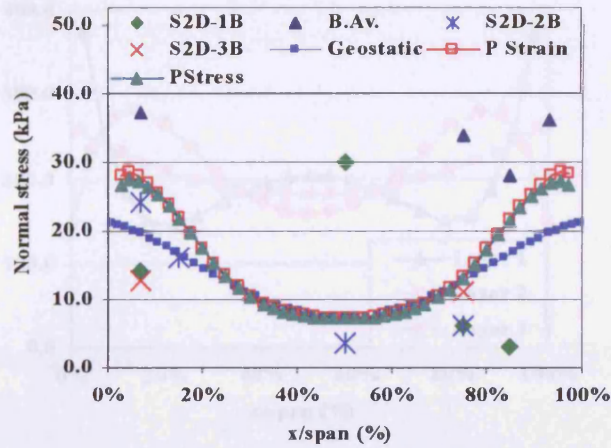


Figure 7-4: Normal stress on shallow arch barrel extrados

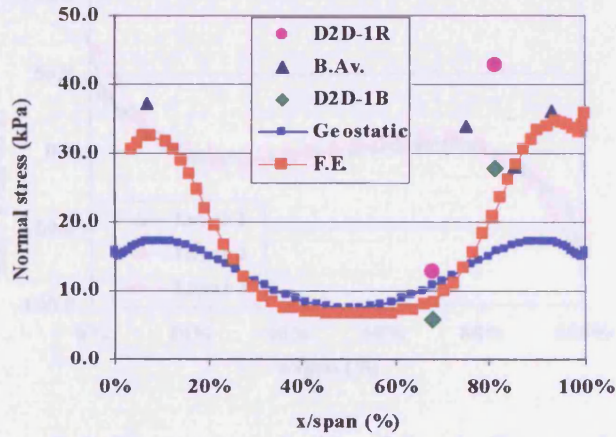


Figure 7-5: Normal stress on deep arch barrel extrados

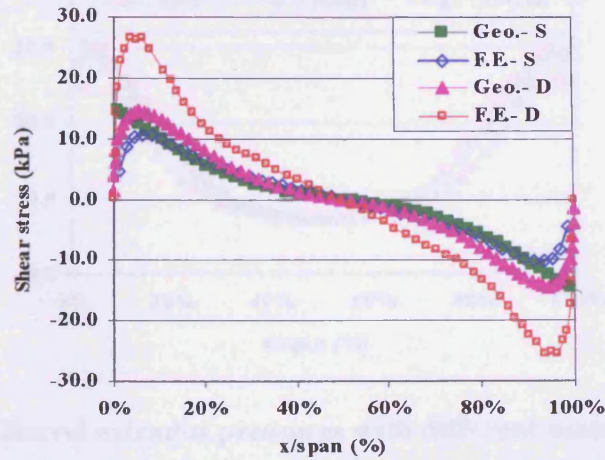


Figure 7-6: Shear stress on the shallow and deep arch extrados



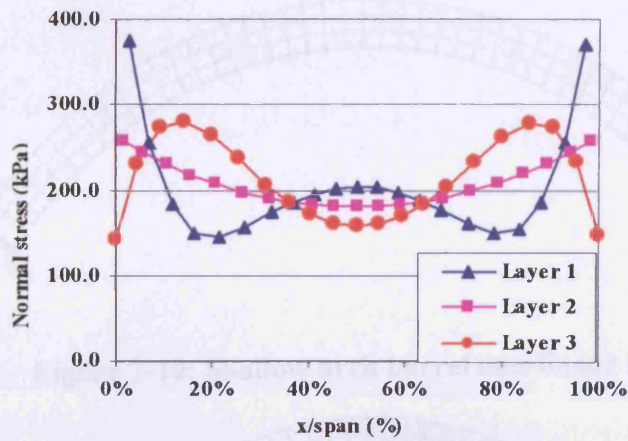


Figure 7-7: Normal stress inside of the shallow arch barrel

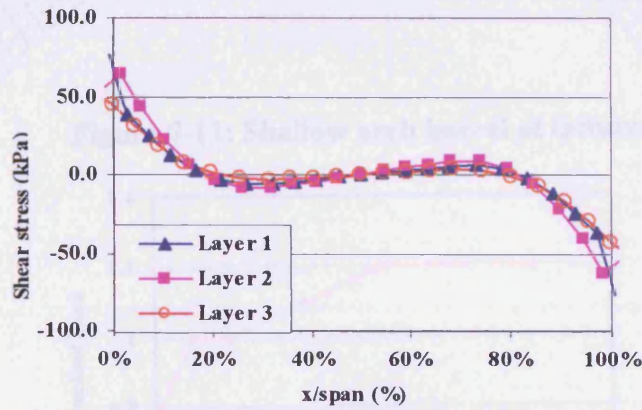


Figure 7-8: Shear stress inside of the shallow arch barrel

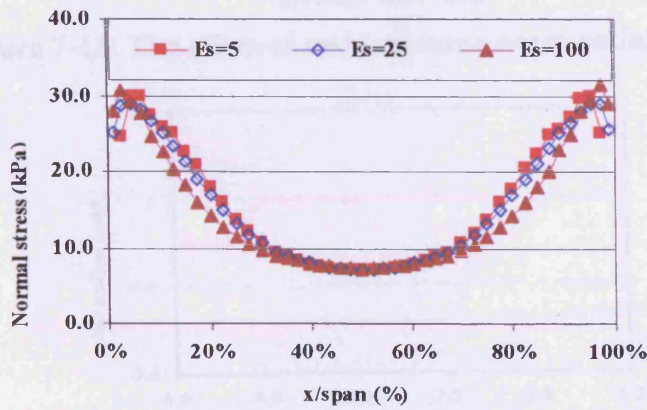
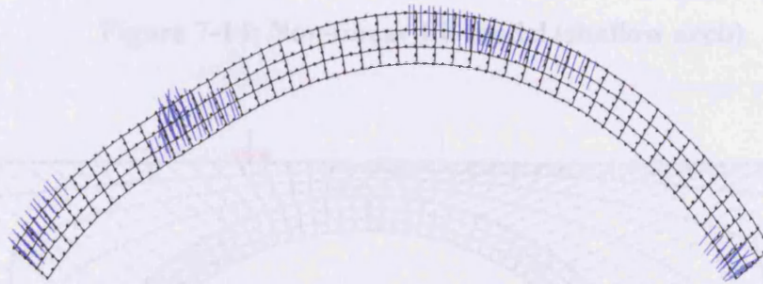


Figure 7-9: Barrel extrados pressures with different material properties



**Figure 7-10: Shallow arch barrel non-linear model**



**Figure 7-11: Shallow arch barrel at failure**

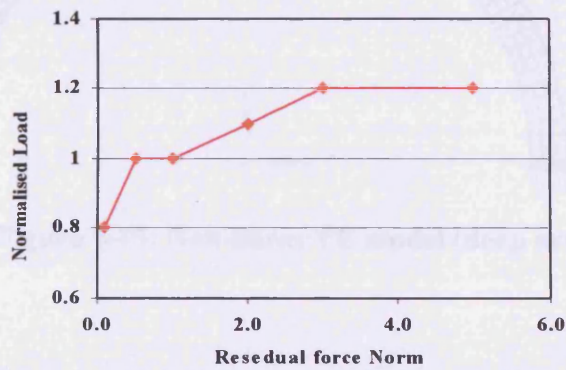


**Figure 7-12: The effect of residual force norm on failure load**

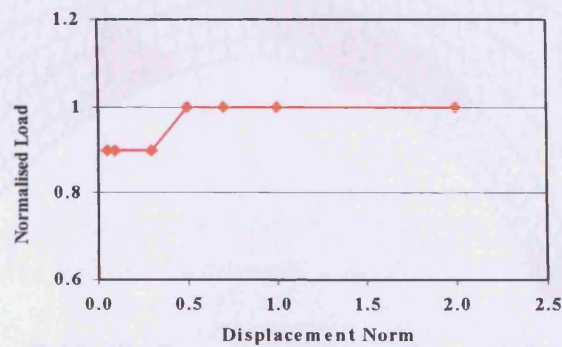


**Figure 7-13: The effect of displacement norm on failure**



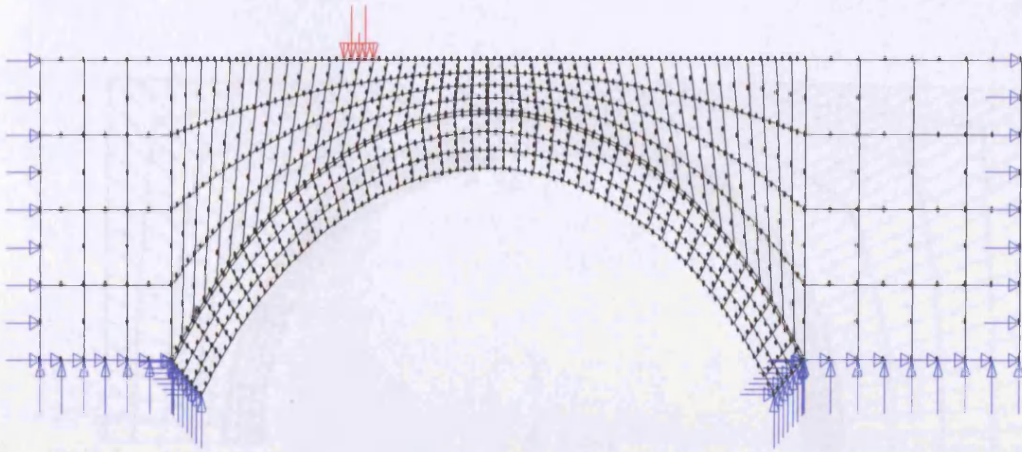


Figure 7-14: Non-linear FE model (shallow arch)

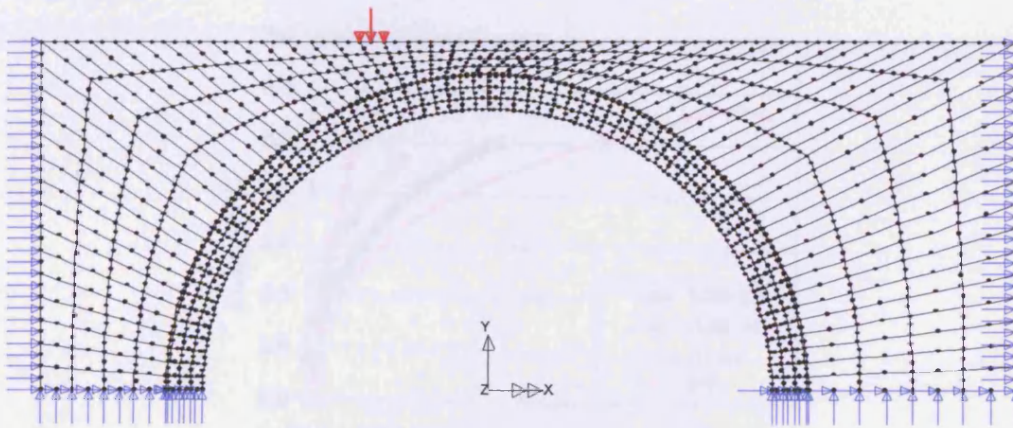


Figure 7-15: Non-linear FE model (deep arch)

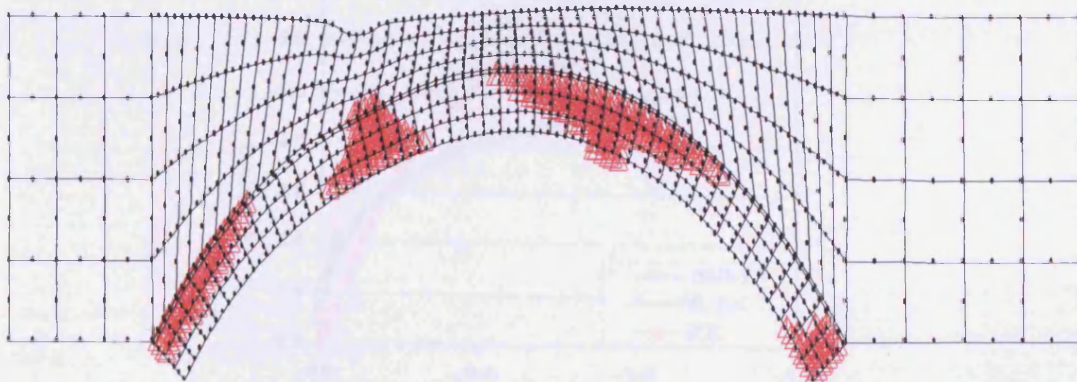


Figure 7-16: Shallow arch deformation at failure load

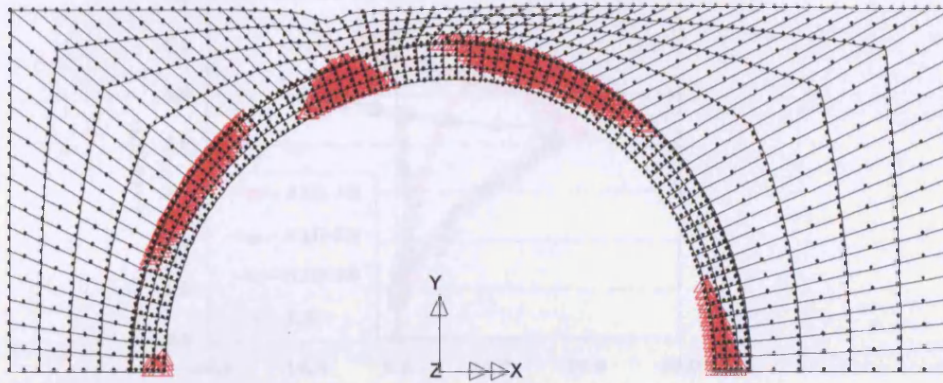


Figure 7-17: Deep arch deformation at failure load

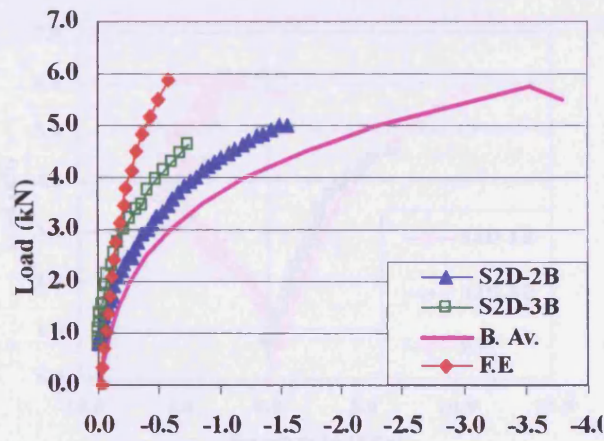


Figure 7-18: Numerical and experimental results comparison (shallow arch)

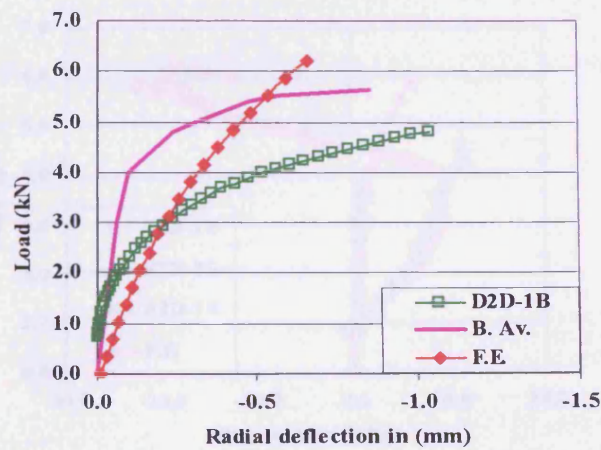
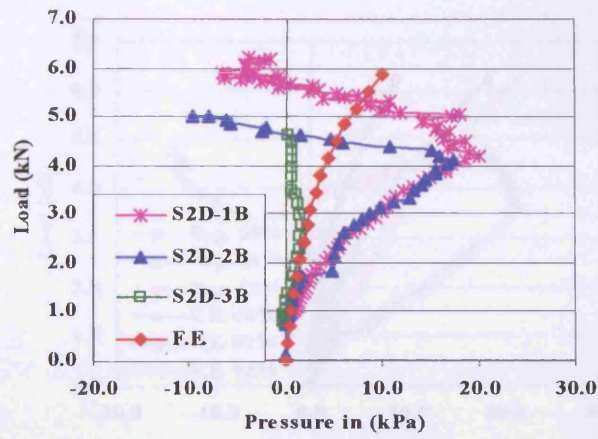
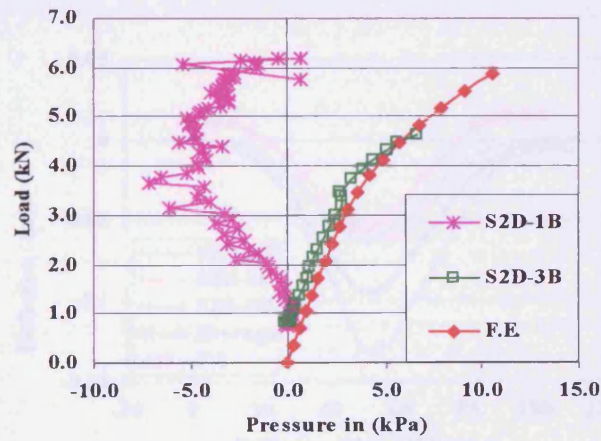


Figure 7-19: Numerical and experimental deflections comparison (deep arch)

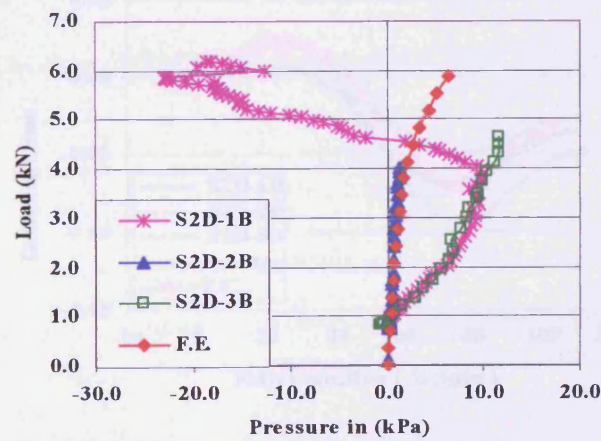




A) 75% Span



B) 85% Span



C) 93% of span

Figure 7-20: Numerical and experimental pressures comparison (shallow arch)

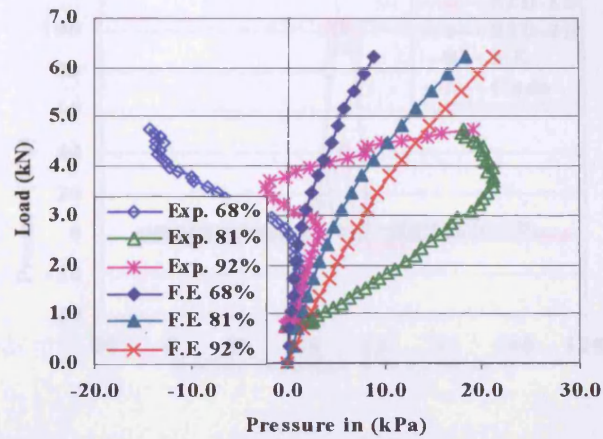
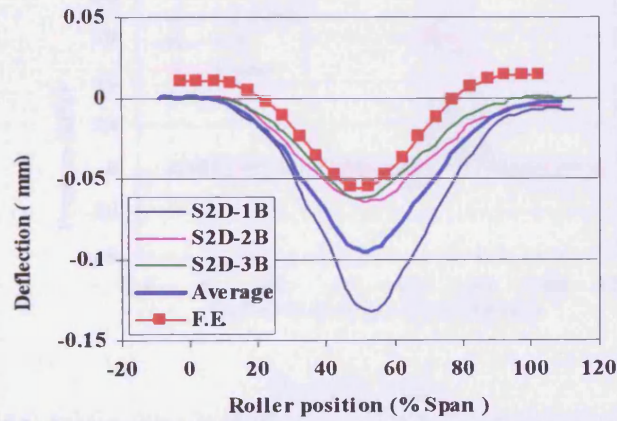
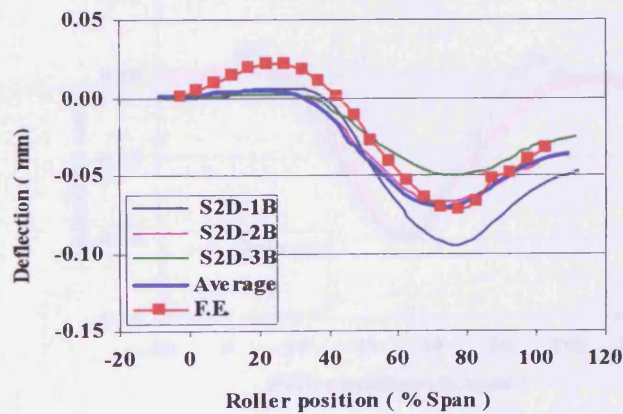


Figure 7-21: Numerical and experimental pressures comparison (deep arch)



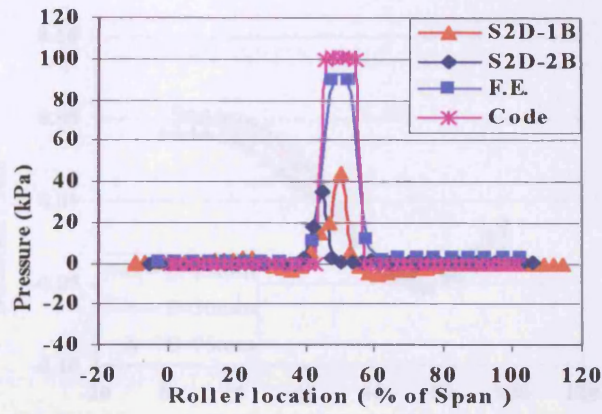
A) 50% of Span



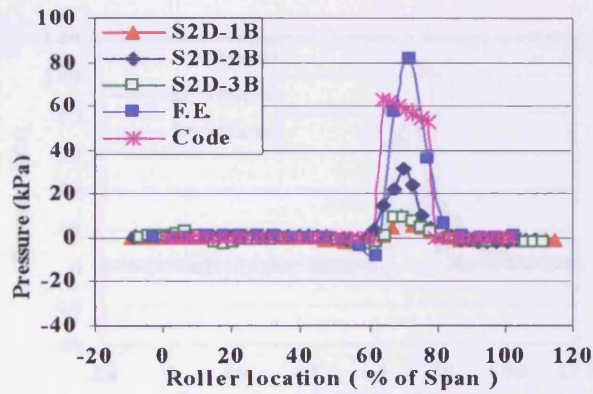
B) At 75% of span

Figure 7-22: Shallow arch deflections at different sections under roller load





A) 50% of span



B) 75% span

Figure 7-23: Pressures at different arch barrel positions (shallow arch)

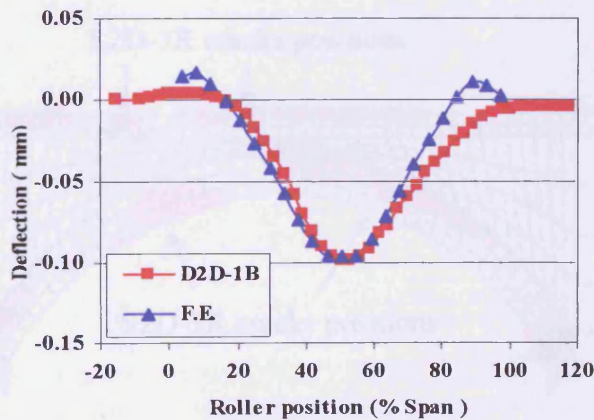


Figure 7-24: Arch deflection against roller location at 50% of span (deep arch)

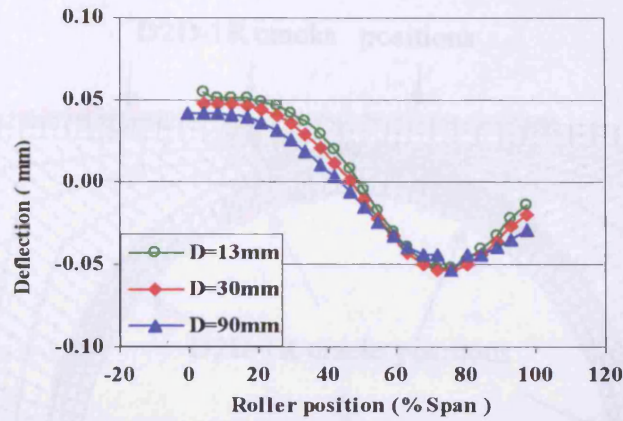


Figure 7-25: Backfill depth effect on arch deflection (75% deep arch)

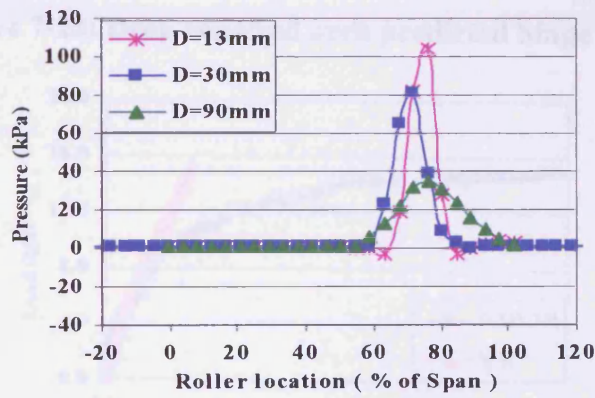


Figure 7-26: Backfill depth effect on predicted extrados pressure (68% deep arch)

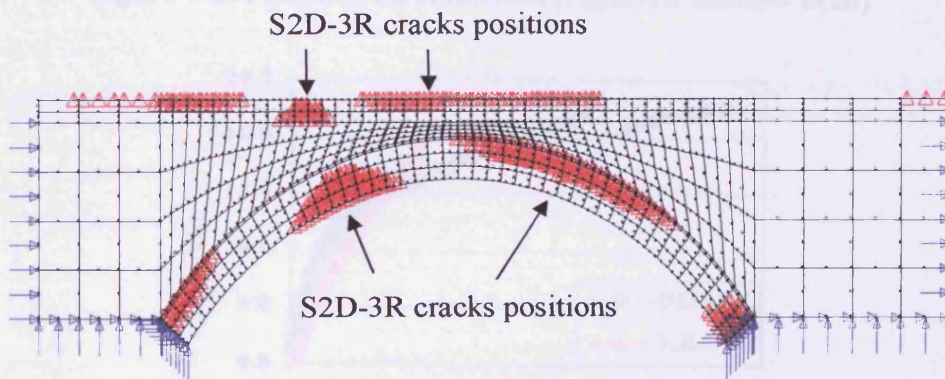


Figure 7-27: Shallow repaired arch predicted hinge position



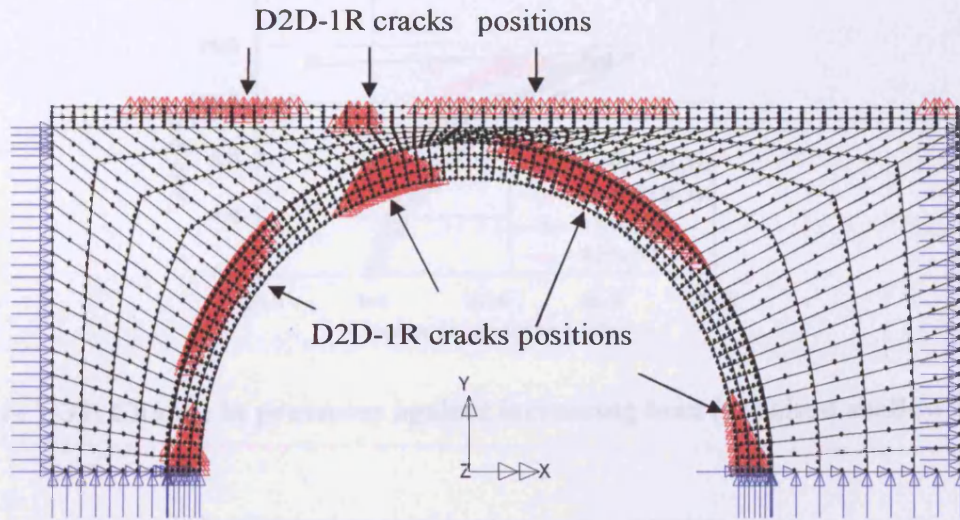


Figure 7-28: Deep repaired arch predicted hinge position

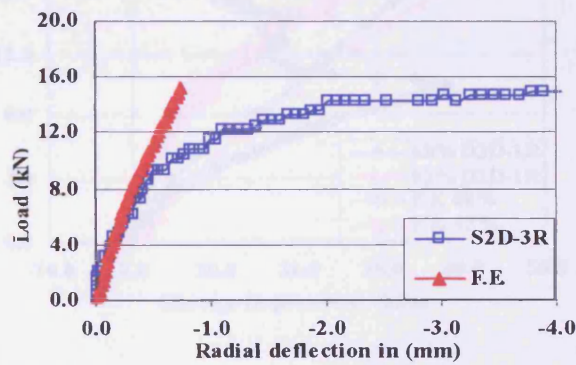


Figure 7-29: Load/arch deflection (repaired shallow arch)

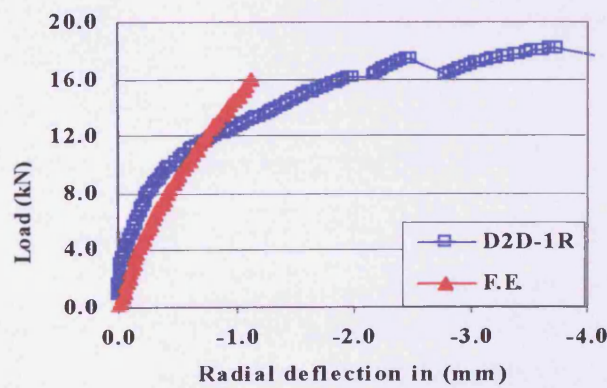


Figure 7-30: Load/arch deflection (repaired deep arch)

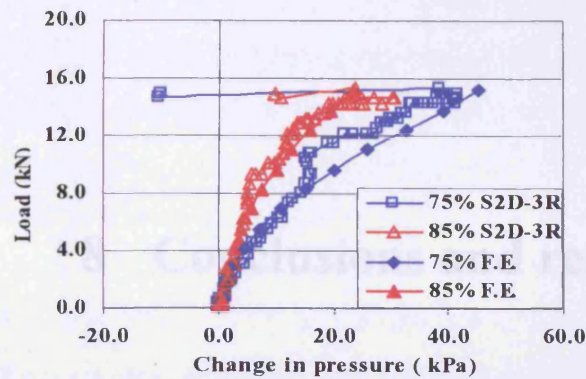


Figure 7-31: Change in pressures against increasing load (repaired shallow arch)

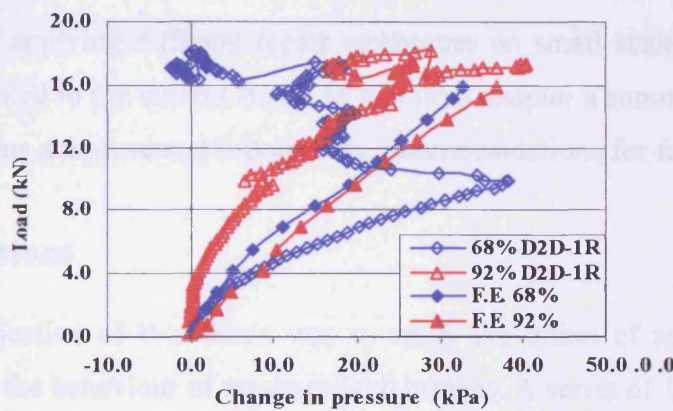


Figure 7-32: Change in pressures against increasing load (repaired deep arch)



## 8 Conclusions and recommendations

### 8.1 Introduction

The effect of applying different repair techniques on small scale centrifuge models has been investigated in the current study. In this final chapter a summary of the observations and conclusions are presented followed by recommendations for future work.

### 8.2 Conclusions

The main objective of this thesis was to study the effect of applying different repair techniques to the behaviour of masonry arch bridges. A series of 1/12<sup>th</sup> scale 2-D and 3-D centrifuge models were tested with rolling and increasing loads. The arches under test were single span, 6m at full size, which were built with both shallow and deep arch geometries. The shallow and deep arches had a span to rise ratio of 4 and 2 respectively. The 2-D models were built with an arch barrel and backfill and the 3-D models in addition included spandrel walls. The models were tested with the rolling loads with a range of 7-15 tonnes at full scale for a 2.5m axle vehicle. The rolling loads were applied to the whole width of the 2-D models and to different locations in the 3-D tests. The arch models were tested in two stages, which were called benchmark and repair tests in the current study. The selected repair methods were applied to the arch models after the benchmark tests and then they were tested to the same rolling and increasing load as the benchmarks. The effect of applying various repair methods was obtained by comparison between the behaviour of arches at the two stages.

Comprehensive arch behavioural information, including arch deformations and pressures on the extrados of the arch barrel were measured for each test. The information considered important is presented in this thesis and the data, in conjunction with the material properties, provides a data bank of well controlled test results that can be useful for future calibration of numerical models.

A 2-D FE model was constructed and the numerical results were compared with those obtained from the experimental tests. The FE model was constructed using the LUSAS commercial FE package and material properties were obtained from related tests on materials during the study. The FE model was used to simulate the arch behaviour under both rolling load and increasing loads at the two stages of benchmark and repaired arch. Both shallow and deep geometries were considered in the numerical study and the concrete slab repair was considered as the only 2-D numerical repaired model.

The following general conclusion can be drawn with regards to the centrifuge benchmark tests:

- Comparison of the results with the previous studies on the same arch geometry and model scale indicate good repeatability of the tests and confirms the value of using centrifuge scale models for studying the behaviour of masonry arch bridges.
- From the test results it can be seen that the maximum part of the load carrying capacity of the arches is resisted before the formation of the first hinge. The results indicated that the load deflection plots are linear approximately up to 50% of the ultimate loads.
- Plastic behaviour of the arches under test was observed at low load levels and only a small part of the deflections were recovered after reloading the arches even at about 30% of the ultimate load capacity.
- The 3-D arch models show out of plane bending of the arches even under symmetrical low load application. This out of plane behaviour and larger deflections along the centreline of the arch are considerable even under the rolling loads (about 30% of the average ultimate load capacity).
- The recorded pressures on the extrados of the arch barrels indicates considerably smaller values in comparison with UK practice and elastic methods. The measured values also indicated that the full passive pressures were not observed during the

tests. The measured values are about 30% of the full passive pressures on parts remote from the applied load location.

The following conclusions can be drawn with regards to the comparison between the 2-D and 3-D benchmark tests:

- In terms of deflections the 3-D arch displacements show smaller values compared with 2-D tests with the same geometry and under the same applied loads. This confirms the spandrel walls effect in restricting of the arch movements.
- The 3-D results highlight the greater variability in the stiffness and failure load compared with the 2-D tests because of their more complex behaviour and because more parameters effect the arch capacity.
- In terms of pressures on the extrados of the arch barrel no significant difference between the 2-D and 3-D results was obtained during the tests and all recorded pressures are approximately in the same range.

After completion of the benchmark tests the arch models were repaired using the selected repair methods and retested using a similar method to the benchmark tests. The following conclusions can be drawn with regards to the repair tests:

- The use of plastic mesh reinforcement in the middle depth of the backfill, at the crown, had no significant effect on the arch load capacity and pressure distribution under the applied loads. Load deflection comparison under increasing load indicated no significant difference between the benchmark and repaired arch behaviour. Larger deflections were observed under the rolling load in the repaired arch which it is suggested is as a result of the separation between the soil layers above and below the plastic mesh.
- The applied concrete slab on top of the backfill increased the ultimate load significantly for both the shallow and the deep arch tests. The ultimate load of the shallow repaired model was 3.4 times that of the benchmark model and 2.7 times the average benchmark results with of the same geometry. The ultimate load for the deep arch was, respectively, 3.7 and 3.2 times as strong as the benchmark test and the average load capacity of a series of deep arch tests. The application of the

slab to the surface appears to be at least equivalent to application directly to the arch intrados and extrados. A concrete slab on top of the fill redistributes the pressure and decreases the recorded pressure on the arch barrel significantly. A significant decrease in the arch barrel deflection was observed under the rolling load.

- The first shallow 3-D arch was repaired using stitching bars applied to the arch barrel and stainless steel bars to connect the extrados ring and spandrel walls to each other. Test results showed limited prevention of ring separation by the stitching bars but an increase of 50% in the ultimate arch load capacity following application of this method.
- Applying a partial saddle concrete on part of the arch barrel in addition to the stainless steel bar connection of the concrete to the spandrel wall increased the arch load capacity and the stiffness of the arch. The arch load capacity was improved by about 2.0 and 2.5 times for the shallow and the deep arch geometry, which is comparable with applying the same concrete on top and beneath the arch barrel in 2-D model tests.
- Two arches were repaired by applying a 17mm reinforced slab of micro-concrete on part of the inside of the spandrel walls. The extent was limited to that reasonably attainable in the field. Test results indicated a significant improvement in the load capacity of the repaired arch. The loads at the failure of the repaired models were approximately twice the benchmark failure load for both the shallow and deep arch geometries. At a low level of applied load and under the rolling load the repaired arch demonstrated much stiffer behaviour compared with the benchmark arch. The strengthened spandrel walls were seen to restrain the arch barrel and the recorded change in pressure on the extrados of the arch barrel, due to barrel movement, is smaller than the benchmark arch.

A 2-D FE model was constructed and tested under the rolling and increasing loads. From the FE results and comparison with the experimental results the following conclusion can be drawn:

- The 2-D FE can simulate the general behaviour of the arch with good consistency. The comparisons between the experimental and numerical results indicate that FE predicted the hinges locations very well.
- The FE model arch models failed due to the formation of four hinges, while in the experimental models some tests failed by ring separation propagation. More detailed definition of the shear joints along the ring needs to be added to the FE model to simulate this behaviour.
- The failure defining criteria according to the crack propagation in the arch barrel can be used to predict the collapse loads. The FE model predicted the arch failure loads for both geometries very well but in terms of deflections the FE model is much stiffer than the experimental models. The pressures on the extrados of the arch barrel determined using the FE model are consistent with those obtained from the centrifuge tests however, some difference were observed particularly near to the failure loads.
- The FE model can simulate the arch behaviour under the rolling load with reasonable accuracy. The general behaviour of the FE model obtained is consistent with the experimental results. The arch deflections under the rolling loads were predicted well but the calculated pressures are significantly more than the experimentally registered values but they are consistent with those predicted by current UK practice.
- The FE model can be used to simulate the repaired arch model using a concrete slab on the top surface of the backfill. The repaired FE results predicted the hinge positions and general behaviour of the repaired arch at failure loads with good consistency. The FE model predicted collapse loads that were approximately the same as those obtained from the tests on both arch geometries.

### **8.3 Recommendations for future research**

According to the results obtained during the study it seems that the research can be extended to some more areas, which were not covered by this thesis due to the time limitation of the project. It is suggested that the study can be extended to the following areas:

- The current test programme was restricted to the testing of non-skewed, single span structures. It is suggested that this study can be extended to the skewed and multi span arches.
- The 2-D FE model of arches was constructed and the numerical results were compared to those obtained from the experimental tests in the current study. There is sufficient data available from the 3-D experimental tests to make a 3-D numerical model of the arches. The effect of the unsymmetrical rolling loads can be considered in such a 3-D numerical model.
- In this 2-D model, the effect of applying the concrete slab on the top surface of the backfill was considered. The study can be extended to the 3-D FE model and study behaviour of the repaired arches using the other repair methods. The effect of a partial concrete slab repair and also spandrel wall strengthening can be an extended area of the current study.



**REFERENCES:**

- Ashurst, D. (1992). "An assessment of repair and strengthening techniques for brick and stone masonry arch bridges." *Contractor Report, TRRL 284*, Transport and Road Research Laboratory, Crowthorne.
- Ayres, D. J. (1990). "Mechanical (or pressure) pointing." *The Maintenance of Brick and Stone Masonry Structure*, A. M. Sowden, ed., E. & F.N. Spon, London, 223-227.
- Baker, G. M. (1996). "Finite element analysis of masonry with application to arch bridges," PhD, University of Wales, Cardiff.
- Baralos, P. (2002). "The small-scale modelling of repair techniques for masonry arch bridges using a geotechnical centrifuge.," PhD, University of Wales, Cardiff.
- Begimgil, M. (1995). "Behaviour of restrained 1.25m span model masonry arch bridge." *First International Conference on Arch bridges*, C. Melbourne, ed., Thomas Telford, Bolton, UK, 321-325.
- Boothby, T. E., Domalik, D. E., and Dalal, V. A. (1998). "Service load response of masonry arch bridges." *Journal of Structural Engineering*, 124(1), 17-23.
- Boothby, T. E., Erdogmus, E., and Yurianto, Y. (2004). "Transverse strength of model masonry arch bridge " *Arch Bridge IV*, P. Roca and C. Molins, eds., Barcelona, Spain, 411-424.
- Boothby, T. E., and Roberts, B. J. (2001). "Transverse behaviour of masonry arch bridges." *The Structural Engineer*, 79(9), 21-26.
- Bridle, R. J., and Hughes, T. G. (1990). "Energy method for arch bridge analysis." *Proceedings of the Institution of Civil Engineers, Part 2*, 89(Sep), 375-385.
- Brookes, C. L., and Tilly, G. P. (1999). "Novel method of strengthening masonry arch bridges." *8th International Conference on Structural Faults and Repair [CD Rom]*, M. C. Forde, ed., Engineering Technics Press, Edinburgh.
- Broomhead, S. F., and Clarke, G. W. (1995). "Strengthening masonry arch." *Bridge modification*, Thomas Telford, London, 174-184.
- BS1377. (1990). *Methods of test for soils for Civil Engineering purposes*, British Standards Institution, London.
- BS 12. (1991). *Specification for ordinary and rapid hardening Portland cement*, British Standards Institution, London.

- BS 890. (1995). *Specification for building limes*, British Standards Institution, London.
- BS 1377-2. (1990). *Methods of test for soils for Civil Engineering purposes, Classification tests*, British Standard Institution, London.
- BS 1377-4. (1990). *Methods of test for soils for Civil Engineering purposes, Compaction related tests*, British Standard Institution, London.
- BS 1377-7. (1990). *Methods of test for soil for Civil Engineering purposes, Shear strength tests*, British standard Institution, London.
- BS 1881-116. (1983). *Testing concrete - Method for determination of compressive strength of concrete cubes*, British Standard Institution, London.
- BS 1881-121. (1983). *Testing Concrete - Method for determination of static modulus of elasticity in compression*, British Standard Institution, London.
- BS 3921. (1985). *Specification for clay bricks*, British Standard Institution, London.
- BS 4551-1. (1998). *Methods of testing mortars, screeds and plasters*, British standard Institution, London.
- Burroughs, P. O. (2002). "A study of parameters that influence the strength of masonry arch bridges using a geotechnical centrifuge," PhD, University of Wales, Cardiff.
- Burroughs, P. O., Baralos, P., Hughes, T. G., and Davies, M. C. R. (2001). "Serviceability load effects on masonry arch bridges." ARCH01, Third international arch bridges conference, C. Abdunur, ed., Paris, 397-402.
- Burroughs, P. O., Baralos, P., Hughes, T. G., and Davis, M. C. R. (2000). "Soil effects and the service loading of masonry arch bridges." 12th International Brick/Block Masonry Conference, Madrid, Spain, 341-350.
- Burroughs, P. O., Hughes, T. G., Hee, S., and Davis, M. C. R. (2002). "Passive pressure development in masonry arch bridges." *Proceedings of the Institution of Civil Engineers, Structure and Buildings*, 152(4), 331-339.
- Carl, L. B., and Graham, P. T. (1999). "Novel method of strengthening masonry arch bridges." 8th International Conference on Structural Faults and Repair [CD ROM], M. C. Forde, ed., Engineering Technics press, London.
- Castigliano, C. (1879). *Elastic stresses in structures. Translation by Andrews, ES*, Scott Greenwood & Son, London.

- Chen, Y., Ashour, A. F., and Garrity, S. W. (2001). "Numerical prediction of the behaviour of masonry arch bridges with near-surface reinforcement." ARCH01, Third international arch bridges conference, C. Abdurnur, ed., Paris, 553-559.
- Cheney, J. A., and Fragaszy, R. J. (1984). "The Centrifuge as a Research Tool." *Geotechnical Testing Journal*, 7(4), 182-187.
- Chettoe, C. S., and Henderson, W. (1957). "Masonry arch bridges: a study." *Proceeding of the Institution of Civil Engineers*, 7(Aug), 723-744.
- Choo, B. S., Coutie, M. G., and Gong, N. G. (1991). "Finite-element analysis of masonry arch bridges using tapered elements." *Proceeding of the Institution of Civil Engineers, Part 2*, 91(Dec), 755-770.
- Choo, B. S., Peaston, C. H., and Gong, N. G. (1995). "Relative Strength of Repaired Arch Bridges." First International Conference on Arch bridges, C. Melbourne, ed., Bolton, UK, 579-588.
- Cox, D., and Hsall, R. (1996). *Brickwork Arch Bridges*, Brick Development Association, Windsor.
- Crisfield, M. A. (1985). "Finite element and mechanism methods for the analysis of masonry and brickwork arches." *TRRL Research Report 19*, Department of Transport, Crowthorne.
- Crisfield, M. A., and Packham, A. J. (1987). "A mechanism program for computing the strength of masonry arch bridges." *TRRL Research Report 124*, Department of Transport, Crowthorne.
- Crisfield, M. A., and Page, J. (1990). "Assessment of the load carrying capacity of arch bridges." *The Maintenance of Brick and Stone Masonry Structures*, A. M. Sowden, ed., E&F.N. Spon, London, 81-113.
- Crisfield, M. A., and Wills, J. (1986). "Nonlinear analysis of concrete and masonry structures." *Finite element methods for nonlinear problems*, Bergan, ed., Springer-Verlag, Berlin, 639-652.
- Davey, N. (1953). "Tests on road bridges." *National Building Studies*, Research Paper No 16, London: HMSO.
- Department of Transport. (1997a). "BA 16/97 - The Assessment of Highway Bridges and Structures." HMSO, London.

- Department of Transport. (1997b). "BD 21/97 - The Assessment of Highway Bridges and Structures." HMSO, London.
- Egermann, R., Cook, D. A., and Anzani, A. (1991). "An investigation into the behaviour of scale model brick walls." 9th International Brick/Block Masonry Conference, DGfM, ed., Berlin, 628-635.
- Ellis, I. W. (1990). "Stitching." *The maintenance of Brick and Stone Masonry Structure*, A. M. Sowden, ed., E. & F.N.Spon, London, 263-270.
- Fairfield, C. A., and Ponniah, D. A. (1993). "Geotechnical considerations in arch bridge assessment." *J. Instn. Highways & Transportation*, 40(7), 11-16.
- Fairfield, C. A., and Ponniah, D. A. (1994a). "Model tests to determine the effect of fill on buried arches." *Proceedings of the Institution of Civil Engineers, Structure and Buildings*, 104(Nov), 471-482.
- Fairfield, C. A., and Ponniah, D. A. (1994b). "The effect of fill buried model arches." *Proceedings of the Institution of Civil Engineers, Structures and Buildings*, 358-371.
- Fairfield, C. A., and Ponniah, D. A. (1996). "A method of increasing arch bridge capacity economically." *Proceedings of the Institution of Civil Engineers, Structures and Buildings*, 116(Feb), 109-115.
- Falconer, R. E. (1997). "Strengthening masonry arch bridges using stainless steel reinforcement." 11th International Brick/Block Masonry Conference, Shanghai, 463-483.
- Fanning, P. J., and Boothby, T. E. (2001a). "Nonlinear three dimensional simulations of service load tests on a 32m stone arch bridge in Ireland." ARCH01, Third international arch bridges conference, C. Abdunur, ed., Presses Ponts et chaussees, Paris.
- Fanning, P. J., and Boothby, T. E. (2001b). "Three-dimensional modelling of full scale testing of stone arch bridges." *Computer & Structures*, 79, 2645-2662.
- Fanning, P. J., Boothby, T. E., and Roberts, B. J. (2001). "Longitudinal and transverse effects in masonry arch assessment." *Construction and Building Materials*, 15, 51-60.
- FEA Ltd. (2001a). *LUSAS Element Reference Manual, Version 13*, FEA Ltd, Kingston upon Thames, Surrey, UK.

- FEA Ltd. (2001b). *LUSAS Modeller user Manual, Version 13*, FEA Ltd, Kingston upon Thames, Surrey, UK.
- FEA Ltd. (2001c). *LUSAS Theory Manual, Version 13*, FEA Ltd, Kingston upon Thames, Surrey, UK.
- Forde, T. E., Augarde, C. E., and Tuxford, S. S. (2003). "Modelling Masonry Arch Bridges using Commercial Finite Element Software." 9th International Conference on Civil and Structural Engineering Computing [CD Rom], B. H. V. Topping, ed., Civil-Comp Press, Stirling, Scotland, Paper 101.
- Garrity, S. W. (1995a). "Retro - reinforcement - a proposed repair system for masonry arch bridge." First International Conference on Arch bridges C. Melbourne, ed., Thomas Telford, Bolton, UK, 557-563.
- Garrity, S. W. (1995b). "Testing on small scale masonry arch with surface reinforcement." 6th International Conference on Structural Faults & Repair, M. C. Forde, ed., Engineering Technics Press, Edinburgh, 409-418.
- Garrity, S. W. (2001). "The strengthening of single span masonry arch bridges using near-surface reinforcement." ARCH01, Third international arch bridges conference, C. Abdunur, ed., Paris, 301-307.
- Garrity, S. W., and Toropova, I. L. (2001). "A finite element study of a single span masonry arch bridge with near-surface reinforcement." ARCH01, Third international arch bridges conference, C. Abdunur, ed., Paris, 567-572.
- Gilbert, M. (1993). "The behaviour of masonry arch bridges containing defects.," PhD, University of Manchester, Manchester.
- Harvey, W. J. (1988). "Application of the mechanism analysis to masonry arches." *The Structural Engineer*, 66(5), 77-84.
- Harvey, W. J., Vardy, A. E., Craig, R. F., and Smith, F. W. (1989). "Load test on a full scale model four metre span masonry arch bridge." *TRRL Contractor Report 155*, Department of Transport, Crowthorne.
- Hendry, A. W. (1986). "Load test to collapse on a masonry arch bridge at Bargower, Strathclyde." *TRRL Contractor Report 26*, Department of Transport, Crowthorne.
- Hendry, A. W. (1990). "Masonry properties for assessing arch bridges." *TRRL Contractor Report 244*, Department of Transport, Crowthorne.

- Hendry, A. W., Davies, S. R., and Royles, R. (1985). "Test on stone masonry arch at Bridgemill-Girvan." *TRRL Contractor Report 7*, Department of Transport, Crowthorn, UK.
- Heyman, J. (1980). "The estimation of the strength of masonry arches." *Proceeding of the Institution of Civil Engineers.*, 69, 921-937.
- Heyman, J. (1982). *The masonry arch*, Ellis Horwood Ltd., Chichester.
- Howe, M. A. (1987). *A treatise on arches*, John Wiley and Sons, New York.
- Hughes, T. G., and Blackler, M. J. (1997). "A review of the UK masonry arch assessment methods." *Proceeding of the Institution of Civil Engineers, Structures and Building*, 122(Aug), 305-315.
- Hughes, T. G., Davis, M. C. R., and Taunton, P. R. (1998). "The small scale modelling of masonry arch bridges using centrifuge." *Proceedings of the Institution of Civil Engineers, Structures and buildings*, 128(Feb), 49-58.
- Hughes, T. G., and Kitching, N. (2000). "Small scale testing of masonry." 12th International Brick/Block Masonry Conference, Madrid-Spain, 893-902.
- Hughes, T. G., and Miri, M. (2004). "Three dimensional behaviour of masonry arch bridges under service load " 13th International Brick/Block Masonry Conference, D. Martens and A. Vermeltfoort, eds., Schaubroeck NV, Amsterdam, 157-164.
- Long, W. B. (1990). "Sprayed concrete." *The Maintenance of Brick and Stone Masonry Structures*, A. M. Sowden, ed., E. & F.N. Spon, London, 239-251.
- Loo, Y. C. (1995). "Collapse load analysis of masonry arch bridges." First International Conference on Arch bridges, C. Melbourne, ed., Thomas Telford, Bolton, UK, 167-174.
- Loo, Y. C., and Yang, Y. (1991a). "Cracking and failure analysis of masonry arch bridges." *Journal of Structural Engineering*, 117(6), 1641-1659.
- Loo, Y. C., and Yang, Y. (1991b). "Tensile strength, strain softening and the failure analysis of masonry arch bridges." *Computational Mechanics*, Lee and Leung, eds., A.A. Balkema, Rotterdam, Hong Kong, 191-196.
- Melbourne, C. (1990a). "The Behaviour of Brick Arch Bridges." *British Masonry Society Proceedings*, 4, 54-57.
- Melbourne, C. (1990b). "The behaviour of masonry arch bridge - the effect of defects." 4th Rail Bridge Centenary Conference, B. H. V. Topping, ed., Edinburgh.



- Melbourne, C. (1991). "Conservation of masonry arch bridges." 9th International Brick / Block masonry conference, DGfM, ed., Berlin, 1563-1570.
- Melbourne, C. (2001). "An overview of experimental masonry arch bridge research in UK." ARCH01, Third international arch bridges conference, C. Abdunur, ed., Paris, 343-350.
- Melbourne, C., Begimgil, M., and Gilbert, M. (1995). "The load test to collapse of a 5M span brickwork arch bridge with tied spandrel walls." First International Conference on Arch bridges, C. Melbourne, ed., Tomas Telford, Bolton, 509-517.
- Melbourne, C., and Gilbert, M. (1993). "A study the effects of ring separation on the load carrying capacity of masonry arch bridges." Bridge Management 2, J. E. Harding, G. A. R. Parke, and M. J. Ryall, eds., Thomas Telford, Guildford, UK, 244-253.
- Melbourne, C., and Gilbert, M. (1995). "The behaviour of multi ring brickwork arch bridges." *The Structural Engineer*, 73(3), 39-47.
- Melbourne, C., and Wagstaff, M. (1993). "Load tests to collapse of three large-scale multi-span brickwork arch bridges." Bridge Management 2, J. E. Harding, G. A. R. Parke, and M. J. Ryall, eds., Thomas Telford, Guildford, UK, 227-235.
- Melbourne, C., and Walker, P. J. (1988). "Load test to collapse of model brickwork masonry arches." 8th International Brick/Block Masonry Conference, Elsevier Applied Science, New York, 991-1002.
- Melbourne, C., and Walker, P. J. (1990). "Load test to collapse on a full scale model six metre span brick arch bridge." *TRRL Contractor Report 189*, Department of Transport, Crowthorne.
- Miri, M., and Hughes, T. G. (2004). "Increased load capacity of arch bridges using slab reinforced concrete." Arch Bridge IV, P. Roca and E. Onate, eds., CIMN, Barcelona, 469-478.
- Mohammed, A., and Hughes, T. G. (2005). "Comparison of prototype and 1/6th model scale behaviour under compressive loading." 10th Canadian Masonry Symposium, Shelley Lissel, Mark Benz, Casie Yuen, and N. Shrive, eds., University of Calgary, Banff, Alberta, Canada, 454-464.
- Ng, K. H. (1999). "Analysis of masonry arch bridges," PhD, Nappier University, Edinburgh.

- Ng, K. H., and Fairfield, C. A. (1999). "Collapse Load Repeatability Tests on Brickwork Arches." 8th International Conference on Structural Faults & Repair [CD Rom], M. C. Forde, ed., Engineering Technics Press, London.
- Ng, K. H., Fairfield, C. A., and Sibbald, A. (1999). "Finite-element analysis of masonry arch bridges." *Proceedings of the Institution of Civil Engineers, Structures and Buildings*, 134(2), 119-127.
- Page, J. (1987). "Load tests to collapse on two arch bridges at Preston, Shropshire and Prestwood, Staffordshire." *TRRL Research Report 110*, Department of Transport, Crowthorne.
- Page, J. (1988). "Load tests on two arch bridges at Torrksey and Shinafoot." *TRRL Research Report 159*, Department of Transport, Crowthorn, UK.
- Page, J. (1989). "Load tests to collapse on two arch bridges at Strathmashie and Barlae." *TRRL Research Report 201*, Department of Transport Crowthorne.
- Page, J. (1993). *Masonry arch bridge- state of the art review*, Transport Research Laboratory, HMSO, London.
- Page, J. (1996). "A guide to repair and strengthening of masonry arch highway bridges." Department of Transport, Crowthorne.
- Page, J., Ives, D. A., and Ashurst, D. (1991). "Deterioration and repair of masonry arch bridges." 9th International Brick/Block Masonry Conference, DGfM, ed., Berlin, 1591-1599.
- Pippard, A. J. (1951). "A study of the voussoir arch." National Building Studies, Research Paper No 11., London.
- Pippard, A. J., and Ashby, R. J. (1939). "An experimental study of the voussoir arch." *Proceeding of the Institution of Civil Engineers*, 10(Jan), 383-406.
- Pippard, A. J., and Chitty, L. (1941). "Repeated load tests on a voussoir arch." *Proceeding of the Institution of Civil Engineers*, 17, 79-86.
- Pippard, A. J., and Chitty, L. (1942). "Repeated load tests on a voussoir arch." *Proceeding of the Institution of Civil Engineers.*, 79-86.
- Pippard, A. J., Tranter, E., and Chitty, L. (1936). "The mechanics of the voussoir arch." *Proceeding of the Institution of Civil Engineers*, 4(Dec), 281-306.
- Ponniah, D. A. (1987). "Stress dispersal in arch bridges." Third International Conference on Structural Faults & Repairs, London, 311-316.

- Ponniah, D. A., Fairfield, C. A., and Prentice, D. J. (1997). "Fill stresses in a new brick arch bridge subject to heavy axle-load tests." *Proceedings of the Institution of Civil Engineers, Structures and Buildings*, 123(May), 173-185.
- Poulos, H. G., and Davis, E. H. (1974). *Elastic solutions for soil and rock mechanics*, John Wiley and Sons, New York.
- RILEM. (1994). *Technical recommendations for the testing and use of construction materials*, E&FN SPON, London.
- Roberts, B. J., and Boothby, T. E. (1999). "Transverse strength of masonry arch bridges." 8th North American Masonry Conference [CD Rom], Austin, Texas, USA.
- Royles, R., and Hendry, A. W. (1991). "Model tests on masonry arches." *Proceedings of the Institution of Civil Engineers, Structure and Buildings*, 91(June), 299-321.
- Sicilia, C. (2001). "A study of 3D masonry arch structures using centrifuge model and FE analysis," PhD, University of Wales, Cardiff.
- Sicilia, C., Pande, G. N., and Hughes, T. G. (2001). "Numerical modelling of masonry arch bridges." *Computer Methods in Structural Masonry*, T. G. Hughes and G. N. Pande, eds., Computers & Geotechnics LTD, Rome, 20-27.
- Smith, F. W. (1991). "Load path analysis of masonry arches," PhD, University of Dundee, Dundee.
- Smith, F. W., and Harvey, W. J. (1989). "Full-scale test of a masonry arch." SERC Conference Repair, Maintenance and Operation in Civil Engineering, Engineering Technics Press, London, 21-27.
- Sumon, S. K. (1997). "Repair and strengthening of a damaged arch with built in ring separation." 7th International Conference on Structural Faults and Repair, Engineering Technics press, Edinburgh, 69-75.
- Sumon, S. K. (1998). "Repair and strengthening of five full scale masonry arch bridges." Second International Conference on Arch Bridges, Venice, Italy, 407-415.
- Sumon, S. K. (1999). "Strengthening methods for ring-separated masonry arch bridges." 8th International Conference on Structural Faults and Repair-99 [CD ROM], M. C. Forde, ed., Engineering Technics press, London.
- Sumon, S. K., and Ricketts, N. (1995). "Repair and Strengthening of Masonry Arch Bridges." First International Conference on Arch bridges, C. Melbourne, ed., Tomas Telford, Bolton, 501-508.

- Sunley, V. K. (1990). "The experimental investigation of defects." *The Maintenance of Brick and Stone Masonry Structures*, A. M. Sowden, ed., E. & F.N. Spon, London, 63-80.
- Taunton, P. R. (1997). "Centrifuge modelling of soil/masonry structure interaction," PhD, University of Wales, Cardiff.
- Taylor, R. N. (1995). "Geotechnical centrifuge technology." Blackie Academic and professional, Chapman and Hall, London, 19-33.
- Temple, B. P., and Kennedy, A. (1989). "The engineering properties of old bricks, Technical Memorandum TM CES 128." British Rail Research, Derby.
- TENAX. (2002). "Ground Reinforcement and Erosion Control, Product Guide and Price list." Tenax UK Limited.
- Thavalingam, A., Bicanic, N., Robinson, J. I., and Ponniah, D. A. (2001). "Computational framework for discontinuous modelling of masonry arch bridges." *Computers & Structures*, 79(19), 1821-1830.
- Towler, K. (1985). "Applications of non-linear finite element codes to masonry arches." Second International Conference on Civil and Structural Engineering Computing, Civil-Comp Press, Edinburgh.
- Towler, K., and Sawko, F. (1982). "Limit state behaviour of brickwork arches." 6th International Brick Masonry Conference, Rome, Italy, 422-429.
- Van Beek, G. W. (1987). "Arches and vaults in ancient Near East." *Scientific American*(Jul), 78-85.

## Appendix:

LVDT serial number	LVDT type	Manufacturer calibration (mV/V)	Modified calibration (mV/mm)
6460	D2/ 100A	N/A	163.92
6449	D2/ 200A	160.02	159.08
6451	D2/ 200A	N/A	152.13
5691	D2/ 200A	165.53	173.85
5692	D2/ 200A	163.39	171.80
5694	D2/ 200A	165.36	165.57
5675	D2/ 100A	157.11	164.88
6944	D2/ 100A	159.06	159.83
6963	D2/ 100A	168.99	170.63
6961	D2/ 100A	174.05	175.44
6960	D2/ 100A	174.19	175.24
6959	D2/ 100A	168.86	169.87
6958	D2/ 100A	145.53	146.69
6957	D2/ 100A	161.69	163.07
102357	DCR15	280.00	287.10
102358	DCR15	280.00	276.45

Table A-1: LVDT Calibration Factors

Kyowa identification	Calibration (kPa/mV)	Calibration (mV/V)
K1-K15	165.9	0.985
K16-K20	153.3	1.066
K21-K24	179.6	0.910
K24-K30	190.7	0.874

Table A-2: Kyowa calibration factors

